Development of bio-based systems as pollutants removal for water remediation.

by

Diego Gomez-Maldonado

A dissertation submitted to the Graduate Faculty of
Auburn University
in partial fulfillment of the
requirements for the Degree of
Doctorate in Philosophy

Auburn, Alabama
May 1, 2021

Keywords: water treatment, adsorption systems, bio-based systems, cellulose nanofibrils, polysaccharides

Approved by

Dr. Maria Soledad Peresin, Chair, Assistant Professor of Forest Biomaterials
Dr. Matthew Neal Waters, Associate Professor of Environmental Sciences
Dr. Brian K. Via, Region Bank Professor of Forest Products
Dr. Graeme Lockaby, Clinton McClure Professor of Wetland Biogeochemistry and Environmental Health
Dr. Wim Thielemans, Professor of Chemical Engineering
Dr. Paul Carver Bartley, University Reader, Assistant Professor of Horticulture

Abstract

In the search of bio-based alternatives to develop systems that can improve water quality, cellulose nanofibril (CNF) were studied as scaffolds for the development of adsorbents for emerging and unregulated pollutants; in particular, the cyanotoxin microcystin-LR. To ensure the capacity of polysaccharides to capture the toxin, modification of the fibrils with β-cyclodextrin (CD) were evaluated in this dissertation. β-cyclodextrin was immobilized directly onto the cellulose nanofibril by epoxy-based reaction and by an indirect adsorption after its immobilization to chitosan following a TEMPO oxidation and EDC/NHS chemistry. A fundamental study on the impact on the adsorption capacity after changing the spatial configuration, the different immobilization approaches, and ratios of chitosan/cyclodextrin were studied using Quartz Crystal Microbalance with Dissipation monitoring (QCM-D).

To develop applicable systems with the above-mentioned materials, different three-dimensional structures were generated, characterized, and applied to remove microcystin-LR from controlled samples; the adsorption kinetic of these systems was monitored with High-Pressure Liquid Chromatography (HPLC). Specific, aerogels were generated by solvent exchange (ethanol and tert-butanol) and freeze-drying with the best performing configuration of the epoxy-based immobilized CD on CNF. Meanwhile, the chitosan mediated adsorption was used as coating for hydrogels produced by solubilizing CNF on cold sodium hydroxide/urea and regenerating on acid, and on aerogels from delignified wood (nanowood) air-dried after solvent exchange (ethanol, isopropanol, and octane). Finally, the coated nanowood was tested on lake water from Ogleetree Lake spiked with a known concentration of microcystin-LR.

Acknowledgments

The author wants to formally acknowledge his major advisor Dr. Maria Soledad Peresin for the trust placed with this opportunity, and for the constant mentoring and guidance not only on regards to research, but also forwarding the academic and professional development as well as personal growth. Thank you for always having your door open for questions, conversation or venting, those little moments always helped. Also, gratitude is due to the members of the PhD committee members, through their guidance, patience and comments this dissertation was possible. The author would also like to acknowledge Dr. Ilari Filpponen for the time invested in conversations, planning and see through the research as well as to Dr. Iris Beatriz Vega Erramuspe, her time and detail helped to form this work.

The author would like to thank his current and former working peers, thank you for your encouragement, company and the high-quality research that inspired me, Celeste, Simon, Marina, Javier, Sydney, Yufei, Alfredo, Osei, Charles, Andrea, Diego Sanchez, and Tao. Likewise, thanks to the undergrads that placed their trust and time in the work that is being developed in the center, Philip, Jacob, Joseph, Samuel, Cassidy, Brieanne, Samir, Evie, Florrie, Emmie. And especial thanks to Autumn Reynolds whom without this work would not have the broadness and quality, thanks for being my partner in this journey.

Thank you are also due to Dr. Leena-Sisko Johansson for her help on the XPS analysis, to Dr. Maria Lujan Auad and Dr. Ronald Dute for their help with the AFM access and their invaluable teachings, to Dr. Sushil Adhikari, Dr. Oladiran Fasina, Vivek Patil and Poulami Roy for their help with the TGA measurements, to Dr. Daniel Burnett for the DVS measurements and analysis, to Dr. Jayachandra Ramapuram and Manjusha Annaji for their help with the HPLC, to Dr. Matthew

Waters and his team for their help with the Elemental Analysis and their friendship. And especial thanks to Dr. Virginia Davis, Dr. Silvia Ponce, Dr. Adriana Restrepo, Dr. Sarah Zohdy and Dr. Paul Bartley as you helped me to develop in fields, applications, and work beyond the one here presented.

Thank you to all the staff, faculty members, colleges and friends from the School of Forestry and Wildlife Sciences for your patience, help and friendship in these years that formed me beyond the professional matter. Especial thanks to Dr. Stephen Ditchkoff, for his friendship, tips, teachings, and personal support.

In giving appreciation, the author wants to thank his parents Gabriela and Julio Cesar and dear siblings Cristina and Sebastian, thank you for always being there to hear and encourage. Thanks to his aunts Edith, Maria Dolores “Lolis”, Elizabeth, Tania, Lidia, and his uncle Jorge for being present even in the distance, as well as his other siblings Alejandra, Carlos, Arturo, Jorge, Renata, Carolina, Lucia, Alain, Erick, Nestor, and Eduardo having your support and love keeps pushing me forward. The author would also like to thank the extended families Gomez and Maldonado.

The author wants to thank likewise his former advisor Dr. Jose Campos Teran and his former co-workers and colleges at UAM-Cuajimalpa, Universidad de Guadalajara, and Aalto University. Thanks to his friends back home and through the distance, Dulce, Owen, Mauricio, Rebeca, Marcus, Heber, Manuel, Nele, Elisa, Ingrid, Veronica, Devi, Cynthia, and Itzel. Finally, the author wants to exceptionally thanks those that became his family and support system at Auburn, Cele, Fer, Laura, Simon, Abel, Anthony, Mariano, Nicole, Jessica, and Monet.

Table of Contents

Abstract ii
Acknowledgments iii
Table of Contents v
List of Tables x
List of Figures xi
List of Publications and Contributions xiv
1. Background 1
1.1. Water access and pollutants 1
1.2. Current treatment of drinking water pre-consumption 2
1.3. Natural Polymers 5
1.4. Polysaccharides 5
1.4.1. Cellulose 7
1.4.2. Chitin 21
1.4.3. Chitosan 28
1.4.4. Alginate 44
1.4.5. Hemicelluloses 57
1.4.6. Starch: Amylose and amylopectin 64
1.5. Cyclodextrins 71
1.6. Conclusions 86
1.7 Future work 88
1.7. Literature Cited: 89
2. Research objective and hypotheses 129
2.1. General objective 129
2.2 Objectives for each chapter 129
Chapter 1 129
Chapter 2 129
Chapter 3 130
Chapter 4 130
Chapter 5 130

Chapter 6 131
Chapter 7 131
2.3. Hypotheses 131
2.4. Fundamentals and limitations 131
2.4.1. Fundamental interactions 132
2.4.2. Limitation on mass and concentration quantification 141
2.5. Conclusions 145
2.6. Literature cited. 146
3. Cellulose-cyclodextrin co-polymer for removal of cyanotoxins on water sources 153
3.1. Abstract 153
3.1.1. Index Words: 153
3.1.2. Project Partners: 153
3.2. Introduction 154
3.3. Materials and Methods 159
3.3.1. Materials 159
3.3.2. Cellulose nanofibril characterization 160
3.3.3. Polymerization of β-cyclodextrin 161
3.3.4. Preparation of CNF/ β-cyclodextrin co-polymers 162
3.3.5. Characterization techniques 162
3.3.6. Quartz Crystal Microbalance with Dissipation Monitoring (QCM-D) 164
3.4. Results and Discussion 166
3.4.1. Characterization of CNF and the modified polysaccharides 166
3.4.2. Formation of surfaces in situ on QCM-D and adsorption of microcystin-LR 171
3.5. Conclusion 180
3.6. Future work 181
3.7. Literature Cited 183
4. Fabrication of aerogels from cellulose nanofibril grafted with β-cyclodextrin for capture of water pollutants. 190
4.1. Abstract 190
4.1.1. Index Words 191
4.1.2. Project Partners 191
4.2. Introduction 192

4.3. Materials and Methods 195
4.3.1. Materials 195
4.3.2. Cellulose nanofibrils (CNF) production 196
4.3.3. Synthesis of crosslinked cellulose nanofibrils/β-cyclodextrin (CNF-CD) 196
4.3.4. Aerogels formation 197
4.3.5. Characterization techniques 197
4.3.6. Adsorption Experiments 202
4.4. Results and Discussions 203
4.4.1. Synthesis of CNF-CD. 203
4.4.2. Aerogel formation. 207
4.4.3. Molecular interactions 210
4.5. Conclusion 214
4.6. Future Work 215
4.7. Literature Cited: 216
5. Oriented β-cyclodextrin/chitosan polymer as an active coating on 2D and 3D nanocellulose surfaces and its efficiency in microcystin-LR capture 225
5.1. Abstract 225
5.1.1. Index Words 226
5.1.2. Project Partners 226
5.2. Introduction 226
5.3. Materials and Methods 232
5.3.1. Materials 232
5.3.2. Synthesis of TEMPO oxidized β-cyclodextrin (TOCD). 232
5.3.3. Synthesis of chitosan-cyclodextrin polymers (Ch-TOCD). 233
5.3.4. Nanocellulose bead generation. 233
5.3.5. Characterization techniques 234
5.4. Results and Discussion 239
5.4.1. TEMPO oxidation of β-cyclodextrin. 239
5.4.2. TOCD grafting to chitosan. 241
5.4.3. Adsorption of Ch-TOCD onto CNF and microcystin-LR capture on surface 244
5.4.4. Adsorption of Ch-TOCD onto CNF and microcystin-LR capture on beads. 247
5.5. Conclusions 251

5.6. Future work 251
5.7. Literature Cited 253
6. Delignified wood aerogel as scaffolds coated with chitosan-cyclodextrin co-polymer for removal of microcystin-LR. 264
6.1. Abstract 264
6.1.1. Index Words 264
6.1.2. Project Partners 265
6.2. Introduction 265
6.3. Materials and Methods 268
6.3.1. Materials 268
6.3.2. Synthesis of TEMPO oxidized β-cyclodextrin (TOCD). 269
6.3.3. Synthesis of chitosan-cyclodextrin polymers (Ch-CD). 269
6.3.4. Delignified wood aerogels (nanowood) production. 270
6.3.5. Coating of wood aerogels. 270
6.3.6. Adsorption of microcystin-LR (MC) by High Pressure Liquid Chromatography (HPLC). 270
6.3.7. Characterization 271
6.4. Results and Discussion 274
6.4.1. TEMPO oxidation of β-cyclodextrin and grafting to chitosan. 274
6.4.2. Characterization of nanowood and coated nanowood. 276
6.4.3. Microcystin adsorption 281
6.5. Conclusions 283
6.6. Future Work 284
6.7. Literature Cited 285
7. Adsorption of microcystin-LR by coated nanowood aerogels from spiked samples of Lake Ogletree of Auburn, AL 293
7.1. Abstract 293
7.1.1. Index Words 293
7.1.2. Project Partners 293
7.2. Introduction 294
7.3. Materials and Methods 297
7.3.1. Materials 297
7.3.2. Water sample of Lake Ogletree 298

7.3.3. Synthesis of TEMPO oxidized β-cyclodextrin (TOCD). 299
7.3.4. Synthesis of chitosan-cyclodextrin polymers (Ch-CD)..... 300
7.3.5. Delignified wood aerogels (nanowood) obtention. 300
7.3.6. Coating of wood aerogels and characterization..... 300
7.3.7. Adsorption of microcystin-LR (MC) by High Pressure Liquid Chromatography (HPLC). 301
7.4. Results and discussion 302
7.4.1. Lake water characterization..... 302
7.4.2. Coated Nanowood characterization..... 304
7.4.3. Adsorption of microcystin from the spiked Ogletree water 305
7.5. Conclusions..... 308
7.6. Future Work..... 309
7.7. Literature Cited..... 310

List of Tables

Table 1.1. Cellulose-derived Materials and Pollutants Adsorbed..... 19
Table.1.2. Chitin- derived materials and pollutants adsorbed 27
Table 1.3. Chitosan-derived Materials and Pollutants Adsorbed 42
Table 1.4. Alginate-derived Materials and Pollutants Adsorbed..... 55
Table 1.5. Hemicelluloses-derived Materials and Pollutants Adsorbed..... 62
Table 1.6. Starch-derived Materials and Pollutants Adsorbed 70
Table 1.7. Cyclodextrin-derived Materials and Pollutants Adsorbed..... 84
Table 3.1. Roughness comparison between the systems surfaces 176
Table 4.1. Charge density values of the different elements used..... 204
Table 4.2. Physical properties of the CNF and CNF-CD aerogels 208
Table 4.3. Parameters for adsorption of microcystin-LR (MC) and methylene blue (MB) by aerogel filters 214
Table 5.1. Elemental Analysis of Chitosan derivates and Degree of substitution estimation. ... 242
Table 6.1. Results from the elemental analysis of the wood, nanowood and coated nanowood.278
Table 6.2. Porosity and SEM image comparison between pinewood before and after treatment. 279
Table 7.1. Characterization of the water obtained from Lake Ogletree..... 303

List of Figures

Figure 1.1. Structure of cellulose monomer..... 8

Figure 1.2. Structure of chitin monomer..... 22

Figure 1.3. Structure of chitosan monomers..... 29

Figure 1.4. Structure of alginates monomers. 45

Figure.1.5. Structures of xylan (left) and glucomannan (right) 58

Figure 1.6. Two glucose molecules joined by α 1, 4 linkage, which originates backbone of amylose and amylopectin 64

Figure 1.7. Structure of β-cyclodextrin..... 72

Figure 3.1. Neutron diffraction structure of β-cyclodextrin with ethanol complex. The hydrogen bonding capability can be observed through dash-lines. (Saenger & Steiner, 1998) Reproduced with the permission of International Union of Crystallography (https://journals.iucr.org/)..... 156

Figure 3.2. Expected structure of β-cyclodextrin crosslinked with other hydroxyl group from polysaccharides (cellulose or other cyclodextrins) through epichlorohydrin 157

Figure 3.3. Basic chemical structure of microcystins. Amino acid residues 2 and 4 are interchangeable 158

Figure 3.4. FTIR-ATR spectra of cyclodextrin and poly(cyclodextrin) obtained by crosslinking with epichlorohydrin..... 167

Figure 3.5.. Aluminum pans with the materials used for this work, from left to right: CD, PCD, CNF-PCD, CNF-CD, and CNF suspensions 168

Figure 3.6. FTIR-ATR spectra comparing cellulose nanofibrils (CNF) and modified cellulose nanofibrils (CNF-CD and CNF-PCD) 169

Figure 3.7. XPS wide energy region spectra comparing a pure cellulose reference, cellulose nanofibrils (CNF) and modified cellulose nanofibrils (CNF-CD and CNF-PCD). The insert shows the high-resolution C 1s spectra..... 170

Figure 3.8 Thermogravimetric analysis of the CNF, CD, and the modified cellulose nanofibrils (CNF-CD and CNF-PCD). The thermogram (left) shows the behavior of the material, and the table (right) presents the main extracted data for each sample..... 171

Figure 3.9. Scheme of the sequece used in the QCM-D to monitor the adsorption of the microcystinon the generated (co)polymerlayers..... 172

Figure 3.10. QCM-D sensograms of the in situ surface generation from (a) CNF, (b) CNF and flushed CD (CNF+CD), (c) CNF-CD, and (d) CNF-PCD. CNF, cellulose nanofibrils; CD, cyclodextrin; CNF-CD, cellulose nanofibrils grafted with cyclodextrin; CNF-PCD, cellulose nanofibrils grafted with poly-cyclodextrin 173

Figure 3.11. AFM images of the cellulose nanofibrils (CNF) and the modified cellulose nanofibrils (CNF-CD and CNF-PCD) and the average rugosity (Ra), each row was generated by a different technique, while the last one was measured after adsorption of microcystin in the QCM-D..... 175

Figure 3.12. QCM-D sensograms of the adsorption of microcystin in water and Tris-HCl buffer from (a) CNF, (b) CNF and flushed CD (CNF+CD), (c) CNF-CD, and (d) CNF-PCD. CNF, cellulose nanofibrils; CD, cyclodextrin; CNF-CD, cellulose nanofibrils grafted with cyclodextrin; CNF-PCD, cellulose nanofibrils grafted with poly-cyclodextrin 178

Figure 3.13. Charts of the mass obtained after the modeling the frequency and dissipation shift of the QCM-D sensograms in QSense DFind software. (a) Mass contribution of each layer added to the surfaces, and (b) microcystin-LR adsorption capability of each CNF polymer. CNF, cellulose nanofibrils; CD, cyclodextrin; CNF-CD, cellulose nanofibrils grafted with cyclodextrin; CNF-PCD, cellulose nanofibrils grafted with poly-cyclodextrin 180

Figure 4.1.Schematic outline of this work 195

Figure 4.2. Chemical and thermal comparison of the used cellulose nanofibrils (CNF), β-cyclodextrin (CD), and the crosslinked CNF-CD. (A) FTIR spectra; (B) XPS wide energy region spectra and inserts showing the high-resolution C 1S spectra and the elemental data 205

Figure 4.3. Thermograms comparing the used cellulose nanofibrils (CNF), β-cyclodextrin (CD) and inserts of the first derivate and the main thermal degradation data..... 206

Figure 4.4 AFM images of spin coated surfaces from CNF (left) and CNF-CD (right). 207

Figure 4.5. Comparison between on surface energy (a), wettability (b), water uptake (c), and swelling (d) of the aerogels obtained from the CNF and the modified CNF-CD..... 210

Figure 4.6. (a) Adsorption of microcystin-LR from solutions with concentrations 0.8 and 1.5 µg/mL by aerogels prepared with CNF and CNF-CD. 212

Figure 4.7. (A) Adsorption and (B) desorption of methylene blue (MB) from a 15 mg/L solution by aerogels prepared with CNF and CNF-CD. 214

Figure 5.1. Basic structure of microcystins, where residues 2 and 4 show variability in residues, those variations are used to name the different molecules derivates, being microcystin-LR the most prominent related to liver cancer and other hepatoxic reactions. 231

Figure 5.2. Conductivity and pH titration of TEMPO oxidized beta-cyclodextrin (left) and determination of inflexion points for volumes determination (right). 240

Figure 5.3. FT-IR spectrum (KBr method) of the acid TEMPO-mediated oxidization of beta-cyclodextrin..... 241

Figure 5.4 XPS wide energy region spectra of chitosan and its derivates. High resolution C 1s graphs (left) and N (left). 243

Figure 5.5 FTIR spectra comparison of the chitosan derivatives and the pristine materials. 244

Figure 5.6. QCM-D isotherms of surface generation with chitosan and derivates, followed by adsorption of microcystin on 50 mM NaOAc buffer. Chitosan surface (a), Chitosan-TOCD molar ratio 1:2 (b), 1:1 (c), and 3:1 (d). 246

Figure 5.7. Mass adsorbed onto the CNF layers of each component (left), and microcystin adsorbed on each chitosan derivate (right). 247

Figure 5.8. Physicochemical comparison of the uncoated CNF beads coated with chitosan (Ch) and chitosan modified with oriented cyclodextrin (Ch-TOCD) in the proportions 3:1, 1:1, and 1:2 by a) solid content: b) elemental analysis; and c) FTIR spectra. 248

Figure 5.9. Adsorption kinetics of the CNF beads and CNF beads coated with Ch-TOCD 1:2 on a 6.5µg/mL solution over 24 h..... 249

Figure 5.10. Pseudo-second order kinetic model for the CNF beads and CNF beads coated with Ch-TOCD 1:2..... 250

Figure 6.1. pH titration of TEMPO oxidized β-cyclodextrin (TOCD) and 2 derivate to identify inflexion groups for DO determination..... 274

Figure 6.2. FTIR-ATR spectra of the TEMPO oxidized β-cyclodextrin (TOCD), chitosan and the grafter material of both (Ch-CD). There the formation of the C-N bond is visible ca. 1490 cm^{-1} as well as the reduction of the carboxyl bond at 1750 cm^{-1}added to TOCD, confirming the reaction. 275

Figure 6.3. (a) FTIR-ATR spectra of the wood, nanowood and coated nanowood and (b) shows the thermogravimetrical analysis of the three components with an insert table presenting the onset and max degradation temperatures of each one. 277

Figure 6.4. (a) Plot comparing the water uptake on wood, nanowood and coated nanowood and (b) swelling percentage of each material after stability. 280

Figure 6.5. Adsorption kinetic of wood, nanowood and the coated nanowood on a 5.4 µg/mL on a solution for 6 h. 282

Figure 6.6. Pseudo-second order kinetic model and data of the adsorption of microcystin-LR with wood, nanowood and the coated nanowood. 283

Figure 7.1. Water Treatment Process of the City of Auburn (The Water Works Board of The City of Auburn, 2019). 295

Figure 7.2. Location where the water samples were obtained. 299

Figure 7.3. FTIR-ATR spectra of the wood and coated nanowood. 305

Figure 7.4. Adsorption kinetic of wood and coated nanowood on water from Lake Ogleetree spiked with 5.4 µg/mL. 307

Figure 7.5. Pseudo-second order kinetic model and data of the adsorption of microcystin-LR with wood and the coated nanowood from spiked water of Ogletree Lake. 308

List of Publications and Contributions

Papers derived from dissertation

Paper I **Gomez-Maldonado, D.**; Vega Erramuspe, I. B.; Peresin, M. S. Natural Polymers as Alternative Adsorbents and Treatment Agents for Water Remediation. *BioResources* **2019**, *14* (4). https://doi.org/10.15376/biores.14.4.Gomez-Maldonado.

Paper II **Gomez-Maldonado, D.**; Vega Erramuspe, I. B.; Filpponen, I.; Johansson, L.-S.; Lombardo, S.; Zhu, J.; Thielemans, W.; Peresin, M. S. Cellulose-Cyclodextrin Co-Polymer for the Removal of Cyanotoxins on Water Sources. *Polymers (Basel).* **2019**, *11* (12), 2075. https://doi.org/10.3390/polym11122075.

Paper III **Gomez-Maldonado, D.**; Reynolds, A. M.; Johansson., L.-S.; Burnett, D.; Jayachandra, R.; Waters, M. N.; Vega Erramuspe, I. B.; Peresin, M. S. Fabrication of aerogels from cellulose nanofibril grafted with β-cyclodextrin for capture of pollutants for water remediation. (Submitted to *Journal of Porous Materials 03/03/2021*)

Paper IV **Gomez-Maldonado, D.**; Vega Erramuspe, I. B.; Filpponen, I.; Johansson, L.-S.; Jachandra, R.; Waters, M.N.; Peresin, M. S. Oriented β-cyclodextrin/chitosan polymer as an active coating on 2D and 3D nanocellulose surfaces and its efficiency in microcystin-LR capture. (In preparation)

Paper V **Gomez-Maldonado, D.**; Reynolds, A.M.; Burnett, D.; Jayachandra, R.; Waters, M. N.; Peresin, M. S. Delignified wood aerogel as scaffolds coated with an oriented chitosan-cyclodextrin co-polymer for removal of microcystin-LR. (In preparation)

Paper VI **Gomez-Maldonado, D.**; Reynolds, A.M.; Jayachandra, R.; Waters, M. N.; Lockaby, A.G.; Peresin, M. S. Adsorption of microcystin-LR by coated nanowood aerogels from spiked samples of Lake Ogletree of Auburn, AL. (In preparation)

Contributions not included in dissertation.

Peer-review articles

Iglesias, M. C.; **Gomez-Maldonado, D.**; Via, B. K.; Jiang, Z.; Peresin, M. S. Pulping Processes and Their Effects on Cellulose Fibers and Nanofibrillated Cellulose Properties: A Review. *For. Prod. J.* **2020**, *70* (1), 10–21. https://doi.org/10.13073/FPJ-D-19-00038.

Sánchez-Osorno, D. M.; **Gomez-Maldonado, D.**; Castro, C.; Peresin, M. S. Surface Interactions between Bacterial Nanocellulose and B-Complex Vitamins. *Molecules* **2020**, *25* (18), 4041. https://doi.org/10.3390/molecules25184041.

Gomez-Maldonado, D.; Peresin, M. S.; Verdi, C.; Velarde, G.; Saloni, D. Thermal, Structural, and Mechanical Effects of Nanofibrillated Cellulose in Polylactic Acid Filaments for Additive Manufacturing. *BioResources* **2020**, *15* (4), 7954–7964. https://doi.org/10.15376/biores.15.4.7954-7964.

Gomez-Maldonado, D.; Filpponen, I.; Hernandez Diaz, J.A.; Waters, M.N.; Auad, M.L.; Johansson, L.-S.; Vega Erramuspe, I. B.; Peresin, M. S. Simple functionalization of cellulose beads with pre-propargylated chitosan for clickable scaffold substrates (In press *Cellulose* 01/04/2021).

Gomez-Maldonado, D.; Filpponen, I.; Johansson, L.-S.; Waters, M.N.; Vega Erramuspe, I. B.; Peresin, M. S. Environmentally dependent adsorption of 2,4-dichlorophenol on cellulose-chitosan self-assembled composites (Submitted to *Biopolymers* 02/10/2021).

Nori, U. M.; **Gomez-Maldonado, D.**; Saha, P.; Ashurst, W.R., Peresin, M.S., Davis, V. A. Surface Modified Cellulose Nanocrystal Probes for Potential Bio-sensing Applications (submitted to *Biomacromolecules*)

Gomez-Maldonado, D.; Ponce, S., Peresin, M.S. Formation of Nanocellulose/Tara gum hydrogel beads as adsorbents in dye capture. (In Preparation)

Refereed book chapter

Gómez-Maldonado, D.; Hernández-Guerrero, M.; López-Simeon, R.; Arroyo-Maya, I. J.; Campos-Terán, J. Lignocellulosic-Derived Nanostructures from Latin American Natural Resources: Extraction, Preparation, and Applications. In *Lignocellulosics*; Elsevier, 2020; pp 91–115. https://doi.org/10.1016/B978-0-12-804077-5.00004-X.

1. Background

1.1.Water access and pollutants

One of the inherent human rights is the access to water and sanitation (United Nations, 2010; United Nations Department of Economic and Social Affairs, 2014), which means that each person should have daily access to in between 50 and 100 liters. This water should also be safe and affordable (less than 3% of household income). However, 29% of the global population do not have access to safely managed drinking water (World Health Organization, 2017).

For the water to be considered safe, the World Health Organization (WHO) recommends that local and country-based regulations base their water standards in the Guidelines for Drinking-water quality, 2011 (World Health Organization, 2014) where 41 organisms and over 80 components are identified as pollutants, which need to be monitored and controlled to assure no health risk. However, the increase in local industrial activities, as well as intensive agricultural activity, mining, and global warming of water sources generates in point pollution that needs to be identify by each entity and controlled by local regulations. For this, the United States Environmental Protection Agency also has the Fourth Unregulated Contaminant Monitoring Rule (USEPA - Office of Ground Water and Drinking Water, 2017) in which 30 more elements that are known to present a health risk have to also be monitored and controlled.

In general, the components that are considered as pollutants in water are soluble molecules and ions that present a risk for human health in low quantities. The nature of these pollutants' ranges from metals, radioactive materials, halogenated compounds, persistent organic pollutants, bioaccumulative and toxic molecules, among others. From the different regulation organs some or the share points include: copper (Cu(II)), chromium (Cr(VI)), mercury (Hg(II)), and lead (Pb(II)) for heavy metals; ammonium ($NH4^{+}$), chloride (Cl^{-}), aluminum (Al(III)), manganese (Mg(II)),

nitrate ($NO3^-$), and sodium (Na^+), which are considered soft ions; and organic molecules including benzene and some derivates, organochlorides like 1,2-dichloroethane, acrylamide, epichlorohydrin, trihalomethanes, and other polycyclic aromatic hydrocarbons, toxins and pesticides, like microcystin-LR, DDT and anatoxin. The microorganisms are more variable between regulations, as the organisms are more native or not to the region. However, the common ones are *Escherichia coli* and *Pseudomonas aeruginosa,* as well as a general count for coliform bacteria; this as they represent the more harmful gram-negative bacteria.

Beside this regulated and monitored pollutants, there exist the category of emerging contaminants (EC), which are molecules or microorganisms that have been often found in multiple water sources in low quantities and are not monitored. However, these new molecules are known or suspected to have an adverse effect on the environment or in human health (Rosenfeld & Feng, 2011). Some of the most common origin for this EC are municipal wastewater carrying pharmaceuticals, pesticides, personal care products and surfactants that are of daily use in residential houses and get reintroduced on drinking water by the flow of rivers and groundwater leaching (Khaoulani et al., 2015).

1.2.Current treatment of drinking water pre-consumption

The most common remediation treatments are precipitation, filtration, chlorination, and ozonation (Hitzfeld et al., 2000; Mahfoudhi & Boufi, 2017). **Ozone treatment** was developed in 1886 and is based on the formation of ozone from molecular oxygen present in the air by an induced electric field. Ozone is a reactive form of oxygen that is able to oxidize minerals, eliminate color and turbidity from water, degrade organics, and inactivate microorganisms (Camel & Bermond, 1998; Glaze et al., 1987; Langlais et al., 1991). This process was relegated after World War I, as chlorine was easier to obtain. In an analogous way, **chlorination** is able to disrupt cellular

processes and structures due to the interactions with cell-membrane proteins, inactivating microorganisms, and generating a long-term resistance, as ions stay in the water for a longer period of time inhibiting the microorganisms' growth (Du et al., 2017; Rosenblum et al., 2017). The downside of these processes is that chlorination generates halogenated compounds and ozone can generate other organic compounds. Often these by-products present a higher risk than the original compounds (Mao et al., 2018).

The **precipitation and filtration** methods are linked processes, as a lot of the precipitated components should then be removed from the water source by filtration, especially when they remain suspended instead of sedimenting as sludge. Aside from being retained by size, some compounds can be adsorbed directly into the material base of the filters, making adsorption the most convenient water treatment method, as components can be directly removed and treated (Faisal et al., 2017; Xin Luo et al., 2013; Mahfoudhi & Boufi, 2017).

The principle of the precipitation method is the use of pH changes or increase in ionic strength, which turns the excess nutrients (*i.e.* nitrates or phosphates) or other heavy ions into salts or gelatinous precipitates that can easily be removed from water lines and treatment plants. Depending on the substance that needs to be removed, a combination of buffer salts can be added to improve the salting out of the pollutants; some examples are the use of calcium salts for phosphate anions removal or sodium carbonate with iron trichloride for radioactive strontium removal (D. H. Kim et al., 2009; Lemlikchi et al., 2012; Xin Luo et al., 2013; Nyberg et al., 1994; Tomson & Vignona, 1984). With the precipitates formed and the newly added ions free in the water, the filtration and adsorption to the filter are key points for the improvement of the water quality. This last step involves the isolation of precipitate products and the removal of any by-product generated during the previous steps of the treatment. The process's capability of removal

is influenced by the surface area, which shows the dominance of interfacial phenomena, the specificity of the surface of the materials, and the mechanical and structural integrity of the selected material (Ali & Gupta, 2007; Mahfoudhi & Boufi, 2017; Z.-Y. Zhou et al., 2011).

The materials used for treatment by filtration of the water flow can be roughly categorized into inorganic, carbon-based, polymeric, and bio-based. Depending on the pollutant to be removed and the media conditions, the selection of the ideal material should be completed and then adjusted to make it as selective as needed. Apart from these common materials, new filtration systems have been developed with enhanced activity via the addition of nanoparticles and by composite generation (Shrivastava, 2010; Trujillo-Reyes et al., 2014). The use of nanoparticles immobilized on the surface of a solid support seems to be a good alternative, as the system usually shows good mechanical stability and prevents the leaching of the nanoparticles into the water that is being purified, preventing contamination with metals or molecules that formed the nanoparticle (Tyagi et al., 2012). It is vital to understand that the nature of the scaffolds selected for the nanoparticles are going to have an impact on the reactivity of the particles, which can either enhance or eliminate the activity (Haruta, 1997).

Even with all the regulations and newly developed technologies, the investment into environmental remediation generally has not been a priority for companies or industries, as it is a low profit activity with high operating costs. For this reason, the systems generated must have a minimum energy consumption, economic feasibility, and be environmental friendly to avoid further contamination (Haruta, 1997; Shrivastava, 2010; Tyagi et al., 2012). To accomplish this, bio-based materials are of primary interest, as they are renewable and low priced. They can be highly versatile, especially when biopolymers are used, as they have a wide range of systems that

can be developed from them, such as nanoparticles, nanofibers, scaffolds, hydrogels, and more (Klemm et al., 2005; Nevárez et al., 2011; Renard et al., 1997).

1.3. Natural Polymers

Biological systems bio-synthetize three main polymer types: nucleic acids, proteins, and polysaccharides; these are the major macromolecules that constitute any organism or biosystem, as they sustain metabolic and structural functions, as well as energy storage, carrying and effecting genetic information, and synthesis of analogous molecules by the enzymes and complex that are formed from the interaction between them (Smith & Wood, 1997). Other polymers present in biosystems include polyesters (*i.e.* PHAs), polyisoprene (rubber), polyethers (lignin), and other complex polyaromatics (melanin and suberin) (Meyers et al., 2008).

The use of natural polymers eliminates steps in industrial processing, as the need for industrial synthesis is avoided, and the purification can be completed using more environmentally friendly solvents. As many of these polymers are already residues from other industrialized processes, they represent a major advantage relative to the generation of new materials, which may be needed to address day-to-day problems, lowering costs and emissions. From this wide variety of available polymers, polysaccharides are generally more abundant, cheap, and easy to extract, as they have less variation within than nucleic acids and proteins; therefore, polysaccharides are ideal materials with which to develop remediation target systems.

1.4.Polysaccharides

As the name suggests, polysaccharides are polymers formed from sugar monomers (saccharides) linked by a glycoside bond with a general formula of $[C_n(H_2O)_n]_m$, where m is

between 40 to 3,000 units (P. Y. Chen et al., 2012; IUPAC, 2014). Smaller chains are called oligosaccharides, which have their own diversity and helpfulness in environmental remediation, as they have higher reactivity and more conformational states. Between these, one can highlight cyclodextrins and derived surfactants, such as *N*-alkylmaltonamides (del Valle, 2004; Saeki et al., 2009; Tianhong Zhang & Marchant, 1996).

Among polysaccharides, **cellulose** and **chitin** are the most abundant, being structural building blocks in plants and animals, respectively (P. Y. Chen et al., 2012; Xiaogang Luo et al., 2016). Furthermore, chitin can be deacetylated to become chitosan, which maintains the characteristics that can be favorable for environmental and biomedical uses (*e.g.* biocompatibility, biodegradability, non-toxicity, among others); at the same time, it increases the reactivity of the molecule, as amino functional groups are now present in the structure and have been found to have antibacterial properties in acidic conditions, which is convenient for environmental applications (Pavinatto et al., 2010; Rinaudo, 2006). Another highly used linear polysaccharide is **alginate**, which has a high water absorption capability due to the abundance of carboxyl groups; it also can be easily crosslinked to generate hydrogels and embed other active compounds in a matrix or as beads (Kuen Yong Lee & Mooney, 2012).

Branched polysaccharides provide different characteristics, as they contain a higher density of surface groups such as acetyls, hydroxyls, and carboxyls, which can be used for immobilization or for modification. However, the branches also give these polysaccharides a more challenging morphology. Of these, **hemicelluloses** and **amyloses** are the main alternatives, as they are highly abundant and have good water uptake and have a low extraction cost (Hult et al., 2002; Wittaya, 2012).

1.4.1. Cellulose

As previously mentioned, cellulose is the most abundant polymer worldwide, accounting for about 45% of dry weight of wood, around 33% of all plants, between 20 and 30% in green algae, and a byproduct of some bacteria and a few animals (Klemm et al., 2005; Xiang et al., 2016; Y. Zhao et al., 2015). Because of this abundancy and the easiness to obtain, cellulose is a referent in the generation of systems for environmental remediation, especially because of the numerous modification options that the hydroxyl groups present, involving both chemical and physical phenomena. These groups can be exploited to generate selective and self-standing approaches (Mahfoudhi & Boufi, 2017).

Cellulose is rarely found as a single molecule, as it tends to form networks or fibers that have intermolecular hydrogen bonding between the hydroxyl groups. The cellulose chains acquire a supra-structure that will further interact with the other cell components; because of this, different methods have been developed to extract and purify the fibers from natural resources. When brought to the nanoscale, cellulose has shown desirable properties for water remediation, such as a low solubility in water, a tunable surface-volume ratio, and surface charge depending on the raw material and extraction method utilized. As surface area is maximized and interfacial phenomena can occur, the more reactive and energetic points are exposed (Z.-Y. Zhou et al., 2011). Thus, the use of nanocellulose is an attractive alternative that promises more efficient adsorbents with better binding affinities (Ali, 2012; Carpenter et al., 2015).

Cellulose, without any further modification, is composed of anhydro-glucose units linked by a β-1-4 glycosidic bond (Figure 1.1). These result in a linear polymer that has 3 hydroxyl groups in the C2, C3, and C6 positions of each anhydroglucose unit. This polymer presents an isoelectric point between 2.5 and 3.7, depending on the literature source (Koon Yang Lee et al., 2011; Sookne

& Harris, 1941), and a its hydroxyl groups present dissociation constant (pKa) values between 10 and 12 for the secondary hydroxyl groups and approximately 14 for the primary group (Feng et al., 2013). The described properties make cellulose negatively charged in most media and prone to interact with molecules and ions that are suspended or diluted at the same media (Stana-Kleinschek et al., 1999).

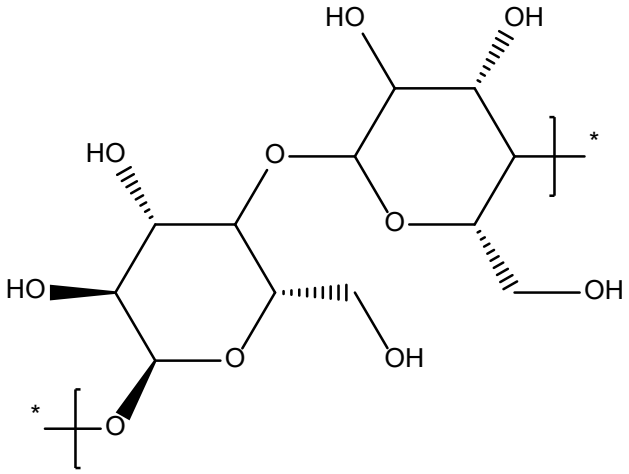

Figure 1.1. Structure of cellulose monomer

The interaction mechanisms with cellulose-derived materials depend on the solute that is to be removed from the contaminated water. In the case of ions and cationic molecules, it has been characterized that adsorption affects the pores and surfaces; the mechanisms of ion exchange, chelation and complexation, and chemisorption by coordination bonding are understood as being the most likely (Hokkanen et al., 2013; Lawrance, 2013; Olivera et al., 2016). Meanwhile, for anions or larger molecules, hydrogen bonding and electrostatic interactions with the hydroxyl groups seem to be the more likely processes (Jin et al., 2015; Olivera et al., 2016). Interestingly, it has also been studied that crystallinity has an effect on the adsorption capability of the fibers; organic molecules, such as benzophenone, tend to adsorb into amorphous regions on the fibers,

but at low concentrations, these molecules are more prone to be adsorbed onto the crystalline region (Ilharco et al., 1997).

The negative nature of the cellulose has been exploited mainly for the removal of cations, as cellulose and especially nanocellulose fibers have been shown to be able to adsorb metals such as Cd(II), Pb(II), and Ni(II) in concentrations of 9.7, 9.42, and 8.55 mg/g, respectively; this was tested in metal solutions with initial concentrations of 25 mg/L (Kardam et al, 2014). Regeneration was obtained with 0.5 M hydrochloric acid and nitric acid, this can be done for up to 3 cycles with similar adsorption outcomes (Kardam et al., 2014). Usually, this negative charge characteristics can be further enhanced by the addition of negative moieties, such as carboxylate, phosphates, and phosphoryl groups (Hokkanen et al., 2013; P. Liu et al., 2015; Olivera et al., 2016; Suopajärvi et al., 2015).

Carboxylation has proven to be one of the easiest and most used methods to raise the negative charge character of cellulosic surfaces, and by it, the adsorption of cations. Fibers that have been oxidized with 2,2,6,6-tetramethyl-1-piperidinyloxy (TEMPO) have demonstrated the capability to adsorb up to 67.2 mg/g of Cu(II) (*ca.* 43.6 mg/L), where the degree of substitution (DO) was 1.5 and the concentration was 200 mg/L (P. Liu et al., 2016). In fibers with a degree of oxidation (DO) of 0.34 at pH 6.2, the removal of Cu(II) was 135.5 mg/g, and the solution had the same initial ion concentration as the previous case (Sehaqui et al., 2014). The same type of fibers, but with a DO of 0.26, also presented adsorptions of 58 mg/g of Cr(III), 49 mg/g of Ni(II), and 66 mg/g of Zn(II) (Sehaqui et al., 2014). Similarly, fibers with a DO of 0.075 (1.4 mmol of carboxylic groups per gram) presented an adsorption capability of 167 mg/g of UO_2(II), with the side effect that this ion gelled the fibers (Ma et al., 2012).

TEMPO oxidation is not the only path to obtaining carboxylated cellulose, as nanocellulose with low crystallinity (~ 35%) and DO of 0.062 (1.15 mmol of carboxyl /g) was obtained using nitric acid and sodium nitrite for 12 h at 50 °C (Sharma, Joshi, et al., 2017). These fibers proved to be also effective to the removal of 1470 mg/g of UO_2(II) (Sharma, Chattopadhyay, et al., 2017), 2270 mg/g of Pb(II) (Sharma, Chattopadhyay, Zhan, et al., 2018), and 2550 mg/g of Cd(II) (Sharma, Chattopadhyay, Sharma, et al., 2018).

Other modifications with the same aim of increasing the negative charge density with carboxylic and carbonyl groups have also proved to be effective in the immobilization and removal of metallic ions. For example, a modification to mercerized nanocellulose fibers with succinic anhydride was able to successfully remove 231.8 mg/g of Cd(II), 120.7 mg/g of Cu(II), 105.3 mg/g of Zn(II), 78.8 mg/g of Co(II), and 43.7 mg/g of Ni(II) (Hokkanen et al., 2013). This was not as high as when only cellulose microfibers were used, which had the removal values of 153.8 mg/g for Cu(II), 249.8 mg/g for Cd(II), and 500.0 mg/g for Pb(II) (Gurgel et al., 2008). Even when the microfibrillar cellulose appears to have higher removal values, nanocellulose proved to be regenerated with high efficiency using nitric acid and sonication.

As previously mentioned, carboxylation is not the only modification available. Enzymatic phosphorylated nanocellulose adsorbed 120 mg/g of Ag(I), 114 mg/g of Cu(II), and 73 mg/g of Fe(III), this with an initial concentration of 62.5 mg/L using 0.2 g of the nanocellulose; this work also found that when used in a mixture, CNF adsorbed more Fe than Cu, with final concentrations of 109 and 59 mg/g, respectively, while Ag adsorption was kept constant (P. Liu et al., 2015). Sulfonated nanocellulose was used to eliminate Pb(II); these fibers had a DO of 0.024 (0.45 mmol sulfonic acid /g) and were able to remove efficiently 248.6 mg/g of Pb(II), which was 15x greater than CNF without the modification (Suopajärvi et al., 2015). Fibers modified with taurine also

present a sulfonate group exposed at the surface; these fibers were found to be efficient for the recovery of suspended Au(III) with a capacity calculated with Langmuir isotherms of 34.5 mg/g, which can still be adsorbed even when other ions such as Ni(II), Cr(VI), Cd(II), Co(II), and As(V) are present (Dwivedi et al., 2014). Even though the main objective of the study was not for environmental purposes, the modification approach can be oriented to it, especially as metal desorption was achieved using acidic thiourea.

Aside from adding functional groups, whole molecules can be used as the modifier moieties. Exploiting the inherent reactivity of silanes to react with hydroxyl groups, cellulose microfibers were modified with aminopropyltriethoxysilane (APS), which gave the surface of the fibers a surface positive charge, as amino groups were exposed; herein the maximum adsorption was of 160.5 mg/g for Ni(II), 200.2 mg/g for Cu(II), and 471.6 mg/g of Cd(II). These adsorption values were between 1 and 2 orders higher with the modification than with the raw microfiber, as the metals are able to coordinate with the exposed nitrogen of the amino group (Hokkanen et al., 2014). Other modifications explored for Cr(III) and Cr(VI) are with paraben and (2,3-epoxypropyl) trimethylammonium chloride, respectively. This work obtained a maximum sorption capacity of 23.9 mg of Cr(III) and 24.0 mg of Cr(VI) per g of sorbent (Jain et al., 2016). Both final modifications used an epoxy group to modify the surface hydroxyl groups, taking advantage of the non-directed reactivity of this group that can easily react with polysaccharides.

Besides epoxy groups, anhydrides can be used as reactive groups too; for instance, ethylenediaminetetraacetic acid (EDTA, PubChem CID: 6049) was used as a grafting molecule when transformed to its anhydride form in pyridine and then reacted in a cellulose paper filter to improve the capacity to remove metal ions from water solutions. In the study Ag(I), Pb(II), Cd(II), Ni(II), Zn(II), Sn(II), and Cu(II) were tested with removal efficiency between 90 and 95%. Among

all of the tested cations, adsorption of Pb and Cd ions were modeled by Langmuir isotherms showing a maximum adsorption capacity of 227.3 mg/g and 102 mg/g respectively, and 5 cycles of recyclability for Pb(II) in 0.5 M HCl, with non-apparent loss of adsorption efficiency (D'Halluin et al., 2017).

The structure of the sorbent also has proved to be an important variable in the adsorption capability of the cellulose nanofibers, as surface area will be affected by the conformations that the systems can acquire. Thus, cellulose hydrogels with TEMPO-oxidized cellulose were also found to adsorb Cu(II) with a maximum of 268.2 mg/g, which after regeneration was also used with other ions combined such as Zn(II), Fe(III), Cd(II), and Cs(I) (Isobe et al., 2013). Likewise, a nanofiber network embedded with TEMPO-oxidized cellulose nanocrystals (CNC) was used to adsorb Ag(I), Cu(II), and Fe(III), presenting capabilities of 0.023, 33, and 55 mg/g, respectively (Karim et al., 2016); the results in these two studies indicate that further modification by incrementing the structural complexity has an impact in the area exposed to retain these metal ions and other organic molecules.

Moreover, the structural modification can also be achieved when nanocomposites are generated; the grafting of other polymers, the entrapping of nanoparticles, or the boosting of an interaction due to different layers are some of the main strategies used for the formation of these materials. Grafting from polymers to cellulose fibers can be done using two approaches, "grafting from" and "grafting to" (Hatton et al., 2015). The "grafting from" approach is when a surface group is used as an anchoring point from where the monomers will generate the branches as they polymerize and elongate the chains. On the other hand, the "grafting to" approach is when the polymer is already generated and is only going to be attached to the cellulose fibers.

A “grafted from” polyaniline on cellulose was used to adsorb two model dye molecules, methyl orange ($C_{14}H_{14}N_3NaO_3S$, PubChem CID:23673835) and eosin yellow ($C_{20}H_6Br_4Na_2O_5$, PubChem CID: 11048); this system removed 20.9 and 58.1 mg/g, respectively, with maximum concentrations of 10 and 30 mg/L (Bhowmik et al., 2018). A similar method was used with poly (glycidyl methacrylate) (GMA) and copolymerized with acrylic acid, acrylamide, or acrylonitrile; these different modified celluloses were characterized and used to remove Fe(II), Cu(II), and Cr(VI). To further understand the effects of the functional groups added to the cellulose, the polymers were partially hydrolyzed with 0.5 N NaOH for 48 h at room temperature. All systems were tested in a solution containing 0.1 g of polymer in 20 mL of solution containing 20 mg of metal salt per liter; the best performance for Cr(VI) before hydrolysis was of 24.6% removal from the cellulose grafted with glycidyl methacrylate and acrylamide and co-grafted with acrylonitrile, which after hydrolysis removed 16.4%. For Cu(II), the best uptake was by the co-grafted with acrylic acid, removing 22.8 and 68.9% before and after hydrolysis, respectively. Finally, for Fe(II) before hydrolysis the best one was the cellulose-g-poly (glycidyl methacrylate), which removed 51.9% of the metal content in the solution, but after hydrolysis, this underperformed, removing only 74.6%, while the co-grafted polymers with acrylamide and acrylic acid removed 100% (G. S. Chauhan et al., 2005).

Polymers also were synthetized on okra cellulose fibers; the system was an aminoxide version of poly(acrylonitrile-co-methacrylic acid) and was evaluated under different pH ranges, which influenced the adsorption capacity. The best performance for Cu(II) was at pH 5.5 with a maximum of 76.8 mg/g; at the same pH, this system removed 268.3 mg/g of Pb(II). For Cd(II) at pH 6, the adsorption was of 141.7 mg/g, and for Zn(II) the maximum was of 62.9 mg/g at pH 6.5 (Singha & Guleria, 2014). Poly(methacrylic acid-co-maleic acid) fibers were grafted from a CNF

aerogel using Fenton's reagent; these branches decreased the specific surface area from 85 to 65 m^2/g but increased the carboxyl content from 0.54 to 7.5 mmol/g. All experiments were done at a constant pH of 5, which allowed for the study of only the effects of the COO^- concentration. Therefore, this high negative surface charge was used to efficiently remove up to 95% of Pb(II), Cd(II), Zn(II), and Ni(II) when the solution had concentrations lower than 10 ppm (mg/L) and ranging from 90 to 60 % with higher concentrations, obtaining a maximum of 165.8, 134.9, 136.0, and 115.6 mg/g for Pb(II), Cd(II), Zn(II), and Ni(II), respectively. Regeneration of the material was possible with 1 mM EDTA solution pH 5 (Maatar & Boufi, 2015). This last work also demonstrated that the initial ionic strength (KCl) of the media has an effect on the adsorption capability of the different metals; the higher the salt concentration, the lower the adsorption capacity of the aerogel to adsorb the metals through coordination with exposed oxygen atoms of the side chains.

As for the "grafted to," TEMPO-oxidized cotton nanofibers (TOCNF) were used to generate an aerogel with branched polyethyleneimine (bPEI) in a ratio 1:2; the resulting sponge was used to serve as an adsorbent for some organic pollutants (p-nitrophenol, 2,4,5-trichlorophenol, and amoxicillin) and some metals (Cu, Co, Ni, and Cd). When a Langmuir isotherm was evaluated, the adsorption capability observed for the organic pollutants in a solution with initial concentrations of ranging from 0.1 and 50 mM was determined to be 1630, 205 and 556 mg/g, for p-nitrophenol, 2,4,5-trichlorophenol, and amoxicillin, respectively. Meanwhile for metals, the maximum absorption with an initial concentration of 0.1M was of 89.0, 57.2, 155.1, and 64.6 mg/g for Cu(II), Co(II), Cd(II), and Ni(II). When the four metals were mixed together, the Cu(II) was the most compatible with the gel, as it removed around 69.9 mg/g and only 8.8, 36.0, and 8.8 mg/g of Co(II), Cd(II) and Ni(II), respectively (Melone et al., 2015). A similar system

was also tested for Cu(II) and Pb(II), but herein the nanofibers were from bleached softwood, and a ratio of 1:1 was selected. With the Langmuir model of an initial concentration of 3 mM, it was found that the maximum adsorption was of 175.4 and 357.1 mg/g (Jian Li et al., 2018). When compared, the 2:1 ratio adsorbed 89.0 mg/g of Cu(II), while the 1:1 captured 175.4 mg/g; this could be due to the difference of the origin of the CNF or from the concentrations of the initial solution, even though, these systems showed a non-specific selection, which provides versatility in the application possibilities.

The versatility and efficiency of these grafting processes can provide highly engineered material, with exciting designs and high selectivity in its performance; for example, an electrospun polyacrylonitrile scaffold was infused with ultrafine cellulose fibers, which were TEMPO oxidized and crosslinked to the scaffold through a carbodiimide reaction. This membrane was able to retain bacteria including *E. coli* and even viruses (MS2), improving the applications in the water treatment field (Sato et al., 2011). Another engineered grafted system for water treatment was generated with polyhedral oligomeric silsesquioxanes bearing multi-*N*-methylol groups (R-POSS) grafted to cellulose using citric acid and $MgCl_2$ as linker and catalyst, respectively (Xie et al., 2010). This system proved to be effective in the removal of the reactive dyes Yellow B-4RFN and Blue B-RN. The removal was dependent upon the temperature; the higher it was, the less dye was adsorbed. Maximum capture for both was at 293 K with 16.6 and 14.4 mg/g, respectively (Xie et al., 2011).

As cellulose in the nanoscale enhances the surface area and availably of negative moieties, other nanoparticles have catalytic activities or a strong affinity to molecules that can be used in parallel for water treatment (Adeleye et al., 2016; Shrivastava, 2010; Tyagi et al., 2012); when these nanoparticles are used as a composite with cellulose, the specific properties of both materials

can be used in an additive way to obtain a better performance than when used alone. For example, hydroxyapatite is known to have an affinity for fluoride, which is a WHO regulated compound; because of it, a cellulose nanocomposite was developed with cotton fibers where hydroxyapatite was grown at the surface. When the material was immersed in a solution with 10 mg of F^- /L, the removal capacity reached a Langmuir maximum capacity of 4.2 mg/g, which is higher than the nano-hydroxyapatite *per se* (1.457 and 0.489 mg/g) and did not show any decrease in adsorption when other anions (NO_{3-}, SO_4^{2-}, and PO_4^{3-}) were present (Yu et al., 2013). A similar study was performed, but herein the fibers were from bleached birch, and the aim was the removal of Cr(VI); the adsorption at 25 °C was of 2.21 mg/g. Interestingly, this system appeared to have a buffering effect in the solutions, so there was no impact from the pH to the removal capacity, but temperature seemed to have a positive relationship; this means that at a higher temperature a higher adsorption was obtained (Hokkanen et al., 2016).

Metallic nanoparticles, such as titanium dioxide, also have been used to develop photocatalytic nanocomposites with cellulose nanofibers. In one study that explains this, *Eucalyptus* TEMPO oxidized nanofibers were decorated with titanium dioxide particles to degrade a model organic molecule solution (0.01 g/L of methylene blue, $C_{16}H_{18}ClN_3S$, PubChem CID: 6099); simultaneously, two films were also decorated with Au and Ag nanoparticles above the preexisting titanium ones. The base film was able to degrade 60% of the methylene blue in the solution, while both Au and Ag charged specimens degraded 75%. As reusability is desired, mechanical tests were performed after each cycle, where the Ag-TiO_2-CNF composite outperformed the others (Snyder et al., 2013). Another study was done on carboxymethyl cellulose (CMC) coated with zero-valent iron particles for the removal of trichloroethylene; herein, from a 10 mg/L solution, this system was able to extract only 9.7%, which is not the best performance but

demonstrated the concept that this modified cellulose could be used for composites with metallic particles (Han et al., 2016). CMC was also used with hydroxyethyl cellulose as a citrate cross-linked hydrogel carrying potassium copper hexacyanoferrate; this system was generated to selectively capture cesium in seawater. From a solution with 19.9 mg/L of Cs^{+}, 12.4 g/L of Na^{+}, 2.3 g/L of Mg^{2+}, 469.1 mg/L of K^{+}, and 148.3 mg/L of Ca^{2+}, the hydrogel was able to remove 90.1% of Cs (*ca*. 265.8 mg/g) in only 1 h (Y. Kim et al., 2017).

The use of ceramic and metallic particles is non-exclusive, as demonstrated by the use of a cellulose composite with magnetite that entrapped acid activated bentonite for the removal of Pb(II). This composite was evaluated at a range of 60 to 160 mg/L and at 298, 303, and 313 K; the Langmuir maximum capacity of the material was 2.86 mg/g at 298 K (Xiaogang Luo et al., 2016). Herein, the purpose of each component was different, as bentonite was the one targeting Pb(II), cellulose was the matrix, and the function of magnetite was to allow the separation and recovery of the material. The use of these specific properties creates the possibility of solving different limitations that water remediation systems present nowadays.

As previously mentioned, non-reactive interactions between cellulose and other materials can also provide composites with valuable properties. For example, a diaminobutane base poly(propyleneimine) dendrimer carrying 16 thiol groups was embedded in cellulose and used to reduce the permeability of metals from a 1 mmol solution of Cd(II), Hg(II), and Pb(II) at about 20% for the Cd(II) and 45% for the two latter mentioned (Algarra et al., 2014). Furthermore, an already modified cellulose can be used to generate the composites; hence, complex systems are obtained. For instance, a cystine grafted nanocellulose was embedded in an electrospun polyacrylonitrile, where the large resulting area and high surface thiol groups of the cysteine

(109 mg/g) were used to adsorb Cr(VI) and Pb(II) with a removal capacity of 87.5 and 137.7 mg/g, respectively (R. Yang et al., 2014).

The use of these complex structures when the conforming materials are from different chemical natures can generate composites that are not selective adsorbents, but which have a hierarchical structure that gives them the potential to perform phase separations, extraction of oils, or the adsorbance of organic molecules with low solubility and hydrophobic domains. For example, a designed layered double hydroxide (LDH) composite based on alumina modified cotton cellulose fibers (Tao Zhang et al., 2014) was used as a template for an auto-assembled superhydrophobic-superoleophilic membrane with steric acid being deposited to the surface; this system proved to have a separation efficiency above 95% with various oil/water mixtures regardless of the mass ratio and was reused for up to 10 cycles (Yue et al., 2017). The same aim was accomplished by drop-casting steric acid and graphite flakes onto a cellulose 3-D scaffold (stabilized with polyethylene and polypropylene); the drop-casted materials provided a non-selective cellulose with a hydrophobic nature that allowed the adsorption of oils and organic solvents without an intake of water. The adsorption capacity of these sponges was reduced to 60% at the third cycle; but this level of uptake was fairly constant for 11 more cycles, in all tested oils (Calcagnile et al., 2017).

The numerous systems mentioned above demonstrate the use of cellulose for generation systems with environmental targeted applications, such as organic molecule removal, or more general, such as oil/water separation. The main advantage of cellulose is its high availability and the wide range of specific properties to select from, such as degree of crystallinity, aspect ratio, surface charge, among others, which makes the design of the systems as broad as the imagination can get.

Table 1.1. Cellulose-derived Materials and Pollutants Adsorbed

Material	DS	Pollutant	Capacity [mg/g]	Regeneration	Reference
Nanocellulose fibrils		Cd (II)	9.7	0.5 M HCl/ 0.5 M HNO_3	Kardam *et al.* 2014
		Pb (II)	9.42		
		Ni (II)	8.55		
TEMPO-oxidized fibers	1.5	Cu(II)	67.2		Liu *et al*. 2016
	0.34	Cu(II)	135.5		Sehaqui *et al*. 2014
	0.26	Cr(III)	58		
		Ni (II)	49		
		Zn(II)	66		
	0.075	UO_2 (II)	167		Ma *et al*. 2012
Carboxylated fibrils	0.062	UO_2 (II)	1470		Sharma *et al*. 2017a
		Pb (II)	2270		Sharma *et al*. 2018b
		Cd (II)	2550		Sharma *et al*. 2018a
Nanocellulose with succinic anhydride		Cd (II)	231.79		Hokkanen *et al.* 2013
		Cu (II)	120.73		
		Zn (II)	105.26		
		Co (II)	78.85		
		Ni (II)	43.67		
Cellulose microfibers with succinic anhydride		Cu (II)	153.84		Gurgel *et al*. 2008
		Cd (II)	249.77		
		Pb (II)	499.97		
Phosphorylated nanocellulose		Ag (I)	120		Liu *et al.* 2015
		Fe (III)	73		
		Cu (II)	114		
		Fe (III)/Cu (II)	109/59		
Sulfonated nanocellulose	0.024	Pb (II)	248.64		Suopajärvi *et al.* 2015
		Au (III)	34.5	Acidic thiourea	Dwivedi *et al*. 2014
APTS modified microfibers		Ni (II)	160.47		Hokkanen *et al.* 2014
		Cu (II)	200.17		
		Cd (II)	471.56		
(2,3-epoxypropyl) trimethylamm		Cr(III)	23.92		Jain *et al.* 2016
		Cr (VI)	23.99		

onium modified fibers					
EDTA modified microfibers		Pb (II)	227.3	0.5 M HCl	D'Halluin *et al.* 2017
		Cd (II)	102		
TEMPO-oxidized nanocellulose hydrogel		Cu (II)	268.2		Isobe *et al.* 2013
Nanocellulose hydrogel with TEMPO-oxidized CNC		Ag (I)	0.023		Karim *et al.* 2016
		Cu (II)	33		
		Fe (III)	55		
Cellulose-g-polyaniline		Methyl orange	20.87		Bhowmik *et al.* 2018
		Eosin yellow	58.14		
Cellulose-g-poly(acrylonitrile-co-methacrylic acid)		Cu(II)	76.82		Singha *et al.* 2014
		Pb (II)	268.32		
		Cd (II)	141.73		
		Zn (II)	62.89		
Cellulose nanofibrils-g-poly(methacrylic acid-co-maleic acid)		Pb (II)	165.76	1 mM EDTA solution pH 5	Maatar *et al.* 2015
		Cd (II)	134.89		
		Zn (II)	135.99		
		Ni (II)	115.62		
TEMPO oxidized cotton nanofibers with polyethyleneimine (1:2)		p-nitrophenol	1630		Melone *et al.* 2015
		2,4,5-trichlorophenol	205		
		amoxicillin	556		
		Cu (II)	88.96		
		Co (II)	57.16		
		Cd (II)	155.13		
		Ni (II)	64.56		
		Cu(II)/Co(II)/Cd(II)/Ni(II)	69.90/8.84/35.97/8.8		
TEMPO oxidized bleach softwood nanofibers with polyethyleneimine (1:1)		Cu (II)	175.44		Li *et al.* 2018
		Pb (II)	357.14		

R-POSS grafted to nanocellulose		Yellow B-4RFN	16.61		Xie *et al.* 2011
		Blue B-RN	14.4		
Cotton fiber with hydroxyapatite		F-	4.2		Yu *et al.* 2013
Cotton fiber with nanohydroxyapatite		F-	1.45		
Bleached birch fibers with hydroxyapatite		Cr (VI)	2.208		Hokkanen *et al*. 2016
CMC/hydroxyethyl cellulose with potassium copper hexacyanoferrate		Ce (I)	265.8		Kim *et al.* 2017
Cellulose with magnetite and bentonite		Pb (II)	2.86		Luo *et al.* 2016
Cysteine-g-nanocellulose embedded in electrospun polyacrylonitrile		Cr (VI)	87.5		Yang *et al*. 2014
		Pb (II)	137.7		

1.4.2. Chitin

Chitin, as cellulose, is a linear polymer that is a widely available structural polymer and is considered the second most abundant natural polysaccharide on earth. Chitin is composed of β(1 → 4) 2-acetamido-2-deoxy-β-D-glucose (Fig. 1.2); therefore, the structure is akin to that of cellulose, except that it has acetamide functional groups at the carbon 2 position (Kumar Dutta et al., 2004). Even though the backbone is structurally alike, properties of both differ importantly;

chitin is highly hydrophobic and insoluble in water and most organic solvents, therefore stable at natural environment. Also chitin is prone to interact with calcium and proteins, which can also be easily removed when necessary for reuse (Syahmani et al., 2018).

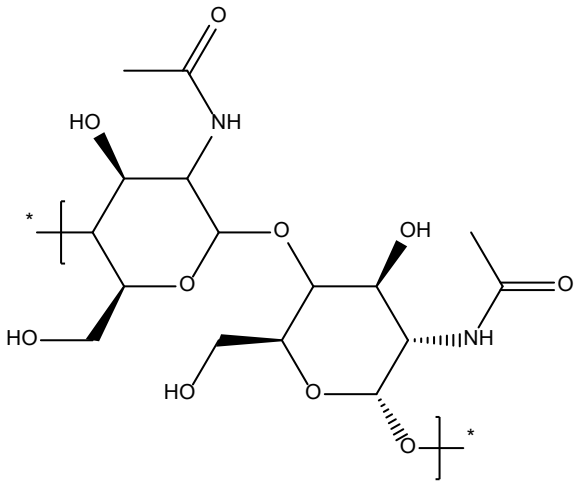

Figure 1.2. Structure of chitin monomer

The acetyl amine groups allow the formation of hydrogen bonds and allows the chitin to serve as an excellent base material to design and develop water treatment systems. This capacity was shown when black water -waste water from toilets- carrying Fe and Mn flowed through a column filled with newly extracted chitin from shrimp shell waste. The original water sample contained 10.34 and 0.20 mg/L, Fe and Mn, respectively, 210 mg/L of organic matter, and was dark brown colored with a pH of 3.88. After flowing through 25 cm of the column, 86.7% and 91.8% of the two metals, and 98.7% of the organic matter were removed from the solution, leaving a final stream with a pH 6.5 and a colorless flow (Syahmani et al., 2018). This simple experiment confirms the capacity of the chitin for entrapping metals and organic molecules, which also proved to be reversible in the case of metals when using a nitrite acid 0.5 M, providing the chance for reuse of the system. Moreover, chitin has proven to be even a better adsorbent than cellulose (cellulose Iα, Iβ, and cellulose triacetate) to eliminate insensitive munitions compounds such as

2,4-dinitroanosole (DNAN), 3-nitro-1,2.4-triazol-5-one (NTO), nitroguanidine (NQ), and 1,1-diamono-2,2-dinitroethene (FOX7), due to the stronger interaction and lower energies required for the compounds to interact with the resulting composite surface (Todde et al., 2018).

Compared to the other polysaccharides, chitin presents facility to obtain derivatives with surface group modifications; the most common reaction for chitin is deacetylation to obtain chitosan, but this will be addressed in its own following section. Meanwhile, other modifications, such as the addition of new groups or oxidation of the acetylamine (like carboxylic groups via TEMPO oxidation) can also be utilized to obtain functional materials. TEMPO oxidation demonstrated that, when performed before fibrillation, the surface area can be increased by about 25% compared with untreated chitosan nanofibrils (ChNF) and reduce the mean diameter of the fibers (Saito & Isogai, 2004). When these two fibers were tested against CNF and TOCNF in Cu(II) adsorption at pH 6.2, TOCNF had the best performance with a removal of 135 mg/g; TOChNF removed 55 mg/g, ChNF 27 mg/g, and CNF 13 mg/g (Sehaqui et al., 2014). This last experiment showed how TEMPO-oxidation of the fibers enhances the adsorption capacity of both systems. The main difference is that the degree of oxidation of the TOChNF was not reported, while for TOCNF it was 0.34; this has an impact on the surface charge content (SCC) and, therefore, in the adsorption capacity. For example, CNF has a SCC of 0.1 mmol/g, and ChNF has 0.88 mmol/g, so a higher adsorption is expected of the ChNF. Another modification that was demonstrated was to thiol-functionalize (*ca.* 1.1 mmol/g) ChNF with cysteine via NHS/EDS coupling. From a range of 4 to 11 in pH and concentrations of 10 to 100 ppm of As(III), this system had the best capturing performance at a pH 7, having a calculated maximum adsorption of 149 mg/g (R. Yang et al., 2015).

As surface area is fundamental for adsorption capacity, methodologies to increase it have been developed; the most commonly reported are the mechanical treatments such as fibrillation by grinding (D. Liu et al., 2013; Oh et al., 2015), crystal generation (Y. Fan et al., 2009; J. Jiang et al., 2018), micro-structuration of particles (Gotoh et al., 2004; Yuntao Wang, Li, et al., 2015), and ultrasonication (Dotto et al., 2015).

The latter approach was shown to adsorb methylene blue when supported on a sand bed (5 g of ultrasonicated chitin and 180 g of sand); herein a MB solution with 50 mg/L flowed at a rate of 10 mL/min for 370 min through a column with 2.5 cm of internal diameter and 25 cm height. This system presented a maximum adsorption capacity of 51.8 mg/g, which represents 51.5% of removal and maintained this performance for up to 5 cycles after washings with 300 mM HCl solutions (Dotto et al., 2015).

When comparing chitin microparticles (ChMP) with nanofibers (ChNF) regarding their capacity to eliminate different metals such as Cd(II), Ni(II), Cu(II), Zn(II), Pb(II), and Cr(III), it was found that the nanomaterial was able to adsorb between 5 to 6 times more ions per gram of adsorbent and with less time to reach the saturation capacity (approximately 10 min for 80% of saturation). ChMP removed 59.4, 42.6, 23.4, 38.4, 198.2, and 6.4 mg/g respectively; while with ChNF, the maximum adsorption capacity was of 330.2, 134.7, 141.1, 134.0, 303.5, and 16.3 mg/g of Cd(II), Ni(II), Cu(II), Zn(II), Pb(II), and Cr(III), respectively (D. Liu et al., 2013).

Chitin microspheres were used as templates for immobilization of α-amylose to generate catalytic composites with Au and magnetic composites modified with Reactive Black 5 ($C_{26}H_{21}N_5Na_4O_{19}S_6$, PubChem CID: 5360531) to adsorb methylene blue (Yuntao Wang, Li, et al., 2015). Herein, it was demonstrated that 2 g of the microspheres were able to eliminate all color in a 10 mg/L solution, and when the initial concentration was of 80 mg/L, the system presented a

maximum adsorption capability of 46 mg/g. Similarly, a chitin microsphere-clay composite was used to capture methylene blue, with a maximum capacity of 156.7 mg/g estimated with a Langmuir isotherm, when using an aqueous solution of 10 mg/mL in 20 min, with a small decrease in removal efficiency of 1% after 5 cycles with desorption through 1 M NaOH aqueous solutions (R. Xu et al., 2018).

A composite with bentonite was studied for Cr(VI) adsorption at varying pH to find the optimal conditions. The results showed that the maximum adsorption occurred at pH 4 and declined while pH increased, except that beyond pH 9 the Cr(VI) became insoluble, precluding the adsorption; herein it was also found that when concentrations of sorbent exceeded 1 g/ 100 mL of ion solution, the adsorption capacity decreased. After the Langmuir isotherm (from 5 to 1000 mg/L) was generated, the maximum adsorption capacity was found to be of 443.7 mg/g (Saravanan et al., 2013).

Chitin-derived structures can also be used for photocatalytic systems, to not only capture but also to degrade the organic pollutants in water sources. For example, Cu_2O nanoparticles were synthetized on the surface of a regenerated chitin/graphene oxide film; this was tested for 3 h to degrade methyl orange. The best performance was when 4.5 g of chitin had 80 mg of graphene oxide and nanoparticles were obtained from a solution of 0.2 mol/L; this system was tested with concentrations of 10, 25, and 50 mg/L, reaching a removal of 92.1%, 72.3%, and 48.3%, respectively and degradation rates of 7.6, 15.6, and 20.1 mg/g h (Yuntao Wang, Pei, et al., 2015). Another catalytic system was inspired by the tunicate tunichrome that selectively captures metals from water. To mimic it, ChNF that were homogenized by a high-performance grinder was used, and as a side effect of this treatment, fiber loss was approximately 11.2% of its surface acetyl groups. Then, the hydroxyl groups on the surface of these fibers were subjected to chemical

reactions with maleic acid; the aim was to capture Au(III), and while doing so, to generate gold nanostructures on the surface of the fibers that were used as catalyst to degrade 4-nitrophenol. The maximum adsorption capacity of gold on the system was of 532.5 mg/g and with it, 0.5 mg/g*h of the organic compound was degraded (Dwivedi et al., 2017).

Elsewhere, a polyurethane matrix was imbedded with chitin (*ca.* 99% and *ca.* 79% of acetylation), a polymeric amine as an additive, and two different catalysts, one being a hydroxyl substituted amine, while the second being a tertiary amine. All the combinations were used as an optimization platform for fluoride removal from a 15 mg/L solution for 72 h. The results showed that the best composition was 60% chitin (*ca*. 79%), 40% polymer, 2% of the catalyst with the tertiary amine, and no additive; this system was able to adsorb 0.29 mg/g at a pH of 5 (Davila-Rodriguez et al., 2009). A similar system, 53% chitin, 47% polymer, and 2% catalyst, was packed in columns and tested with natural waters containing carbonites, chloride, fluoride, sulfates, and organics for the same fluoride concentration of 5.1 mg/L. These tests resulted in an efficiency of about 85%, with 50 bed volumes treated in 20 min, and the system was regenerated with only 4 bed volumes of 0.1 M sodium hydroxide (Davila-Rodriguez et al., 2012).

Not only have chitin fibers been used by themselves, but also with nanocrystals (ChNC), which are usually referred to as nanowhiskers. ChNC have been used to develop composite fibers by electrospinning. One example is an electrospun membrane with polyvinylidene fluoride (PVDF) as a matrix carrying the ChNC, which was used to adsorb indigo carmine ($C_{16}H_8N_2Na_2O_8S_2$, PubChem CID: 5284351). This system had a maximum adsorption capability of 72.6 mg/g and a removal efficiency of 88.9% within 4 h of contact (Gopi et al., 2017). A less specific system was developed to separate oil-in-water emulsion by generating a super-hydrophilic membrane using ChNC in a matrix of N, N-isopropylacrylamide (NIPAAm) copolymerized with

methylolacrylamide (NMA). The test sample was made by adding 30 mL of toluene to 970 mL of deionized water with 10 mg of polysorbate 80 (Tween-80, $C_{32}H_{60}O_{10}$, PubChem CID: 5281955) and flowed through the membrane with a driving pressure of 0.3 bar. Here, the fibers containing 10% of ChNC proved to be structurally stable under different pH conditions and salinity (2 M NaCl) with a removal of about 99% for up to 15 cycles in all of these treatments (J. X. Wu et al., 2018).

Therefore, the use of chitin in water treatment systems seems to be an easy approach for pollutant removal, as it also has low cost, is easy to obtain, and has the advantage of the characteristic moiety that allows for an easier modification approach. The system can be exploited to both main approaches, adsorption or to generate composites with higher specificity.

Table.1.2. Chitin- derived materials and pollutants adsorbed

Material	Pollutant	Capacity [mg/g]	Regeneration	Reference
Chitin nanofibrils	Cu(II)	27		Sehaqui *et al.* 2014
TEMPO chitin nanofibrils		55		
Chitin nanofibrils with cysteine	As(III)	149		Yang *et al.* 2015
Ultrasonicated chitin	Methylene Blue	51.8	300 mM HCl	Dotto *et al*. 2015
Chitin microparticles	Cd(II)	59.42		Liu *et al*. 2013
	Ni(II)	42.62		
	Cu(II)	23.45		
	Zn(II)	38.36		
	Pb(II)	198.19		
	Cr(III)	6.4		
Chitosan nanofibrils	Cd(II)	330.15		
	Ni(II)	134.72		
	Cu(II)	141.08		
	Zn(II)	134.03		
	Pb(II)	303.49		
	Cr(III)	16.28		

Chitin microspheres with Au, magnetic particles and Reactive Black 5	Methylene Blue	46		Wang *et al.* 2015a
Chitin/clay microsphere	Methylene Blue	156.7	1 M NaOH	Xu *et al*. 2018
Chitin-bentonite composite	Cr(VI)	443.71		Saravanan *et al*. 2013
Chitin nanofibrils with maleic acid	Au(III)	532.5		Dwivedi *et al*. 2017
Polyurethane/chitin and tertiary amine	F-	0.29		Davila-Rodriguez *et al.* 2009
polyvinylidene electrospun with chitin nanocrystals	Indigo carmine	72.6		Gopi *et al.* 2017

1.4.3. Chitosan

Chitosan is the main derivative of chitin; it is obtained through the hydration of the amide moiety by concentrated NaOH and heat (40% at 120 °C for 1-3 h) or through enzymatic hydrolysis with chitin deacetylase (Shukla et al., 2013). This derivative is more often used in bio-applications than chitin due to its better solubility in water and in organic acids; this property is caused by the basic nature of this polysaccharide, which contrasts with the natural acidic nature of most other polysaccharides (Kumar Dutta et al., 2004).

Because of the deacetylation, chitosan is defined as a copolymer of β-(1→4) linked D-glucosamine and N-acetyl-D-glucosamine (Fig. 1.3). The main difference between chitin and chitosan lies in the number of glucosamine groups, or the degree of deacetylation (DD). The latter, as well as the molecular weight, purity and polymorphous structure are usually reported as important parameters that will define the properties of the consequent materials, such as viscosity, polyelectrolyte behavior, metal chelation, polyoxysalt formation, optical properties, and film formation (Kumar Dutta et al., 2004; Struszczyk, 2002). Depending on the DD, the pK_a also varies, but it is usually close to 7. When the DD is in a range of 70 to 80% the reported pK_a value is

approximately 6.5, which leads to a majority of deprotonated groups when the pH is above this value, challenging the interactions with other systems above this value (Orelma et al., 2012). Additionally, chitosan, as well as other polysaccharides with (1 → 4)-β-D linked glucans, have been found to adhere irreversibly to cellulose and between them, being an useful property to generate composites with low energy consumption (Mishima et al., 1998; Orelma et al., 2011).

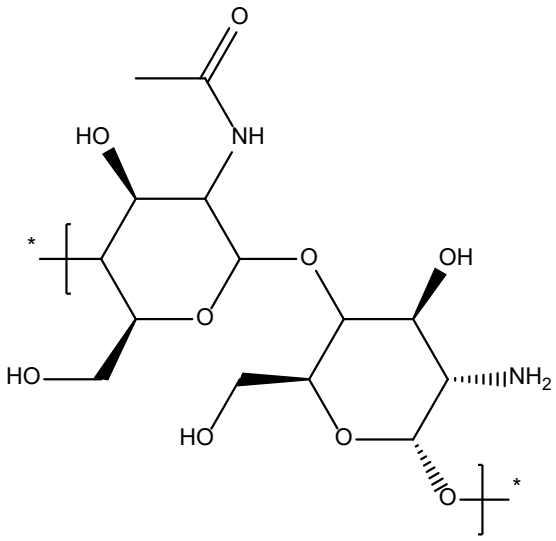

Figure 1.3. Structure of chitosan monomers

The importance for water treatment of the molecular weight DD, and viscosity is clearly shown by the work from the group of Lopez Maldonado and coworkers (Meraz et al., 2016), where two different chitosan products were compared to flocculate organic compounds suspended in waste water from the maize industry (nejayote). The first chitosan had high molecular weight, 85% of DD and dynamic viscosity of 2.35 Pa/s, while the second one had low molecular weight, 95% of DD and a viscosity of 0.39 Pa/s. The sample wastewater was pretreated by centrifugation (3500 rpm for 5 min) in order to remove the non-colloidal particles. The final total organic carbon was 9836 mg/L, and the initial ζ was -6.62 mV. It was later mixed with 10, 15, 20, 25, 30, and 50

mg of the chitosan solutions (from a stock of 1% w/w using acetic acid 1% v/v), stirred for 1 min at 800 rpm, followed by 5 min at 200 rpm, and characterized by ζ-potential measurements. Results showed a high dependency of pH, having the best performance at 5.5, with 80% of turbidity removal with only 2.35 g of chitosan of low molecular weight (MW) and 2.9 g of chitosan with high MW (Meraz et al., 2016). The paper shows how even the same material, without further modification can have an impact on the removal of contaminants and final applications and how easily chitosan can be used to adjust wastewater to meet regulations with simple measurement techniques.

Even though chitosan has been shown to be a good adsorbent material because of the surface charge provided by the acetyl amine and amine functional groups in the backbone, its interactions are not specific; for this, further modification can be done to add moieties or structures that add as selective attractors to the pollutants. For example, carboxymethyl groups were grafted to the surface of chitosan beads to make them selective to Cu(II) when a blend of Pb(II) and Mg(II) was also present; herein, the effects of pH, temperature, and adsorption equilibrium were studied. For the first part, the pH ranged from 1 to 5 with a constant concentration of 6 mmol/L; the best adsorption was found at a pH of 5. The temperature and equilibrium were therefore studied at this condition. The concentration for the equilibrium was variated from 40 to 450 mg/L, and the temperatures studied were 10, 21, 30, and 40 °C. The carboxylic groups had a higher preference for the Cu(II) ions over the other two metals and proved to be independent from the temperature. In all cases the maximum Langmuir adsorption calculated was of 130 mg/g for the modified chitosan, which was almost 2.5x greater than in pristine chitosan beads. When cycles of regeneration were performed using 0.1 M HCl, the system showed the same removal for 6 cycles without significant recovery lost; additionally, it was found that once the Cu(II) was adsorbed, the

system was able to uptake 58 mg/g of phosphates, which would not happen without the metal (Yan et al., 2011).

A similar study was performed, but with a chitosan crosslinked covalently by epichlorohydrin and ionicly by triphosphate (CTS-ECH-TPP) and adsorbing Cu(II), Cd(II) and Pb(II); it was also studied how many protons were titratable. The optimal adsorption pH was found to be of 5 for Pb(II), 6 for Cu(II), and 7 for Cd(II) with a maximum adsorption capability of 166.9, 130.7, and 83.8 mg/g, respectively, as calculated by Langmuir isotherms. In parallel fashion, 0.1 M nitric and hydrochloric acids proved to be the best eluents for the system for recycling the system with around 90% desorption (Laus et al., 2010).

This ionic crosslinking was also used to provide structure to chitosan microspheres that were later dried (80% of final porosity) and used for the separation of an oil/water solution in a packing column (7.8 mm * 200 mm). This material was able to reduce by 90% (180 ppm) the average oil concentration with a flow of 3 mL/min and 7 mL/min, keeping its shape and with minimum porosity lost (final of 78%) after treating up to 50 L and 28 L for each flow, respectively (Grem et al., 2013).

As iron is the fourth most abundant material in the earth's crust and is non-toxic, cheap, easy to reduce and process, and has a redox potential of -0.44 V by which its reactivity with other metals is enhanced, it is widely proposed for composites that will be facilitating the removal of metals and other pollutants from water sources (Fu et al., 2014). When used in oxide form, the resulting nanoparticles also have a low toxicity, are easy to manipulate and modify, and especially, present super-paramagnetism, which can be used to recover and extract materials and sorbents from water solutions (P. Xu et al., 2012). Because of this and its easy interaction with chitosan by

the simple dipping process, iron in different forms has been widely used in composites with this material.

One example of the use of iron for water treatment is the comparison of chitosan iron coated flakes and iron-doped-glutaraldehyde-crosslinked chitosan granules for the removal of As(II) and As(V) from groundwater; experiments were performed using 0.1 g in 20 mL of solution pH 7 at 25 °C for 4 h, with As concentrations from 1 to 10 mg/L. Langmuir isotherms presented a maximum adsorption capacity of 2.32 and 2.24 mg/g of As(III) and As(V), respectively, for the granules, and 16.15 and 22.47 mg/g for the flakes. Both systems showed little interference from common anions (sulfate, phosphate, and silicates) present in the solutions, and they were able to be reused after regeneration with 0.1 M NaOH, for at least two cycles in a column reactor approach (Gupta et al., 2009).

Another type of iron used for As removal is a Fe-Mn binary oxide that was impregnated to chitosan beads; sorption isotherms were made using 1 g/L of the system at pH 7 and varying As concentrations from 5 to 60 mg/L with a contact time of 36 h on an orbital shaker at 180 rpm and 25°C. The pH influence was evaluated in the range of 5.5 to 11.5 with 50 mg of sorbent in a solution with 10 mg/L of As, while competitivity of other ions (SO_4^{2-}, HCO_3^-, SiO_3^{2-}, HPO_4^{2-}, Ca^{2+}, Mg^{2+}) was tested in a 10 mg/L As concentration using 1 g/L of sorbent and a fixed pH of 7, all with the same contact time. The Langmuir maximum adsorption capacity was 39.1 mg/g for As(V) and 54.2 mg/g for As(III); adsorption efficiency decreased as the pH increased, but pH showed no significant impact from a range of 6 to 8 for As(V) and from 6 to 9 for As(III). For the ion's competition, SO_4^{2-} did not present a significant effect, a slight inhibition was present with HCO_3^- and SiO_3^{2-}, and a significant decrease was consequent with the presence of HPO_4^{2-}. On the contrary, cations seemed to have a small enhancing effect on the adsorption. This system was also

evaluated for reusability with 0.5 M NaOH; herein, efficiency dropped to 85 and 83% for As(III) and As(V), respectively, after the forth regeneration; however, the system showed good mechanical stability with no apparent crushing or mass loss (Qi et al., 2015).

For magnetic iron nanoparticles, more work is allowed, as the magnetic properties provide an extra push, and a more convenient recovery can be performed. For example, a spun hollow chitosan fiber was used as a scaffold to generate magnetic iron oxide (Fe_3O_4) nanoparticles (FeONP), which were then tested to adsorb Se(IV). In this work, to determine which variables were the more influential on the adsorption kinetics, a second order polynomial model was generated, and an Analysis of Variance (ANOVA) test was performed; the obtained results showed that only pH and sorbent concentration had a large effect on the experimental adsorption capacity of the Se(IV), which in optimum conditions (291.36 µg/L of Se(IV) diluted, 92.97 mg/L of fibers, 3.67 pH, and 109.22 min of contact) was of 1.34 mg/g. When a Langmuir equilibrium model was generated, the maximum adsorption capacity was 15.6 mg/g. Finally, the presence of other recurring ions was tested at optimum conditions to see whether they have a negative effect on adsorption when concentrations of 1 to 10 mM were added to the solution; chloride and nitrates had no significant effect on the adsorption, but phosphate and bicarbonate did significantly reduce the capacity of the material for removal (Seyed Dorraji et al., 2017).

A more complex structure was obtained when using the chelating agents: ethylenediaminetetraacetic acid (EDTA) or diethylenetriaminepentaacetic acid (DTPA, $C_{14}H_{19}N_3O_8$ PubChem CID: 100825), to crosslink and functionalize magnetic chitosan, and to then remove Cd(II), Pb(II), Co(II), and Ni(II) from wastewater with an adjusted pH of 3.5, using 2 g/L of the sorbents and a contact time of 16 h. Herein, the maximum adsorption capacity for the systems linked with EDTA was 168.5, 213.4, 72.8, and 81.0 mg/g, respectively, and 175.5, 181.9,

66.0, and 69.7 mg/g for the beads crosslinked with DTPA. These systems were reused for 10 cycles using a 2 M HNO_3 solution for regeneration; the EDTA maintained an efficiency above 90% until the eight cycle, while the DTPA derivatives lost this threshold at the sixth cycle. The main advantage of both systems is the green chemistry employed for the synthesis and the easiness to recuperate them after use by the magnetic properties (F. Zhao et al., 2015).

Composite systems have also been developed with this magnetic chitosan, and they have been found to benefit from the functional groups of other materials and the electrostatic and entropic interactions that come with them. For example, a covalently bonded composite of carboxymethyl chitosan was generated with the highly amine dense branched polyethyleneimine for Pb(II) removal. Here the Langmuir isotherm was not the best fit, as the R^2 was 0.9531, with a maximum adsorption capacity of 114.7 mg/g; the Langmuir-Freundlich isotherm had an R^2 fit of 0.9952 and a maximum of 124.0 mg/g. In this study, the optimal conditions were obtained using a contour plot with a fixed time of 3 h and a solution initial concentration of 50 mg/L; the optimum pH was 4.5 with a dosage of sorbent of 0.4 mg/L. Thermodynamic parameters were calculated, finding a negative ΔG (~-9.5 kJ/mol) at the studied temperatures (303, 313, and 323 K) and an entropic gain of 21.80 J/mol K. Finally, recycling was tested using three different eluents with 0.1M concentration for all (EDTA, HCl, and NaOH). EDTA had the best performance, with 90% desorption efficiency; after 5 cycles this system still maintained about 85% removal efficiency, but some mass losses were observed (Yaoguang Wang et al., 2017).

This magnetic chitosan system has also been further composited with graphene oxide (GO) to adsorb different pollutants; for example, the adsorption of methylene blue was demonstrated in this system with a Langmuir isotherm calculation of the maximum adsorption capacity of 180.8 mg/g. The effect of pH was also studied in this experiment, and it was found that the optimal

adsorption was obtained when the solution's pH was 10, and the system was recuperated without complication using a magnet, which made it an efficient adsorbent for dyes in water suspension (L. Fan et al., 2012). Another pollutant that was removed with this system was the drug ciprofloxacin, which presented a maximum adsorption capacity of 282.9 mg/g when a Langmuir isotherm was generated using 10 mg of sorbent in 30 mL of ciprofloxacin solution at pH 5. Subsequently, effects of ionic strength and pH were studied with a fixed concentration of 20 mg/L for ionic strength NaCl (20 and 200 mM) and $CaCl_2$ (1 and 10 mM). For the pH effect, it was shown that when the pH was below range for the species to be in its zwitterionic form (between 6.1 and 8.7), the adsorption was enhanced, which indicates that the electrostatic interaction is favored when is at the cationic state and was optimal at a pH of 5. With respect of the effects of the ions, both species decreased the interaction with the sorbent on 40.9 and 37.5%, respectively, probably due to the preferred interaction with these ions than to the drug and the interference with the π-π interactions of the drug with the GO. Finally, regeneration was suitable for 3 cycles; the regenerated material presented a remaining 72% adsorption capacity when methanol (100%) was selected as eluent (F. Wang et al., 2016). For metal adsorption, the system was impregnated with an ionic liquid, specifically tetraoctylammonium bromide ($C_{32}H_{68}BrN$, PubChem CID: 2734117) in methanol (6.6%). This system was tested with Cr(VI) and described by a Langmuir isotherm to present a maximum adsorption capacity of 145.4 mg/g; the optimal pH was found to be in the range of 3 to 4 due to the protonated state of the hydroxyl and amino surface groups. Above this range the adsorption decreased around 20%. The system was evaluated for multiple cycles using HCl for desorption, but after the third cycle, adsorption capacity started to drop drastically, retaining a capacity of 20 mg/g at the 10^{th} cycle (L. Li et al., 2014).

Another composite generated with the ferromagnetic nanoparticles used them as seeds to grow a shell with ZrO_2 for a photocatalytic system with chitosan that can recover Cr(VI) and degrade 4-chlorophenol. Here, the nanoparticles with and without the chitosan matrix were tested using 50 mg of the sample in 100 mL of a solution with 70 mg/L of $K_2Cr_2O_7$ with pH of 2 at 30 ± 0.5 °C. For the chlorophenol, 0.01 g were added to 100 mg with 20 mg/L under natural sunlight for 3 h, and for the reuse, 6 continuous cycles were performed with a duration of 2 h for Cr(VI) and 3 h for the 4-chlorophenol. The NP by themselves presented a reduction of Cr of 71.2%, but when anchored to chitosan, this reduction increased to 84.7%; these results were improved by the addition of 0.2 mL of ethanol or isopropanol, to 92.4% and 98.5%, which was explained by a side reaction. The process also showed the influence of pH, as the performance decreased when pH become higher. Reductions of 84.7%, 61.2%, 40.5%, and 28.7 % were obtained with the pH of 2, 4, 6, and 8, respectively. For the 4-chlorophenol, degradation was of 66% with the nanoparticles alone, and of 88.6% when they were in with chitosan; the normal mechanism is the generation of –OH, which will attack and lead to dechlorination to produce 1,4-benzenediol or other alcohols with further nucleophilic reactions. Adsorption of the phenol was also measured in dark conditions to avoid the degradation; herein, it was 7.3% for the nanoparticles alone, while the chitosan adsorbed 22%, which facilitates the degradation and explains the better performance that this system has in the degradation. Finally, regarding reusability, for the Cr(VI), the photoreduction capability of the system with chitosan decreased after the 6 cycles from 87.1% to 85.1%, while for the 4-chlorophenol it changed from 71.2% to 67.3%. These results show that the systems with chitosan and magnetic nanoparticles are not only effective and easy to recuperate, but also are versatile in the systems that can degrade and adsorb, eliminating them from water sources and waste streams (Kumar et al., 2016).

Hydrous zirconium oxide (HZO) was also used in chitosan beads crosslinked with triphosphate for the removal of F^- and Pb(II). Here, studies to find the best ratio of HZO and chitosan were performed; the conditions for the study were 2.5 g/L of the adsorbents, a pH of 5 for 160 h, and initial concentrations of 10.2 and 46.1 mg/L of F^- and Pb(II), respectively. The best ratio was found to be 2:2.5 chitosan:HZO. However, such combinations were observed to have bad stability, so the ratio 2:2 was selected for the adsorption experimentation. The Langmuir isotherm presented a maximum adsorption capacity of 22.1 mg/g for fluoride and 222.2 mg/g for Pb(II); interestingly, the pH influence was inverse for the elements, as fluoride adsorption peaked at pH 3 and Pb(II) at pH 7, demonstrating that it is possible to select the element needs to be preferentially removed with the same system (Cho et al., 2016).

Zirconium (IV)-chitosan coordinated composites have also been of interest lately, as they prove to have a good ion exchange mechanism, which was used to remove Cr(VI) and V(V) from water (Lingfan Zhang et al., 2013, 2014). For Cr(VI), the Langmuir modeling showed a maximum adsorption capacity of 175 mg/g in a solution with pH 5 and 30 °C; this pH makes the interactions occur via electrostatic forces and ligand-exchange mechanism, because when pH decreases or increases, the efficiency plummets. Also, when ions ($Cl^–$, $NO^{–3}$, and $SO_4^{2–}$) are present in the solution, the adsorption capability is decreased by more than 60% as a result of the competition of the ions for the active spaces (Lingfan Zhang et al., 2013). For V(V), the Langmuir isotherm model maximum adsorption capacity is 208 mg/g at 30 °C, but in this case the optimum pH was found to be 4; this is a consequence of the other vanadium oxidation states that are formed a higher pH, which affects the composite's adsorption capacity. Regarding the ions' competitivity, chloride and nitrite had little effect, but the sulfite ion reduced the effectiveness when tested in a solution with 500 mg/L of SO_4^{2-} and 30 mg/L of V(V) (Lingfan Zhang et al., 2014). Both systems were evaluated

for regeneration by 0.01 M NaOH solutions, which maintained 89% of the initial capacity after 5 cycles, and with a 0.05 M NaOH, for which the effectiveness was of 90% after 3 cycles for the Cr(VI) tests.

Zinc oxide (ZnO), as with the other oxide and metallic nanoparticles considered, has shown good efficiency for the removal of metals from water (Trujillo-Reyes et al., 2014); the generation of composites with natural polymers can then enhance these existing properties to maximize the removal performance. For example, ZnO nanoparticles coated with chitosan were tested to eliminate Pb(II), Cd(II), and Cu(II) and to study the viability of the reuse of this system. Langmuir isotherm modeling presented a maximum adsorption capacity of 476.1, 135.1, and 117.6 mg/g, respectively, with optimum pH at 6, 6.5, and 4. These values are close to the pKa of chitosan, which helps the adsorption add less competition between protons and the ions is present. As previously mentioned, the system was tested for reusability; for this, 0.01 M of EDTA was used as a regeneration solution. Herein, after 4 cycles, the system preserved > 90% of the removal capacity for all ions. Finally, three wastewater samples were used to analyze the viability in an uncontrolled environment; the results were satisfactory, as all metals were removed with efficiencies of more than 90%, with the decrease in uptake being linked to the concentrations of calcium, sodium, and potassium ions in the sample (Saad et al., 2018).

Metal-chitosan composites can be employed in many versatile ways to purify water; for example, an aluminum oxyhydroxide-chitosan was shown to be a good base system to modify with iron-zero valent, MnO_2 nanoparticles, or silver nanoparticles, all to use as a filter for different proposes. The first was established for As(V) and Fe(II) removal, the second modification for Pb(II) removal, and the silver composite was used for the controlled release of Ag ions, exploiting the bactericidal properties of the ion. The system was tested first in a batch mode for the

antimicrobial activity, using 2 g of the silver carrying system; it was shown that after 500 batches, only 29% of the silver nanoparticles were released, maintaining always below the safety threshold concentrations, and *E. coli* growth was eliminated completely. After this, all the systems were tested with a flow of 50 mL/min in a filter, where 1500 L of solution was passed with concentrations of 1.5*105 CFU, 5 mg/g of Fe(II), and 150 mg/g of Pb(II). 400 mL of a 1 mg/L solution of As(V) was also tested. All solutions were purified with final concentrations below the permitted regulations, presenting evidence of the feasibility of the systems to be cheap and useful in low income houses (Sankar et al., 2013).

A non-metal oxide that has also been used for water treatment is SiO_2. Herein, like the last case, the oxide-chitosan (silicagel/chitosan) composite was used to adsorb another compound; in this case, La(III) was used, as it generates a better interaction with the fluoride ion that needs to be removed. When tested for adsorption in a solution with 10 mg/L and an initial dosage of 0.1 g of the materials at 303 K and pH 7, the system with La(III) removed 4.9 mg/g, while the system with only oxide-chitosan had an adsorption capacity of only 1.56 mg/g; it was also found that these adsorption values were relatively constant from pH 3 to 9 for the metal-containing version, and from 3 to 7 for the oxide-chitosan version. After the high extreme, the adsorption capacity decreased significantly and had little impact on the adsorption when Cl^-, $SO_4^{2-}$and NO^{3-} ions were present, but HCO^{3-} reduced the adsorption capability. When the Langmuir isotherm was modeled, the maximum adsorption capability was of 3.33 mg/g at 303 K, and ΔG was negative in all temperatures modeled (303, 313, and 323 K) with a small $\Delta S = 0.05$, indicating a spontaneous process (Viswanathan et al., 2014). A closed system was also used for the fluoride removal, but herein, instead of SiO_2, bentonite was used in the generation of the base sorbent. This system presented an adsorption capacity at pH 5 and 30 °C of 2.87 mg/g, and when modeled with a

Langmuir isotherm, the maximum adsorption capacity was of 8.6 mg/g at 30 °C, decreasing as temperature increased. Contrary to the previous system, this presented a decrease of capacity moving in both extremes of pH, as the performance at 3 was as low as at 9, a similar behavior with co-existing ions, with the carbonate ions affecting the adsorption more. Finally, the system was tested for 10 cycles of reuse using 0.5 M NaOH as a regeneration solution. A stable adsorption was maintained for 8 cycles, where only the 17% capacity was lost gradually, which indicates the good performance of the system through time (Y. Zhang et al., 2014).

A more ambitious system was prepared in chitosan beads containing a combination of activated carbon and montmorillonite ($(Ca_{0.13}Na_{0.34}K_{0.03})$ $[Al_{3.04}Fe(III)_{0.41}Mg_{0.49}Ti_{0.01}]$ $[Si_{7.98}Al_{0.02}]O_{20}(OH)_4$, PubChem CID: 71586775). The objective of this combination was to remove metals, but also some cationic and anionic organic pollutants in a one-step system. For this Zn, metoprolol (MTP, $C_{15}H_{25}NO_3$, PubChem CID: 4171) and clofibric acid (CBA, $C_{10}H_{11}ClO_3$, PubChem CID: 2797) were selected to act as a metal mode, a cationic beta blocker, and an anionic anti-cholesterol. The adsorption capacity was tested in a solution of the model substances with an initial concentration of 1.5 mmol/L with pH 6.5 at 25 °C using 200 mg of the system and controls. The results showed that the composites had indeed a better adsorption of the samples, but the most effective adsorbent was the chitosan with 1.5% of activated carbon, with an adsorption maximum of 10, 26, and 21 mg/g for Zn(II), MTP, and CBA, respectively; while the three components system had an adsorption of 10, 19, and 16 mg/g, respectively. Interestingly, for the anionic model, the montmorillonite-chitosan system presented the best performance with 30 mg/g for MTP, which was not the behavior when the base materials were tested alone, and activated carbon performed better (Bouyahmed et al., 2018). Overall, this system was able to capture all type of pollutants in good proportions, which has to be the ultimate goal of remediation systems.

As it has been shown, chitosan is easily molded into beads that can be packed into columns, while keeping a high surface area; another structure that can be considered for similar system design are foams that can be obtained when different polymers are mixed, entangled, and/or crosslinked. An example of this design is a foam composite generated with polyurethane and chitosan, which was tested for adsorption of an acid dye, acid violet 48 ($C_{37}H_{38}N_2Na_2O_9S_2$, PubChem CID: 11969493). Performance of the foam was studied variating pH, initial concentrations, and chitosan composition variance from 5 to 20% (w/w). The Langmuir isotherm model showed that the maximum adsorption capability was of 29.6 mg/g when the chitosan concentration was 20%, and decreasing as the concentration decreased; meanwhile, the best adsorption was at pH 3, decreasing gradually up to pH 8, and plummeting in a higher pH range (H. C. Lee et al., 2009).

Cellulose-chitosan composites are also interesting, as they are cheap and abundant raw materials, and, as seen in the previously and in this section, they have a large variety of sorbates, which can also be further improved with structure, group addition, or composite generations. An example of fiber combinations for a homogeneous membrane generation was completed using butyl methylimmidazilium chloride [$BMIm^+Cl^-$] ionic liquid in a recovery variation of the process. This system was used to adsorb a cyanotoxin called microcystin-LR (MC, $C_{49}H_{74}N_{10}O_{12}$, PubChem CID: 445434), which is one of the 80 reported variants of microcystins, but is linked with liver cancer and is closely monitored by the U.S. EPA (U.S. Environmental Protection Agency, 2012). For the composite formation, a 10% solution was generated in the ionic liquid in the range 100 to 110 °C and using a 75% deacetylated chitosan to reach a final concentration of the dry composite between 20 and 67%, wherein the solutions were stirred for about 6 to 8 h. When a pure cellulose membrane was tested with no adsorption of MC, when the 20% was evaluated the

adsorption capacity obtained by a pseudo-second order model was of 42 mg/g, while the 67% presented an adsorption capacity of 96 mg/g. An interesting point in this work is that the increase in chitosan also came with a swelling increase of 29.2% when 20 and 67% were compared. Lastly, reusability of the membrane was determined by putting the charged membrane in ultrapure water, resulting in the release of all the adsorbed MC and allowing the system to re-adsorb at the similar concentration on a second use (Tran et al., 2013).

Table 1.3. Chitosan-derived Materials and Pollutants Adsorbed

Material	Pollutant	Capacity [mg/g]	Regeneration	Reference
Chitosan Beads with carboxymethyl groups	Cu(II)	130	0.1 M HCl	Yan *et al*. 2011
Chitosan with epichlorohydrin and triphosphate	Cu(II)	130.72	0.1 HCl and HNO_3	Laus *et al.* 2010
	Cd(II)	83.75		
	Pb(II)	166.94		
Chitosan iron coated flakes	As(III)	16.15	0.1 M NaOH	Gupta *et al.* 2009
	As(V)	22.47		
Iron draped glutaraldehyde crosslinked chitosan granules	As(III)	2.32		
	As(V)	2.24		
Chitosan beads impregnated with Fe-Mn oxide	As(III)	54.2	0.5 M NaOH	Qi *et al*. 2015
	As(V)	39.1		
Chitosan spun hollow fiber with iron oxide nanoparticles	Se(IV)	15.62		Seyed Dorraji *et al*. 2017
Magnetic chitosan with EDTA	Cd(II)	168.5	2 M HNO_3	Zhao *et al.* 2015a
	Pb(II)	213.41		
	Co(II)	72.84		
	Ni(II)	81.05		
Magnetic chitosan with DTPA	Cd(II)	175.47		
	Pb(II)	181.92		
	Co(II)	66		
	Ni(II)	69.66		
Magnetic carboxymethyl chitosan/branched PEI	Pb(II)	114.7	0.1 M EDTA	Wang *et al.* 2017

Magnetic chitosan/ graphene oxide	Methylene blue	180.83		Fan *et al*. 2012
	Ciprofloxacin	282.9	Methanol	Wang *et al*. 2016
Magnetic chitosan/ graphene oxide/tetractylammonium bromide	Cr(VI)	145.35	HCl	Li *et al*. 2014
Chitosan beads with triphosphate and hydrous zirconium oxide	F-	22.1		Cho *et al*. 2016
	Pb(II)	46.1		
Zirconium (IV)-chitosan	Cr(VI)	175	0.01 M NaOH	Zhang *et al.* 2013a
	V(V)	208		Zhang *et al.* 2014a
ZnO nanoparticles coated with chitosan	Pb(II)	476.1	0.01 EDTA	Saad *et al*. 2018
	Cd(II)	135.1		
	Cu(II)	117.6		
Silica gel-chitosan	F-	1.55		Viswanathan *et al*. 2014
Silica gel-chitosan with La(III)	F-	4.9		
Bentonite-chitosan with La(III)	F-	8.54	0.5 M NaOH	Zhang *et al.* 2014d
Chitosan beads/ activated carbon	Zn(II)	10		Bouyahmed *et al*. 2018
	Metoprolol	26		
	Clofibric acid	21		
Chitosan beads/montmorillonite	Zn(II)	6		
	Metoprolol	30		
	Clofibric acid	8		
Chitosan beads/activated carbon/montmorillonite	Zn(II)	10		
	Metoprolol	19		
	Clofibric acid	16		
Chitosan/polyurethane foam	Acid violet	29.6		Lee *et al.* 2009
Cellulose/chitosan (20%)	Microcystin-LR	42	H_20	Tran *et al.* 2013
Cellulose/chitosan (67%)		96		

As the use of ionic liquids is still a work in progress, another approach to combining these two natural polymers was by imbedding cellulose nanocrystals (CNC) in a chitosan matrix and then freeze-drying and compacting the material, which was crosslinked with glutaraldehyde for further stability. This system was tested for the removal of three dyes: Victoria Blue 2B (VB, $C_{29}H_{32}ClN_3$, PubChem CID: 16599), Methyl Violet 2B (MV, $C_{25}H_{30}ClN_3$, PubChem CID:

11057), and Rhodamine 6G (R6G, $C_{28}H_{31}ClN_2O_3$, PubChem CID: 13806). The maximum removal was found when pH was at 5 but was stable up to 9 for the VB and R6G, but it decreased for MV. Initial concentration also had an impact on the removal percentage, as it saturates faster; for an initial concentration of 1 mg/L, the removal efficiency was of 91, 70, and 98% for MV, R6G, and VB, respectively, but when the concentration was 10 mg/L, the percentage decreased to 48, 13, and 88%. Part of the comparison was the impact of the crosslinking of the chitosan, assuming that it had an impact on MV and R6G adsorption but not on VB, which can be explained by the greater contribution of the hydrogen bonding mechanism employed by the latter, instead of electrostatic interactions where the sulfate, amino, and acetyl groups are the driving force (Karim et al., 2014).

This section has overviewed some approaches taken by researchers to improve water by adsorption with a low-cost biopolymer that possesses charged surface groups. These groups are the main driving force in adsorption for a lot of the cases considered. The groups also are a crucial factor when structure is desired, as these interactions with the media present the opportunity of precipitate in the generation of beads when pH is changed drastically and are anchoring points for the chemical and ionic crosslinks between the materials.

1.4.4. Alginate

Alginates are also linear polymers consisting of (1→4) β-D-mannuronic acid (M) and α-L-guluronic acid (G), which are part of the structural components of algae and are an exopolymer of bacteria matrixes (Figure 1.4). The blocks that are formed with the monomers depend highly on the origin and provide the resulting alginate with different properties, as the ease of hydrolysis and crosslinking depends on those. The blocks can be obtained by hydrolysis and

fractionation, as consecutive G or M residues (GGGGGG or MMMMMM). These have low solubility and are more resistant to the attack of extreme pH or enzymes; meanwhile alternated blocks (GMGMGM) are degraded more quickly (Kuen Yong Lee & Mooney, 2012).

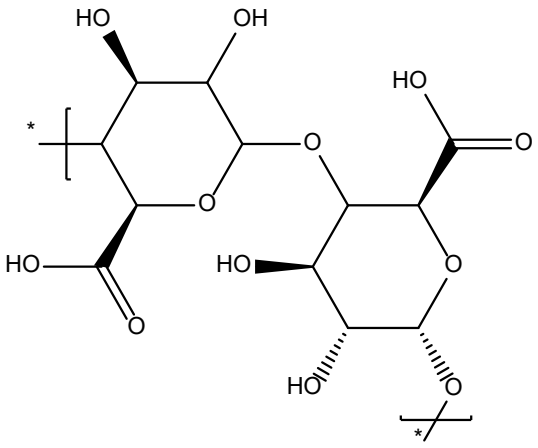

Figure 1.4. Structure of alginates monomers.

The attractiveness in the use of alginate, apart from the low toxicity, relatively low cost, and biocompatibility, is the mild gelation that occurs when divalent cations are present in the media (that presented in decreasing affinity order are Pb > Cu > Cd > Ba > Sr > Ca >Co, Ni, Zn > Mn) or when pH is below the pK_a value of the uronic acids (3 to 3.5). It is important to highlight that only G-blocks are believed to be responsible for crosslinking while interacting with divalent cations; as the natural source dictates this G/M ratio, it is always important to characterize this to understand the physical and chemical characteristics of the generated hydrogels (Kuen Yong Lee & Mooney, 2012; Pawar & Edgar, 2012).

Another interesting behavior of these resulting hydrogels is that they present a huge water uptake, which frequently has been used to maintain stable conditions for encapsulation and improvement of the persistency of sensitive molecules or systems such as cells. Similarly, the

molecular weight of the raw material will have an impact on the properties, as when low molecular weight is used, the polymer solution or hydrogels generated can be plasticly modified and have been widely used to inject into the muscles or ingested orally for drug delivery and personal medicine; but when high molecular weight is preferred, higher mechanical properties and viscosity are provided, which lead to better water resistance and durability (Pawar & Edgar, 2012; J. S. Yang et al., 2011).

A simple, direct, and effective way to use this polymer to improve the purity of water was tested by the addition of alginate and calcium to a sample water as a coagulant system and therefore reduce turbidity. In this study (Devrimci et al., 2012), 3 samples were tested with initial turbidities of 10, 80, and 150 NTU obtained by adding smectite clay; for treatment, concentrations of calcium ranged from 30 to 200 mg/L and alginate from 0.001 to 10 mg/L with low viscosity. For most of the samples, concentrations as small as 80 mg/L of calcium were used, and alginate concentrations varied from sample to sample; for 150 NTU, the lowest concentration to obtain an NTU of 1 or lower was 2 mg/L, while for 80 NTU the lowest alginate concentration was of 0.4 mg/L. For 10 NTU, two alginates were tested with low and high viscosities; herein, the low molecular weight was unable to reduce the turbidity below 4 NTU, but the high molecular weight accomplished it with a concentration of 2 mg/L and 120 mg/L of calcium. The most significant contribution of this system is that it works at neutral pH conditions, while aluminum, which is the most common coagulant, has to change pH to alkali conditions to work and produce a higher volume of slurry compared to the alginate treatment; therefore, alginate can act as a more feasible alternative that would also simplify downstream processes (Devrimci et al., 2012).

A more standard process to eliminate pollutants is the Polymer Assisted Filtration (PAF), where a polymer is pre-dissolved to enhance the precipitation of ions in a solution and then be

removed by filtration. For this application, the polymer should have some inherent interaction with the ions, but nowadays, synthetic polymers are mainly used, even when these could have a certain toxicity or low solubility. Looking for alternatives, an alginate with M/G ratio of 1:1.5 and MW between 12 to 80 kDa was studied to eliminate divalent ions such as Pb(II), Cu(II), Zn(II), and Ni(II). Herein, it was observed that alginate was able to eliminate the Pb(II), Cu(II), and Zn(II) in concentrations as low as 4 x 10^{-2} M, but Ni(II) was adsorbed between 3 to 5 orders of magnitude less than the other metals, which was explained because of the soft ion nature of the Ni(II), which prefers to bind with ligands with softer interactions. The regeneration of the alginate was also demonstrated in acid conditions with times between 2 to 20 min depending on the pH (Fatin-Rouge et al., 2006).

For a less specific treatment, alginate proved to be able to separate oil and water efficiently for emulsification when a surface modification with dodecanol was performed to obtain a hydrophobic system. The emulsion was obtained using sunflower oil at 10 wt% and with the synthetized alginate having a substitution ratio of 8.47%. It was found that with only 0.8%, the emulsion was stable for up to one month, presenting no creaming or face visible phase separation and with less viscosity than the sodium alginate by itself (J. S. Yang et al., 2012), presenting it as a good system to separate oil when it could be incorporated to a complex composite.

As mentioned before, alginate has the inherent ability to generate beads when divalent cations are in the media. Exploiting this property, beads were generated with silver particles (AgNP) using three different approaches: 1) entrapping premade AgNP, 2) reduction of Ag+ in premade beads, and 3) a simultaneous gelation and reduction. The systems were then tested for bactericidal performance in a column though which 10^5 to 10^6 CFU *E. coli*/mL flowed. The results showed that the systems with the reduction *in situ* the CFU was decreased to non-measurable

quantities in only 1 min of retention in the column, but the reduction in premade beads liberated high quantities of ions, up to 22 ppm, which was not the case in the simultaneous gelation and reduction-derived beads. This last observation implies that the latter might have a longer life-time, which is highly desirable for feasible water purification systems (S. Lin et al., 2013).

Even when beads are the most common structure generated by alginate coagulation, hollow fibers can also be prepared successfully; an example is the hollow fibers generated with TiO_2 for a photocatalytic reactor that was tested with the degradation of methyl orange. These fibers were tested wet and dried by supercritical CO_2 exchange. The fibers contained 41.7% of TiO_2, and the dry fibers had better permeability than the theoretical calculation predicted, with a BET of 94 m^2/g instead of 46, a pore volume of 0.46 mL/g instead of 0.36, and a mean pore radius was of 9.7 nm, while the prediction was of 16 nm. From an initial concentration of 6.4 mg/L, the efficiency of removal in flow without UV irradiation was of 0.08 mg/L, but with the UV was of 0.64 mg/L, which is much higher than what was obtained with the oxide nanoparticles alone. This was related to the high surface area, the adsorption to the alginate matrix, and the better dispersion of the nanoparticles due to the moieties form the alginate (Papageorgiou et al., 2012).

Iron oxides have also been used with alginate on account of their magnetic properties and adsorption capability. One example of the first property is a system developed in which alginate nanogel carrying tetra- sodium thiacalix[4]arene tetrasolfonate and synthetized nanoparticles for easier recuperation in metal water treatment. When solutions with 50 ppm of Co(II), Cd(II), Pb(II), Cu(II), Ni(II), and Cr(III) were tested with a pH of 7, the adsorptions ranged between 87 and 96.5%, with an apparent increase in adsorption when the magnetic particles were present compared to the system without them; the order of interaction was Pb(II) > Cd(II) > Cu(II) > Cr(III) > Co(II) > Ni(II) (Lakouraj et al., 2014). Meanwhile, the capture by adsorption was tested with As(III) and

As(V) in alginate beads impregnated with iron oxide; herein, two loads were studied, 10, 20, and 30% of hydrous iron oxide using a constant concentration of 1 g/L in solutions that contained only one of the two arsenic species. Results showed that the total removal for As(II) was higher when the load was 30% but the rate of adsorption was lower, with 10% being the fastest. As for As(V), 20% was the best adsorption performance, but only around 60% was adsorbed. Also, phosphate salts appeared to have an effect on the adsorption, as the removal efficiency was lower when these ions were present. For the Langmuir model isotherms, the maximum adsorption capacity was 393.7 mg/g for As(III) and 200.4 mg/g for As(V). Finally, regeneration was possible with agitation in a 0.05 M NaOH solution for 24 h and continued to work for 8 cycles; no significant loss in efficiency was observed for both arsenic species, but bead mass decreased between 15 to 20% after the cycles for As(III) and As(V), respectively (Sigdel et al., 2016).

Another tested alginate composite for arsenic removal consisted of beads imbedded with zirconium oxide. This system was also tested with Cu(II), and the effects of the mixing of both arsenic and cooper were tested, as well; separately, maximum adsorption capabilities were 32.3, 28.5, and 69.9 mg/g for As(III), As(V), and Cu(II), respectively, and when mixed, the As(V) was enhanced and more than doubling adsorption, while As(III) adsorption decreased, and no significant effect in Cu(II) adsorption was observed. Initial concentration and pH had a larger effect on copper adsorption than in the arsenic species, with optimum conditions at 300 mg/L and a pH of 9. The main contribution of this system is the simultaneous adsorption of cations and anions from wastewaters (Kwon et al., 2016).

In the above studies, a specific oxide was used for the arsenic removal, but solid waste material that contains oxides can be used, also. To demonstrate this, a residue from an electroplating industry containing Fe, Ni, Cu, and Cr oxides was prepared in alginate beads and

tested in sample waters. The optimum pH for this system was found to be 8, with 48 h to reach the plateau in a solution with an initial concentration of 15 mg/L. The Langmuir model maximum adsorption capacities were 126.5 mg/g for As(III) and 41.6 mg/g for As(V), which are about 60% higher than that of the raw material, leading to an improvement in the uses of waste products in other industries for water treatment (Escudero et al., 2009).

Ceramics have also been impregnated in alginate beads for organics and metals adsorption. For example, attapulgite ($Al_2H_{29}Mg_2O_{15}Si_4^-$, PubChem CID: 56842194) was encapsulated via freeze-drying, cross-linked with a calcium solution, and later tested for Cu(II) and Cd(II) adsorption. When the ratio load was 1:4 between the clay and alginate, the Langmuir modeling showed that the maximum adsorption capacity of this material was 119 and 160 mg/g, respectively. The pH seemed to have no impact when it was higher than 4, but at lower pH, the adsorption decreased. The optimal concentration for Cu(II) was 200 mg/L, while for Cd(II), it was 400 mg/L. Finally, the recyclability was tested with mild acid washing (0.2 M HCl) for 1 h; the copper adsorption efficiency was decreased by 32% after the second cycle and remained constant for the following 4 cycles; meanwhile, cadmium adsorption increased 26%, which was explained by the exchange of calcium from the material with more active sites for adsorption and possibly by the release of Ca ions, which transform the active sites to alginic acid. This is also consistent with a 23% weight loss in the first acid washing (Yaquan Wang et al., 2018).

While for organics, imbedded nano-goethite in a fixed ratio of 3:1 alginate: clay was used for the adsorption of Congo red ($C_{32}H_{22}N_6Na_2O_6S_2$, PubChem CID: 11313). For this system, the optimum pH was 3 with a maximum adsorption capability of 181.1 mg/g. For reusability, 0.1 M NaOH was tested for 5 cycles with a desorption efficiency of 94%, but a loss of efficiency was observed after 4 cycles, decreasing from 85% to 76%, which is still acceptable for multiple uses

(Munagapati & Kim, 2017). Another commonly used clay is bentonite; when beads carrying it were tested for methylene blue adsorption, it was found that the optimal pH was between 7 to 10 with a maximum adsorption capability estimated by Langmuir isotherm of 799.4 mg/g. Herein, the efficiency loss after 6 cycles with acid washings in water pH 3, was only 7%; since the initial efficiency was a high value of 94%, the system was judged to be promising for the removal of the cationic dye MB (Djebri et al., 2016).

As activated carbon is one of the main adsorbents available, the use of other forms of carbon serve as an attractive alternative to replace this market; they have some of the same effects, but when nanomaterials are used, some can leak to water streams, resulting in micro-pollution. To prevent this, carbon nanotubes were immersed in alginate (1:1.5) and then wet spun and freeze-dried; performance was evaluated for Cu(II) adsorption in a solution with 20 mg/L, an ionic strength of 0.1 M using $NaNO_3$, and a pH between 2 and 7. It was found that good adsorption was present for the composite in all pH ranges, but it reached an optimal performance at pH 5 of 83.3%; higher pH presented precipitation of the copper species. Lastly, the maximum adsorption capability was modeled by Langmuir isotherms and was determined to be 84.9 mg/g, which was higher than previous studies using the separate components and other natural derivates as waste yeast, lignin, or activated sludge (Y. Li et al., 2010). Another carbon-containing system, alginate-bentonite-activated carbon beads, were tested for methylene blue adsorption; herein, it was observed that after pH 6, maximum adsorption was reached and was stable to higher potentials. Interestingly, Langmuir isotherm models were made at three different temperatures 30, 40, and 50 °C having a maximum adsorption capability of 757.0, 982.5, and 994.1 mg/g, respectively. The first one was lower than a simple bentonite-alginate composite (Djebri et al., 2016), but there was a clear relationship between the increase in temperature and the adsorption capacity of the system.

Also, the Gibbs free energy was increased from -5.92 to -5.72 kJ/mol, presenting a higher tendency to adsorb at lower temperatures; this indicates that there were other phenomena involved in the adsorption than physisorption, which is always a spontaneous process. Finally, regeneration was tested with methanol washes for 6 cycles, and adsorbance efficiency decreased from 94.4 to 75.4%, which are good values for the rehabilitation of contaminated water (Benhouria et al., 2015).

Like the previous cases, combinations with other polysaccharides or synthetic polymers can help gain better properties, generating composites with improved interactions with the pollutants. For example, three freeze-dried alginate-CNF (7:1) aerogels were generated for oil/water separation with a difference of how freezing was done to the mixture: direct refrigeration, unidirectional freezing, or bidirectional. Herein, cellulose was used only as a mechanical reinforcer, but also it helped to improve the hydrophobicity as hydroxyl groups were added and silanized, too. In this work, the structure of the aerogel was the main difference, with the bidirectionally frozen aerogel performing better when compression cycles were applied with almost non-stress reduction or plastic deformation compared with the others after 10 cycles. The contact angle for oil in this aerogel was 0° and of 148.7° for water, assessing the superhydrophobic nature of it, and when this aerogel was tested for the selectively pump oils from a water mixture, it showed adsorption capacities between 15 and 35 g/g for hexane, hexadecane, silicon oil, pump oil, toluene, colza oil, and chloroform in this order, with the same results for up to 10 cycles when regeneration was obtained by mechanical squeezing with 80% strain (J. Yang et al., 2018).

Meanwhile, alginate-chitosan beads were generated for divalent ion adsorption. These beads were generated by spraying an alginate-chitosan solution into a 0.15 M $CuCl_2$ solution and then exchanging the Cu(II) ions for H^+ in a 0.1 M HCl solution; these beads were tested for Cu(II), Co(II), and Cd(II), having a maximum adsorption capacity of 8.39, 3.18, and 6.63 mg/g,

respectively and reaching saturation around 10 min in solutions with 5 mM of the chloride from of the metal (Gotoh et al., 2004). Similarly, nano-chitosan-alginate-cellulose (2:8:1) nano-beads were generated and tested for Pb(II) ions adsorption. Optimal adsorption conditions were found to be pH 6, initial concentration of 62.5 mg/L, dosage of 4 g and temperature of 50 °C; regeneration of the beads was also obtained using 0.1 M HCl solutions. The nano-chitosan comes from the addition of tripolyphosphate as an ionic pre-crosslinker to the chitosan solution before mixing with alginate and cellulose, which generates nanoparticles with a sharp distribution peak at 100 nm when observed in DLS. Langmuir isotherms were calculated, but no correlation was found, suggesting a different adsorption mechanism, which fit in a Freundlich model with an n value of 1.4916 (Vijayalakshmi et al., 2017). It is important to remember that this model is used when the energy term (b) in the Langmuir model is a function of surface storage, suggesting a heterogeneous phenomenon and using n as a constant that describes the shift from linearity, with 1 being the value that indicates linearity (Novotny, 2003).

Also, polymers synthetized in the alginate matrix have been studied for metal removal. For example, alginate-polyaniline nanofibers were tested for Cr(VI); here calcium was not used as a crosslinker, as H-binding was done with the N groups of the aniline structure. This system was able to eliminate 78.6% from a solution with an initial concentration of 100 mg/L of Cr(VI) in 60 min. The system efficiency also showed to be highly dependent on pH, decreasing efficiency as the pH increased from 2 to 10. Furthermore, the optimal dosage of material was found to be 150 mg. When other ions were tested in the solution, a decrease in the adsorption of the metal was observed when bicarbonate ions were present, but no significant loss was observed with chloride, sulphates, or nitrate ions. The maximum adsorption capability was modeled with Langmuir isotherms with values of 73.3, 74.5, and 75.8 mg/g at 303, 313, and 323 K, respectively and ΔG

of -10.48, -10.43, and -10.0 kJ/mol for each. Regeneration was also obtained with a 0.5 M NaOH solution with non-significant loss after 3 cycles, indicating that the system can be used as an alternative for the removal of this ion (Karthik & Meenakshi, 2015).

One of the main advantages of the synthesis *in situ* of the polymer for the composite is that physical entanglement and van der Waals interactions will be the main forces holding the composite together, leaving available the inherent functional groups of the polymers, *i.e.*, the carboxylic and hydroxyl groups of the alginate, which could then be leveraged for adsorbing the pollutants. Examples of this are beads of sodium alginate and poly [2-acrylamido-2-methylpropa-1-propanesulfonic acid] (PAMPS) which were evaluated for the adsorption of methylene blue (MB), Congo red (CR), methylene violet (MV, $C_{14}H_{12}N_2OS$, PubChem CID: 73024), amaranth red (AR, $C_{20}H_{11}N_2Na_3O_{10}S_3$, PubChem CID: 5359521), and metal ions such as Cu(II), Pb(II), Cd(II), and Ni(II). The tested system had a Young's modulus of 191 kPa, a compression strength of 48 kPa, and a water uptake of approximately 30%. For MB adsorption, pH did not seem to have a major impact on the adsorption efficiency; on the contrary, the initial concentration of MB had an effect, increasing removal capacity as the concentration increased. When the Langmuir model isotherm was used, the maximum adsorption capacity was 2273 mg/g, which was close to the experimental values. When tested with the other dyes, AR and CR, which are anionic, it did not present a measurable adsorption, mainly due to the electrostatic repulsion; while cationic dye MV presented an adsorption of 2105 mg/g, which valued closely to the 2977 mg/g of MB. For the metal ions, adsorption capacity was 2042 mg/g for Pb(II), whith lower values of 254, 50, and 843 mg/g for Cu(II), Ni(II), and Cd(II), respectively. Finally, recyclability of MB adsorption was tested for 5 cycles using NaCl as a desorbing agent, reaching a removal ratio of 90%, which leads to a

possible industrial application as a broad quantity of cationic species adsorbed in high amounts (Z. jian Shao et al., 2018).

As previously mentioned, alginate presents the advantage of being highly hygroscopic, enabling the use of encapsulated microorganisms for bioremediation. Some examples of this are the use of *Zoogloea ramigera* for Cu(II) removal in filters with different flow rates; the best removal obtained was of 94.3% of a solution with 50 mg/L and using 20 g of the sorbent with a flow of 3.6 mL/min and maintaining this efficiency after flowing 2700 mL. The only downside of this system was that mass transfer was slower than with the alginate beads, taking between 100 and 200 min to reach the maximum capacity. Recovery of the Cu(II) was obtained by washing with 0.005 M H_2SO_4 and a pH of 2, which allowed for a reutilization of the system (Sag et al., 1995). Similar systems can be generated with multiple organisms; for example, microalgae *Chlorella vulgaris* was co-immobilized with the bacteria *Azospirillum brasilense* and was used for the removal of ammonium and phosphorus ions.

Table 1.4. Alginate-derived Materials and Pollutants Adsorbed

Material	Pollutant	Capacity [mg/g]	Regeneration	Reference
Alginate beads with iron oxide	As(III)	393.7	0.05 M NaOH	Sidgel *et al.* 2016
	As(V)	200.4		
Alginate beads with zirconium oxide	As(III)	32.3		Kwon *et al*. 2016
	As(V)	28.5		
	Cu(II)	69.9		
Alginate beads with Fe, Ni, Cu, and Cr oxides	As(III)	126.5		Escudero *et al*. 2009
	As(V)	41.6		
Alginate beads with attapulgite	Cu(II)	119	0.2 M HCl	Wang *et al*. 2018
	Cd(II)	160		

Alginate beads with nano-goethite	Congo red	181.1	0.1 M NaOH	Munagapati *et al.* 2017
Alginate beads with bentonite	Methylene blue	799.4	H_2O pH 3	Djebri *et al*. 2016
Alginate with carbon nanotubes	Cu(II)	84.88		Li *et al*. 2010
Alginate beads with bentonite and activated carbon	Methylene blue	756.97	Methanol	Benhouria *et al*. 2015
Alginate-chitosan beads	Cu(II)	8.39		Gotoh *et al*. 2004
	Co(II)	3.18		
	Cd(II)	6.63		
Alginate-polyaniline nanofibers	Cr(VI)	73.34	0.5 M NaOH	Karthik *et al*. 2015
Alginate beads with PAMPS	Methylene blue	2272.73	NaCl	Shao *et al.* 2018
	Methylene violet	2105		
	Pb(II)	2042		
	Cu(II)	254		
	Ni(II)	50		
	Cd(II)	843		

When an initial concentration of ammonium was of 3 mg/L, 93% was eliminated in the first 2 days and 99% after the 6th day. Meanwhile, phosphorous at concentrations above 20 mg/L presented no change in concentration, but in a solution of 15 mg/L, 75% was eliminated in 2 days with no further change. When both ions were present, 91% of ammonium was eliminated after 2 days, but no change in phosphorous concentrations was observed; this suggests a higher affinity to the ammonium than to phosphorous. It is important to say that the use of alginates allowed for the use of these organisms in continuous and semi-continuous systems, so when the sample water was recirculated, drops in phosphorous concentrations were observed after the 3rd cycle, indicating some mass transfer phenomena occurring (De-Bashan et al., 2002).

An advantage of bioremediation is the use of intrinsic biochemical routes and defense mechanisms of the bacteria to accumulate the pollutants and easily recuperate them. For instance,

mercury was stored by *Enterobacter* sp. that was entrapped in alginate beads. For this experiment, 30 g of the wet sorbent were used in a solution with 5 mg/L of $HgCl_2$ at 30 °C and in a more complex water sample obtained from an industrial discharge in India and enriched with 7.3 mg/L of Hg(II). The reusability of the beads was assessed by 3 washes in ultrapure water. Complete removal was obtained in both samples after 72 h with the bacteria immobilized in the beads, while free bacteria only removed 69%, and the beads alone 19%. No more than two cycles were permitted, as for the fourth efficiency decreased to a 49%. The loss of efficiency was attributed to the loss of cells from the washes with ultrapure water. The mercury here was found stored as nanoparticles (3.75 ± 0.03 nm) at the cytoplasm of the bacteria with a change of Hg(II) to Hg(0), due to the presence of reductase found in this organism, thus showing the advantage of using more complicated biosystems for water remediation when treating toxic pollutants (Arvind Sinha & Khare, 2012).

This section showed advantages of using inherent properties of the polysaccharides, such as alginate, that can be exploited to provide structure, for direct adsorption, or as carriers of other components including nanoparticles, polymers, or microorganisms, presenting more options of hygroscopic materials for water treatment.

1.4.5. Hemicelluloses

Hemicelluloses are another class of widely abundant heteropolymers, as they constitute about 25 to 35% of wood mass (Smook, 2016). The major monomeric units in the polymers are hexoses (D-glucose, D-mannose, and D-galactose), pentoses (L-arabinose, D-xylose), and uronic acids (D-glucuronic acid, 4-O-methyl-D-glucuronic acid, and D-galacturonic

acid) (Gírio et al., 2010; Salam, Pawlak, et al., 2011). These monomers form branched chains with both α and β linkages with lower molecular weights than the other polysaccharides. These formed polymers can be divided into four groups: xylans, mannans, xyloglucans, and mixed-linkage β-glucans.

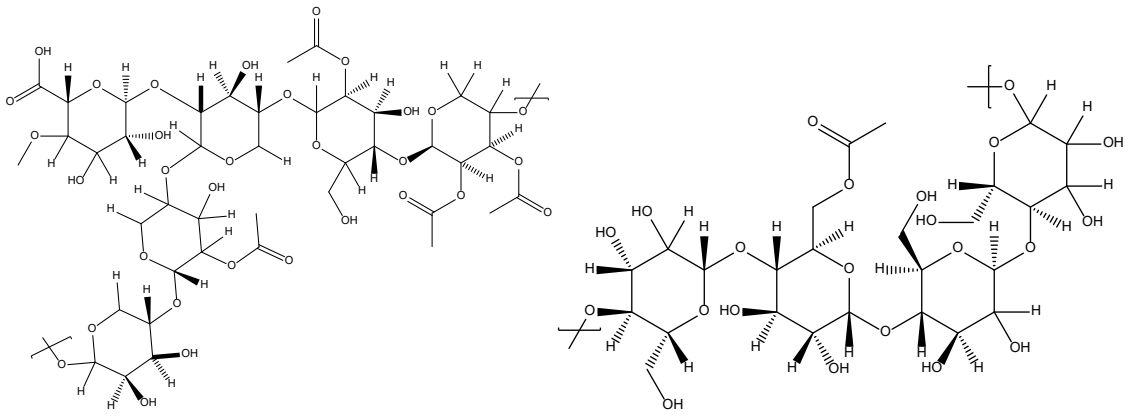

Figure.1.5. Structures of xylan (left) and glucomannan (right)

Among these groups, xylans the most abundant (Fig. 1.5, left), as they represent the major components of hemicelluloses in hardwoods and about half of the tissue in cereal grains (Wang *et al.* 2013; Sixta 2006); while mannan-type, such as glucomannans (Fig. 1.5, right) and galactoglucomannans, are mainly found in the secondary cell wall of softwoods (Gírio et al., 2010).

The main disadvantage that these polysaccharides present is their high solubility in water; therefore, a great portion of them are lost in the downstream processes of pulping, turning them into residue that is usually burned to obtain energy. Nevertheless, some work has been done to obtain added-value products targeting water remediation systems. For example, the modification of xylan with organic acids, such as citrate, succinic anhydride, and sodium monochloroacetate, was performed to increase the carboxyl content 2x in the three cases and to increase the water

absorption from 200% in natural xylan to 500% when modification with citrate was done (Salam, Pawlak, et al., 2011). This modification with citric acid, with and without catalyst (sodium hypophosphite, SHP), was then used to study the adsorption capability of this material for Cu(II) and methyl orange. The adsorption experiments were done using a slurry of the material with the following standard solutions: 500 mg/L of $Cu(NO_3)_2$ at room temperature, pH 4.5, and 400 rpm for 24 h; methyl orange was done with 20 mg/L pH 2.5 for the same time at room temperature. Herein, the study showed that the catalyst increased the crosslink reaction instead of enhancing the carboxyl group content, and consequently the carboxylated xylan without the catalyst had the better adsorption capacity with 83.8 mg/g of Cu(II) and 1.69 mg/g methyl orange when the weight ratio of citric acid/xylan was 3.6. In contrast, the unmodified xylans had a binding capacity of 11.4 and << 0.1, respectively, for Cu(II) and MO, demonstrating the potential to use these hemicelluloses that were modified with green chemistry and that can provide hydrogels with high water intake and can be easily degraded after usage (Wang *et al.* 2013).

Another work with hemicelluloses used pressurized hot water extracted polysaccharides from *Pinus wallichiana* and modified all the hydroxyls to improve the adsorption of malachite green (MG, $C_{23}H_{25}ClN_2$, PubChem CID: 11294). Herein, C6 was first acetylated, while C3 and C2 were carboxylated via aldehyde formation. Adsorption capability was tested with 5 g of the sorbent in a solution with 100 mg/L of MG at 50 °C. After confirmation of the adsorbance capacity, ranges of pH (3 to 9), temperature (20 to 90 °C), and concentration (10 to 120 mg/L) were also studied. The optimal concentration was found to be 98.2 mg/g at 70 °C and pH 6.5. Reusability was also tested for 16 cycles, where 67% of the capacity was possible, removing a total amount of 1294 g/g in the 16 cycles. Finally, kinetics and thermodynamics were studied. The Langmuir isotherm model showed a maximum adsorption capacity of 456.2 mg/g with the

following thermodynamic parameters at 343 K: ΔG of -16.62 kJ/mol, ΔH of 49.9 kJ/mol, and ΔS of 172.02 J/mol K. This demonstrates the great capacity of hemicellulose for use as an adsorbent for this dye or similar cationic organic molecules (Gautam et al., 2018).

Similar to the polysaccharides mentioned above, composites can play an important role in enhancing the adsorption capacity of hemicelluloses. For example, konjac glucomannan was crosslinked via calcium ions with graphene oxide and tested for the adsorption of methyl orange and methyl blue. In this work adsorption capacity was modeled with Langmuir and Freundlich isotherms, finding that the latter gave a better estimate with maximum capacities of 51.6 and 92.3 mg/g for MO and MB, respectively, and n value higher than 1. Interestingly, the composite swelled approximately one third less than the one without the graphene, but adsorption of the dyes was almost doubled, which was attributed to π-π stacking and ionic interactions with the oxide and the available hydroxyl groups (Gan et al., 2015). In the same way, MB was adsorbed to corn stover hemicelluloses hydrogels containing a variety of swellable clay (Laponite XLG, $Mg_{5.34}Li_{0.66}Si_8O_{20}(OH)_4Na_{0.66}$) to improve the adsorption capability. In this case, the cross-linkage was done with polyethylene glycol diglycidyl ether (PEGDE). Concentrations of each component were varied to understand the mechanical and rheological behavior, but adsorption was performed only in the hydrogels that had 1.5 M PEGE/ 1 M hemicelluloses and with 2 M of clay. Adsorption experiments were carried out with 100 mg of a freeze-dried sample in a solution at 25 °C and pH ranging from 2 to 9 to find the optimal conditions. The pH study results show that efficiency was low in acidic conditions, but when pH 6 was reached, adsorption stabilized at the maximum efficiency. For the modeling, Freundlich and Langmuir equations were tested in the isotherms; results varied, as the hydrogels without clay fit the a Freundlich model, while the one with incorporated clay fit the Langmuir monolayer model with a maximum adsorption capacity

calculated of 148.8 mg/g (Cheng et al., 2016). This last result makes evident how nanocomposites can improve the adsorption capacity by changing the mechanism in which the pollutant interacts with the hydrogels; in both cases, water adsorption was reduced, but mechanical stability was achieved by simple crosslinking of the hemicelluloses.

As previously mentioned, one of the main drawbacks of the use of hemicelluloses is their low molecular weight compared to other polysaccharides, such as cellulose. Therefore, the mechanical properties of materials prepared with these polysaccharides are somehow inferior compared to others such as cellulose; to remediate this, the incorporation of other polymers, such as chitosan, can improve the final mechanical properties. A crosslinked aerogel with tri-carboxylated hemicellulose-chitosan (1:1) has been developed and tested for swelling stability in water and saline solutions. This system presents only 8% mass loss in water and a gain of 9.3% in the saline solution, also having a tensile strength of 1.61 N/mm^2. An interesting point is that the volume expansion was 110% in water and 240% in saline solutions, but the mass adsorbed was only 80 g of water and 100 g of salts, meaning that the salts improved the swelling by rearranging the hydrogel without degrading the material, as no mass loss was observed, demonstrating that the composite can be used for water treatment in different conditions (Salam, Venditti, et al., 2011). A similar system was generated by grafting pentetic acid (DTPA, $C_{14}H_{23}N_3O_{10}$ PubChem CID: 3053) to hemicelluloses and then crosslinking with chitosan; this hydrogel was tested for the adsorption of Pb(II), Cu(II), and Ni(II) ions and swelling in saline conditions. The results showed that this system was stiffer that the one obtained with carboxylated hemicellulose, as salt uptake was 0.30 g/g, but there were similar losses and gains in water and saline solutions. Meanwhile for the metallic ions, the best conditions were at pH 5 and initial concentration of 5 mg/L, having a maximum adsorption of 2.9, 0.95, and 1.37 mg/g for Pb(II), Cu(II), and Ni(II), respectively

(Ayoub et al., 2013). A more complex hemicellulose-chitosan was generated by adding TiO_2 to the hydrogel to further improve the adsorption of metals. In this case the crosslinking was made by Schiff base linkages between the aldehyde groups of the hemicellulose (xylan) and the amines from chitosan. This hydrogel had a great water intake of 1507% g/g in water and 821% g/g in the saline solution, which is greater than the two previous studies; Langmuir isotherms modeled the adsorption of the metallic ions, giving maximum adsorption capacities for Cu(II), Cr(VI), Ni(II), Cd(II), and Hg(II) of 158.7, 97.1, 96.2, 78.1, and 76.3 mg/g, respectively. Analysis of thermodynamic and kinetic data revealed that the adsorption was spontaneous and endothermic, with ΔG between -7 and -1.55 kJ/mol and positive ΔH (S. Wu et al., 2014). These three studies made it clear that the combination of hemicelluloses and chitosan can help to improve water uptake and stability, allowing the use of hemicelluloses in more complex systems for water treatment.

While chitosan is great for the adsorption of metals due to the amine functional groups, other synthetic polymers can also help in the stability of hemicelluloses, and the generation of materials is applicable to pollutant capture. For instance, butyl acrylate and acrylamide were used jointly to generate hemicellulose-containing latex (HCL), which was studied for the adsorption of MB. An interesting finding with this system was that adsorption was constant between pH 3 to 7 (30.4 mg/g), and in more alkali conditions adsorption increased, reaching a maximum at pH 13 of 97.3 mg/g; this was explained as the more negative surface charge that the composite acquired at lower proton concentration was found.

Table 1.5. Hemicelluloses-derived Materials and Pollutants Adsorbed

Material	Pollutant	Capacity [mg/g]	Regeneration	Reference
	Cu(II)	83.8		Wang *et al*. 2013

Carboxylated xylan with sodium hypophosphite	Methyl orange	1.69		
C6-acetylated, C2, C3-carboxylated hemicelluloses	Malachite green	456.23		Gautam *et al.* 2018
Glucomannan with graphene oxide	Methyl orange	51.6		Gan *et al.* 2015
	Methyl blue	92.3		
Hemicelluloses with PEGDE carrying laponite	Methylene blue	148.8		Cheng *et al*. 2016
Hemicelluloses -g- pentetic acid with chitosan	Pb(II)	2.9		Ayoub *et al*. 2013
	Cu(II)	0.95		
	Ni(II)	1.37		
Hemicellulose-chitosan with TiO2	Cu(II)	158.7		Wu *et al.* 2014
	Cr(VI)	97.1		
	Ni(II)	96.2		
	Cd(II)	78.1		
	Hg(II)	76.3		
Hemicellulose-containing latex	Methylene blue	42.73		Zhang *et al.* 2015b
O-acetyl galactoclucomannan -g- methacylate	As(V)	48.17		Dax *et al.* 2014
	Cr(VI)	40		

The adsorption followed tightly the Langmuir isotherm models, showing a maximum adsorption capability at 25 °C of 42.7 mg/g (J. Zhang et al., 2015). Furthermore, methacrylate was grafted to O-acetyl galactoglucomannan, which was used to generate hydrogels for arsenic and chromium removal. The hydrogel generated with these materials was able to uptake 15 times its initial weight in water after 120 min; the maximum adsorption of the pollutants was observed at pH 9, which ensures that As and Cr must be in their anionic forms. The maximum adsorption obtained with the system was 48.2 mg/g for As(V) with similar results for the Cr(VI), which was constant for Cr(VI) for two more batches but was reduced in one third for As(V) in the subsequent tests (Dax et al., 2014).

Even though the low molecular weight of the hemicelluloses could present a problem for application in more complex materials generation, the addition of functional groups or using crosslinking agents provides an increase in the network generation within the hydrogels. This network generation provides a feasible approach to obtaining materials that can improve water quality using an abundant and underused resource such as the hemicelluloses.

1.4.6. Starch: Amylose and amylopectin

Another important polysaccharide blend is starch, which is produced in plants, tuber crops, and roots for storage of energy (between 16 and 24% mass content) and constitutes an important element in the human diet (Hoover 2001; Sajilata *et al.* 2006). Starch is composed of two main glucose-based polysaccharides: amylose and amylopectin; the first is a linear structure of glucose residues linked by α-D-(1 → 4) glycosidic bonds (Fig. 1.6), which ordinarily constitute between 15 to 20 % of total starch. Amylopectin is a branched structure with both α-D-(1 → 4) and α-D-(1 → 6) glycosidic bonds and in which side chains are typically 20 to 25 glucose units (Hoover 2001; Singh *et al.* 2010).

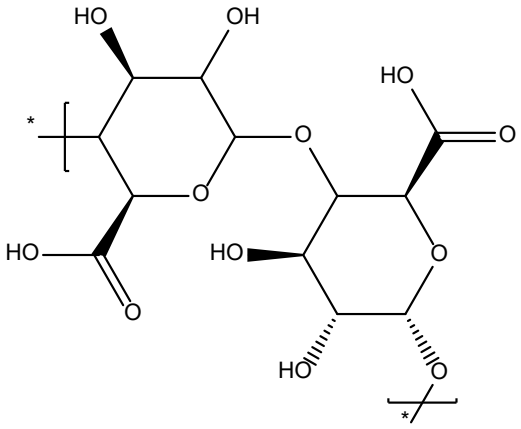

Figure 1.6. Two glucose molecules joined by α 1, 4 linkage, which originates backbone of amylose and amylopectin

Their composition is the same as cellulose, but the difference in the bond orientation (α *vs.* β) causes an important difference in how both polymers pack in the natural environment. Starch polymers forms helices instead of fibers, and these aggregate into granules with 70% of amorphous structure, while the other 30% form a crystalline region in the granules which consists primarily of amylopectin. This difference in cluster formation and in the amorphous proportion makes the starch more susceptible to enzyme degradation than cellulose chains (Sajilata et al., 2006).

Just as in cellulose, the hydroxyl groups in the polymeric backbone of starch permit the formation of highly hygroscopic materials while also allowing the use of hydroxyl groups as reactive points to add moieties to improve the uptake of pollutants or specific molecules. For example, starch was poly-carboxylated at C6 by nitrogen oxides and used to generate a hydrogel that was tested to adsorb Cu(II). The maximum adsorption capacity was 128.3 mg/g, which was obtained with 2 h contact at 40 °C, pH 7, and 50 mg/L initial concentration, following a Langmuir isotherm. A chelation binding mechanism where coordination between the copper, and the carboxyl, hydroxyl, and keto groups of the hydrogel was suggested to be the predominant phenomenon (K. Chauhan et al., 2010). Similarly, N-(3-chloro-2-hydroxypropyl) trimethyl ammonium chloride (CHPTAC) was incorporated into starch as a cationic moiety. This material was tested as a flocculant in 0.25% w/w silica suspensions and compared with other commercial options, showing a decrease from 13 NTU to approximately 4 NTU at neutral conditions and performing better than most of the commercially available options, proving to be a low-cost material with good performance as an option for wastewater treatment systems (Pal et al., 2005).

In the previous cases, cationic groups were added to the surface of hydrogels, and layered double hydroxide (LDH), also called hydrotalcite clay, was used to obtain negative surface charges

(Zubair et al., 2017). An example of this is the use of starch-NiFe-LDH composites in two proportions (1:1 and 1:2) for the removal of methyl orange. The optimum conditions for adsorption were found to be pH 3, initial dosage of 10 mg/L, 180 min, and low concentrations of initial MO dissolved; meanwhile, for the modeling of the isotherms, the Freundlich model was found to fit better than the Langmuir, indicating a heterogeneous adsorption that was favorable, as $1/n$ was lower than 1, with a maximum adsorption capacity of 388 and 358 mg/g, respectively, which was reproducible for 4 cycles using a 0.1 M NaOH solution for regeneration (Zubair et al., 2018).

A less specific adsorption mechanism has been shown by carbon nanotubes. To improve the biocompatibility of these materials, starch is a good alternative that has many advantages. In the following case, carbon nanotubes were covalently linked to starch (14.3 %) and iron oxide nanoparticles for facilitating the removal from solutions. This system was then tested for the removal of methylene blue and methyl orange in solutions containing 500 mg/L of the material with 373.9 and 327.3 mg/L of the MB and MO, respectively. An adsorption of 135 mg/g for MO and 94 mg/g for MB was obtained for the samples with starch in 10 min of contact, whereas, in the absence of starch, the removal capacity was approximately half of the uptake with starch, and it took approximately 30 min. As planned with the magnetic nanoparticles, these sorbents were quickly separated from the solution, with a visible diminution of the color concentration, which presents a good alternative for the elimination of organic pollutants by either adsorption to the nanotubes and starch or by using different catalytic nanoparticles that can be grown onto the carbon nanotubes such as ZnO, Ag, or TiO_2 (Chang et al., 2011).

Composites with polysaccharides also serve as an alternative to use either as a continuous phase or as a dispersed phase with special properties or moieties. Like the hemicelluloses, chitosan is a predilect material due to the difference in surface groups and the high abundance of it.

Examples of composites of starch/chitosan are reported in the literature. For instance, a cationic starch was composited with chitosan and tested as a flocculant. The starch was prepared by microwave irradiation with sodium hydroxide and 2,3-epoxypropyltrimethylammonium chloride, resulting in a DS of 0.31. The material was then crosslinked with chitosan in the presence of a crosslinker. The optimal conditions for the synthesis were a temperature of crosslinking at 70 °C, a ratio of 5:1 cationic starch: chitosan, and a ratio of 0.75 mL/g of catalyzer for 1.5 h. This system performed better in clarifying water at 5 °C and pH 5 with efficiencies around 88%; this provides a new alternative for flocculation in atypical systems (You et al., 2009). A similar composite was generated with starch and chitosan, but instead of the cationic starch, citrate-modified starch was used to further crosslink the chitosan to the starch molecules and generate a hydrogel with high water and saline adsorption. An important finding in this study was that the temperature used for the cross linkage had an effect on the properties of the swelling and tensile strength, increasing from 1.44 to 1.81 N/mm^2 for the latter and from 1940 to 2780% w/w from water adsorption when temperature changed from 100 to 120 °C. This behavior was similar in the saline solution, but larger mass loss was found in the foam generated at 120 °C, showing how the properties can be adjusted as desired by changing temperature conditions and maintaining pH, ratio, and solid-liquid proportions. One of the main advantages of this strategy is that the incorporation of the citrate as a crosslinker increased the thermal stability, water adsorption, and strength while decreasing weight loss compared to normal starch-chitosan composites (Salam et al., 2010).

As noted, starch is usually grafted to allow interactions with the other materials; for this, latexes are great materials to consider, as they can be used as an interface or as a point to graph from the polymer to form the composites. An example of the first strategy is a composite that was generated with starch grafted with poly-acrylic acid and CNC. This system aimed to be a fast

removal agent of methylene blue (MB), for which the pH was studied as the isoelectric point of the material changed as the concentration of CNC increased. The optimal CNC concentration for maximum adsorption was found to be 5% at a pH 5; this adsorption was modeled by Langmuir isotherms as 2240 mg/g with around 90% of total removal in 1 h. Reusability was also tested, finding that when it was immersed in a solution with pH 1, 60% of the adsorbed material was released and available for reusability; similar results were observed for the only grafted hydrogel that did not contain the CNC, but maximum adsorption was only of 2040 mg/g (Gomes et al., 2015). When sodium humate was used for the composite instead of CNC, the obtained system was able to form complexes with Cu(II). Herein different added percentages were tested (0, 5, 10, 15, and 20); from these, the best performance was found in the hydrogel containing 5% in a pH range of 2.7 to 5 and a maximum adsorption capacity modeled by Langmuir isotherm of 2.83 mg/g, which decreased as the content of sodium humate increased, which also gave some support to the hypothesis that the adsorption mechanisms were ion-exchange and chelation with the carboxylic groups. Lastly, regeneration was evaluated with 0.1 M NaOH, which, similar to the adsorption, was better in hydrogels containing sodium humate. Adsorption even improved after the first cycle, but after 4 cycles the efficiency had decreased by almost 40% (Zheng et al., 2010). Another system that used the grafted polymers as an interface was one with polyacrylamide grafted starch that contained clay (bentonite, kaolinite, or sercite). These were only tested for water absorption capacity, which reached 4000 g H_2O/g in 120 min, which apparently was mostly influenced by the presence of kaolinite, as the composite with only this clay absorbed almost 2500 g/g on its own but needed the three to enhance swelling (J. Wu et al., 2000).

Meanwhile, the “grafted from” approach can use different monomers to obtain sidechains with different properties and surface interactions. For example, aniline was used to form a hydrogel

for the removal of reactive dyes, Reactive Black 5 (RB, $C_{26}H_{21}N_5Na_4O_{19}S_6$, PubChem CID: 44134920) and Reactive Violet 4 (RV, $C_{20}H_{16}CuN_3Na_3O_{15}S_4$, PubChem CID: 129818966). The composite was able to remove 99% of RB and 98% of RV at pH 3 from solutions with 0.5 mM of the dyes; higher pH resulted in lower adsorption efficiency, with only 65% at pH 9. This was explained by the dissociation of the sodium from the sulfur groups at low pH, increasing the adsorption. When isotherms were performed, the Toth model fit the data better than the Langmuir or Freundlich, giving maximum adsorption capacities of 808 mg/g of RB and 667 mg/g of RV. A benefit of this study is an adsorption study done with a dye bath effluent containing RB (0.5 mM), RV (0.5 mM), sodium chloride (355 mM), sodium carbonate (61 mM), sodium hydroxide (6.5 mM), and acetic acid (6.5 mM) with pH 5, which is closer to a mixture that could represent a real scenario. With this solution, the removal efficiency was 87% and the isotherm fit into a modified Freundlich model, which changed the concentration term for an absorbance term; this gave an adsorption capacity of 1.97 mg/g. Finally, desorption was tested for reusability with a 0.1 M NaOH solution, which was 93% for RV, 94.2% for RB, and only 89.4% for the dye solution; when tested again for sorption, a reduction of 4% was observed, which is considered negligible, showing the good performance of the composite which is inexpensive and eco-friendly (Janaki et al., 2012). Similarly for dye adsorption, N,N-Diethylamino ethyl methacrylate was grafted from starch to remove Direct Red 81 (DR, $C_{29}H_{19}N_5Na_2O_8S_2$, PubChem CID: 9570117). Different grafting yields were tested, and the best one had a 50% yield, with an adsorbent concentration of 2.5 g/L and pH 1, obtaining a 95.6% efficiency after 50 min; the isotherm was modeled by Langmuir, giving a maximum adsorption capacity of 112 mg/g (Abdel-Halim, 2013).

Table 1.6. Starch-derived Materials and Pollutants Adsorbed

Material	Pollutant	Capacity (mg/g)	Regeneration	Reference
C6-carboxylated starch hydrogel	Cu(II)	128.26		Chauhan *et al.* 2010
Starch NiFe-LDH composite	Methyl orange	358.42	0.1 M NaOH	Zubair *et al.* 2018
Carbon nanotubes-starch/iron oxide	Methylene blue	94		Chang *et al.* 2011
	Methyl orange	327.33		
Starch-g-polyacrylic acid	Methylene blue	2043	H_2O pH 1	Gomes *et al.* 2015
Starch-g-polyacrylic acid/CNC		2236		
Starch-g-polyacrylic acid/sodium humate	Cu(II)	2.83	0.1 M NaOH	Zheng *et al*. 2010
Aniline/starch	Reactive black 5	808.11	0.1 M NaOH	Janaki *et al.* 2012
	Reactive violet 4	667.09		
Starch-g-N,N-Diethylamino ethyl methacrylate	Direct red 81	112		Abdel-Halim *et al.* 2013
Starch/Polyvinyl alcohol	Fe(II)	37.07	2 M HCl	Chowdhury *et al.* 2015
	As(III)	22.11	2 M NaOH	

"Grafting from" can also be used for metal removal; for example, polyvinyl alcohol was used in different starches, wheat-flour, rice-powder corn-starch, and maize-starch. The corn-starch composite performed best in the adsorption of Fe(II) and As(III) with 37.1 and 22.1 mg/g, respectively, and was reused for up to 3 cycles with efficiencies between 95 and 88%; herein, a 2 M HCl solution was used for Fe(II) desorption and a 2 M NaOH solution for As(III). Also, this composite presented 600% swelling when placed in water, which helped when tests of metals adsorption were performed using neutral pH and concentrations of 100 mg/L were given using

0.5 g of the sorbent; herein, adsorptions were of ~20, 22, 37, 7.5, 18, 4, and 22 mg/g for Cr(VI), Mn(II), Fe(II), Ni(II), Cu(II), Pb(II), and As(III), respectively (Chowdhury et al., 2015).

As presented, starch is a low-cost option for the development of hydrogels, with high water adsorption and pollutant removal capacity. Simple chemistry can be used to adjust the surfaces generated and improve composite interactions for chelation and adsorption of metals and dyes, respectively.

1.5.Cyclodextrins

Cyclodextrins are cyclic oligosaccharides formed by α-1,4-glucopyranose units (Fig. 1.7), that have inherent properties of biocompatibility and non-toxicity. These cyclic molecules are obtained by the enzymatic degradation of starch by cyclodextrin glucanotransferase (CGTase) enzyme, which can result in structures containing six (α), seven (β), or eight (γ) units (del Valle, 2004; Kurkov & Loftsson, 2013; Villiers, 1891).

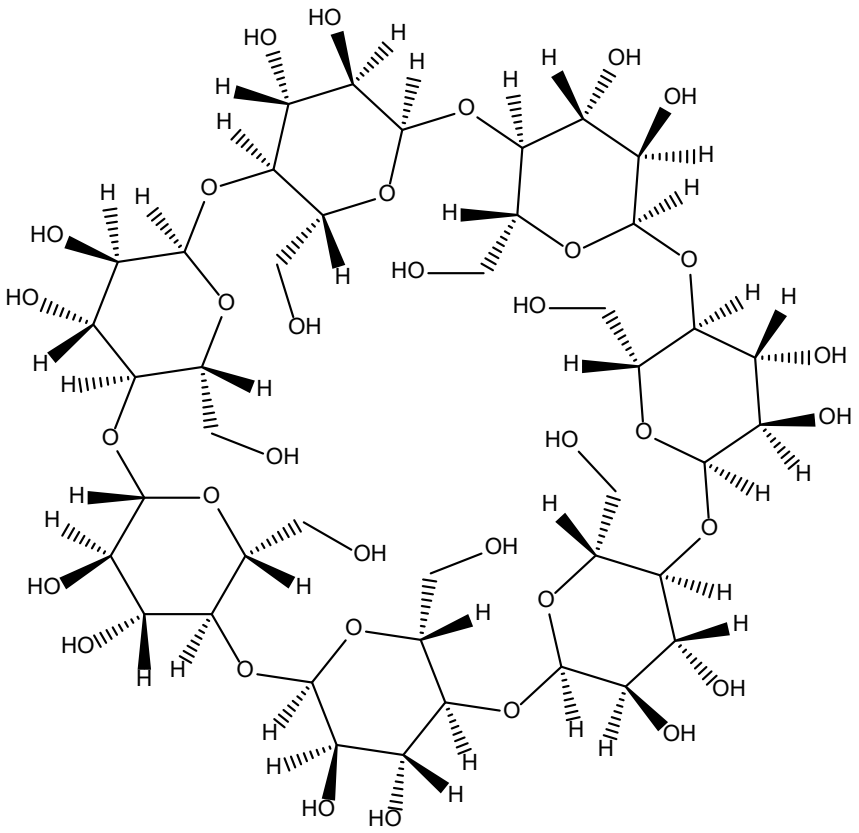

Figure 1.7. Structure of β-cyclodextrin

The glucose units here are spatially immobilized in a $^4C_1$-chair conformation, which gives the structure the shape of a truncate cone with an internal cavity with diameters between 6 to 10 Å. Because of this conformation, the primary hydroxyl groups end up oriented to the exterior of the cone, making the exterior part highly hydrophilic and the interior hydrophobic. Meanwhile, the secondary hydroxyls are on the edges of the cavity forming H-bonds between them, leading the non-bonding electron pairs to be oriented towards the cavity interior, conferring a Lewis-like base character (Szejtli *et al.* 1982; Szejtli 1998; Cova *et al.* 2018).

Due to the structure of cyclodextrin (CD), it has between three to five times more resistance to hydrolysis than linear polymers, and as the hydroxyl groups are used to form the H-bond, they also have a lower solubility. The number of units has an impact on these properties, as well; for

example, β-CD is known to be more rigid and less soluble than the other two possible CDs, as they use all the secondary oxygens to stabilize the ring compared to the α-CD, which only forms 4 of 6 possible bonds and is more rigid because of the seven units, which make it less flexible and more planar than γ-CD. Similarly, the half-life of the structure of β-CD is approximately 15 h in an aqueous solution at 70 °C and pH 1.1; this is 1.5 times greater than γ-CD and 1.5 times less than α-CD (Kurkov & Loftsson, 2013).

As previously mentioned, the structure of the CD provides a hydrophobic cavity that can form highly stable host-guest complexes with alkyl chains or aromatic compounds. These complexes are stabilized by different electrostatic Van der Waals, charge-transfer interactions, and other H-bonds that could be formed between the guest molecules and the oxygens in the ring or the primary hydroxylic groups. All of these interactions can then be used for the improvement of solubility, capture, or control of organics, volatiles, and antioxidant molecules (Cova et al., 2018; X. Guo et al., 2005; Kurkov & Loftsson, 2013; L. Liu & Guo, 2004; Saenger & Steiner, 1998). The high structural and thermal stability of β-CD has made it the predominant cyclodextrin on the market, causing the production cost to go down and increasing the availability of derivatives with almost 86% of the market in medicine (Kurkov & Loftsson, 2013).

For environmental applications, the low molecular weight of β-CD (1135 Da) makes it important to generate composites for its use in aqueous media. One of the most widespread approaches is the generation of a polymer with epichlorohydrin or other agents capable of esterification (Gidwani & Vyas, 2014; Morin-Crini et al., 2018; Morin-Crini & Crini, 2013). The main objective when crosslinking is to increase size and efficiency without loss by steric effects. An example of a study using this analysis is one that a Canadian group performed where 5 types of crosslinker agents were used to examine the effectiveness in decolorizing a solution with

phenolphthalein ($3.6*10^{-5}$ M in 0.1 M sodium hydrogen carbonate buffer pH 10.5); the crosslinkers used were epichlorohydrin (EP), sebacoyl chloride (SCL), terephthaloyl chloride (TCL), glutaraldehyde (GLU), and poly(acrylic acid) (PAA). From these, the TCL with proportions 1:1, the GLU 1:3, and 1:15 molar ratio was the one with a better performance, with 72.4, 68.7, and 64.6 % of accessible β-CD in the polymer, respectively. Even when accessibility varied between the systems, ΔG from all copolymers ranged between -27.6 and -30.9 kJ/mol, demonstrating the favorable complex formation between the aromatic compound and the β-CD (Mohamed et al., 2012). Another group tried tetrafluoroterephthalonitrile as a linker and compared it with polymers with epichlorohydrin and activated carbon; this system was tested for the adsorption of 0.1 mM bisphenol-A solutions. The system generated with high surface porosity had an efficiency of 80%, sustaining it for 5 cycles, while the same polymer without a porous formation had an efficiency around 30%, like the epichlorohydrin-linked system. The activated carbon systems ranged between 60 to 10% efficiency. For a better understanding of the binding, the porous system was tested to adsorb other compounds, bisphenol S, 2-naphthol, 1-naphthyl amine, 2,4-dichlorophenol, metolachlor, ethinyl oestradiol, and propranolol hydrochloride. In all of these, removal efficiencies ranged from 70 to 90%, outperforming activated carbon and EP-CD (Alsbaiee et al., 2016).

Differences in the CD can also modify the adsorption behavior of molecules in the polymer with the same crosslinker. For instance, the use of 2-hydroxypropyl β-CD (HPCDP), random methyl-β-CD (RMCDP), or a blend with β-CD polymer for the removal of pollutants show different removal efficiencies depending on the selected pesticide when spheres with EP were prepared. The 4 systems (RMCDP, HPCDP, βCD, and the Multiplex) were studied for adsorbance of 10 aromatic pesticide (fomesafen, bromacil, simazine, atrazine, fenamiphos, fipronil, benalaxyl,

butene-fipronil, pretilachlor, and butachlor) and all fit Langmuir isotherms. The mixture of the different CD proved to be the most effective, with maximum adsorption capacities greater in almost all cases but the benalaxyl, where HPCDP had a maximum of 28.0 mg/g, while the multiplex had 22.7 mg/g (H. Liu et al., 2011). When compared to the pristine polymers, the addition of moieties did not always help to improve, as βCD had a better adsorption of fomesafen, simazine, and pretilachlor, but HPCDP was better for bromacil, fenamiphos, fipronil, and benalaxyl, leaving the rest working better with the random methylated material. This means that interactions are guided by different mechanisms, and the inclusion of aliphatic moieties can improve adsorption and to form better complexes when the surface is chemically uneven.

The main focus of the use of these hydrophobic materials for water treatment in studies is when dyes and other aromatic structures are to be removed. For example, in a study in 2008, CDP with EP was used to eliminate Basic Blue 3 (BB3, $C_{33}H_{32}ClN_3$, PubChem CID: 17407), basic violet 3 (BV3, $C_{25}H_{30}ClN_3$, PubChem CID: 11057), and basic violet 10 (BV10, $C_{28}H_{31}ClN_2O_3$, PubChem CID: 6694) from standard solutions with concentration 40 mg/L. These polymers had a maximum adsorption capacity of 42.4, 35.8, and 53.2 mg/g, respectively, when modeled by Langmuir isotherms. A clear relationship between the adsorbent mass (that allows and estimation of the number of hydrophobic cavities available) with the removal of pollutants was found. This suggests a chemisorption of the dyes from the hydrophobic cavities in the polymer (Crini, 2008). Similarly, azo dyes with more elaborate structures were studied, but with polymers were crosslinked with 4,4-methylene-bisphenyldiisocyanate (MDI) or hexamethylenediisocyanate (HMDI). Generally, the one with the phenolic groups had a better adsorption capacity than the linear one, probably due to the increase of immobilization by π-π interactions; the tested dyes were Evans Blue (EB, $C_{34}H_{24}N_6Na_4O_{14}S_4$, PubChem CID: 9566057) and Chicago Sky Blue (CSB,

$C_{34}H_{24}N_6Na_4O_{16}S_4$, PubChem CID: 5359775). The ideal pH for these systems was 3, and the maximum adsorption capacities were 9.6 and 7.6 mg/g for the HMDI derivate and 10.59 and 12.09 mg/g respectively for the MDI polymer (Yilmaz et al., 2010).

As observed, the linkers can provide advantages in the interactions with the pollutants, but those linkers can also serve as points to further design the polymer. For example, four polymers were generated using toluene diisocyanate (TDI), isophorone diisocyanate (IPDI), hexamethylene diisocyanate (HMDI), and carbonyl diimidazole (CDI) as a cross-linker and then the material was doped with TiO_2 for the photocatalytic reaction of the adsorbed pollutants. From this, the polymer that used TDI had the best retention of total organic carbon (TOC), with a maximum of 93% (Khaoulani et al., 2015).

Another commonly used approach to increase molecular weight and facilitate the recovery of the CD from solutions is the generation of a composite with magnetic particles, especially Fe_3O_4 nanoparticles, as they are easily synthetized and can be adsorbed to the β-CD without changing their potential to eliminate pollutants. An example of the use of this system was to degrade bisphenol-A (BPA) and malachite green (MG); for these experiments, 100 mg of the composite were immersed in solutions with 20 mg/L of BPA or 9.27 mg/L of MG. The system was able to photodegrade 70% of BPA, and when reused 6 times, degradation decreased to 64.2%; meanwhile for GM, almost a complete removal was obtained, decreasing to 90.1% after 6 cycles (Kumar et al., 2015). Other experiments were also performed to test the adsorptions of different organics and metal ions. For example, 1-naphthylamine (60 mg/L) was tested at different pH, ionic strength, concentrations, and β-CD content; the ideal conditions were between 5.5 and 7.5, with ionic strength < 0.05, initial sorbent concentration of 1 g/L, and β-CD content > 6.84. Different concentrations were tested and fit the Langmuir isotherm, with a maximum adsorption

concentration of 144.7 mg/g and thermodynamic parameters of -4.7 kJ/mol for ΔG, 50.6 j/mol K for ΔS, and ΔH of 10.7 kJ/mol at 303 K. In this same article, adsorption of Cu(II) was tested in solutions with an initial concentration of 10 mg/L; when the pH was varied, ideal conditions were found to be at pH ≥ 8, and recycling was completed 5 times after washing with HNO_3 (pH~2), decreasing from an initial adsorption of 9.04 mg/g to 8.6 mg/g. When these data were fit to the Langmuir model, the maximum adsorption capacity was 9.04 mg/g, the same as achieved in the experimental data (Jie Li et al., 2013). Similarly, 1-naphthol and Co(II) were tested separately and in a mixed solution. In this set of experiments, the grafted amount of β-CD was 115 mg/g, and concentrations of 1-naphthol and Co(II) were 50 mg/L and 10 mg/L, respectively. For Co(II), optimal conditions were: pH above 8.3, 2 h of contact, and a maximum adsorption capacity 38.0 mg/g at 293 K; for 1-naphthol, optimal contact time was of 4 hours, at a pH of 9, with an effect on adsorption diet to ionic strength after this pH, presenting a better adsorption at 0.7 mol/L NaCl, the fitting into the Langmuir model by the isotherms with a maximum adsorption capacity of 235.1 mg/g at 293 K. Probably the most interesting analysis of this paper is the effect of each of these on the adsorption of the CD-nanoparticle. It was observed that the concentration of the organic had an effect on the adsorption of Co(II), peaking when 80 mg/L of 1-naphthol was present; this is attributed to the adsorption of the hydrophobic part of the alcohol into the cavities, while the hydroxyl groups were available to form active sites with the ion. In lower concentrations, the tri-complex formation was not saturated in the surface, while at higher concentrations of naphthol, the complex naphthol-Co(II) were formed in solution, decreasing the capacity to adsorb into the material. On the other hand, changes in the concentration of Co(II) did not affect the capacity of the 1-naphthol to get captured by the CD, sustaining the idea of the capture of the alcohol by hydrophobic interactions (X. Zhang et al., 2014).

Another element that has been shown to adsorb into the magnetic CD composite is the rare earth Eu(III); this was tested at pH 3.5 and 5, where the ionic species were present for adsorption and using an initial concentration of $2.3*10^{-4}$ mg/L. Also, different ionic strengths were tested observing no significant effect due to the change of salt concentrations. When the adsorption isotherms were fit to a Langmuir model, the maximum adsorption capacities were calculated as $3.31*10^{-4}$ and $5.49*10^{-4}$ mg/g for pH 3.5 and 5, respectively; these values were highly efficient considering their price and eco-friendly production compared to clay and other commercial sorbents (Z. Guo et al., 2015).

Like the other polymers, the addition of CD moieties helps to extract heavy metals from wastewaters. For example, a carboxymethyl-β-CD was polymerized with EP, used to coprecipitate with Fe_3O_4 nanoparticles, and used to extract Pd(II), Cd(II), and Ni(II). The system was shown to be dependent on pH, ionic strength, and temperature; optimal pH seemed to be > 5.5 for all cases with higher temperatures, and ionic strength decreased the adsorption capacity. The Langmuir model fit the isotherms through maximum adsorption capacities of 64.5, 27.7, and 13.2 mg/g for Pd(II), Cd(II), and Ni(II), respectively. When reversibility was studied, three eluent solutions were tested: 0.01 M nitric acid, 0.1 M Na_2EDTA, and 0.02 M phosphoric acid; nitric acid and EDTA were better eluents for Pb(II), and the phosphoric acid for Ni(II). Overall, Pb(II) was easier to remove from the sorbent, followed by Cd(II), and lastly Ni(II). Pb(II) was able to be reused for adsorption for up to 4 cycles without significant loss, proving to be an easy, convenient, and efficient nanocomposite for the removal of ions (Badruddoza et al., 2013).

Although Fe_3O_4-CD is a nanomaterial with high surface area, it can be improved when the composite is built-up with other high surface colloidal particles, such as silica or graphene. When this was studied and tested for microcystin-LR adsorption, a cyanotoxin related to liver cancer

consisting of a 7 amino acid cycle, it was observed that any composite with α, β, or γ-CD adsorbed into the materials between 16 to 19% w/w, but only the one on the graphene surface had a good capture performance, with removal capacities of 80, 140, and 160 mg/g for α, β, and γ-CD, respectively (Arjyabaran Sinha & Jana, 2015). The main contribution of this paper is the use of cyclodextrin to remove complex molecules, such as microcystin-LR in a high surface nanomaterial, combining specific properties of each material: complex formation with CD and microcystin, high surface area by the graphene and the magnetic properties for the removal of the Fe_3O_4 nanoparticles.

Just like graphene, multiwalled carbon nanotubes (MWCNT) can be used to support β-CD and increase the contact area; this grafting is achieved in reactors where only N2 atmosphere is permitted while heating, avoiding its degradation or the formation of oxides. This high surface material was used to remove polychlorinated biphenyls (PBCs) from a solution with an initial concentration of 4.1 mg/L, pH 3.5, ionic strength 0.01 M $NaClO_4$, and *T* of 20 °C; the PBCs tested were 4,4'-dichlorobiphenyls (4,40-DCB) and 2,3,3'-trichlorobiphenyl (2,3,30-TCB) that when fitted to the Langmuir isotherm models had a maximum adsorption capacity of 261 and 235 mg/g, respectively. The effects of pH and ionic force were also tested but were found to have little to no influence on the adsorption between pH 3 to 10 and concentrations ranging from 0.001 to 0.05 M (D. Shao et al., 2010). Similar to the previous case, the MWCNT can be further composited with other nanoparticles, such as iron oxides, to enhance adsorption and add properties to the sorbent like magnetic properties for its separation. In one study, this was used to eliminate 1-naphthylamine; when fitted to a Langmuir model, the maximum adsorption capacity of the system was 200 mg/g. It was also found that pH had an effect on the adsorption, as it was only when the pH was higher than the pK_a that there was significant adsorption was observed, especially after pH

5.5. Interestingly, when a higher initial concentration was used (60 mg/L instead of 32 mg/L), a decrease in adsorption was observed after pH 8.5, which was explained due to an electron-donor-acceptor interaction and Lewis acid-base interaction between the CNT and the 1-naphthylamine after this pH value (Hu et al., 2011).

Another alternative to increase both contact area and recovery after the adsorption, is the use of polymer fibers as substrates to immobilize the CD. Following the scope of the review, natural fibers have been used for their abundancy, mechanical properties, and high surface area (Dong et al., 2014; Ghorpade et al., 2017; N. Lin & Dufresne, 2013; Medronho et al., 2013; Prabaharan & Gong, 2008; Ruiz-Palomero et al., 2015; Lingzhi Zhang et al., 2013). Cellulose is the most abundant polysaccharide and can be used to enhance the water adsorption of materials as well as for an easy recovery of hydrogels or films. An example of this composite using nanofibrils was used for the adsorption of phenol; herein, adsorption was done using different structures (fibers, membranes, and aerogels) with different initial weight concentrations (1 to 3%). From these, the best performance was obtained with the 3% aerogel, as the porosity of the obtained material increased significantly the surface area, favoring the adsorption kinetics. This result was more apparent when isotherms were made with the 3% materials, where the maximum adsorption was of 13.9 mg/g for the aerogel, 3.67 mg/g for the membrane, and 5.93 mg/g for the fibers. Adsorption also decreased as the temperature increased from 20 to 40 °C, and when the pH was above 9, dependency of the adsorption to these parameters was shown (F. Zhang et al., 2015).

Another method to obtain high surface materials is by electrospinning, which generate mats that can also be modified with CD to adsorb pollutants; an example of this was done by electrospinning regenerated cellulose acetate fibers which were modified with CDs (α, β, and γ) by citric acid and sodium hypophosphite hydrate (SHPI) and were used to adsorb toluene. This

regenerated material had an average diameter distribution between 226.5 and 364.5 nm, with the best adsorption rate given by the γ-CD modified fibers with 86% in 180 min at 60 °C (Yuan et al., 2017).

As previously mentioned, cellulose is easily modifiable to adsorb metals; therefore, if these modifications are partnered with cyclodextrin, a material with wider adsorption capability can be obtained. To verify this, cellulose powder was grafted with glycidyl methacrylate monomers, with β-CD, and quaternary ammonium groups and used to remove Cr(VI) form aqueous solutions. When the Langmuir isotherm was modeled, a maximum adsorption capacity of 61.0 mg/g was found, with an optimum pH range between 3.5 to 6 and a slight decrease in adsorption when other ions were present between 1 to 7% depending on the ion diversity. Reusability was possible using sodium hydroxide (0.5 mg/L) as a desorption agent for up to 5 cycles with minimal loss of efficiency (Y. Zhou et al., 2011).

One way to improve the adsorption is to promote the exposure of the cavity from β-CD; for this, different alternatives have been tested, but the use of "click" chemistry stands out as it is uses aqueous and green chemistry. For example, a membrane from acetate nanocellulose – azide-β-CD was electrospun and used to remove phenanthrene; in this set of experiments, it was observed that the grafting of the CD modified the spinnablility of the nanofibers, as more roughness was seen in the microscopies, but the final membrane was still obtained with continuous fibers. When tested for the adsorption of the aromatic compound, it was observed that the final concentration after 480 h was 5% for the modified membrane and 15% for the unmodified membrane, demonstrating the enhanced activity due to the hydrophobic cavities attached with the β-CD (Celebioglu et al., 2014).

A reduction of the modification steps can be done when chitosan is used, due to its advantage of keeping the desired properties of polysaccharides while a nitrogen is already placed in the structure for use as an anchoring point for a modified cyclodextrin. This application has been used to test the adsorption of methyl orange; for the design of the material, maleoyl chains were used as linkers between the chitosan and CD, followed with glutaraldehyde to generate a stable structure. The adsorption was made using 10 mg of the adsorbent with 50 mL of solution with different concentrations, pH, and temperature from which it was found that the optimal conditions were at pH 5, room temperature (25 °C), and dosage of 200 mg/L; when this was fitted into a Langmuir isotherm, the maximum adsorption capacity was of 392 mg/g, one of the highest reported (Y. Jiang et al., 2018). Even though this system showed good performance, higher surface area can be obtained when the modified chitosan is attached to another material; examples of this are the use of a similarly prepared chitosan/β-CD attached to magnetic nanoparticles and graphene for it removal and stabilization. This was tested to remove methylene blue, which had a better performance at higher pH values, reaching a maximum adsorption capacity calculated at 84.3 mg/g (L. Fan et al., 2013). Another example was the adsorption of β-CD/chitosan to cellulose yarns generated by spinning; however, in this case, the β-CD was previously TEMPO-oxidized and immobilized to chitosan that was available in the surface of the yarn by EDC/NHS. This system was used to adsorb 17 α-ethinyl estradiol (EE2) and followed by surface plasmon resonance (SPR) and by UV-Vis measurements with solutions at pH 7.4 in a 50 mM phosphate buffer with concentrations of 0, 0.1875, 0.375, 0.75, and 1.25 μg/mL; the system presented an immobilization of EE2 in SPR of 0.15 degrees, which correspond to an adsorption of 2.5 mg/g (Orelma et al., 2018).

Synthetic polymers can also provide some properties that can be explored for other applications; similar to the regenerated cellulose (Yuan et al., 2017), electrospun polyethylene terephthalate (PET) mats were modified with different cyclodextrins and were tested for the adsorption of phenanthrene, with no significant difference between CD efficiency. However, the addition of them was found to enhance the removal of the compound from aqueous solutions (Kayaci et al., 2013). Poly(methyl methacrylate) was also electrospun with β-CD in different concentrations (10, 25, 50% w/w) without any chemical modification; these mats were then tested for the adsorption of organic vapors (styrene, toluene, and aniline) which was later quantified by direct pyrolysis mass spectrometry. In all cases, changes in the degradation were only observable when CD was present, and the intensity increased as the percent grafted increase, assuring the interaction between the oligosaccharide and the solvents. Interestingly, the ways they interact differ in some degree, as aniline interacted in only one degradation peak, which sustains the theory of inclusion complex formation. Styrene had a broader interaction with β-CD, possibly due to inclusion complex formation, but also due to adsorption mechanism. Finally, toluene had two temperature peaks, which indicates also the formation of complex and some other kind of interactions (Uyar et al., 2010).

As a last example, poly(urethane) was also copolymerized with β-CD and used to test the sorption of chlorinated aromatic compounds, which are a main source of concern; the tested compounds were pentachlorophenol (PCP, C_6Cl_5OH, PubChem CID: 992), 2,4-dichlorophenol ($C_6H_4Cl_2O$, PubChem CID: 8449), and 2,4-dichlorophenoxy acetic acid ($C_8H_6Cl_2O_3$, PubChem CID: 1486). Here, the cross-linkage was done using two components: methylenediphenyl diisocyanate (MDI) and dicyclohexylmethane-4,4’-disiisocyante (CDI), which apparently have some differences when the isotherms were generated at 295 K and pH 9. For this case, the Sips

isotherm model, which is a corrected version of the Langmuir isotherm, was used. For pentachlorophenol, the maximum adsorption capacities were 14.9 and 22.9 mg/g for the CDI and MDI crosslinked material; the low capacity was probably due to the size of the pollutant compared with the cavity of β-CD. The capacities for the other aromatics were: for 2,4-dichlorophenol, 98.9 and 6.4 mg/g for MDI and CDI, respectively, and for 2,4-dichlorophenoxy acetic acid, 119.3 and 250.8 mg/g for the same polymers (Wilson et al., 2011). All the above examples show how cyclodextrins can be widely used for the removal of pollutants, especially because they possess the capacity to capture aromatic molecules in hydrophobic cavities.

Table 1.7. Cyclodextrin-derived Materials and Pollutants Adsorbed

Material	Pollutant	Capacity [mg/g]	Regeneration	Reference
2-hydroxypropyl β-cyclodextrin with EP	Benalaxyl	27.99		Liu *et al.* 2011
2-hydroxypropyl/ methyl/ pristine β-cyclodextrins with EP		22.74		
Cyclodextrin polymer with EP	Basic blue 3	42.4		Crini *et al.* 2008
	Basic violet 3	35.8		
	Basic violet 10	53.2		
Cyclodextrin polymer with MDI	Evans blue	10.59		Yilmaz *et al.* 2010
	Chicago sky blue	12.09		
Cyclodextrin polymer with HMDI	Evans blue	9.58		
	Chicago sky blue	7.63		
β-cyclodextrin with Fe_3O_4 nanoparticles	Naphthylamine	144.74		Li *et al.* 2013
	Cu(II)	9.04		
	1-naphthol	235.06		Zhang *et al.* 2014c
	Co(II)	38.03		
	Eu(III)	5.49 * 10^-4		Guo *et al.* 2015

Carboxymethyl β-cyclodextrin polymer with EP	Pb(II)	64.5	0.01 M HNO_3/ 0.1 M Na_2EDTA /0.02 M H_3PO4	Badruddoza *et al.* 2013
	Cd(II)	27.7		
	Ni(II)	13.2		
α-cyclodextrin/ graphene/ Fe_3O_4	Microcystin-LR	80		Sinha and Jana, 2015
β-cyclodextrin/ graphene/ Fe_3O_4		140		
γ-cyclodextrin/ graphene/ Fe_3O_4		160		
Multiwalled carbon nanotubes/ β-cyclodextrin	4,4'-dichlorobiphenyl	261		Shao *et al.* 2010
	2,3,3'-trichlorobiphenyl	235		
Multiwalled carbon nanotubes/ β-cyclodextrin/ iron oxide	1-naphthylamine	200		Hu *et al.* 2011
β-cyclodextrin/ cellulose nanofibers	Phenol	5.93		Zhang *et al.* 2015a
β-cyclodextrin/ cellulose aerogels		13.93		
β-cyclodextrin/ cellulose membranes		3.67		
Cellulose powder-g-glycidyl methacrylate/ ammonium/ β-cyclodextrin	Cr(VI)	61.05	NaOH	Zhou *et al.* 2011a
Chitosan/ cyclodextrin/ glutaraldehyde	Methyl orange	392		Jiang *et al.* 2018
Chitosan/ cyclodextrin/ graphene/ magnetic nanoparticles	Methylene blue	84.32		Fan *et al.* 2013
	Pentachlorophenol	22.9		Wilson *et al.* 2011

Polyurethane/ cyclodextrin with MDI	2,4-dichlorophenoxy acetic acid	119.26		
	2,4-dichlorophenol	98.94		
Polyurethane/ cyclodextrin with CDI	Pentachlorophenol	14.38		
	2,4-dichlorophenoxy acetic acid	250.84		
	2,4-dichlorophenol	6.42		

1.6.Conclusions

In conclusion, the recent development of adsorbents from polysaccharides seems to be a feasible approach for generating materials of low cost and high performance with a wide variety of possible functionalization that can further improve the interactions between pollutants and fibers. Among the different polysaccharides, cellulose and chitosan have been the most studied, which derives from their wide availability and the deep knowledge on processing technologies held by the scientific community. Furthermore, surface modification of these polysaccharides for adding new functional groups with little environmental impact, such as TEMPO oxidation, has been the method of choice for modification of the polysaccharide surfaces and improvement of the targeting of water contaminants. When surface modification using greener chemistry is not an option, the generation of composite materials by combining polysaccharides with other polymers containing the functional groups is a low-cost approach that can provide great impact in removing the wide variety of pollutants, such as metallic and organic ions, pesticides, dyes, dissolved organic pollutants such as toxins, and oils.

The formation of composites with other polysaccharides (*i.e.* cyclodextrins), nanoparticles, clays, or even other complex polymers can further increase the substrate surface area, while adding additional functionalities that will increase their selectivity, such as catalytic properties.

The low-cost, reusability and extended life cycle of polysaccharide materials are key points that all research must consider when developing composites, in particular for their utilization in water remediation. Even though some synthetic polymers have shown improved potential to be utilized for the uptake of water pollutants, the complexity and toxicity, as well as the high cost of the involved chemistry has made them less attractive. Additionally, most of them involve organic solvents as media for polymer functionalization, which offers more reasons to opt for the natural polysaccharides as the option of choice.

The main challenge that polysaccharide-derived materials must address is the recycling of the adsorbent, as well as the manufacturing cost. This could be addressed by either slowing down degradation or increasing the pollutant uptake per cycle. On the one hand there is potential to increase the manufacturer's profitability by adding value to the capacity of the manufacturer. On the other hand, it is possible to increase the material's life for the end users.

Regarding cost analysis of composite materials based in natural polymers, it can be argued that production costs will be higher in the case of composite materials and/or modified polysaccharides. However, efforts are being made to lower these prices on a daily basis based on optimization of current production methods. Furthermore, the superior performance of the (nano) composites materials open a clear pathway in which the captured pollutant can be purified or re-integrated to upstream production, providing some return in the process besides the obvious environmental benefits of the water quality improvement. For these reasons, natural fibers are exiting materials to develop and improve so that the commercial application of versatile systems

with low cost that improve water quality and increase life expectancy can be possible in the near future.

1.7 Future work

Based on the environmental stress that cyanotoxins will present to the Auburn City area, this dissertation will focus mainly on the removal of microcystin-LR. Thus, after this literature review, cyclodextrins -in specific β-cyclodextrin- were used due to its capacity to form complexes with the toxin. However, as it was mentioned above, cyclodextrin is highly soluble and therefore need to be immobilized for its use in water treatment.

As cellulose is the most abundant and can be structured into different films, aerogels or hydrogels this material was selected as the primary material to conjugate with β-cyclodextrin. Finally, chitosan was used as intermediary between cellulose and cyclodextrin. As mentioned, chitosan has amino groups that allowed to use green chemistry to immobilize cyclodextrin, and due to its β-glucan nature, adsorption onto cellulose can be done without energy inputs.

An edited version of this chapter was published as:

Gomez-Maldonado D, Vega Erramuspe IB, Peresin MS (2019) Natural Polymers as Alternative Adsorbents and Treatment Agents for Water Remediation. BioResources 14:4. https://doi.org/10.15376/biores.14.4.Gomez-Maldonado

1.7. Literature Cited:

Abdel-Halim, E. S. (2013). Preparation of starch/poly(N,N-Diethylaminoethyl methacrylate) hydrogel and its use in dye removal from aqueous solutions. *Reactive and Functional Polymers*, *73*(11), 1531–1536. https://doi.org/10.1016/j.reactfunctpolym.2013.08.003

Abdolali, A., Guo, W. S., Ngo, H. H., Chen, S. S., Nguyen, N. C., & Tung, K. L. (2014). Bioresource Technology Typical lignocellulosic wastes and by-products for biosorption process in water and wastewater treatment : A critical review. *Bioresource Technology*, *160*, 57–66. https://doi.org/10.1016/j.biortech.2013.12.037

Adeleye, A. S., Conway, J. R., Garner, K., Huang, Y., Su, Y., & Keller, A. A. (2016). *Engineered nanomaterials for water treatment and remediation : Costs , benefits , and applicability*. *286*, 640–662.

Algarra, M., Isabel, M., Alonso, B., María, C., Casado, J., & Benavente, J. (2014). *Characterization of an engineered cellulose based membrane by thiol dendrimer for heavy metals removal*. *253*, 472–477.

Ali, I. (2012). New generation adsorbents for water treatment. *Chemical Reviews*, *112*(10), 5073–5091. https://doi.org/10.1021/cr300133d

Ali, I., & Gupta, V. K. (2007). Advances in water treatment by adsorption technology. *Nature Protocols*, *1*(6), nprot.2006.370. https://doi.org/10.1038/nprot.2006.370

Alsbaiee, A., Smith, B. J., Xiao, L., Ling, Y., Helbling, D. E., & Dichtel, W. R. (2016). Rapid removal of organic micropollutants from water by a porous β-cyclodextrin polymer. *Nature*, *529*(7585), 190–194. https://doi.org/10.1038/nature16185

Archimandritis, A. S., Papadimitriou, T., Kormas, K. A., Laspidou, C. S., Yannakopoulou, K., &

Lazarou, Y. G. (2016). Theoretical investigation of microcystin-LR, microcystin-RR and nodularin-R complexation with α-, β-, and γ-cyclodextrin as a starting point for the targeted design of efficient cyanotoxin traps. *Sustainable Chemistry and Pharmacy*, *3*, 25–32. https://doi.org/10.1016/j.scp.2016.02.001

Ayoub, A., Venditti, R. A., Pawlak, J. J., Salam, A., & Hubbe, M. A. (2013). Novel hemicellulose-chitosan biosorbent for water desalination and heavy metal removal. *ACS Sustainable Chemistry and Engineering*, *1*(9), 1102–1109. https://doi.org/10.1021/sc300166m

Badruddoza, A. Z. M., Shawon, Z. B. Z., Tay, W. J. D., Hidajat, K., & Uddin, M. S. (2013). Fe 3O 4/cyclodextrin polymer nanocomposites for selective heavy metals removal from industrial wastewater. *Carbohydrate Polymers*, *91*(1), 322–332. https://doi.org/10.1016/j.carbpol.2012.08.030

Benhouria, A., Islam, M. A., Zaghouane-Boudiaf, H., Boutahala, M., & Hameed, B. H. (2015). Calcium alginate-bentonite-activated carbon composite beads as highly effective adsorbent for methylene blue. *Chemical Engineering Journal*, *270*, 621–630. https://doi.org/10.1016/j.cej.2015.02.030

Bhowmik, K. L., Deb, K., Bera, A., Debnath, A., & Saha, B. (2018). Interaction of anionic dyes with polyaniline implanted cellulose: Organic π-conjugated macromolecules in environmental applications. *Journal of Molecular Liquids*, *261*, 189–198. https://doi.org/10.1016/j.molliq.2018.03.128

Bouhadiba, A., Belhocine, Y., Rahim, M., Djilani, I., Nouar, L., & Khatmi, D. E. (2017). Host-guest interaction between tyrosine and β-cyclodextrin: Molecular modeling and nuclear studies. *Journal of Molecular Liquids*, *233*, 358–363.

https://doi.org/10.1016/j.molliq.2017.03.029

Bouyahmed, F., Cai, M., Reinert, L., Duclaux, L., Dey, R., Youcef, H., Lahcini, M., Muller, F., & Delpeux-Ouldriane, S. (2018). A Wide Adsorption Range Hybrid Material Based on Chitosan, Activated Carbon and Montmorillonite for Water Treatment. *C*, *4*(2), 35. https://doi.org/10.3390/c4020035

Briggs, D., & Beamson, G. (1993). XPS Studies of the Oxygen 1s and 2s Levels in a Wide Range of Functional Polymers. *Analytical Chemistry*, *65*(11), 1517–1523. https://doi.org/10.1021/ac00059a006

Calcagnile, P., Caputo, I., Cannoletta, D., Bettini, S., Valli, L., & Demitri, C. (2017). *A bio-based composite material for water remediation from oily contaminants*. *134*, 374–382.

Camel, V., & Bermond, A. (1998). Review Paper the Use of Ozone and Associated Oxidation. *Water Research*, *32*(11), 3208–3222.

Carpenter, A. W., de Lannoy, C.-F., & Wiesner, M. R. (2015). Cellulose Nanomaterials in Water Treatment Technologies. *Environmental Science & Technology*, *49*(9), 5277–5287. https://doi.org/10.1021/es506351r

Celebioglu, A., Demirci, S., & Uyar, T. (2014). Cyclodextrin-grafted electrospun cellulose acetate nanofibers via “click” reaction for removal of phenanthrene. *Applied Surface Science*, *305*, 581–588. https://doi.org/10.1016/j.apsusc.2014.03.138

Chang, P. R., Zheng, P., Liu, B., Anderson, D. P., Yu, J., & Ma, X. (2011). Characterization of magnetic soluble starch-functionalized carbon nanotubes and its application for the adsorption of the dyes. *Journal of Hazardous Materials*, *186*(2–3), 2144–2150. https://doi.org/10.1016/j.jhazmat.2010.12.119

Chauhan, G. S., Guleria, L., & Sharma, R. (2005). Synthesis, characterization and metal ion sorption studies of graft copolymers of cellulose with glycidyl methacrylate and some comonomers. *Cellulose*, *12*(1), 97–110. https://doi.org/10.1023/B:CELL.0000049349.66326.5e

Chauhan, K., Chauhan, G. S., & Ahn, J. H. (2010). Novel polycarboxylated starch-based sorbents for Cu2+ ions. *Industrial and Engineering Chemistry Research*, *49*(6), 2548–2556. https://doi.org/10.1021/ie9009952

Chen, L., Zhu, J. Y., Baez, C., Kitin, P., & Elder, T. (2016). Highly thermal-stable and functional cellulose nanocrystals and nanofibrils produced using fully recyclable organic acids. *Green Chem.*, *18*(13), 3835–3843. https://doi.org/10.1039/C6GC00687F

Chen, P. Y., McKittrick, J., & Meyers, M. A. (2012). Biological materials: Functional adaptations and bioinspired designs. *Progress in Materials Science*, *57*(8), 1492–1704. https://doi.org/10.1016/j.pmatsci.2012.03.001

Cheng, H., Feng, Q., Liao, C., Liu, Y., Wu, D., & Wang, Q. (2016). Removal of methylene blue with hemicellulose/clay hybrid hydrogels. *Chinese Journal of Polymer Science*, *34*(6), 709–719. https://doi.org/10.1007/s10118-016-1788-2

Cho, D. W., Jeon, B. H., Jeong, Y., Nam, I. H., Choi, U. K., Kumar, R., & Song, H. (2016). Synthesis of hydrous zirconium oxide-impregnated chitosan beads and their application for removal of fluoride and lead. *Applied Surface Science*, *372*, 13–19. https://doi.org/10.1016/j.apsusc.2016.03.068

Chowdhury, M. N. K., Ismail, A. F., Beg, M. D. H., Hegde, G., & Gohari, R. J. (2015). Polyvinyl alcohol/polysaccharide hydrogel graft materials for arsenic and heavy metal removal. *New*

Journal of Chemistry, *39*(7), 5823–5832. https://doi.org/10.1039/c5nj00509d

Cova, T. F. G. G., Murtinho, D., Pais, A. A. C. C., & Valente, A. J. M. (2018). Combining cellulose and cyclodextrins: fascinating designs for materials and pharmaceutics. *Frontiers in Chemistry*, *6*(July), 271. https://doi.org/10.3389/fchem.2018.00271

Crini, G. (2008). Kinetic and equilibrium studies on the removal of cationic dyes from aqueous solution by adsorption onto a cyclodextrin polymer. *Dyes and Pigments*, *77*(2), 415–426. https://doi.org/10.1016/j.dyepig.2007.07.001

D'Halluin, M., Rull-Barrull, J., Bretel, G., Labrugère, C., Le Grognec, E., & Felpin, F. X. (2017). Chemically modified cellulose filter paper for heavy metal remediation in water. *ACS Sustainable Chemistry and Engineering*, *5*(2), 1965–1973. https://doi.org/10.1021/acssuschemeng.6b02768

Davila-Rodriguez, J. L., Escobar-Barrios, V. A., & Rangel-Mendez, J. R. (2012). Removal of fluoride from drinking water by a chitin-based biocomposite in fixed-bed columns. *Journal of Fluorine Chemistry*, *140*, 99–103. https://doi.org/10.1016/j.jfluchem.2012.05.019

Davila-Rodriguez, J. L., Escobar-Barrios, V. A., Shirai, K., & Rangel-Mendez, J. R. (2009). Synthesis of a chitin-based biocomposite for water treatment: Optimization for fluoride removal. *Journal of Fluorine Chemistry*, *130*(8), 718–726. https://doi.org/10.1016/j.jfluchem.2009.05.012

Dax, D., Chávez, M. S., Xu, C., Willför, S., Mendonça, R. T., & Sánchez, J. (2014). Cationic hemicellulose-based hydrogels for arsenic and chromium removal from aqueous solutions. *Carbohydrate Polymers*, *111*, 797–805. https://doi.org/10.1016/j.carbpol.2014.05.045

De-Bashan, L. E., Moreno, M., Hernandez, J. P., & Bashan, Y. (2002). Removal of ammonium

and phosphorus ions from synthetic wastewater by the microalgae Chlorella vulgaris coimmobilized in alginate beads with the microalgae growth-promoting bacterium Azospirillum brasilense. *Water Research*, *36*(12), 2941–2948. https://doi.org/10.1016/S0043-1354(01)00522-X

del Valle, E. M. M. (2004). Cyclodextrins and their uses: A review. *Process Biochemistry*, *39*(9), 1033–1046. https://doi.org/10.1016/S0032-9592(03)00258-9

Devrimci, H. A., Yuksel, A. M., & Sanin, F. D. (2012). Algal alginate: A potential coagulant for drinking water treatment. *Desalination*, *299*, 16–21. https://doi.org/10.1016/j.desal.2012.05.004

Djebri, N., Boutahala, M., Chelali, N. E., Boukhalfa, N., & Zeroual, L. (2016). Enhanced removal of cationic dye by calcium alginate/organobentonite beads: Modeling, kinetics, equilibriums, thermodynamic and reusability studies. *International Journal of Biological Macromolecules*, *92*, 1277–1287. https://doi.org/10.1016/j.ijbiomac.2016.08.013

Dong, C., Qian, L. Y., Zhao, G. L., He, B. H., & Xiao, H. N. (2014). Preparation of antimicrobial cellulose fibers by grafting β-cyclodextrin and inclusion with antibiotics. *Materials Letters*, *124*, 181–183. https://doi.org/10.1016/j.matlet.2014.03.091

Dotto, G. L., Santos, J. M. N. dos, Rosa, R., Pinto, L. A. A., Pavan, F. A., & Lima, E. C. (2015). Fixed bed adsorption of Methylene Blue by ultrasonic surface modified chitin supported on sand. *Chemical Engineering Research and Design*, *100*, 302–310. https://doi.org/10.1016/j.cherd.2015.06.003

Du, Y., Lv, X. T., Wu, Q. Y., Zhang, D. Y., Zhou, Y. T., Peng, L., & Hu, H. Y. (2017). Formation and control of disinfection byproducts and toxicity during reclaimed water chlorination: A

review. *Journal of Environmental Sciences*, *58*, 51–63. https://doi.org/10.1016/j.jes.2017.01.013

Dwivedi, A. D., Dubey, S. P., Hokkanen, S., Fallah, R. N., & Sillanpää, M. (2014). Recovery of gold from aqueous solutions by taurine modified cellulose: An adsorptive-reduction pathway. *Chemical Engineering Journal*, *255*, 97–106. https://doi.org/10.1016/j.cej.2014.06.017

Dwivedi, A. D., Permana, R., Singh, J. P., Yoon, H., Chae, K. H., Chang, Y. S., & Hwang, D. S. (2017). Tunichrome-Inspired Gold-Enrichment Dispersion Matrix and Its Application in Water Treatment: A Proof-of-Concept Investigation. *ACS Applied Materials and Interfaces*, *9*(23), 19815–19824. https://doi.org/10.1021/acsami.7b03064

Escudero, C., Fiol, N., Villaescusa, I., & Bollinger, J. C. (2009). Arsenic removal by a waste metal (hydr)oxide entrapped into calcium alginate beads. *Journal of Hazardous Materials*, *164*(2–3), 533–541. https://doi.org/10.1016/j.jhazmat.2008.08.042

Espinosa, E., Tarrés, Q., Delgado-Aguilar, M., González, I., Mutjé, P., & Rodríguez, A. (2016). Suitability of wheat straw semichemical pulp for the fabrication of lignocellulosic nanofibres and their application to papermaking slurries. *Cellulose*, *23*(1), 837–852. https://doi.org/10.1007/s10570-015-0807-8

Example, A. (1991). Dissipative QCM. *Langmuir*, 1–3.

Faisal, A. A. H., Sulaymon, A. H., & Khaliefa, Q. M. (2017). A review of permeable reactive barrier as passive sustainable technology for groundwater remediation. *International Journal of Environmental Science and Technology*, 1–16. https://doi.org/10.1007/s13762-017-1466-0

Fält, S., Wågberg, L., & Vesterlind, E. L. (2003). Swelling of model films of cellulose having

different charge densities and comparison to the swelling behavior of corresponding fibers. *Langmuir*, *19*(19), 7895–7903. https://doi.org/10.1021/la026984i

Fan, L., Luo, C., Sun, M., Li, X., Lu, F., & Qiu, H. (2012). Preparation of novel magnetic chitosan/graphene oxide composite as effective adsorbents toward methylene blue. *Bioresource Technology*, *114*, 703–706. https://doi.org/10.1016/j.biortech.2012.02.067

Fan, L., Luo, C., Sun, M., Qiu, H., & Li, X. (2013). Synthesis of magnetic β-cyclodextrin-chitosan/graphene oxide as nanoadsorbent and its application in dye adsorption and removal. *Colloids and Surfaces B: Biointerfaces*, *103*, 601–607. https://doi.org/10.1016/j.colsurfb.2012.11.023

Fan, Y., Saito, T., & Isogai, A. (2009). TEMPO-mediated oxidation of β-chitin to prepare individual nanofibrils. *Carbohydrate Polymers*, *77*(4), 832–838. https://doi.org/10.1016/j.carbpol.2009.03.008

Fatin-Rouge, N., Dupont, A., Vidonne, A., Dejeu, J., Fievet, P., & Foissy, A. (2006). Removal of some divalent cations from water by membrane-filtration assisted with alginate. *Water Research*, *40*(6), 1303–1309. https://doi.org/10.1016/j.watres.2006.01.026

Feng, S., Bagia, C., & Mpourmpakis, G. (2013). Determination of proton affinities and acidity constants of sugars. *Journal of Physical Chemistry A*, *117*(24), 5211–5219. https://doi.org/10.1021/jp403355e

Filpponen, I., Kontturi, E., Nummelin, S., Rosilo, H., Kolehmainen, E., Ikkala, O., & Laine, J. (2012). Generic method for modular surface modification of cellulosic materials in aqueous medium by sequential “click” reaction and adsorption. *Biomacromolecules*, *13*(3), 736–742. https://doi.org/10.1021/bm201661k

Fu, F., Dionysiou, D. D., & Liu, H. (2014). The use of zero-valent iron for groundwater remediation and wastewater treatment: A review. *Journal of Hazardous Materials*, *267*, 194–205. https://doi.org/10.1016/j.jhazmat.2013.12.062

Gan, L., Shang, S., Hu, E., Yuen, C. W. M., & Jiang, S. X. (2015). Konjac glucomannan/graphene oxide hydrogel with enhanced dyes adsorption capability for methyl blue and methyl orange. *Applied Surface Science*, *357*, 866–872. https://doi.org/10.1016/j.apsusc.2015.09.106

Gautam, D., Kumari, S., Ram, B., Chauhan, G. S., & Chauhan, K. (2018). A new hemicellulose-based adsorbent for malachite green. *Journal of Environmental Chemical Engineering*, *6*(4), 3889–3897. https://doi.org/10.1016/j.jece.2018.05.029

Ghorpade, V. S., Yadav, A. V., & Dias, R. J. (2017). Citric acid crosslinked β-cyclodextrin/carboxymethylcellulose hydrogel films for controlled delivery of poorly soluble drugs. *Carbohydrate Polymers*, *164*, 339–348. https://doi.org/10.1016/j.carbpol.2017.02.005

Gidwani, B., & Vyas, A. (2014). Synthesis, characterization and application of Epichlorohydrin-β-cyclodextrin polymer. *Colloids and Surfaces B: Biointerfaces*, *114*, 130–137. https://doi.org/10.1016/j.colsurfb.2013.09.035

Gírio, F. M., Fonseca, C., Carvalheiro, F., Duarte, L. C., Marques, S., & Bogel-Łukasik, R. (2010). Hemicelluloses for fuel ethanol: A review. *Bioresource Technology*, *101*(13), 4775–4800. https://doi.org/10.1016/j.biortech.2010.01.088

Glaze, W. H., Kang, J.-W., & Chapin, D. H. (1987). *The chemistry of water treatment processes involving ozone, hydrogen peroxide and ultraviolet radiation*.

Gomes, R. F., de Azevedo, A. C. N., Pereira, A. G. B., Muniz, E. C., Fajardo, A. R., & Rodrigues, F. H. A. (2015). Fast dye removal from water by starch-based nanocomposites. *Journal of*

Colloid and Interface Science, *454*, 200–209. https://doi.org/10.1016/j.jcis.2015.05.026

Gomez-maldonado, D., Vega Erramuspe, I. B., & Peresin, M. S. (2019). Natural Polymers as Alternative Adsorbents and Treatment Agents for Water Remediation. *BioResources*, *14*(4). https://doi.org/10.15376/biores.14.4.Gomez-Maldonado

Gopi, S., Balakrishnan, P., Pius, A., & Thomas, S. (2017). Chitin nanowhisker (ChNW)-functionalized electrospun PVDF membrane for enhanced removal of Indigo carmine. *Carbohydrate Polymers*, *165*, 115–122. https://doi.org/10.1016/j.carbpol.2017.02.046

Gotoh, T., Matsushima, K., & Kikuchi, K. I. (2004). Preparation of alginate-chitosan hybrid gel beads and adsorption of divalent metal ions. *Chemosphere*, *55*(1), 135–140. https://doi.org/10.1016/j.chemosphere.2003.11.016

Grem, I. C. da S., Lima, B. N. B., Carneiro, W. F., Queirós, Y. G. de C., & Mansur, C. R. E. (2013). Chitosan microspheres applied for removal of oil from produced water in the oil industry. *Polímeros Ciência e Tecnologia*, *23*(6), 705–711. https://doi.org/10.4322/polimeros.2014.008

Guo, X., Abdala, A. A., May, B. L., Lincoln, S. F., Khan, S. A., & Prud'homme, R. K. (2005). Novel associative polymer networks based on cyclodextrin inclusion compounds. *Macromolecules*, *38*(7), 3037–3040. https://doi.org/10.1021/ma050071o

Guo, Z., Li, Y., Pan, S., & Xu, J. (2015). Fabrication of Fe3O4@cyclodextrin magnetic composite for the high-efficient removal of Eu(III). *Journal of Molecular Liquids*, *206*, 272–277. https://doi.org/10.1016/j.molliq.2015.02.034

Gupta, A., Chauhan, V. S., & Sankararamakrishnan, N. (2009). Preparation and evaluation of iron-chitosan composites for removal of As(III) and As(V) from arsenic contaminated real life

groundwater. *Water Research*, *43*(15), 3862–3870. https://doi.org/10.1016/j.watres.2009.05.040

Gurgel, L. V. A., Júnior, O. K., Gil, R. P. de F., & Gil, L. F. (2008). Adsorption of Cu(II), Cd(II), and Pb(II) from aqueous single metal solutions by cellulose and mercerized cellulose chemically modified with succinic anhydride. *Bioresource Technology*, *99*(8), 3077–3083. https://doi.org/10.1016/j.biortech.2007.05.072

Han, J., Xin, J., Zheng, X., Kolditz, O., & Shao, H. (2016). Remediation of trichloroethylene-contaminated groundwater by three modifier-coated microscale zero-valent iron. *Environmental Science and Pollution Research*, *23*(14), 14442–14450. https://doi.org/10.1007/s11356-016-6368-z

Haruta, M. (1997). Size- and support-dependency in the catalysis of gold. *Catalysis Today*, *36*(1), 153–166. https://doi.org/10.1016/S0920-5861(96)00208-8

Hatton, F. L., Malmström, E., & Carlmark, A. (2015). Tailor-made copolymers for the adsorption to cellulosic surfaces. *European Polymer Journal*, *65*, 325–339. https://doi.org/10.1016/j.eurpolymj.2015.01.026

Hitzfeld, B. C., Hoger, S. J., & Dietrich, D. R. (2000). Cyanobacterial Toxins : Removal during Drinking Water Treatment , and Human Risk Assessment Cyanobacteria. *Environmental Health Perspectives*, *108*(1), 113–122.

Hokkanen, S., Bhatnagar, A., Repo, E., Lou, S., & Sillanpää, M. (2016). Calcium hydroxyapatite microfibrillated cellulose composite as a potential adsorbent for the removal of Cr(VI) from aqueous solution. *Chemical Engineering Journal*, *283*, 445–452. https://doi.org/10.1016/j.cej.2015.07.035

Hokkanen, S., Repo, E., & Sillanpää, M. (2013). Removal of heavy metals from aqueous solutions by succinic anhydride modified mercerized nanocellulose. *Chemical Engineering Journal*, *223*, 40–47. https://doi.org/10.1016/j.cej.2013.02.054

Hokkanen, S., Repo, E., Suopajärvi, T., Liimatainen, H., Niinimaa, J., & Sillanpää, M. (2014). Adsorption of Ni(II), Cu(II) and Cd(II) from aqueous solutions by amino modified nanostructured microfibrillated cellulose. *Cellulose*, *21*(3), 1471–1487. https://doi.org/10.1007/s10570-014-0240-4

Hoover R. (2001). *Composition, molecular structure, and physicochemical properties of tuber and root starches: a review. Carbohydr Polym. 45*(3), 2001.

Hu, J., Shao, D., Chen, C., Sheng, G., Ren, X., & Wang, X. (2011). Removal of 1-naphthylamine from aqueous solution by multiwall carbon nanotubes/iron oxides/cyclodextrin composite. *Journal of Hazardous Materials*, *185*(1), 463–471. https://doi.org/10.1016/j.jhazmat.2010.09.055

Hult, E. L., Larsson, P. T., & Iversen, T. (2002). A comparative CP/MAS13C-NMR study of the supermolecular structure of polysaccharides in sulphite and kraft pulps. *Holzforschung*, *56*(2), 179–184. https://doi.org/10.1515/HF.2002.030

Ilharco, L. M., Garcia, A. R., Lopes da Silva, J., & Vieira Ferreira, L. F. (1997). Infrared Approach to the Study of Adsorption on Cellulose: Influence of Cellulose Crystallinity on the Adsorption of Benzophenone. *Langmuir*, *13*(15), 4126–4132. https://doi.org/10.1021/la962138u

Isobe, N., Chen, X., Kim, U. J., Kimura, S., Wada, M., Saito, T., & Isogai, A. (2013). TEMPO-oxidized cellulose hydrogel as a high-capacity and reusable heavy metal ion adsorbent.

Journal of Hazardous Materials, *260*, 195–201. https://doi.org/10.1016/j.jhazmat.2013.05.024

IUPAC. (2014). Compendium of Chemical Terminology (the "Gold Book"). In M. Nič, J. Jirát, B. Košata, A. Jenkins, & A. McNaught (Eds.), *IUPAC Compendium of Chemical Terminology* (2nd ed.). Blackwell Scientific Publications. https://doi.org/10.1351/goldbook

Jagur-Grodzinski, J. (2006). Nanostructured polyolefins / clay composites : role of the molecular interaction at the interface. *Polym. Adv. Technol.*, *17*(April), 395–418. https://doi.org/10.1002/pat

Jain, P., Varshney, S., & Srivastava, S. (2016). Functionalized nanobiomaterials: high-performance sorbents for chromium remediation from water streams [Springer Berlin Heidelberg]. In *International Journal of Environmental Science and Technology* (Vol. 13, Issue 12). https://doi.org/10.1007/s13762-016-1115-z

Janaki, V., Vijayaraghavan, K., Oh, B. T., Lee, K. J., Muthuchelian, K., Ramasamy, A. K., & Kamala-Kannan, S. (2012). Starch/polyaniline nanocomposite for enhanced removal of reactive dyes from synthetic effluent. *Carbohydrate Polymers*, *90*(4), 1437–1444. https://doi.org/10.1016/j.carbpol.2012.07.012

Ji, B., Tang, P., Yan, K., & Sun, G. (2015). Catalytic actions of alkaline salts in reactions between 1,2,3,4-butanetetracarboxylic acid and cellulose: II. Esterification. *Carbohydrate Polymers*, *132*, 228–236. https://doi.org/10.1016/j.carbpol.2015.06.070

Jiang, J., Ye, W., Yu, J., Fan, Y., Ono, Y., Saito, T., & Isogai, A. (2018). Chitin nanocrystals prepared by oxidation of α-chitin using the O2/laccase/TEMPO system. *Carbohydrate Polymers*, *189*(August 2017), 178–183. https://doi.org/10.1016/j.carbpol.2018.01.096

Jiang, Y., Liu, B., Xu, J., Pan, K., Hou, H., Hu, J., & Yang, J. (2018). Cross-linked chitosan/β-cyclodextrin composite for selective removal of methyl orange: Adsorption performance and mechanism. *Carbohydrate Polymers*, *182*(July 2017), 106–114. https://doi.org/10.1016/j.carbpol.2017.10.097

Jin, L., Sun, Q., Xu, Q., & Xu, Y. (2015). Adsorptive removal of anionic dyes from aqueous solutions using microgel based on nanocellulose and polyvinylamine. *Bioresource Technology*, *197*, 348–355. https://doi.org/10.1016/j.biortech.2015.08.093

Johansson, L. S., & Campbell, J. M. (2004). Reproducible XPS on biopolymers: Cellulose studies. *Surface and Interface Analysis*, *36*(8), 1018–1022. https://doi.org/10.1002/sia.1827

Johansson, L. S., Tammelin, T., Campbell, J. M., Setälä, H., & Österberg, M. (2011). Experimental evidence on medium driven cellulose surface adaptation demonstrated using nanofibrillated cellulose. *Soft Matter*, *7*(22), 10917–10924. https://doi.org/10.1039/c1sm06073b

Kardam, A., Raj, K. R., Srivastava, S., & Srivastava, M. M. (2014). Nanocellulose fibers for biosorption of cadmium, nickel, and lead ions from aqueous solution. *Clean Technologies and Environmental Policy*, *16*(2), 385–393. https://doi.org/10.1007/s10098-013-0634-2

Karim, Z., Claudpierre, S., Grahn, M., Oksman, K., & Mathew, A. P. (2016). Nanocellulose based functional membranes for water cleaning: Tailoring of mechanical properties, porosity and metal ion capture. *Journal of Membrane Science*, *514*, 418–428. https://doi.org/10.1016/j.memsci.2016.05.018

Karim, Z., Mathew, A. P., Grahn, M., Mouzon, J., & Oksman, K. (2014). Nanoporous membranes with cellulose nanocrystals as functional entity in chitosan: Removal of dyes from water. *Carbohydrate Polymers*, *112*, 668–676. https://doi.org/10.1016/j.carbpol.2014.06.048

Karthik, R., & Meenakshi, S. (2015). Removal of Cr(VI) ions by adsorption onto sodium alginate-polyaniline nanofibers. *International Journal of Biological Macromolecules*, *72*, 711–717. https://doi.org/10.1016/j.ijbiomac.2014.09.023

Kasemo, B., Fant, C., Sott, K., Elwing, H., & Qcm-d, T. (2001). *Variations in Coupled Water , Viscoelastic Properties , and Film Thickness of a Mefp-1 Protein Film during Adsorption and Cross-Linking : A Quartz Crystal Microbalance with Dissipation Monitoring , Ellipsometry , and Surface Plasmon*. *73*(24), 5796–5804.

Kayaci, F., Aytac, Z., & Uyar, T. (2013). Surface modification of electrospun polyester nanofibers with cyclodextrin polymer for the removal of phenanthrene from aqueous solution. *Journal of Hazardous Materials*, *261*, 286–294. https://doi.org/10.1016/j.jhazmat.2013.07.041

Khaoulani, S., Chaker, H., Cadet, C., Bychkov, E., Cherif, L., Bengueddach, A., & Fourmentin, S. (2015). Wastewater treatment by cyclodextrin polymers and noble metal/mesoporous TiO2photocatalysts. *Comptes Rendus Chimie*, *18*(1), 23–31. https://doi.org/10.1016/j.crci.2014.07.004

Kim, D. H., Cha, J. H., Hong, S. H., Kim, D. Y., & Kim, C. W. (2009). Control of corrosive water in advanced water treatment plant by manipulating calcium carbonate precipitation potential. *Korean Journal of Chemical Engineering*, *26*(1), 90–101. https://doi.org/10.1007/s11814-009-0015-z

Kim, S., Yun, Y. S., & Choi, Y. E. (2018). Development of waste biomass based sorbent for removal of cyanotoxin microcystin-LR from aqueous phases. *Bioresource Technology*, *247*(June 2017), 690–696. https://doi.org/10.1016/j.biortech.2017.09.164

Kim, Y., Kon, Y., Kim, S., Harbottle, D., & Lee, J. W. (2017). *Nanostructured potassium copper*

hexacyanoferrate-cellulose hydrogel for selective and rapid cesium adsorption. *313*, 1042–1050.

Klemm, D., Heublein, B., Fink, H. P., & Bohn, A. (2005). Cellulose: Fascinating biopolymer and sustainable raw material. In *Angewandte Chemie - International Edition* (Vol. 44, Issue 22, pp. 3358–3393). https://doi.org/10.1002/anie.200460587

KSV Instruments Ltd. (2002). *What Is a Quartz Crystal Microbalance – Qcm* (pp. 1–10).

Kumar, A., Guo, C., Sharma, G., Pathania, D., Naushad, M., Kalia, S., & Dhiman, P. (2016). Magnetically recoverable ZrO2/Fe3O4/chitosan nanomaterials for enhanced sunlight driven photoreduction of carcinogenic Cr(VI) and dechlorination & mineralization of 4-chlorophenol from simulated waste water. *RSC Advances*, *6*(16), 13251–13263. https://doi.org/10.1039/c5ra23372k

Kumar, A., Sharma, G., Naushad, M., & Thakur, S. (2015). SPION/β-cyclodextrin core-shell nanostructures for oil spill remediation and organic pollutant removal from waste water. *Chemical Engineering Journal*, *280*, 175–187. https://doi.org/10.1016/j.cej.2015.05.126

Kumar Dutta, P., Dutta, J., & Tripathi, V. S. (2004). Chitin and chitosan: Chemistry, properties and applications. *Journal of Scientific & Industrial Research*, *63*(January), 20–31. https://doi.org/10.1002/chin.200727270

Kuo, P. Y., Barros, L. de A., Yan, N., Sain, M., Qing, Y., & Wu, Y. (2017). Nanocellulose composites with enhanced interfacial compatibility and mechanical properties using a hybrid-toughened epoxy matrix. *Carbohydrate Polymers*, *177*(August), 249–257. https://doi.org/10.1016/j.carbpol.2017.08.091

Kurkov, S. V., & Loftsson, T. (2013). Cyclodextrins. *International Journal of Pharmaceutics*,

453(1), 167–180. https://doi.org/10.1016/j.ijpharm.2012.06.055

Kwon, O. H., Kim, J. O., Cho, D. W., Kumar, R., Baek, S. H., Kurade, M. B., & Jeon, B. H. (2016). Adsorption of As(III), As(V) and Cu(II) on zirconium oxide immobilized alginate beads in aqueous phase. *Chemosphere*, *160*, 126–133. https://doi.org/10.1016/j.chemosphere.2016.06.074

Lahti, K., Rapala, J., Färdig, M., Niemelä, M., & Sivonen, K. (1997). Persistence of cyanobacterial hepatotoxin, microcystin-LR in particulate material and dissolved in lake water. *Water Research*, *31*(5), 1005–1012. https://doi.org/10.1016/S0043-1354(96)00353-3

Lakouraj, M. M., Mojerlou, F., & Zare, E. N. (2014). Nanogel and superparamagnetic nanocomposite based on sodium alginate for sorption of heavy metal ions. *Carbohydrate Polymers*, *106*(1), 34–41. https://doi.org/10.1016/j.carbpol.2014.01.092

Langlais, B., Reckhow, D. A., & Brink, D. R. (1991). *Ozone in Water Treatment: Application and Engineering*. Taylor & Francis. https://books.google.com/books?id=1mT8GYBMoZgC

Laus, R., Costa, T. G., Szpoganicz, B., & Fávere, V. T. (2010). Adsorption and desorption of Cu(II), Cd(II) and Pb(II) ions using chitosan crosslinked with epichlorohydrin-triphosphate as the adsorbent. *Journal of Hazardous Materials*, *183*(1–3), 233–241. https://doi.org/10.1016/j.jhazmat.2010.07.016

Lawrance, G. A. (2013). *Introduction to Coordination Chemistry*. Wiley. http://doi.wiley.com/10.1002/9780470687123

Lee, H. C., Jeong, Y. G., Min, B. G., Lyoo, W. S., & Lee, S. C. (2009). Preparation and acid dye adsorption behavior of polyurethane/chitosan composite foams. *Fibers and Polymers*, *10*(5), 636–642. https://doi.org/10.1007/s12221-010-0636-1

Lee, J., & Walker, H. W. (2011). Adsorption of microcystin-Lr onto iron oxide nanoparticles. *Colloids and Surfaces A: Physicochemical and Engineering Aspects*, *373*(1–3), 94–100. https://doi.org/10.1016/j.colsurfa.2010.10.032

Lee, Koon Yang, Quero, F., Blaker, J. J., Hill, C. A. S., Eichhorn, S. J., & Bismarck, A. (2011). Surface only modification of bacterial cellulose nanofibres with organic acids. *Cellulose*, *18*(3), 595–605. https://doi.org/10.1007/s10570-011-9525-z

Lee, Kuen Yong, & Mooney, D. J. (2012). Alginate: Properties and biomedical applications. *Progress in Polymer Science (Oxford)*, *37*(1), 106–126. https://doi.org/10.1016/j.progpolymsci.2011.06.003

Lemlikchi, W., Sharrock, P., Mecherri, M. O., Fiallo, M., & Nzihou, A. (2012). Treatment of textile waste waters by hydroxyapatite co-precipitation with adsorbent regeneration and reuse. *Waste and Biomass Valorization*, *3*(1), 75–79. https://doi.org/10.1007/s12649-011-9096-0

Li, C., Wen, T., Yan, L., Li, B., Wang, W., Yang, J., Xu, M., T-f, W., L-n, Y., W-t, W., J-y, Y., & M-q, X. (2017). Develpment of waste biomass based sorbent for removal of cyanotoxin microcystin-LR from aqueous phases. *Bioresource Technology*. https://doi.org/10.1016/j.ijsu.2017.05.034

Li, Jian, Zuo, K., Wu, W., Xu, Z., Yi, Y., Jing, Y., Dai, H., & Fang, G. (2018). Shape memory aerogels from nanocellulose and polyethyleneimine as a novel adsorbent for removal of Cu(II) and Pb(II). *Carbohydrate Polymers*, *196*(April), 376–384. https://doi.org/10.1016/j.carbpol.2018.05.015

Li, Jie, Chen, C., Zhao, Y., Hu, J., Shao, D., & Wang, X. (2013). Synthesis of water-dispersible

Fe3O4β-cyclodextrin by plasma-induced grafting technique for pollutant treatment. *Chemical Engineering Journal*, *229*, 296–303. https://doi.org/10.1016/j.cej.2013.06.016

Li, L., Luo, C., Li, X., Duan, H., & Wang, X. (2014). Preparation of magnetic ionic liquid/chitosan/graphene oxide composite and application for water treatment. *International Journal of Biological Macromolecules*, *66*, 172–178. https://doi.org/10.1016/j.ijbiomac.2014.02.031

Li, R., Yu, J. C., Jiang, Z. T., Zhou, R. H., & Liu, H. Y. (2003). A solid-phase fluorescent, quenching method for the determination of trace amounts of nitrite in foods with neutral red. *Journal of Food and Drug Analysis*, *11*(3), 251–257.

Li, Y., Liu, F., Xia, B., Du, Q., Zhang, P., Wang, D., Wang, Z., & Xia, Y. (2010). Removal of copper from aqueous solution by carbon nanotube/calcium alginate composites. *Journal of Hazardous Materials*, *177*(1–3), 876–880. https://doi.org/10.1016/j.jhazmat.2009.12.114

Lin, N., & Dufresne, A. (2013). Supramolecular hydrogels from in situ host-guest inclusion between chemically modified cellulose nanocrystals and cyclodextrin. *Biomacromolecules*, *14*(3), 871–880. https://doi.org/10.1021/bm301955k

Lin, S., Huang, R., Cheng, Y., Liu, J., Lau, B. L. T., & Wiesner, M. R. (2013). Silver nanoparticle-alginate composite beads for point-of-use drinking water disinfection. *Water Research*, *47*(12), 3959–3965. https://doi.org/10.1016/j.watres.2012.09.005

Liu, D., Zhu, Y., Li, Z., Tian, D., Chen, L., & Chen, P. (2013). Chitin nanofibrils for rapid and efficient removal of metal ions from water system. *Carbohydrate Polymers*, *98*(1), 483–489. https://doi.org/10.1016/j.carbpol.2013.06.015

Liu, H., Cai, X., Wang, Y., & Chen, J. (2011). Adsorption mechanism-based screening of

cyclodextrin polymers for adsorption and separation of pesticides from water. *Water Research*, *45*(11), 3499–3511. https://doi.org/10.1016/j.watres.2011.04.004

Liu, L., & Guo, Q. X. (2004). Use of quantum chemical methods to study cyclodextrin chemistry. *Journal of Inclusion Phenomena and Macrocyclic Chemistry*, *50*(1), 95–103. https://doi.org/Doi 10.1007/10.1007/S10847-003-8847-3

Liu, P., Borrell, P. F., Božič, M., Kokol, V., Oksman, K., & Mathew, A. P. (2015). Nanocelluloses and their phosphorylated derivatives for selective adsorption of Ag^{+}, Cu^{2+} and Fe^{3+} from industrial effluents. *Journal of Hazardous Materials*, *294*, 177–185. https://doi.org/10.1016/j.jhazmat.2015.04.001

Liu, P., Oksman, K., & Mathew, A. P. (2016). Surface adsorption and self-assembly of Cu(II) ions on TEMPO-oxidized cellulose nanofibers in aqueous media. *Journal of Colloid and Interface Science*, *464*, 175–182. https://doi.org/10.1016/j.jcis.2015.11.033

Lombardo, S., & Thielemans, W. (2019). Thermodynamics of adsorption on nanocellulose surfaces. *Cellulose*, *26*(1), 249–279. https://doi.org/10.1007/s10570-018-02239-2

Luo, Xiaogang, Lei, X., Xie, X., Yu, B., Cai, N., & Yu, F. (2016). *Adsorptive removal of Lead from water by the effective and reusable magnetic cellulose nanocomposite beads entrapping activated bentonite*. *151*, 640–648.

Luo, Xin, Zhang, G., Wang, X., & Gu, P. (2013). Research on a pellet co-precipitation micro-filtration process for the treatment of liquid waste containing strontium. *Journal of Radioanalytical and Nuclear Chemistry*, *298*(2), 931–939. https://doi.org/10.1007/s10967-013-2495-x

Ma, H., Hsiao, B. S., & Chu, B. (2012). Ultrafine cellulose nanofibers as efficient adsorbents for

removal of UO22+in water. *ACS Macro Letters*, *1*(1), 213–216. https://doi.org/10.1021/mz200047q

Maatar, W., & Boufi, S. (2015). Poly(methacylic acid-co-maleic acid) grafted nanofibrillated cellulose as a reusable novel heavy metal ions adsorbent. *Carbohydrate Polymers*, *126*, 199–207. https://doi.org/10.1016/j.carbpol.2015.03.015

Mahfoudhi, N., & Boufi, S. (2017). Nanocellulose as a novel nanostructured adsorbent for environmental remediation: a review. *Cellulose*, *24*(3), 1171–1197. https://doi.org/10.1007/s10570-017-1194-0

Mao, Y., Guo, D., Yao, W., Wang, X., Yang, H., Xie, Y. F., Komarneni, S., Yu, G., & Wang, Y. (2018). Effects of conventional ozonation and electro-peroxone pretreatment of surface water on disinfection by-product formation during subsequent chlorination. *Water Research*. https://doi.org/10.1016/j.waters.2017.12.019

Medronho, B., Andrade, R., Vivod, V., Ostlund, A., Miguel, M. G., Lindman, B., Voncina, B., & Valente, A. J. M. (2013). Cyclodextrin-grafted cellulose: Physico-chemical characterization. *Carbohydrate Polymers*, *93*(1), 324–330. https://doi.org/10.1016/j.carbpol.2012.08.109

Melone, L., Rossi, B., Pastori, N., Panzeri, W., Mele, A., & Punta, C. (2015). TEMPO-Oxidized Cellulose Cross-Linked with Branched Polyethyleneimine: Nanostructured Adsorbent Sponges for Water Remediation. *ChemPlusChem*, *80*(9), 1408–1415. https://doi.org/10.1002/cplu.201500145

Meraz, K. A. S., Vargas, S. M. P., Maldonado, J. T. L., Bravo, J. M. C., Guzman, M. T. O., & Maldonado, E. A. L. (2016). Eco-friendly innovation for nejayote coagulation-flocculation process using chitosan: Evaluation through zeta potential measurements. *Chemical*

Engineering Journal, *284*, 536–542. https://doi.org/10.1016/j.cej.2015.09.026

Meriluoto, J., & Codd, G. A. (2005). *Cyanobacterial Monitoring and Cyanotoxin Analysis*. https://doi.org/10.1002/9781119068761

Meyers, M. A., Chen, P. Y., Lin, A. Y. M., & Seki, Y. (2008). Biological materials: Structure and mechanical properties. *Progress in Materials Science*, *53*(1), 1–206. https://doi.org/10.1016/j.pmatsci.2007.05.002

Mishima, T., Hisamatsu, M., York, W. S., Teranishi, K., & Yamada, T. (1998). Adhesion of β-D-glucans to cellulose. *Carbohydrate Research*, *308*(3–4), 389–395. https://doi.org/10.1016/S0008-6215(98)00099-8

Mohamed, M. H., Wilson, L. D., Pratt, D. Y., Guo, R., Wu, C., & Headley, J. V. (2012). Evaluation of the accessible inclusion sites in copolymer materials containing β-cyclodextrin. *Carbohydrate Polymers*, *87*(2), 1241–1248. https://doi.org/10.1016/j.carbpol.2011.09.011

Morin-Crini, N., & Crini, G. (2013). Environmental applications of water-insoluble β-cyclodextrin- epichlorohydrin polymers. *Progress in Polymer Science*, *38*(2), 344–368. https://doi.org/10.1016/j.progpolymsci.2012.06.005

Morin-Crini, N., Winterton, P., Fourmentin, S., Wilson, L. D., Fenyvesi, É., & Crini, G. (2018). Water-insoluble β-cyclodextrin–epichlorohydrin polymers for removal of pollutants from aqueous solutions by sorption processes using batch studies: A review of inclusion mechanisms. *Progress in Polymer Science*, *78*, 1–23. https://doi.org/10.1016/j.progpolymsci.2017.07.004

Munagapati, V. S., & Kim, D. S. (2017). Equilibrium isotherms, kinetics, and thermodynamics studies for congo red adsorption using calcium alginate beads impregnated with nano-

goethite. *Ecotoxicology and Environmental Safety*, *141*(August 2016), 226–234. https://doi.org/10.1016/j.ecoenv.2017.03.036

Nevárez, L. A. M., Casarrubias, L. B., Celzard, A., Fierro, V., Muñoz, V. T., Davila, A. C., Lubian, J. R. T., & Sánchez, G. G. (2011). Biopolymer-based nanocomposites: effect of lignin acetylation in cellulose triacetate films. *Science and Technology of Advanced Materials*, *12*(4), 045006. https://doi.org/10.1088/1468-6996/12/4/045006

Novotny, V. (2003). *Water quality : diffuse pollution and watershed management*. J. Wiley. https://books.google.com/books?hl=es&lr=&id=dodtuLJBxhAC&oi=fnd&pg=PR19&dq=Novotny+ecology+engineering&ots=RuEZECwcoW&sig=iYqfhhb-yurdOrWdHkq8MqpyhFU#v=onepage&q=Novotny ecology engineering&f=false

Nyberg, U., Andersson, B., Aspegren, H., & Ødegaard, H. (1994). The Use of Polymer in the Pre-precipitation Step of a Wastewater Treatment System for Extended Nutrient Removal. In R. Klute & H. H. Hahn (Eds.), *Chemical Water and Wastewater Treatment III: Proceedings of the 6th Gothenburg Symposium 1994 June 20 -- 22, 1994 Gothenburg, Sweden* (pp. 211–219). Springer Berlin Heidelberg. https://doi.org/10.1007/978-3-642-79110-9_15

Oh, D. X., Kim, S., Lee, D., & Hwang, D. S. (2015). Tunicate-mimetic nanofibrous hydrogel adhesive with improved wet adhesion. *Acta Biomaterialia*, *20*, 104–112. https://doi.org/10.1016/j.actbio.2015.03.031

Olivera, S., Muralidhara, H. B., Venkatesh, K., Guna, V. K., Gopalakrishna, K., & Kumar K., Y. (2016). Potential applications of cellulose and chitosan nanoparticles/composites in wastewater treatment: A review. *Carbohydrate Polymers*, *153*, 600–618. https://doi.org/10.1016/j.carbpol.2016.08.017

Orelma, H., Filpponen, I., Johansson, L.-S., Laine, J., & Rojas, O. J. (2011). Modification of Cellulose Films by Adsorption of CMC and Chitosan for Controlled Attachment of Biomolecules. *Biomacromolecules*, *12*(12), 4311–4318. https://doi.org/10.1021/bm201236a

Orelma, H., Filpponen, I., Johansson, L. S., Österberg, M., Rojas, O. J., & Laine, J. (2012). Surface functionalized nanofibrillar cellulose (NFC) film as a platform for immunoassays and diagnostics. *Biointerphases*, *7*(1–4), 1–12. https://doi.org/10.1007/s13758-012-0061-7

Orelma, H., Virtanen, T., Spoljaric, S., Lehmonen, J., Seppälä, J., Rojas, O. J., & Harlin, A. (2018). Cyclodextrin-Functionalized Fiber Yarns Spun from Deep Eutectic Cellulose Solutions for Nonspecific Hormone Capture in Aqueous Matrices. *Biomacromolecules*, *19*(2), 652–661. https://doi.org/10.1021/acs.biomac.7b01765

Pal, S., Mal, D., & Singh, R. P. (2005). Cationic starch: An effective flocculating agent. *Carbohydrate Polymers*, *59*(4), 417–423. https://doi.org/10.1016/j.carbpol.2004.06.047

Papageorgiou, S. K., Katsaros, F. K., Favvas, E. P., Romanos, G. E., Athanasekou, C. P., Beltsios, K. G., Tzialla, O. I., & Falaras, P. (2012). Alginate fibers as photocatalyst immobilizing agents applied in hybrid photocatalytic/ultrafiltration water treatment processes. *Water Research*, *46*(6), 1858–1872. https://doi.org/10.1016/j.watres.2012.01.005

Parvinzadeh, M., Alimohammadi, F., & Shamei, A. (2012). Surface & Coatings Technology Preparation of water-repellent cellulose fi bers using a polycarboxylic acid / hydrophobic silica nanocomposite coating. *Surface & Coatings Technology*, *206*(14), 3208–3215. https://doi.org/10.1016/j.surfcoat.2012.01.006

Pavinatto, F. J., Caseli, L., & Oliveira, O. N. (2010). Chitosan in nanostructured thin films. *Biomacromolecules*, *11*(8), 1897–1908. https://doi.org/10.1021/bm1004838

Pawar, S. N., & Edgar, K. J. (2012). Alginate derivatization: A review of chemistry, properties and applications. *Biomaterials*, *33*(11), 3279–3305. https://doi.org/10.1016/j.biomaterials.2012.01.007

Pinto, L. M. A., Fraceto, L. F., Santana, M. H. A., Pertinhez, T. A., Oyama, S., & De Paula, E. (2005). Physico-chemical characterization of benzocaine-β-cyclodextrin inclusion complexes. *Journal of Pharmaceutical and Biomedical Analysis*, *39*(5), 956–963. https://doi.org/10.1016/j.jpba.2005.06.010

Prabaharan, M., & Gong, S. (2008). Novel thiolated carboxymethyl chitosan-g-β-cyclodextrin as mucoadhesive hydrophobic drug delivery carriers. *Carbohydrate Polymers*, *73*(1), 117–125. https://doi.org/10.1016/j.carbpol.2007.11.005

Qi, J., Zhang, G., & Li, H. (2015). Efficient removal of arsenic from water using a granular adsorbent: Fe-Mn binary oxide impregnated chitosan bead. *Bioresource Technology*, *193*, 243–249. https://doi.org/10.1016/j.biortech.2015.06.102

Renard, E., Barnathan, G., Deratani, A., & Sebille, B. (1997). Polycondensation of Cyclodextrins With Epichlorohydrin . Influence of Reaction Conditions on the Polymer Structure. *Macromol. Symp.*, *122*, 229–234. https://doi.org/10.1002/masy.19971220136

Rinaudo, M. (2006). Chitin and chitosan: Properties and applications. *Progress in Polymer Science (Oxford)*, *31*(7), 603–632. https://doi.org/10.1016/j.progpolymsci.2006.06.001

Rosenblum, L., Zaffiro, A., Adams, W. A., & Wendelken, S. C. (2017). Effect of chlorination by-products on the quantitation of microcystins in finished drinking water. *Toxicon*, *138*, 138–144. https://doi.org/10.1016/j.toxicon.2017.08.023

Rosenfeld, P. E., & Feng, L. G. H. (2011). Emerging Contaminants. In *Risks of Hazardous Wastes*

(pp. 215–222). Elsevier. https://doi.org/10.1016/b978-1-4377-7842-7.00016-7

Ruiz-Palomero, C., Soriano, M. L., & Valcárcel, M. (2015). β-Cyclodextrin decorated nanocellulose: A smart approach towards the selective fluorimetric determination of danofloxacin in milk samples. *Analyst*, *140*(10), 3431–3438. https://doi.org/10.1039/c4an01967a

Saad, A. H. A., Azzam, A. M., El-Wakeel, S. T., Mostafa, B. B., & Abd El-latif, M. B. (2018). Removal of toxic metal ions from wastewater using ZnO@Chitosan core-shell nanocomposite. *Environmental Nanotechnology, Monitoring and Management*, *9*(August 2017), 67–75. https://doi.org/10.1016/j.enmm.2017.12.004

Saeki, H., Sasaki, M., Komatsu, K., Miura, A., & Matsuda, H. (2009). Oil spill remediation by using the remediation agent JE1058BS that contains a biosurfactant produced by Gordonia sp. strain JE-1058. *Bioresource Technology*, *100*(2), 572–577. https://doi.org/10.1016/j.biortech.2008.06.046

Saenger, W., & Steiner, T. (1998). *Cyclodextrin Inclusion Complexes : Host ± Guest Interactions and Hydrogen-Bonding Networks*. 798–805. https://doi.org/10.1107/S0108767398010733

Sag, Y., Nourbakhsh, M., Aksu, Z., & Kutsal, T. (1995). *Comparison of Ca-alginate and Immobilized 2 . ramigera as Sorbents for Copper Removal*. *30*(2), 175–181.

Saito, T., & Isogai, A. (2004). TEMPO-mediated oxidation of native cellulose. The effect of oxidation conditions on chemical and crystal structures of the water-insoluble fractions. *Biomacromolecules*, *5*(5), 1983–1989. https://doi.org/10.1021/bm0497769

Sajilata, M. G., Singhal, R. S., & Kulkarni, P. R. (2006). Resistant starch - A review. *Comprehensive Reviews in Food Science and Food Safety*, *5*(1), 1–17.

https://doi.org/10.1111/j.1541-4337.2006.tb00076.x

Salam, A., Pawlak, J. J., Venditti, R. A., & El-tahlawy, K. (2011). Incorporation of carboxyl groups into xylan for improved absorbency. *Cellulose*, *18*(4), 1033–1041. https://doi.org/10.1007/s10570-011-9542-y

Salam, A., Pawlak, J. J., Venditti, R. A., El-tahlawy, K., & Carolina, N. (2010). *Synthesis and Characterization of Starch Citrate - Chitosan Foam with Superior Water and Saline Absorbance Properties*. *60 mL*, 1453–1459.

Salam, A., Venditti, R. A., Pawlak, J. J., & El-tahlawy, K. (2011). Crosslinked hemicellulose citrate – chitosan aerogel foams. *Carbohydrate Polymers*, *84*(4), 1221–1229. https://doi.org/10.1016/j.carbpol.2011.01.008

Sankar, M. U., Aigal, S., Maliyekkal, S. M., Chaudhary, A., Anshup, Kumar, A. A., Chaudhari, K., & Pradeep, T. (2013). Biopolymer-reinforced synthetic granular nanocomposites for affordable point-of-use water purification. *Proceedings of the National Academy of Sciences*, *110*(21), 8459–8464. https://doi.org/10.1073/pnas.1220222110

Saravanan, D., Gomathi, T., & Sudha, P. N. (2013). Sorption studies on heavy metal removal using chitin/bentonite biocomposite. *International Journal of Biological Macromolecules*, *53*, 67–71. https://doi.org/10.1016/j.ijbiomac.2012.11.005

Sato, A., Wang, R., Ma, H., Hsiao, B. S., & Chu, B. (2011). Novel nanofibrous scaffolds for water filtration with bacteria and virus removal capability. *Journal of Electron Microscopy*, *60*(3), 201–209. https://doi.org/10.1093/jmicro/dfr019

Sehaqui, H., de Larraya, U. P., Liu, P., Pfenninger, N., Mathew, A. P., Zimmermann, T., & Tingaut, P. (2014). Enhancing adsorption of heavy metal ions onto biobased nanofibers from

waste pulp residues for application in wastewater treatment. *Cellulose*, *21*(4), 2831–2844. https://doi.org/10.1007/s10570-014-0310-7

Seyed Dorraji, M. S., A.R., A.-G., Hanifehpour, Y., Woo Joo, S., Figoli, A., Carraro, M., & Tasselli, F. (2017). Performance of chitosan based nanocomposite hollow fibers in the removal of selenium (IV). *Chemical Engineering Research and Design*, *117*, 309–317.

Shao, D., Sheng, G., Chen, C., Wang, X., & Nagatsu, M. (2010). Removal of polychlorinated biphenyls from aqueous solutions using β-cyclodextrin grafted multiwalled carbon nanotubes. *Chemosphere*, *79*(7), 679–685. https://doi.org/10.1016/j.chemosphere.2010.03.008

Shao, Z. jian, Huang, X. lian, Yang, F., Zhao, W. feng, Zhou, X. zhi, & Zhao, C. sheng. (2018). Engineering sodium alginate-based cross-linked beads with high removal ability of toxic metal ions and cationic dyes. *Carbohydrate Polymers*, *187*(January), 85–93. https://doi.org/10.1016/j.carbpol.2018.01.092

Sharma, P. R., Chattopadhyay, A., Sharma, S. K., Geng, L., Amiralian, N., Martin, D., & Hsiao, B. S. (2018). Nanocellulose from Spinifex as an Effective Adsorbent to Remove Cadmium(II) from Water. *ACS Sustainable Chemistry and Engineering*, *6*(3), 3279–3290. https://doi.org/10.1021/acssuschemeng.7b03473

Sharma, P. R., Chattopadhyay, A., Sharma, S. K., & Hsiao, B. S. (2017). Efficient Removal of UO_2^{2+} from Water Using Carboxycellulose Nanofibers Prepared by the Nitro-Oxidation Method. *Industrial & Engineering Chemistry Research*, *56*(46), 13885–13893. https://doi.org/10.1021/acs.iecr.7b03659

Sharma, P. R., Chattopadhyay, A., Zhan, C., Sharma, S. K., Geng, L., & Hsiao, B. S. (2018). Lead

removal from water using carboxycellulose nanofibers prepared by nitro-oxidation method. *Cellulose*, *25*(3), 1961–1973. https://doi.org/10.1007/s10570-018-1659-9

Sharma, P. R., Joshi, R., Sharma, S. K., & Hsiao, B. S. (2017). A Simple Approach to Prepare Carboxycellulose Nanofibers from Untreated Biomass. *Biomacromolecules*, *18*(8), 2333–2342. https://doi.org/10.1021/acs.biomac.7b00544

Shrivastava, V. . S. (2010). Metallic and organic nanomaterials and their use in pollution control : A Review. *Archives of Applied Science Research*, *2*(6), 82–92.

Shuaiyang, W., Huiling, L., Junli, R., Chuanfu, L., Feng, P., & Runcang, S. (2013). Preparation of xylan citrate - A potential adsorbent for industrial wastewater treatment. *Carbohydrate Polymers*, *92*(2), 1960–1965. https://doi.org/10.1016/j.carbpol.2012.11.079

Shukla, S. K., Mishra, A. K., Arotiba, O. A., & Mamba, B. B. (2013). Chitosan-based nanomaterials: A state-of-the-art review. *International Journal of Biological Macromolecules*, *59*, 46–58. https://doi.org/10.1016/j.ijbiomac.2013.04.043

Sigdel, A., Park, J., Kwak, H., & Park, P. K. (2016). Arsenic removal from aqueous solutions by adsorption onto hydrous iron oxide-impregnated alginate beads. *Journal of Industrial and Engineering Chemistry*, *35*, 277–286. https://doi.org/10.1016/j.jiec.2016.01.005

Singh, J., Dartois, A., & Kaur, L. (2010). Starch digestibility in food matrix: a review. *Trends in Food Science and Technology*, *21*(4), 168–180. https://doi.org/10.1016/j.tifs.2009.12.001

Singha, A. S., & Guleria, A. (2014). Chemical modification of cellulosic biopolymer and its use in removal of heavy metal ions from wastewater. *International Journal of Biological Macromolecules*, *67*, 409–417. https://doi.org/10.1016/j.ijbiomac.2014.03.046

Sinha, Arjyabaran, & Jana, N. R. (2015). Separation of microcystin-LR by cyclodextrin-

functionalized magnetic composite of colloidal graphene and porous silica. *ACS Applied Materials and Interfaces*, *7*(18), 9911–9919. https://doi.org/10.1021/acsami.5b02038

Sinha, Arvind, & Khare, S. K. (2012). Mercury bioremediation by mercury accumulating Enterobacter sp. cells and its alginate immobilized application. *Biodegradation*, *23*(1), 25–34. https://doi.org/10.1007/s10532-011-9483-z

Sixta, H. (2006). *Handbook of pulp* (Vol. 1). Wiley Online Library.

Smith, C. A., & Wood, E. J. (1997). *Moléculas Biológicas*. Addison-Wesley Iberoamericana.

Smook, G. (2016). *Handbook for Pulp and Paper Technologist* (M. Kocurek (ed.); 4th Editio). TAPPI Press.

Snyder, A., Bo, Z., Moon, R., Rochet, J. C., & Stanciu, L. (2013). Reusable photocatalytic titanium dioxide-cellulose nanofiber films. *Journal of Colloid and Interface Science*, *399*, 92–98. https://doi.org/10.1016/j.jcis.2013.02.035

Sookne, A. M., & Harris, M. (1941). Surface characteristics of cotton fibers, as indicated by electrophoretic studies. *Journal of Research of the National Bureau of Standards*, *26*(1), 65. https://doi.org/10.6028/jres.026.041

Stana-Kleinschek, K., Strnad, S., & Ribitsch, V. (1999). Surface characterization and adsorption abilities of cellulose fibers. *Polymer Engineering & Science*, *39*(8), 1412–1424. https://doi.org/10.1002/pen.11532

Struszczyk, M. H. (2002). Chitin and Chitosan. *Polimery*, *47*(5), 316–325. https://doi.org/10.1002/0471440264.pst052

Sun, T., & Lindsay, J. D. (2004). *Cyclodextrins covalently bound to polysaccharides* (Patent No. US 6,689,378 B1).

Suopajärvi, T., Liimatainen, H., Karjalainen, M., Upola, H., & Niinimäki, J. (2015). Lead adsorption with sulfonated wheat pulp nanocelluloses. *Journal of Water Process Engineering*, *5*, 136–142. https://doi.org/10.1016/j.jwpe.2014.06.003

Syahmani, S., Iriani, R., Sanjaya, R. E., & Leny. (2018). Potency of Chitin as an Adsorbent in Black Water Treatment Process at Peatland Environment. *Advances in Social Science, Education and Humanities Research (ASSEHR)*, *147*(Icsse 2017), 316–321.

Szejtli, József. (1998). Introduction and General Overview of Cyclodextrin Chemistry. *Chemical Reviews*, *98*(5), 1743–1754. https://doi.org/10.1021/cr970022c

Szejtli, Jozsef, Zsadon, B., Fenyvesi, É., & Tüdös, F. (1982). *Sorbents of cellulose basis capable of forming inclusion complexes and a process for the preparation thereof* (Patent No. 4,357,468).

TAPPI. (1993). T550 Determination of equilibrium moisture in pulp , paper and paperboard for chemical analysis. *TAPPI T550 Om-08*, 1–3. https://doi.org/10.1002/rcm.5278

Todde, G., Jha, S. K., Subramanian, G., & Shukla, M. K. (2018). Adsorption of TNT, DNAN, NTO, FOX7, and NQ onto cellulose, chitin, and cellulose triacetate. Insights from Density Functional Theory calculations. *Surface Science*, *668*, 54–60. https://doi.org/10.1016/j.susc.2017.10.004

Tomson, M. B., & Vignona, L. (1984). Precipitation of Phosphate Minerals in Waste Water Treatment Systems. In J. O. Nriagu & P. B. Moore (Eds.), *Phosphate Minerals* (pp. 386–399). Springer Berlin Heidelberg. https://doi.org/10.1007/978-3-642-61736-2_13

Tran, C. D., Duri, S., Delneri, A., & Franko, M. (2013). Chitosan-cellulose composite materials : Preparation , Characterization and application for removal of microcystin. *Journal of*

Hazardous Materials, *253*, 355–366.

Trujillo-Reyes, J., Peralta-Videa, J. R., & Gardea-Torresdey, J. L. (2014). Supported and unsupported nanomaterials for water and soil remediation: Are they a useful solution for worldwide pollution? *Journal of Hazardous Materials*, *280*, 487–503. https://doi.org/10.1016/j.jhazmat.2014.08.029

Turon, X., Rojas, O. J., & Deinhammer, R. S. (2008). Enzymatic kinetics of cellulose hydrolysis: A QCM-D study. *Langmuir*, *24*(8), 3880–3887. https://doi.org/10.1021/la7032753

Tyagi, P. K., Singh, R., Vats, S., & Kumar, D. (2012). Nanomaterials Use in Wastewater Treatment. *International Conference on Nanotechnology and Chemical Engineering (ICNCS'2012) December 21-22, 2012 Bangkok (Thailand)*, 65–68.

U.S. Environmental Protection Agency. (2012). Cyanobacteria and Cyanotoxins : Information for Drinking Water Systems. *United States Environmental Protection Agency*, *EPA-810F11001*, 1–9.

United Nations. (2010). *64/292. The human right to water and sanitation*. https://doi.org/10.4324/9781315471532-2

United Nations Department of Economic and Social Affairs. (2014). *International Decade for Action "Water for Life" 2005-2015. Focus Areas: The human right to water and sanitation*. https://www.un.org/waterforlifedecade/human_right_to_water.shtml

USEPA - Office of Ground Water and Drinking Water. (2017). *The Fourth Unregulated Contaminant Monitoring Rule (UCMR 4) Public Meeting and Webinar :*

USEPA - Office of Water. (2016). *Human Health Recreational Ambient Water Quality Criteria or Swimming Advisories for Microcystins and Cylindrospermopsin Draft Human Health*

Recreational Ambient Water Quality Criteria or Swimming Advisories for Microcystins and Cylindrospermopsin (Issue December).

Uyar, T., Havelund, R., Nur, Y., Balan, A., Hacaloglu, J., Toppare, L., Besenbacher, F., & Kingshott, P. (2010). Cyclodextrin functionalized poly(methyl methacrylate) (PMMA) electrospun nanofibers for organic vapors waste treatment. *Journal of Membrane Science*, *365*(1–2), 409–417. https://doi.org/10.1016/j.memsci.2010.09.037

Vijayalakshmi, K., Devi, B. M., Latha, S., Gomathi, T., Sudha, P. N., Venkatesan, J., & Anil, S. (2017). Batch adsorption and desorption studies on the removal of lead (II) from aqueous solution using nanochitosan/sodium alginate/microcrystalline cellulose beads. *International Journal of Biological Macromolecules*, *104*, 1483–1494. https://doi.org/10.1016/j.ijbiomac.2017.04.120

Villiers, A. (1891). Sur la fermentation de la fécule par l'action du ferment butyrique. *Compt. Rend. Acad. Sci*, *112*, 536–538.

Viswanathan, N., Pandi, K., & Meenakshi, S. (2014). Synthesis of metal ion entrapped silica gel/chitosan biocomposite for defluoridation studies. *International Journal of Biological Macromolecules*, *70*, 347–353. https://doi.org/10.1016/j.ijbiomac.2014.06.010

Voinova, M. V., Jonson, M., & Kasemo, B. (2002). "Missing mass" effect in biosensor's QCM applications. *Biosensors and Bioelectronics*, *17*(10), 835–841. https://doi.org/10.1016/S0956-5663(02)00050-7

Voinova, M. V., Rodahl, M., Jonson, M., & Kasemo, B. (1998). *Viscoelastic acoustic response of layered polymer films at fluid-solid interfaces: Continuum mechanics approach*. 1–22. https://doi.org/10.1238/Physica.Regular.059a00391

Walls, J. T., Wyatt, K. H., Doll, J. C., Rubenstein, E. M., & Rober, A. R. (2018). Hot and toxic: Temperature regulates microcystin release from cyanobacteria. *Science of the Total Environment*, *610–611*, 786–795. https://doi.org/10.1016/j.scitotenv.2017.08.149

Wang, F., Yang, B., Wang, H., Song, Q., Tan, F., & Cao, Y. (2016). Removal of ciprofloxacin from aqueous solution by a magnetic chitosan grafted graphene oxide composite. *Journal of Molecular Liquids*, *222*, 188–194. https://doi.org/10.1016/j.molliq.2016.07.037

Wang, R., Chen, L., Zhu, J. Y., & Yang, R. (2017). Tailored and integrated production of carboxylated cellulose nanocrystals (CNC) with nanofibrils (CNF) through maleic acid hydrolysis. *ChemNanoMat*, *3*(5), 328–335. https://doi.org/10.1002/cnma.201700015

Wang, Yaoguang, Wu, D., Wei, Q., Wei, D., Yan, T., Yan, L., Hu, L., & Du, B. (2017). Rapid removal of Pb(II) from aqueous solution using branched polyethylenimine enhanced magnetic carboxymethyl chitosan optimized with response surface methodology. *Scientific Reports*, *7*(1), 1–11. https://doi.org/10.1038/s41598-017-09700-5

Wang, Yaquan, Feng, Y., Zhang, X. F., Zhang, X., Jiang, J., & Yao, J. (2018). Alginate-based attapulgite foams as efficient and recyclable adsorbents for the removal of heavy metals. *Journal of Colloid and Interface Science*, *514*, 190–198. https://doi.org/10.1016/j.jcis.2017.12.035

Wang, Yuntao, Li, Y., Liu, S., & Li, B. (2015). Fabrication of chitin microspheres and their multipurpose application as catalyst support and adsorbent. *Carbohydrate Polymers*, *120*, 53–59. https://doi.org/10.1016/j.carbpol.2014.12.005

Wang, Yuntao, Pei, Y., Xiong, W., Liu, T., Li, J., Liu, S., & Li, B. (2015). New photocatalyst based on graphene oxide/chitin for degradation of dyes under sunlight. *International Journal*

of Biological Macromolecules, *81*, 477–482. https://doi.org/10.1016/j.ijbiomac.2015.08.037

Wilson, L. D., Mohamed, M. H., & Berhaut, C. L. (2011). Sorption of aromatic compounds with copolymer sorbent materials containing β-cyclodextrin. *Materials*, *4*(9), 1528–1542. https://doi.org/10.3390/ma4091528

Wittaya, T. (2012). Rice Starch-Based Biodegradable Films: Properties Enhancement. In *Structure and Function of Food Engineering* (pp. 103–134). https://doi.org/http://dx.doi.org/10.5772/47751

World Health Organization. (2014). Guidelines for drinking-water quality, 2011. *Switzerland: WHO Library Cataloguing-in-Publication Data, Fourth Google Scholar*, *1*, 595. https://doi.org/10.1016/S1462-0758(00)00006-6

World Health Organization. (2017). *WHO | Water safety and quality*. WHO; World Health Organization. http://www.who.int/water_sanitation_health/water-quality/en/

Wu, J., Lin, J., Zhou, M., & Wei, C. (2000). Synthesis and properties of starch-graft-polyacrylamide/clay superabsorbent composite. *Macromolecular Rapid Communications*, *21*(15), 1032–1034. https://doi.org/10.1002/1521-3927(20001001)21:15<1032::AID-MARC1032>3.0.CO;2-N

Wu, J. X., Zhang, J., Kang, Y. L., Wu, G., Chen, S. C., & Wang, Y. Z. (2018). Reusable and Recyclable Superhydrophilic Electrospun Nanofibrous Membranes with in Situ Co-cross-linked Polymer-Chitin Nanowhisker Network for Robust Oil-in-Water Emulsion Separation. *ACS Sustainable Chemistry and Engineering*, *6*(2), 1753–1762. https://doi.org/10.1021/acssuschemeng.7b03102

Wu, S., Hu, J., Wei, L., Du, Y., Shi, X., Deng, H., & Zhang, L. (2014). Construction of porous

chitosan-xylan-TiO2hybrid with highly efficient sorption capability on heavy metals. *Journal of Environmental Chemical Engineering*, *2*(3), 1568–1577. https://doi.org/10.1016/j.jece.2014.07.001

Xiang, Z., Gao, W., Chen, L., Lan, W., Zhu, J. Y., & Runge, T. (2016). A comparison of cellulose nanofibrils produced from Cladophora glomerata algae and bleached eucalyptus pulp. *Cellulose*, *23*(1), 493–503. https://doi.org/10.1007/s10570-015-0840-7

Xie, K., Zhang, Y., & Chen, S. (2010). Synthesis and characterization of reactive polyhedral oligomeric silsesquioxanes (R-POSS) containing multi-N-methylol groups. *Journal of Organometallic Chemistry*, *695*(5), 687–691. https://doi.org/10.1016/j.jorganchem.2009.12.001

Xie, K., Zhao, W., & He, X. (2011). Adsorption properties of nano-cellulose hybrid containing polyhedral oligomeric silsesquioxane and removal of reactive dyes from aqueous solution. *Carbohydrate Polymers*, *83*(4), 1516–1520. https://doi.org/10.1016/j.carbpol.2010.09.064

Xu, P., Zeng, G. M., Huang, D. L., Feng, C. L., Hu, S., Zhao, M. H., Lai, C., Wei, Z., Huang, C., Xie, G. X., & Liu, Z. F. (2012). Use of iron oxide nanomaterials in wastewater treatment: A review. *Science of the Total Environment*, *424*, 1–10. https://doi.org/10.1016/j.scitotenv.2012.02.023

Xu, R., Mao, J., Peng, N., Luo, X., & Chang, C. (2018). Chitin/clay microspheres with hierarchical architecture for highly efficient removal of organic dyes. *Carbohydrate Polymers*, *188*(November 2017), 143–150. https://doi.org/10.1016/j.carbpol.2018.01.073

Yan, H., Dai, J., Yang, Z., Yang, H., & Cheng, R. (2011). Enhanced and selective adsorption of copper(II) ions on surface carboxymethylated chitosan hydrogel beads. *Chemical*

Engineering Journal, *174*(2–3), 586–594. https://doi.org/10.1016/j.cej.2011.09.064

Yang, J. S., Jiang, B., He, W., & Xia, Y. M. (2012). Hydrophobically modified alginate for emulsion of oil in water. *Carbohydrate Polymers*, *87*(2), 1503–1506. https://doi.org/10.1016/j.carbpol.2011.09.046

Yang, J. S., Xie, Y. J., & He, W. (2011). Research progress on chemical modification of alginate: A review. *Carbohydrate Polymers*, *84*(1), 33–39. https://doi.org/10.1016/j.carbpol.2010.11.048

Yang, J., Xia, Y., Xu, P., & Chen, B. (2018). Super-elastic and highly hydrophobic / superoleophilic sodium alginate / cellulose aerogel for oil / water separation. *Cellulose*, *25*(6), 3533–3544. https://doi.org/10.1007/s10570-018-1801-8

Yang, R., Aubrecht, K. B., Ma, H., Wang, R., Grubbs, R. B., Hsiao, B. S., & Chu, B. (2014). Thiol-modified cellulose nanofibrous composite membranes for chromium (VI) and lead (II) adsorption. *Polymer (United Kingdom)*, *55*(5), 1167–1176. https://doi.org/10.1016/j.polymer.2014.01.043

Yang, R., Su, Y., Aubrecht, K. B., Wang, X., Ma, H., Grubbs, R. B., Hsiao, B. S., & Chu, B. (2015). Thiol-functionalized chitin nanofibers for As (III) adsorption. *Polymer (United Kingdom)*, *60*, 9–17. https://doi.org/10.1016/j.polymer.2015.01.025

Yilmaz, E., Memon, S., & Yilmaz, M. (2010). Removal of direct azo dyes and aromatic amines from aqueous solutions using two β-cyclodextrin-based polymers. *Journal of Hazardous Materials*, *174*(1–3), 592–597. https://doi.org/10.1016/j.jhazmat.2009.09.093

You, L., Lu, F., Li, D., Qiao, Z., & Yin, Y. (2009). Preparation and flocculation properties of cationic starch/chitosan crosslinking-copolymer. *Journal of Hazardous Materials*, *172*(1),

38–45. https://doi.org/10.1016/j.jhazmat.2009.06.120

Yu, X., Tong, S., Ge, M., & Zuo, J. (2013). Removal of fluoride from drinking water by cellulose@hydroxyapatite nanocomposites. *Carbohydrate Polymers*, *92*(1), 269–275. https://doi.org/10.1016/j.carbpol.2012.09.045

Yuan, G., Prabakaran, M., Qilong, S., Lee, J. S., Chung, I. M., Gopiraman, M., Song, K. H., & Kim, I. S. (2017). Cyclodextrin functionalized cellulose nanofiber composites for the faster adsorption of toluene from aqueous solution. *Journal of the Taiwan Institute of Chemical Engineers*, *70*, 352–358. https://doi.org/10.1016/j.jtice.2016.10.028

Yue, X., Li, J., Zhang, T., Qiu, F., Yang, D., & Xue, M. (2017). *In situ one-step fabrication of durable superhydrophobic- superoleophilic cellulose / LDH membrane with hierarchical structure for efficiency oil / water separation*. *328*, 117–123.

Zhang, F., Wu, W., Sharma, S., Tong, G., & Deng, Y. (2015). Synthesis of Cyclodextrin-functionalized Cellulose Nanofibril Aerogel as a Highly Effective Adsorbent for Phenol Pollutant Removal. *BioResources*, *10*(4), 7555–7568.

Zhang, J., Xiao, H., & Yang, Y. (2015). Preparation of hemicellulose-containing latex and its application as absorbent toward dyes. *Journal of Materials Science*, *50*(4), 1673–1678. https://doi.org/10.1007/s10853-014-8728-8

Zhang, Lingfan, Liu, X., Xia, W., & Zhang, W. (2014). Preparation and characterization of chitosan-zirconium(IV) composite for adsorption of vanadium(V). *International Journal of Biological Macromolecules*, *64*, 155–161. https://doi.org/10.1016/j.ijbiomac.2013.11.040

Zhang, Lingfan, Xia, W., Teng, B., Liu, X., & Zhang, W. (2013). Zirconium cross-linked chitosan composite: Preparation, characterization and application in adsorption of Cr(VI). *Chemical*

Engineering Journal, *229*, 1–8. https://doi.org/10.1016/j.cej.2013.05.102

Zhang, Lingzhi, Zhou, J., & Zhang, L. (2013). Structure and properties of β-cyclodextrin/cellulose hydrogels prepared in NaOH/urea aqueous solution. *Carbohydrate Polymers*, *94*(1), 386–393. https://doi.org/10.1016/j.carbpol.2012.12.077

Zhang, Tao, Mei, Z., Zhou, Y., Bu, X., Wang, Y., Li, Q., & Yang, X. (2014). Template-controlled fabrication of hierarchical porous Zn-Al composites with tunable micro/nanostructures and chemical compositions. *CrystEngComm*, *16*(9), 1793–1801. https://doi.org/10.1039/c3ce41839a

Zhang, Tianhong, & Marchant, R. E. (1996). Novel polysaccharide surfactants: The effect of hydrophobic and hydrophilic chain length on surface active properties. *Journal of Colloid and Interface Science*, *177*(2), 419–426. https://doi.org/10.1006/jcis.1996.0054

Zhang, X., Wang, Y., & Yang, S. (2014). Simultaneous removal of Co(II) and 1-naphthol by core-shell structured Fe3O4@cyclodextrin magnetic nanoparticles. *Carbohydrate Polymers*, *114*, 521–529. https://doi.org/10.1016/j.carbpol.2014.08.072

Zhang, Y., Xu, Y., Cui, H., Liu, B., Gao, X., Wang, D., & Liang, P. (2014). La(III)-loaded bentonite/chitosan beads for defluoridation from aqueous solution. *Journal of Rare Earths*, *32*(5), 458–466. https://doi.org/10.1016/S1002-0721(14)60094-6

Zhao, F., Repo, E., Sillanpää, M., Meng, Y., Yin, D., & Tang, W. Z. (2015). Green synthesis of magnetic EDTA- And/or DTPA-cross-linked chitosan adsorbents for highly efficient removal of metals. *Industrial and Engineering Chemistry Research*, *54*(4), 1271–1281. https://doi.org/10.1021/ie503874x

Zhao, Y., Zhang, Y., Lindström, M. E., & Li, J. (2015). Tunicate cellulose nanocrystals:

Preparation, neat films and nanocomposite films with glucomannans. *Carbohydrate Polymers*, *117*, 286–296. https://doi.org/10.1016/j.carbpol.2014.09.020

Zheng, Y., Hua, S., & Wang, A. (2010). Adsorption behavior of Cu2+from aqueous solutions onto starch-g-poly (acrylic acid)/sodium humate hydrogels. *Desalination*, *263*(1–3), 170–175. https://doi.org/10.1016/j.desal.2010.06.054

Zhou, Y., Jin, Q., Zhu, T., & Akama, Y. (2011). Adsorption of chromium (VI) from aqueous solutions by cellulose modified with β-CD and quaternary ammonium groups. *Journal of Hazardous Materials*, *187*(1–3), 303–310. https://doi.org/10.1016/j.jhazmat.2011.01.025

Zhou, Z.-Y., Tian, N., Li, J.-T., Broadwell, I., & Sun, S.-G. (2011). Nanomaterials of high surface energy with exceptional properties in catalysis and energy storage. *Chem. Soc. Rev.*, *40*(7), 4167–4185. https://doi.org/10.1039/C0CS00176G

Zubair, M., Daud, M., McKay, G., Shehzad, F., & Al-Harthi, M. A. (2017). Recent progress in layered double hydroxides (LDH)-containing hybrids as adsorbents for water remediation. *Applied Clay Science*, *143*(March), 279–292. https://doi.org/10.1016/j.clay.2017.04.002

Zubair, M., Jarrah, N., Ihsanullah, Khalid, A., Manzar, M. S., Kazeem, T. S., & Al-Harthi, M. A. (2018). Starch-NiFe-layered double hydroxide composites: Efficient removal of methyl orange from aqueous phase. *Journal of Molecular Liquids*, *249*, 254–264. https://doi.org/10.1016/j.molliq.2017.11.022

2. Research objective and hypotheses

2.1. General objective

The aim of this work is to develop novel bio-based materials to remove unregulated and emerging contaminants form water bodies, understanding the interactions between the selected materials forming the sorbent, and these with different pollutants all around the world. The pollutant selected as primary target was the cyanotoxin -microcystin-LR- which has been linked to hepatic damage and is every-year occurrent during and shortly after algae blooms. Furthermore, this toxin has been found in the water supply from Opelika, AL, which in turn supplies the City of Auburn when the capacity of the surface water source of the city is exceeded.

To assure the biological origin and sustainable availability in Alabama, cellulose, *i.e.,* cellulose nanofibrils or wood, and chitosan were selected as primary base materials for the generation of the sorbent.

2.2 Objectives for each chapter

Chapter 1

a. To research the published literature regarding natural polymers to select the best alternatives for water treatment.

Chapter 2

a. To state the objectives and hypotheses for this dissertation
b. To explain the main interactions between the different systems
c. To denote the limitations of the techniques used in this work

Chapter 3

a. To generate a cellulose/cyclodextrin material that can adsorb microcystin-LR
b. To evaluate the effect of spatial configuration on adsorption capacity
c. To characterize the synthetized material by spectroscopy (FTIR), calorimetry (TGA), and microscopy (AFM)
d. To test the adsorption of microcystin-LR by measurements on model surfaces in real time through adsorption in a Quartz Cristal Microbalance with Dissipation monitoring (QCMD)

Chapter 4

a. To generate a 3-D structure for using the formed CNF-CD fibrils
b. To test on adsorption of microcystin-LR
c. To corroborate and understand the driving mechanism between the adsorption of microcystin-LR and the aerogel

Chapter 5

a. To generate an oriented cyclodextrin material for removal of microcystin
b. To characterize the generated material via spectroscopy (FTIR & XPS), elemental analysis (EA)
c. To use the formed material as an active coating for other cellulosic materials
d. To investigate the effect of availability of amino groups will have on coating
e. To evaluate performance in adsorption capacity with microcystin-LR

Chapter 6

a. To generate a nanocellulose structure from wood by top-down approach
b. To characterize the generated material via spectroscopy (FTIR), calorimetry (TGA) and morphology (SEM)
c. To use the formed chitosan-cyclodextrin material with the active coating
d. To evaluate performance in adsorption capacity of microcystin-LR

Chapter 7

a. To obtain and characterize water samples from Ogletree Lake
b. To increase the coating content on the nanowood
c. To test the coated nanowood on spiked lake water sample

2.3. Hypotheses

1. Natural polymers, mainly polysaccharides, can be used in adsorption systems for the effective removal of microcystin-LR from water.
2. The modification of the polysaccharides with β-cyclodextrin will allow to add hydrophobic active points to the sorbents, allowing the capture of the amphipathic toxin.
3. The use of the active material as a coating will allow the diversification of shapes or systems that can be used as sorbent.
4. The selected system will be able to capture the toxin, in both: lab-controlled samples and water obtained from natural sources.

2.4. Fundamentals and limitations

As explored throughout this dissertation, there exists a large interest on utilizing cellulose and other polysaccharide-derived materials to prepare bio-based adsorbents driven by their

abundancy and inherent biocompatibility. However, to be able to best design and utilize these novel adsorbents for the removal of pollutants, it is imperative to understand the fundamental interactions occurring between the adsorbents and the contaminants to be removed.

Likewise, it is important to be aware of the limitations and assumptions that the different techniques utilized in this work present while measuring these interactions. Thus, the values, inferences, and conclusions can be better weighted and compared to results reported in the literature.

Therefore, this chapter concentrates in a more in-depth explanation of the interactions presented and exploited to develop the materials and adsorbents utilized in this dissertation; in specific, between wood components, cellulose -mostly cellulose nanofibril-, chitosan, and β-cyclodextrin. Additionally, driving forces in the complex formation between cyclodextrin and cyanotoxin microcystin-LR are explored. Convergently, the assumptions considered when modeling frequency shifts of the Quartz Crystal Microbalance to calculate mass adsorbed on the surface are described; as well as the limitations on the fitting of data from concentrations found by High Pressure Liquid Chromatography.

2.4.1. Fundamental interactions

As wood is a biosynthesized product, its chemical composition varies depending on the selected tree, genus, specie, geographical location, available soil nutrients, age, environmental condition of farming, droughts, and other factors (Pettersen and Rowell 1984; Iglesias et al. 2020). However, the three main components of wood are cellulose, hemicellulose, and lignin. Within these, the polysaccharide components -cellulose and hemicellulose- account for 65 to 70% of the dry weight (Rowell et al. 2012), which make them the primary contributors of the physicochemical properties of the wood as a material. However, these materials as individual components possess

their own functional groups, thermomechanical properties, and morphological characteristics; those determine in turn the interactions and possible uses that they can have towards adsorbent materials.

Is of particular interest cellulose, as this biopolymer tends to bundle into nano- to microscale fibers, depending on the diameter. When arrange, the cellulose fibril have two differentiable packing conformations, an amorphous and a crystalline domain; the previous can be dissolved by acidic hydrolysis, which when in the nanoscale diameters leaves the crystalline domain as the nanomaterial known as cellulose nanocrystals (Salas et al. 2014).

The chemical composition of these materials, as well as molecular organization in which they can be found, will have great impact in the properties that the materials derived from them will possess. To understand these effects, there are two levels in which to study and understand the causing phenomena: atomic and molecular level.

For the atomic level, the main phenomena to describe are intermolecular forces. Those forces are mostly the molecular expression of the fundamental electromagnetic force, more commonly explained as the electrostatic state. After the development of the quantum theory in the 1920s, it was better understood that this expression of the force could be described by the spatial distribution of the electron clouds, that when considered homogenous could be solved by the traditional inverse-square Coulomb force theorem. However, as the atoms in molecules variate, these interactions are not always static or with the same intensity on attraction force, which have led to a subdivision of them into covalent bonds, ionic bonds, metallic bonds, van der Waals forces, hydrogen bonding, and solvation forces (Israelachvili 2011). Furthermore, attraction can occur also in the materials as a entropic effect which decreases to total energy of the system evaluated, which is called hydrophobic interactions or hydrophobic effect (Blackburn 2004; Israelachvili

2011; Lombardo and Thielemans 2019; Fernandes et al. 2020). Therefore, different equations have been developed to better explain the interactions occurring with each force expression as well as for the entropic contribution on adsorption systems (Lui 2009; Israelachvili 2011).

The covalent forces or bonds are the main force responsible of the formation of the molecules and its functional groups. In the case of cellulose, the sharing of electrons (covalent bond) between $C_6H_{10}O_5$ atoms forms the anhydroglucopyranose unit, which then spatially arrange in the way we know them due to repulsive forces between the position of the rest of electron clouds of the atoms that are not participating on the bond formation. And when the formed units share electrons with other identical structures through the carbons and oxygens that are in position 1 and 4, in a antiparallel formation (β bond), they form the cellulose polymer (OSullivan 1997; Klemm et al. 2002). Similarly, hemicellulose is composed by the covalent bonding of different monosaccharide units, mainly glucose, mannose, galactose, arabinose, and xylose. In this case, the diversity of monomers tends to form smaller chains than cellulose, with branches and a combination of α and β linkages (Tunc and Van Heiningen 2008; Gírio et al. 2010). In the case of the third component of wood: lignin; the polymer is composed by three versions of phenylpropane units (p- coumaryl alcohol, coniferyl alcohol, and sinapyl alcohol) that forms also a branched 3-D structure in wood (Chakar and Ragauskas 2004; Rowell et al. 2012).

A particularity of lignin is that its monomers are based on phenolic structures. These phenyls are groups of 6 carbon on a ring formation, that share 2 electron levels (s and p) which would require strong attraction from other atoms to break. The electron cloud is then contained to the interior axis of the formed molecule, letting the exterior “unprotected” and the protons tightly bound; then restrict the charge flow from other molecules, for example the exchange of hydrogen protons. As this exchange is restricted, more energy is required for this type of molecules to interact

with other molecules such as water, and therefore they tend to decrease the energetic state of the system by interacting with other molecules that have a similar phenomenon, resulting it what is called hydrophobic interactions or hydrophobic effect (Israelachvili 2011). This phenomenon is usually stronger that other weak electrostatic attractive forces such as van der Waals or hydrogen bonding.

Even though van der Waals and hydrogen bonding have smaller magnitudes than the others attractive forces, they are responsible for large properties in the wood components behavior and structure. For example, the formed cellulose chain is kept lineal by the attraction of the hydrogens to the dipoles of the nearby atoms in the same chain (H-bonding), more specifically, between the one connected to carbons 3 and 5 of the monomers (Kontturi et al. 2003). This attraction is also present in contiguous chains, that depending on the position that there are found on the contiguous chain to form bonds between C6 and C3 or C6 and C2, form compact structures known as cellulose I and II, respectively (Kontturi et al. 2003). Furthermore, when these chains connected by hydrogen bonds add up, they form nanometric wide organized structures known as cellulose nanomaterials (Foster et al. 2018).

As described, those atomic level interactions are responsible for the structure and most of the basic physicochemical properties of the biopolymers, such as melting point or density. However, the addition of the forces in their now formed molecules and 3-D forms also add new properties for the materials, especially on the surface. The surface or interface is the region with limited thickness (< 1 μm), which composition and energy state vary from the continuous bulk phase, as not all the atoms are interacting with the same number of contiguous atoms as in the bulk (Wu 1982).

One of these surface properties is surface charge, which is determined by the potential given by the atoms that are not fully interacting with others as the ones in the bulk material. In the cellulosic materials is given mainly by the carboxyl groups that are formed by the oxidation of the alcohol in C6 (Unruh and Kenyon 1946), and sulfate groups for some cellulose nanocrystal (obtained by sulfuric acid hydrolysis) (Sjostrom and Enstrom 1966; Young 1994; Östenson et al. 2006). Other providers of surface charge in lignocellulosic nanomaterial are the residual hemicelluloses and lignin that also have carboxyl groups that are exposed in this interfacial volume (Popescu et al. 2008). Additionally, the extraction process of the cellulose pulp from which the nanomaterial is obtained also modifies the available groups in the surface, with some lignosulfonate compounds formed during sulfite process that would also impact the charge on the surface (Chakar and Ragauskas 2004). This surface charge can be measured by multiple titration processes, where the charges would be neutralized by addition of protons or other polymer ions, as the main intermolecular force present here is the dipole-dipole interactions (Mocchiutti et al. 2016).

The energy of a system is determined by more than just the dipole-dipole interactions measurable by charge density. Overall, the energy on the surface is the resulting from the presence of dispersive intermolecular forces (van der Waals), plus some of the stronger polar interactions (H-bonding, and dipole-dipole interactions), as well as some hydrophobic free energy -cavity work- (Baldwin 2013). The sum of these energies on the surface are called surface free energy (Israelachvili 2011). A formal description of this energetic add-up is as the free energy that is required to transport matter from the bulk to the interfacial zone, and is dependent of the temperature, pressure, area and the total number of moles in the system (Wu 1982). As mention,

the surface groups will contribute to the surface free energy, but other factors such as position, surface structure, atomic neighbors, and even shape would greatly impact the result.

Two advantages of knowing the surface free energy on a solid surface are: 1) allows the prediction of its behavior when interacting with liquids, including water; and 2) indicates the energy required to propitiate the intermolecular and interatomic interactions with other surfaces, which is the phenomena also known as adhesion (Awaja et al. 2009).

The understanding of these two energy expressions, the surface charge, and the molecular interactions that will be present in any determine material were important to understand throughout this dissertation. Primarily, as the developed products were exposed to water, as well as to describe the capability that they would have for targeted removal of pollutants.

Herein, the cellulose nanofibril have a base interaction capacity with the pollutants, determined by the available groups, the surface exposed to the contaminated water, the solubility and nature of the pollutant. Similarly, other factors such as the temperature, pH, and the presence or lack of ions would enhance or decrease the adsorption capacity. In specific, while using the toxin microcystin-LR, which is a cyclic heptamer (7 amino acids: d-Ala-l-Leu-d-MeAsp-l-Arg-Adda-d-Glu-MdhA) as our model pollutant (Kaplan et al. 2012), most of the residues will be sterically (space wise) blocked. Thus, the interactions will be only with smaller molecules such as water (solvation and solubility are determined by these); while the arginine and ADDA residues are long enough to interact with other molecules beside itself. Arginine is an amino-based residue, which means that at the end of its chain it has 2 “free” amine groups that resonate a π electron bond, presenting then a positive charged dipole, which could be attracted to the dipole of the carboxyl groups in the surface of the cellulose.

Even more, as cellulose nanofibrils are organized 3-D structures, part of the properties that the crystalline structure possess, is that one of the faces (i.e., plane 110) is hydrophobic because of the equatorial localization of all hydroxyl groups (Yamane et al. 2006). This hydrophobic plane become a surface on larger scale, where phenolic groups such as the ADDA residue of the toxin, are attracted to, this to decrease the system's free energy. Therefore, there are two mechanisms that could direct the interactions of cellulose and the toxin.

As the general aim of this work was to increase the capturing of the toxin, more surface charge or multiple hydrophobic regions could have been added. As the latter would not depend on the physicochemical conditions to adsorb, the preferred route was the addition of cyclodextrin onto the cellulose nanofibril. Cyclodextrins, and more specifically β-cyclodextrin, is composed from anhydroglucose monomers linked in the carbons in positions 1 and 4, similarly to cellulose; however, in this molecule the seven monomers are linked in an α orientation, given the chain a rotation and its further formation of the cycle. In this molecule, the hydroxyl groups are oriented to the exterior face, leaving the center of the cone-shaped structure deprived from electron clouds, resulting in molecular spaces that would tend to adsorb other molecules or components to decrease their energy, forming hydrophobic active points (Kurkov and Loftsson 2013).

Cellulose and cyclodextrins form covalent bonds with groups like epoxy rings, that when in small molecules such as epichlorohydrin, can form bridges that connect the two structures. This reaction is propitiated by the strong dipole that the epoxy ring forms, that when in contacts other susceptible dipoles like the ones in the hydroxyl groups, can open the ring, providing enough energy to covalently bond the two molecules (Sun and Lindsay 2004). Here the formed material will have on the surface a different energy potential, as some of the carboxyl groups could have been used for the linkage, however, the hydrophobic effect will be potentiated as more

hydrophobic points should be available throughout the material (Archimandritis et al. 2016; Gomez-Maldonado et al. 2019).

The simplest approach is on model flat surfaces, where the surface energy is displacing only on two dimensions; however, in more complex 3-D structures such as aerogels, other factors should be taken into consideration. For instance, the same cellulose-cyclodextrin fibrous material could be compacted through filtration, extracting water molecules that are not interacting with the surface. To form the aerogel, solvent exchanges was done (Chapter 4, Dong et al. 2013; Toivonen et al. 2015; Han et al. 2016), this is done to avoid the dragging effect that water could have with the cellulose fibrils as adhesion and resistive forces will occur between the chains and the water due to the electrostatic and dispersive interactions. Therefore, the different chemical characteristic of the different solvents is the reason to use them as weaker attractions to the surface arise, so when removed drastically (i.e., by freeze-drying), the dragging force will be lower, allowing the fibers to stay in the same position even when liquid is absent. Even when this is done, the fibers in solution would try to encounter special states where the energy of the system is low, so contact between them in the hydrophobic faces can be expected, as well as the formation of some hydrogen bonding between the chains, resulting in agglomeration, and therefore decrease of the surface area. Which as mentioned above, is one of the factors that determine the surface energy and the attraction to other molecules, surfaces, and ions to the surface. Consequently, the ability of the cellulose-cyclodextrin to capture the microcystin is decreased through the addition of all these energetical losses.

In the formation of hydrogels, as done in Chapter 5, the impact of the interactions with media in the properties of the material was clear, mainly in the solubilization of cellulose in the sodium-urea solution. Cellulose is insoluble in water due to the high crystallinity of the formed

molecules and fibers, which due to the high density of H-bonding generated have a stronger interaction between them, than the interactions that could form with the water (Pinkert et al. 2010). However, if these bonds are broken, solubilization of cellulose is possible. For this the ion sodium, has a high electro-attractive force (ion-dipole), high enough that the surface hydroxyl groups release the bound proton and interact with it, breaking some of the H-bonds formed (Beck et al. 2015). However, solvation (the complete surrounding of water to the molecule to become a solvate) is still not possible as other type of interactions are still present, such as hydrophobicity of the surface 110 plane. To eliminate this, urea can attach to the plane on the crystals while also interacting with the water, allowing the dissolution (Zhou and Zhang 2000; Cai and Zhang 2005; Xiong et al. 2014; Huber et al. 2016). The high concentration of the sodium and urea also come with an alkaline pH, so when the solution is dropped into an acid bath, the solubility of the cellulose drops, regenerating its crystalline structure and forming 3-D compacted bead hydrogels (Trivedi et al. 2016). Here, the interactions not only affect the solubility, but also the surface and crystalline structure.

Similarly, modification of chitosan with TEMPO oxidized β-cyclodextrin was possible with green chemistry as molecules intermediaries were used to lower the energy required to form the covalent bond between the carboxyl groups of cyclodextrin and the amino groups of chitosan. Herein, the imide group of 3-(3-Dimethylaminopropil)-1-ethyl-carbodiimide hydrochloride (EDC) is strongly attracted to the carboxyl groups, however the electron imbalance is too strong to form a stable covalent bond. So, in the presence of N-hydroxysuccinimide (NHS), the displacement of the EDC is more favorable than forming the bond, allowing the NHS to link. However, this bond is still to energetically unstable, and in the presence of amine groups -such as the ones from

chitosan- the systems energy is lowered while crosslinking the amino-containing polymer to the carboxyl-containing molecule (Orelma et al. 2012; Vashist 2012).

Likewise, the molecular interactions and its changes can be the only thing needed to generate a 3-D structure; like this, composite materials can also be generated from cellulose without the formation of covalent bonds. As mentioned before, the hydroxyl groups of cellulose are exposed in the equatorial axis (Alekozai 2013), which makes the surface rich in hydroxyl groups. These groups can be used to form H-bonding with other β-lineal polysaccharides, such as chitosan, that are close enough to the surface (de Mesquita et al. 2010; Orelma et al. 2011; Junka et al 2014). Here the surface energy is decreased -and therefore the entropy is increased- by the intermediate state where salts and bound water is displaced by the new polymer (Lombardo and Thielemans, 2019), that once on the surface tis adsorption is enhancing the density of H-bond interactions and irreversibly adsorbing the chitosan onto the surface (de Mesquita et al. 2010; Orelma et al. 2011; Junka et al 2014). The presence of the chitosan either pristine or pre-modified with cyclodextrin is adding functionality to the surface, and therefore surface energy, as the available groups of these new polymers would be exposed in the new generated surface. This mechanism was observed in the 3 different materials –thin films, hydrogels, wood aerogels- coated with the cyclodextrin modified chitosan.

As elucidated by this work, combination of atomic and molecular interactions opens a wide range of possible materials and applications that can be targeted with these renewable and sustainable materials, enhancing the use of the forest, and increasing its potential value.

2.4.2. Limitation on mass and concentration quantification

Throughout this dissertation, mass calculations were done to compare the adsorption capacity of the materials using two main techniques: Quartz Crystal Microbalance with Dissipation

monitoring (QCMD) and High-Pressure Liquid Chromatography (HPLC). However, both techniques have physical and operational limitations on how the samples are processed, as well as resorting to mathematical models to fit the raw data obtained into generalizations on mass values. Therefore, this section aims to point out some of them to have a more informed understanding on the results presented on this work.

2.4.2.1. Quartz Crystal Microbalance with Dissipation monitoring (QCMD)

Fundamentally, QCMD is based on the piezoelectric properties for the quartz-based sensor. Liquids containing the materials to interact with the surface are flown into sealed channel containing the surface immersed into the same liquid. In there its understood that the water adsorbed onto the surface will also be accounted for. This is mainly true for the adsorbed mass calculated with the Sauerbrey correlation (1959, Eq. 8.1) which transforms the changes in frequency into mass. This equation assumes rigid layers, and materials uniformly distributed on the surface of the sensor and with lower values of mass than the mass of the crystal:

$$\Delta m = C * \Delta F * n^{-1} \tag{8.1}$$

Where the constant considers the density and viscosity of the quartz sensor but not of the media, or any changes in pressure due to the flow of the materials and liquid. Furthermore, most of the polymeric systems do not generate a rigid layer, then Sauerbrey's equation underestimates the adsorbed mass. Therefore, some other models have been generated to address the changes of mass, based on Voigt's and Maxwell's mechanical viscoelastic relationships. These models take into the account the density, dynamic and static viscosity of the adsorbed materials as well as the crystal's (Voinova et al., 1998). However, changes pressure or the interactions with dissolved gas are unaccounted for, which happens more often as longer times are used for the measurements and consecutive adsorptions.

Moreover, the dissipation factor ΔD is related to the viscoelastic properties of the layers formed on the crystal, as it translates the relationship of energy dissipation from the sensor to the fluid and the energy stored (8.2); it can be measured as it is inversely proportional to the decay time constant (τ) and the resonant frequency (f) as it is shown in equation 8.3 (Voinova et al., 1998).

$$D = \frac{E_{dissipated}}{2\pi E_{stored}} \tag{8.2}$$

$$D = \frac{1}{\pi f \tau} \tag{8.3}$$

If the generated film is viscous, energy would be dissipated due to the oscillation of the layer, then more energy is loss and longer decay times are present which translates to a decrement in the D factor; while when more energy is stored, as the surface is being rigidize, increments in the D-factor will be observable (Turon et al., 2008). However, localized changes on pH will affect the compaction arrangement of chitosan (Junka et al. 2014), but these changes can be happening at surface level as the immobilized ions and water are being exchanged throughout the adsorption, which in turn are usually overseen and error in the mass transformation would occur.

2.4.2.2. High-Pressure Liquid Chromatography (HPLC).

Conversely, HPLC is a technique that do not performs in real time measurements, which comes with its own complications. As a chromatography the principle is that the interaction between the residual concentration of the pollutant -microcystin-LR for this work- will be captured in a hydrophobic column (C18) and will be only removed in its totality while the solvent is being modified and the flushing will occur at the specific time (4.2 min). However, most times than not, some residual pollutant is retained on the column even after the total solvent change, for which

rinsing with only solvent should done every couple measurement to decrease the error. Furthermore, as the measurement is asynchronous, there is the assumption that no degradation, evaporation, or interactions of the container and pollutant are occurring during the waiting times before running the batch to obtain the data. Finally, as sampling is done from different times for the calculation of kinetics, there is the supposition that the differences are only due to adsorption of the pollutant onto the sorbent, without considering evaporation, osmotic and diffusion profiles, interactions between the pollutant and the container or pipetting equipment.

On the case of the actual conversion to mass, the standard curve is done without any sorbent, and is assuming that the sorbent will not change any properties of the solvent in which the adsorption is being made. However, some natural-based sorbent can release H ions, changing the pH, or release salts and water that were tightly adsorbed on the surfaces but can be less favorable while the adsorption of the pollutant is made.

Beside that mathematical error due to the fitting of the standard curve, the fitting into the pseudo-first and pseudo-second order kinetics is limited in this work (Tran et al., 2013), as the adsorption is not electrostatically driven, there was not a clear equilibrium value. This then do not allow the fitting onto the pseudo-first order kinetics (8.4), as it is not possible to apply natural logarithms to negative values.

$$\ln(qe - qt) = \ln qe - k_1 t \tag{8.4}$$

Furthermore, the data points were of samples obtained from the same experiments, which comes with the error that the data is not independent from each other. To assure reproducibility averages of different experiments are done, but standard deviations are usually big as the microcystin has a high surface activity which competes with the adsorption on the utilized sorbents and drags error to the samples as concentration is not homogenous thought the solution. Finally,

the calculated adsorption capacity in equilibrium can vary depending on the monitored time, as concentration could vary; and the concentrations utilized will affect the percentage of saturation, adding to the error on the capacity (Lombardo and Thielemans, 2019).

Overall, these techniques come with their own limitations and assumptions that can be reduced with fine control of the experimental conditions and multiple repetitions to reduce the mathematical error. However, it is important to be aware of the limitations with asseverations are made in the final conclusions.

2.5. Conclusions

The better understanding of the fine scale interactions and phenomena occurring throughout the design of the material allows to better visualize and anticipate the performance of the sorbents. Furthermore, knowing what to expect can also help to better limit the conditions and experimental design. Knowing the limitations of the different analytical techniques while understanding the systems they are applied to, allows for a better decision making on final applications.

2.6. Literature cited.

Alekozai E (2013) Enhanced Multiscale Sampling of the Cel7A-Cellulose Interaction. Ruperto-Carola University of Heidelberg

Archimandritis AS, Papadimitriou T, Kormas KA, et al (2016) Theoretical investigation of microcystin-LR, microcystin-RR and nodularin-R complexation with α-, β-, and γ-cyclodextrin as a starting point for the targeted design of efficient cyanotoxin traps. Sustain Chem Pharm 3:25–32. https://doi.org/10.1016/j.scp.2016.02.001

Awaja F, Gilbert M, Kelly G, et al (2009) Adhesion of polymers. Prog Polym Sci 34:948–968. https://doi.org/10.1016/j.progpolymsci.2009.04.007

Baldwin, R. L. (2013). The new view of hydrophobic free energy. FEBS Letters, 587(8), 1062–1066. https://doi.org/10.1016/j.febslet.2013.01.006

Beck S, Méthot M, Bouchard J (2015) General procedure for determining cellulose nanocrystal sulfate half-ester content by conductometric titration. Cellulose 22:101–116. https://doi.org/10.1007/s10570-014-0513-y

Blackburn, R. S. (2004). Natural polysaccharides and their interactions with dye molecules: Applications in effluent treatment. Environmental Science and Technology, 38(18), 4905–4909. https://doi.org/10.1021/es049972n

Cai J, Zhang L (2005) Rapid dissolution of cellulose in LiOH/urea and NaOH/urea aqueous solutions. Macromol Biosci 5:539–548. https://doi.org/10.1002/mabi.200400222

Chakar FS, Ragauskas AJ (2004) Review of current and future softwood kraft lignin process chemistry. Ind Crops Prod 20:131–141. https://doi.org/10.1016/j.indcrop.2004.04.016

de Mesquita, J. P., Donnici, C. L., & Pereira, F. V. (2010). Biobased nanocomposites from layer-by-layer assembly of cellulose nanowhiskers with chitosan. Biomacromolecules, 11(2), 473–480. https://doi.org/10.1021/bm9011985

Dong H, Snyder JF, Tran DT, Leadore JL (2013) Hydrogel, aerogel and film of cellulose nanofibrils functionalized with silver nanoparticles. Carbohydr Polym 95:760–767. https://doi.org/10.1016/j.carbpol.2013.03.041

Fernandes, A., Oliveira, J., Fonseca, F., Ferreira-da-Silva, F., Mateus, N., Vincken, J. P., & de Freitas, V. (2020). Molecular binding between anthocyanins and pectic polysaccharides – Unveiling the role of pectic polysaccharides structure. Food Hydrocolloids, 102(September 2019). https://doi.org/10.1016/j.foodhyd.2019.105625

Foster EJ, Moon RJ, Agarwal UP, et al (2018) Current characterization methods for cellulose nanomaterials. Chem Soc Rev 47:2609–2679. https://doi.org/10.1039/c6cs00895j

Gírio FM, Fonseca C, Carvalheiro F, et al (2010) Hemicelluloses for fuel ethanol: A review. Bioresour Technol 101:4775–4800. https://doi.org/10.1016/j.biortech.2010.01.088

Gomez-Maldonado D, Vega Erramuspe IB, Filpponen I, et al (2019) Cellulose-Cyclodextrin Co-Polymer for the Removal of Cyanotoxins on Water Sources. Polymers (Basel) 11:2075. https://doi.org/10.3390/polym11122075

Han S, Sun Q, Zheng H, et al (2016) Green and facile fabrication of carbon aerogels from cellulose-based waste newspaper for solving organic pollution. Carbohydr Polym 136:95–100. https://doi.org/10.1016/j.carbpol.2015.09.024

Howard JL (2016) U . S . Timber Production , Trade , Consumption , and Price Statistics , 1965 – 2013. 1965–2013

Howard JL, Liang S (2019) U.S. Timber Production, Trade, Consumption, and Price Statistics, 1965-2017. 96

Huber T, Starling K, Cen WS, et al (2016) Effect of Urea Concentration on the Viscosity and Thermal Stability of Aqueous NaOH / Urea Cellulose Solutions. 2016:

Iglesias MC, Gomez-Maldonado D, Peresin MS, Via BK (2020) Pulping Processes and Their Effects on Cellulose Fibers and Nanofibrillated Cellulose Properties: A Review. 70:10–21. https://doi.org/10.13073/FPJ-D-19-00038

Israelachvili, J. (2011). Intermolecular and Surface Forces. In Intermolecular and Surface Forces (Third). Elsevier. https://doi.org/10.1016/C2009-0-21560-1

Kaplan A, Harel M, Kaplan-levy RN, et al (2012) The languages spoken in the water body (or the biological role of cyanobacterial toxins). 3:1–11. https://doi.org/10.3389/fmicb.2012.00138

Klemm D, Schmauder HP, Heinze T (2002) Cellulose. In: Vandamme EJ, de Baets S, Steinbüchel A (eds) Biopolymers. Volume 6, Polysaccharides II, polysaccharides from eukaryotes, 1st edn. Wiley-VCH, Chichester, pp 275–287

Köhl M, Lasco R, Cifuentes M, et al (2015) Changes in forest production, biomass and carbon: Results from the 2015 UN FAO Global Forest Resource Assessment. For Ecol Manage 352:21–34. https://doi.org/10.1016/j.foreco.2015.05.036

Kontturi E, Thüne PC, Niemantsverdriet JW (2003) Novel method for preparing cellulose model surfaces by spin coating. Polymer (Guildf) 44:3621–3625. https://doi.org/10.1016/S0032-3861(03)00283-0

Kurkov S V., Loftsson T (2013) Cyclodextrins. Int J Pharm 453:167–180. https://doi.org/10.1016/j.ijpharm.2012.06.055

Lombardo, S., & Thielemans, W. (2019). Thermodynamics of adsorption on nanocellulose surfaces. Cellulose, 26(1), 249–279. https://doi.org/10.1007/s10570-018-02239-2

Liu, Y. (2009). Is the free energy change of adsorption correctly calculated? Journal of Chemical and Engineering Data, 54(7), 1981–1985. https://doi.org/10.1021/je800661q

Mocchiutti P, Schnell CN, Rossi GD, et al (2016) Cationic and anionic polyelectrolyte complexes of xylan and chitosan. Interaction with lignocellulosic surfaces. Carbohydr Polym 150:89–98. https://doi.org/10.1016/j.carbpol.2016.04.111

Munang R, Thiaw I, Thompson J, et al (2011) Sustaining Forests: Sustaining forests : Investing in our common future

Orelma H, Filpponen I, Johansson LS, et al (2011) Modification of cellulose films by adsorption of cmc and chitosan for controlled attachment of biomolecules. Biomacromolecules 12:4311–4318. https://doi.org/10.1021/bm201236a

Orelma, H., Filpponen, I., Johansson, L. S., Österberg, M., Rojas, O. J., & Laine, J. (2012). Surface functionalized nanofibrillar cellulose (NFC) film as a platform for immunoassays and diagnostics. Biointerphases, 7(1–4), 1–12. https://doi.org/10.1007/s13758-012-0061-7

Östenson M, Järund H, Toriz G, Gatenholm P (2006) Determination of surface functional groups in lignocellulosic materials by chemical derivatization ESCA analysis. Cellulose 13:157–170. https://doi.org/10.1007/s10570-005-5855-z

O'Sullivan AC (1997) Cellulose: the structure slowly unravels. Cellulose 4:173–207. https://doi.org/Chemistry and Materials Science

Pettersen RC, Rowell RM (1984) The Chemical Compostition of Wood. In: Rowell R (ed) The chemistry of solid wood. American Chemical Society, Washington, pp 57–126

Pinkert A, Marsh KN, Pang S (2010) Reflections on the solubility of cellulose. Ind Eng Chem Res 49:11121–11130. https://doi.org/10.1021/ie1006596

Popescu CM, Tibirna CM, Raschip IE, et al (2008) Bulk and Surface Characterization of Unbleached and Bleached Softwood Kraft Pulp Fibres. Cellul Chem Technol 42:525–547

Rowell R, Pettersen R, Tshabalala M (2012) Cell Wall Chemistry. In: Handbook of Wood Chemistry and Wood Composites, Second Edition. pp 33–72

Salas C, Nypelö T, Rodriguez-Abreu C, et al (2014) Nanocellulose properties and applications in colloids and interfaces. Curr Opin Colloid Interface Sci 19:383–396. https://doi.org/10.1016/j.cocis.2014.10.003

Sauerbrey G (1959) Verwendung von Schwingquarzen zur Wägung dünner Schichten und zur Mikrowägung. Zeitschrift für Phys 155:206–222. https://doi.org/10.1007/BF01337937

Sjostrom E, Enstrom B (1966) A method for separate determination of sulpho and carboxyl groups in sulphite pulps. Sven PAPPERSTIDNING-NORDISK Cellul 69:55

Sun T, Lindsay JD (2004) Cyclodextrins covalently bound to polysaccharides

Toivonen MS, Kaskela A, Rojas OJ, et al (2015) Ambient-Dried Cellulose Nanofibril Aerogel Membranes with High Tensile Strength and Their Use for Aerosol Collection and Templates for Transparent, Flexible Devices. Adv Funct Mater 25:6618–6626. https://doi.org/10.1002/adfm.201502566

Tran, C. D., Duri, S., Delneri, A., & Franko, M. (2013). Chitosan-cellulose composite materials: Preparation, Characterization, and application for removal of microcystin. Journal of Hazardous Materials, 253, 355–366.

Trivedi P, Trygg J, Saloranta T, Fardim P (2016) Synthesis of novel zwitterionic cellulose beads by oxidation and coupling chemistry in water. Cellulose 23:1751–1761. https://doi.org/10.1007/s10570-016-0939-5

Tunc MS, Van Heiningen ARP (2008) Hemicellulose extraction of mixed southern hardwood with water at 150 oC: Effect of time. Ind Eng Chem Res 47:7031–7037. https://doi.org/10.1021/ie8007105

Turon, X., Rojas, O. J., & Deinhammer, R. S. (2008). Enzymatic kinetics of cellulose hydrolysis: A QCM-D study. Langmuir, 24(8), 3880–3887. https://doi.org/10.1021/la7032753

Unruh CC, Kenyon WO (1946) The Formation and Properties of Oxidized Celluloses. Text Res J 16:1–12. https://doi.org/10.1177/004051754601600101

Vashist, S. K. (2012). Comparison of 1-Ethyl-3-(3-Dimethylaminopropyl) Carbodiimide Based Strategies to Crosslink Antibodies on Amine-Functionalized Platforms for Immunodiagnostic Applications. Diagnostics, 2(3), 23–33. https://doi.org/10.3390/diagnostics2030023

Voinova, M. V., Rodahl, M., Jonson, M., & Kasemo, B. (1998). Viscoelastic acoustic response of layered polymer films at fluid-solid interfaces: Continuum mechanics' approach. 1–22. https://doi.org/10.1238/Physica.Regular.059a00391

Woods S (2016) A History of Wood from the Stone Age to the 21st Century | Architect Magazine. In: Ecobuilding Pulse. https://www.architectmagazine.com/technology/products/a-history-of-wood-from-the-stone-age-to-the-21st-century_o. Accessed 5 May 2020

Wu S (1982) Polymer Interface and Adhesion. Taylor & Francis

Xiong B, Zhao P, Hu K, et al (2014) Dissolution of cellulose in aqueous NaOH/urea solution: role of urea. Cellulose 21:1183–1192. https://doi.org/10.1007/s10570-014-0221-7

Yamane C, Aoyagi T, Ago M, et al (2006) Two different surface properties of regenerated cellulose due to structural anisotropy. Polym J 38:819–826. https://doi.org/10.1295/polymj.PJ2005187

Young RA (1994) Comparison of the properties of chemical cellulose pulps. Cellulose 1:107–130. https://doi.org/10.1007/BF00819662

Zhou J, Zhang L (2000) Solubility of cellulose in NaOH Urea.pdf. 32:866–870

3. Cellulose-cyclodextrin co-polymer for removal of cyanotoxins on water sources

3.1. Abstract

With increasing global water temperatures and nutrient runoff in recent decades, the blooming season of algae lasts longer, resulting in toxin concentrations that exceed safe limits for human consumption and for recreational use. From the different toxins, microcystin-LR has been reported as the main cyanotoxin related to liver cancer, and consequently its abundance in water is constantly monitored. In this work, we report a methodology for decorating cellulose nanofibrils with β-cyclodextrin or with poly(β-cyclodextrin) which were tested for the recovery of microcystin from synthetic water. The adsorption was followed by Quartz Crystal Microbalance with Dissipation monitoring (QCM-D), allowing for real-time monitoring of the adsorption behavior. A maximum recovery of 196 mg/g was obtained with the modified by cyclodextrin. Characterization of the modified substrate was confirmed with Fourier Transform Infrared Spectroscopy (FT-IR), X-ray Photoelectron Spectroscopy (XPS), Thermogravimetric Analysis (TGA), and Atomic Force Microscopy (AFM).

3.1.1. Index Words:

bio-based composite, cellulose Nanofibrils, β-cyclodextrin, surface chemistry, water treatment, cyanotoxins, microcystin-LR.

3.1.2. Project Partners:

Auburn University and the Forest Products Development Center worked in collaboration with the Department of Chemical Engineering of Aalto University, Finland; the Renewable Materials and Nanotechenology research group, from the Department of Chemical Engineering

in KU Leuven, Belgium; and the USDA Forest Products Laboratory. This research was supported by the Alabama Agricultural Experiment Station, and the Hatch program of the National Institute of Food and Agriculture, United States Department of Agriculture. The School of Forestry and Wildlife Sciences at Auburn University financial support to complete this work is greatly appreciated. This work also made use of Aalto University Bioeconomy Facilities (XPS)

3.2. Introduction

Cellulose is the main component of cell wall structures of plants, algae, and a few other organisms. This qualifies it as the most abundant polysaccharide, making it interesting for utilization in renewable materials development (Carpenter et al., 2015; Filpponen et al., 2012; Gomez-maldonado et al., 2019; Kuo et al., 2017). In recent years, the increasing concerns over environmental changes and the decrease in water quality have increased the interest for sustainable and low-cost materials that could be applied to improve it. We are interested in the elimination of toxins that are a consequence of longer algae blooming seasons and cyanobacteria caused by an increasing temperature of water sources and nutrient runoff from agriculture (Hitzfeld et al., 2000; C. Li et al., 2017; Mahfoudhi & Boufi, 2017; Walls et al., 2018).

Cellulose is a linear polysaccharide consisting of anhydroglucose units covalently linked by β-glycosidic bonds β-(1→4). These linear chains tend to form intra- and intermolecular hydrogen (H)-bonds to form bundles of fibrils with a hierarchical structure of varied diameters and lengths; the available ranges of dimensions and aspect ratio provide unique characteristics that can be utilized to design materials with the desired properties for the final use of the generated product. For example, cellulose nanofibrils (CNF), with diameters between 5-50 nm and lengths from hundreds of nanometers up to a few micrometers have a higher surface area than regular cellulose fibers. This in turn means that they have larger amount of free hydroxyl groups on their surface

which leads to a colloidal character and more reactive groups (Mahfoudhi & Boufi, 2017). Also, the abundance of surface hydroxyl groups permits a variety of surface modifications either via chemical modification or physical adsorption. One common methodology is the surface modification to enable specific molecular adsorption, a preferred mechanism in water treatment (Ali & Gupta, 2007; Lombardo & Thielemans, 2019; Mahfoudhi & Boufi, 2017; Z.-Y. Zhou et al., 2011).

β-cyclodextrin has been demonstrated to effectively adsorb cyanotoxins (Archimandritis et al., 2016; S. Kim et al., 2018; Arjyabaran Sinha & Jana, 2015) and it is also compatible with cellulose for producing composites. β-cyclodextrins are a 7-unit cone-shaped cycle of anhydroglucose units bonded by α-(1→4) bonds. The formation of this cone shape orients its hydroxyl groups of C2 and C3 to the wider extreme, leaving C6 and its hydroxyl group in the lower part and at the exterior of the cycle generating an hydrophobic interior than can form inclusion complexes with a wide variety of molecules (Saenger & Steiner, 1998). Figure 3.1 represents a neutron diffraction structure of this oligosaccharide and the bold black bars symbolize the hydroxyl groups of the structure. In the center, one can observe an entrapped ethanol molecule accompanied with three water molecules in the hydrophobic cavity of β-cyclodextrin; Thin solid lines represent the H-bonding between C2 and C3 of the anhydroglucose units, while the dotted lines illustrate the H-bonding with the inclusion molecule. The latter helps to capture and immobilize molecules which can be further occluded by hydrophobic interactions (Pinto et al., 2005).

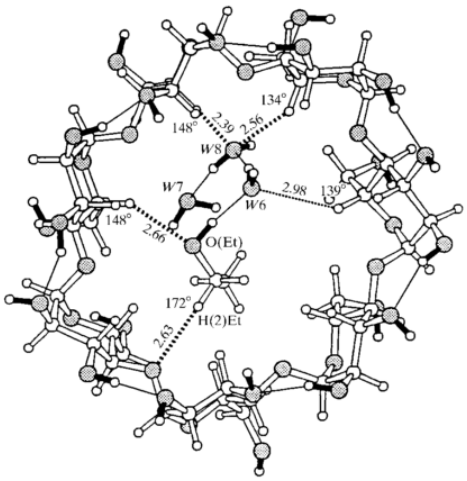

Figure 3.1. Neutron diffraction structure of β-cyclodextrin with ethanol complex. The hydrogen bonding capability can be observed through dash-lines. (Saenger & Steiner, 1998) Reproduced with the permission of International Union of Crystallography (https://journals.iucr.org/).

Grafting of cellulose with cyclodextrin has been demonstrated by different chemical methodologies -most of them- based in the generation of a covalent bond between the hydroxyl groups of both components, using linkers such as epichlorohydrin to form ether bonds (Abdolali et al., 2014; Gidwani & Vyas, 2014; Jagur-Grodzinski, 2006; Sun & Lindsay, 2004; Jozsef Szejtli et al., 1982; F. Zhang et al., 2015); or with poly(carboxylic) acids to form ester bonds (Ji et al., 2015; Medronho et al., 2013; Parvinzadeh et al., 2012). The main operational differences between these two approaches are temperature and grafting medium. Epichlorohydrin modification occurs in water at a mild temperature of 65 °C, while the esterification using polycarboxylic acids requires oven dry conditions at 180 °C. Oven drying has a significant downside when nanocellulose is utilized as a substrate, as fibers tend to aggregate due to hornification (H-bonding) as a consequence of losing the hydration layers which keep them separate. The expected configuration of β-cyclodextrin (CD) and its linkages through epichlorohydrin is schematically shown in Figure 3.2. This crosslinker introduces a new CH_2 and ether linkages to stabilize the structure.

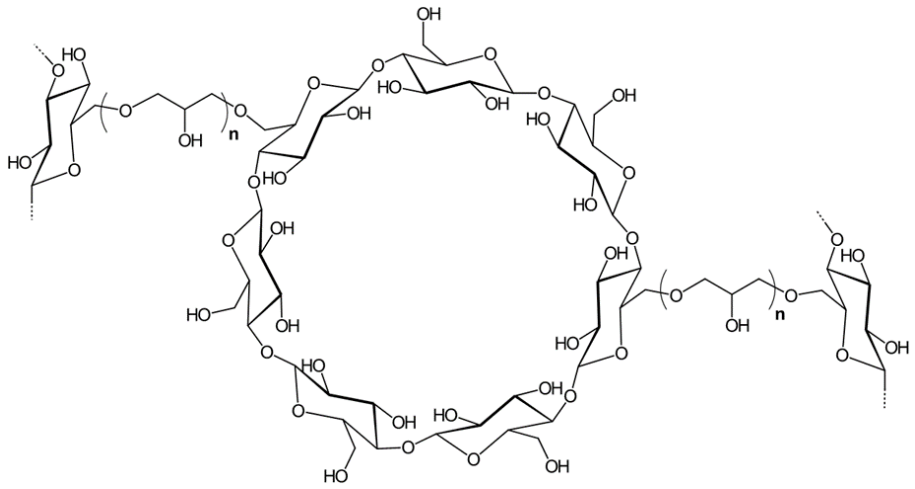

Figure 3.2. Expected structure of β-cyclodextrin crosslinked with other hydroxyl group from polysaccharides (cellulose or other cyclodextrins) through epichlorohydrin

Among the different cyanotoxins, the most notable category are microcystins. These toxins are cyclic heptapeptides with varying amino acids in positions 2 and 4, which give them their particular names. In particular microcystin-LR (Lahti et al., 1997; Meriluoto & Codd, 2005) must be constantly monitored as it has a proven connection to liver cancer. The World Health Organization (WHO) stipulates that the maximum concentration of microcystin-LR in water should not exceed 1 µg/L (World Health Organization, 2014) but the United States' Environmental Protection Agency (USEPA) (USEPA - Office of Water, 2016) found out that up to 30 % of the 1028 water sites tested had microcystin at concentrations between 0.1 µg/L to 225 µg/L with an average of 3.0 µg/L, making this particular cyanotoxin one of the main targets to improve water quality.

The basic chemical structure of microcystin is shown in Figure 3.3. As previously mentioned, amino acid residues 2 and 4 are interchangeable which alters the chemical properties of cyanotoxins. In addition, position 5 presents the amino acid 3-amino-9-methoxy-2,6,8-trimethyl-10-phenyldeca-4,6-dienoic acid (ADDA) which affords more hydrophobic character

because of a long aliphatic chain and aromatic ring and can therefore be exploited for the adsorption via hydrophobic interactions (Meriluoto & Codd, 2005).

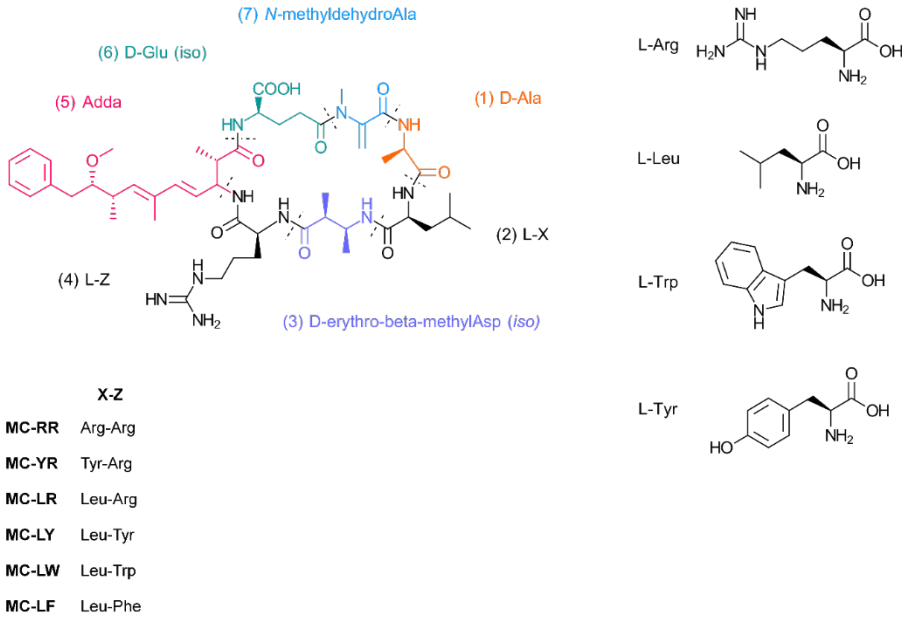

Figure 3.3. Basic chemical structure of microcystins. Amino acid residues 2 and 4 are interchangeable

As previously mentioned, β-cyclodextrin has the tendency to form complexes with the hydrophobic molecules, especially with highly unsaturated structures such as benzene and its derivatives like benzocaine and amino acids such as tyrosine (Bouhadiba et al., 2017; Pinto et al., 2005). It has also been demonstrated that toxins containing ADDA are susceptible to form inclusion complexes with cyclodextrins driven by the hydrophobic interactions. These toxins include microcystin-LR, microcystin-RR, and nodularin-R (Archimandritis et al., 2016; Arjyabaran Sinha & Jana, 2015).

Even though the mechanism of adsorption through the formation of complex β-cyclodextrin/microcystin-LR has been proven, the removal of the complex from water sources has remained a challenge. Different approaches such as magnetic particle carriers have been developed (J. Lee & Walker, 2011; Arjyabaran Sinha & Jana, 2015) but their sustainability and economic

feasibility can be questioned. In this work we aim to compare different configurations for the grafting of β-cyclodextrin onto cellulose nanofibrils as well as their ability to form inclusion complexes with microcystin-LR. To better understand the differences in the adsorption mechanisms, the generated materials were characterized by Fourier-Transform Infrared Spectroscopy with Attenuated Total Reflectance (FTIR-ATR), X-ray Photoelectron Spectroscopy (XPS), Atomic Force Microscopy (AFM), and Thermogravimetric Analysis (TGA); while the adsorption capacity was measured by Quartz Crystal Microbalance with Dissipation monitoring (QCM-D).

3.3. Materials and Methods

3.3.1. Materials

Cellulose nanofibrils (CNF) were prepared by using concentrated di-carboxylic acid hydrolysis with subsequent mechanical fibrillation as described previously (L. Chen et al., 2016; R. Wang et al., 2017) 1 kg (oven dry) of bleached eucalyptus Kraft pulp fibers (BEP) from a commercial source (Aracruz Cellulose, Brazil) were hydrolyzed using aqumeous maleic acid solution of 50 wt.% at 90 °C for 60 min. After separating cellulose nanocrystals through dialysis, the partially hydrolyzed cellulosic solids were fed into a pilot scale homogenizer (GEA Noro Soavi Ariete NS3015, GEA, Germany) for mechanical fibrillation. The resultant CNF were obtained after 5 passes through the homogenizer (L. Chen et al., 2016)(Lot BCNF_M50T90t60, 0.75% wt., pH 7.03, charge density 337.77 ± 62.67 μeq/g); β-cyclodextrin (> 98 %, CD) was purchased from Tokyo Chemical Industry America, epichlorohydrin (99 %, EPI) was purchased from Acros Organics; microcystin-LR (> 95 %, MC) was purchased from Cayman Chemicals, polyvinyl sulfuric acid potassium salt (0.001 N, PVSK) and polydimethyl diallyl ammonium chloride (0.001 N, pDADMAC) were bought from BTG, and sodium hydroxide (50 % w/w) was purchased

from J.T. Baker. The water used was deionized and purified with a Thermo Scientific Barnstead Nanopure (18.2 MΩ cm). Fifty mM Tris- HCl pH 7.4 buffer was used for dissolving microcystin where required in concentrations of 0.5 µg/mL. Polyethyleneimine (PEI) and all other polymeric solutions were utilized at a concentration of 0.1% (m/v) in ultrapure water.

3.3.2. Cellulose nanofibril characterization

3.3.2.1.Dry content determination

Dry content was determined following the TAPPI standard T550 (TAPPI, 1993): Nanocellulose suspensions were weighted in aluminum pans and dried overnight in an oven at 105 °C t. The dry material was weighted and subtracted from the moisture weight. Percentage was calculated based on the moisture content (MC%) according to equation 1.

$$MC\ \% = \frac{mass_{wet} - mass_{dry}}{mass_{wet}} * 100\ \% \qquad (3.1)$$

The average and standard deviation of three replicates was calculated and the dry content was determined as the difference of the 100 % and the MC%.

3.3.2.2. Charge density and pH measurements

Charge density of the CNF was measured using a method adapted from Espinosa *et al.* (Espinosa et al., 2016). Measurements were repeated three times and then averaged. Briefly, CNF suspensions were prepared at 0.04 wt.% and sonicated for 10 min using a Vibra Cell sonicator (Newtown, CA) with 20 KW and 25 % of amplitude to effectively disperse the fibrils. Then, 25 ml of polydimethyl diallyl ammonium chloride (pDADMAC) was added to 15 mL of CNF suspension and mixed for 10 min, followed by centrifugation at 3000 rpm for 15 min. After centrifugation, 10 mL of the supernatant was analyzed in a Laboratory Charge Analyzer Chemtrac LCA-1,

(Norcross, GA). Next, a titration using polyvinyl sulfuric acid potassium salt (PSVK) was performed until the equipment reached a streaming current value (SCV) of zero. The volume of anionic titrant consumed was used for the final calculations using Equation 2.

$$\boldsymbol{Charge\ density} = \frac{\left([\boldsymbol{pDADMAC}] * \boldsymbol{V_{p-DADMAC}}\right) - ([\boldsymbol{PVSK}] * \boldsymbol{V_{PVSK}})}{\boldsymbol{W_{dry\ CNF\ sample}}} \quad (3.2)$$

where $[\boldsymbol{pDADMAC}]$ is the concentration of the cationic polymer, $\boldsymbol{V_{pDADMAC}}$ is the used volume of p-DADMAC, $[\boldsymbol{PVSK}]$ is the concentration of the anionic titrant, $\boldsymbol{V_{PVSK}}$ is the consumed volume of titrant, and $\boldsymbol{W_{dry\ LCNF\ sample}}$ is the weight of the dry CNF sample.

The CNF suspensions were used as received, pH was measured using a SympHony Benchtop Multi Parameter Meter B30PCI (VWR®) equipped with pH and conductivity electrodes. Measurements were repeated 15 times and the average and standard deviation were reported.

3.3.3. Polymerization of β-cyclodextrin

Five grams of β-cyclodextrin was dissolved in 40 mL of 20% NaOH solution. Next, the temperature was raised to 65 °C while 13.8 mL (16.3 g) of epichlorohydrin (≈ 0.8 mL/min) was added dropwise using an addition funnel. The reaction was stopped after 2 h by adding 150 mL of acetone. Once room temperature was reached, the solution was vacuum filtered through a Whatman ashless glass filter paper No 1 and placed in a 100 mL extraction thimble, which was placed into a Soxhlet extractor. The extraction of residual epichlorohydrin was carried out with 150 mL of acetone. After 12 cycles (ca. 3 h) at 80 °C, the solid poly(β-cyclodextrin) (PCD) was recovered, and ground using a mortar and pestle and kept in a desiccator for further use.

3.3.4. Preparation of CNF/ β-cyclodextrin co-polymers

3.3.4.1. Synthesis of CNF-CD

CNF suspension of 0.4 wt.% was stirred at 4 °C for 20 h. Then, the suspension was transferred to a three-neck round bottom flask and 30 mL of NaOH (40%) was added at room temperature to activate the CNF hydroxyl groups. 5 g of β-cyclodextrin was then added to the mixture and stirred for 1 hour. The temperature was raised to 65 °C while adding dropwise 15.2 mL (18 g) of epichlorohydrin (≈ 0.8 mL/min) with an addition funnel. The reaction was carried out for 2 h at 65 °C under stirring at 180 rpm. After cooling down, the solution was filtered under vacuum using PYREX™ Buchner funnel with a fritted disc of pore size 4 – 5.5 µm until no more water was released.

The filtered material was placed into an extraction cellulose thimble in a Soxhlet extractor and washed with 150 mL of acetone at 80 °C for 16 cycles (ca. 16 min/ cycle). The washed material was resuspended into 150 mL of ultrapure water and neutralized using 1 M HCl solution. The neutralized co-polymer was filtered under vacuum and stored at 4 °C.

3.3.4.2.Synthesis of CNF-PCD

The same procedure described above was followed for the synthesis of CNF/poly(β-cyclodextrin) co-polymer. However, in this synthesis 5 g of the poly(β-cyclodextrin) was used instead of pristine β-cyclodextrin.

3.3.5. Characterization techniques

3.3.5.1.Fourier-transform infrared spectroscopy with attenuated total reflectance (FTIR-ATR)

Dry samples were analyzed using a Perkin Elmer Spotlight 400 FT-IR Imaging System (Massachusetts, US) with an ATR accessory with diamond/ZnSe crystal and a resolution of 4 cm^{-}

[1] to reveal surface modification. First, a background spectrum was collected before each set of measurement with the same number of scans. To achieve a high spectra resolution, 1024 scans per spectrum were performed. Data were processed with Spectrum 6 Spectroscopy Software (PerkinElmer, Massachusetts, US).

3.3.5.2.X-Ray Photoelectron Spectroscopy (XPS)

Samples were mounted on XPS sample holder using UHV compatible carbon tape and pre-evacuated overnight together with a piece of pure cellulose as the in-situ reference monitoring analysis conditions during the measurement (Johansson & Campbell, 2004). Data were recorded using monochromatic Al Kα irradiation at only 100W and under neutralization. In data analysis, high-resolution C 1s regions were fitted with Gaussian components of equal half widths, and the binding energies of all spectra were charge-corrected using the main component of cellulose, namely C-O at 286.7 eV, as the BE reference (Briggs & Beamson, 1993).

3.3.5.3.Thermogravimetric analysis (TGA)

Dry samples were tested in aluminum pans in a TGA-50 from Shimadzu (Kyoto, Japan). Samples were heated from room temperature to 600 °C at a rate of 10 °C/min under nitrogen atmosphere and data was processed with TA60 software version 2.11 from Shimadzu.

3.3.5.4.Atomic Force Microscopy (AFM)

Morphological characterization of the nanofibrils in drop-cast and in QCM-D generated surfaces post MC adsorption were observed using a Bunker (formerly Digital Instruments, Veeco) AFM Dimension 3100 (California, US). Topographical images were obtained in tapping mode at 2.35 Hz of amplitude velocity using a Nano World (Innovative Technologies) FM 20 silicon SPM-sensor cantilever at resonance frequency of 75 kHz and force constant of 2.8 N/m; scan sizes were

of 5x5 µm and 1x1 µm. Processing of the images and roughness calculations were made by Gwyddion software 2.49 (SourceForge).

For Spin coated surfaces, A 20 mL of CNF or derivate suspension (0.01% w/w in ultrapure water) were placed in ice bath and sonicated during 5 minutes at 25 % amplitude in a Branson Digital Sonifier 450 (Brandson Ultrasonics corporation, 230 V, 50/60 Hz, USA) with 13 mm solid extender, using 3 sec sonication and 2 seconds standby program. Subsequently, the samples were centrifuged at 10000 rpm during 40 min using mini-spin Eppendorf centrifuge. AFM images were obtained with a NanoScope V controller (Dimension Icon,Bruker Corporation, Billerica, MA), operating in tapping mode. Three scanning areas in all samples were selected: 5µm×5µm, 3µmx3µm, and 1µmx1µm. The image correction applied was flattening during image analysis (NanoScope 8.15 software, Bruker).

3.3.6. Quartz Crystal Microbalance with Dissipation Monitoring (QCM-D)

In situ formation of CNF, CNF-CD, and CNF-PCD surfaces on gold sensors and the adsorption of microcystin-LR (MC) were studied with a QSense Analyzer from Biolin Scientific (Västra Frölunda, Sweden). The basic principle of the QCM-D is the following: Changes in frequency (Hz) of a piezoelectric sensor that has a base resonance of 5 MHz and its overtones 15, 25, 35, 45, 55 and 75 MHz are monitored. This changes in frequency resonance are proportional to a change in mass on the sensor, as only the surface is interacting with a flow of matter, then those changes are correlated to the mass adsorption on the sensor surface (Example, 1991; KSV Instruments Ltd, 2002; Voinova et al., 2002). Sauerbrey determined this relationship for rigid layers ($D > 0$) under uniform mass distribution on the surface and when the mass is much less than the mass of the crystal:

$$\Delta m = C * \Delta f * n^{-1} \quad (3.3)$$

where C is -17.7 ng/cm^2 and is a constant for 5 MHz crystals, Δf is the change of frequency, and n is the overtone number. However, most of the polymeric systems do not generate a rigid layer to result in underestimation of the adsorbed mass using eq. (3). Some other models have been developed to address the change in mass, such as Voigt's and Maxwell's that considered the density, and dynamic and static viscosity of the adsorbed materials, as well as the crystals (Voinova et al., 1998).

The dissipation factor is related to the viscoelastic properties of the layers formed on the crystal, as it translates to the relationship of energy dissipation from the sensor to the fluid and the energy stored (3). It can be measured as inversely proportional to the decay time constant ($\boldsymbol{\tau}$) and the resonant frequency ($\boldsymbol{f}$) as shown in equation 4 (Voinova et al., 1998).

$$D = \frac{E_{dissipated}}{2\pi E_{stored}} \quad (3.4)$$

$$D = \frac{1}{\pi f \tau} \quad (3.5)$$

If the generated film is viscoelastic, energy would be dissipated due to the oscillation of the layer and thus more energy will be lost because of longer decay times, i.e., When more energy is stored, as the surface becomes more rigid, an decrease in the D-factor will be observed (Turon et al., 2008).

Measurements were carried out at 25°C with a constant flow of 150 µL/min on gold coated crystals using PEI as anchoring solution. Crystal sensors were previously placed in Novascan PSD Series Digital UV Ozone System (Iowa, US) for 15 min to eliminate dust and activate the surface.

The active surfaces were generated *in situ* by flowing the polymer solution (0.1 % (m/v)) until stabilization was achieved, followed by adsorption of microcystin-LR (0.5 µg/mL) at the same flow rate. Data was collected at multiple frequencies and only the third overtone is presented on sensogram to facilitate discussion and interpretation. The adsorbed mass was calculated using the Broadfit model (based on the Voight model) with dissipation dependency from frequency changes, using DFind Software from Biolin Scientific (Västra Frölunda, Sweden). Literature densities were used for CNF and microcystin-LR (1.20 and 1.299 g/cm^3), while for the modified polymers, it was calculated by compacting dry material into 1 mL containers and weighing, coming to values of 1.096 and 0.954 g/cm^3 for CNF-CD and CNF-PCD, respectively.

3.4. Results and Discussion

3.4.1. Characterization of CNF and the modified polysaccharides

3.4.1.1.CNF suspensions

The CNF suspension was characterized prior to use and modification with β-cyclodextrin. Solid content of the white milky suspension was determined to be 0.75 wt.%. The suspension pH and charge density were 7.0 and 337.7 ± 62.6 µeq/g, respectively. The latter is due to the carboxylation at cellulose C6 position through esterification by concentrated maleic acid hydrolysis (L. Chen et al., 2016).

3.4.1.2.Synthesis of poly(β-cyclodextrin) (PCD)

The crosslinking of the CD with EPI resulted in a granular texture after vacuum filtration. Reaction was also confirmed by FTIR as shown in Figure 3.4, where spectra of CD and PCD are presented. EPI linkage resulted in spectral changes in the C-H stretching band (2900 cm^{-1}). The

presence of ether bonds was clearly reflected from the significant reduction in the C-O signal (1200 cm^{-1}). Furthermore, the variations between 1400 and 1300 cm^{-1} are mainly due to changes in the bending modes of C-H and in-plane O-H, which may point towards more diverse movement that these groups can undergo through the bridges formed by EPI. It should be noted that the observed spectral characteristics are in agreement with those reported in the literature for crosslinking of cyclodextrin with epichlorohydrin (R. Li et al., 2003).

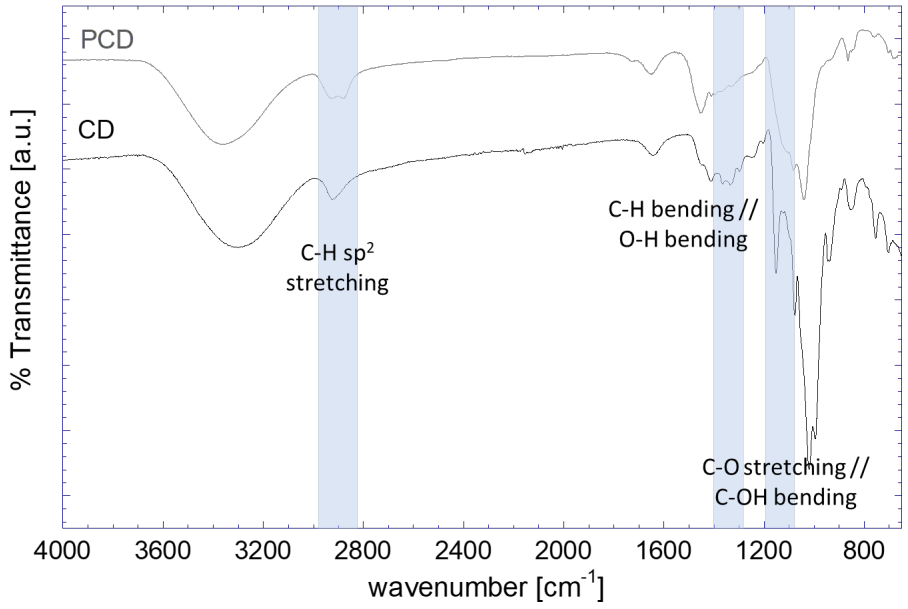

Figure 3.4. FTIR-ATR spectra of cyclodextrin and poly(cyclodextrin) obtained by crosslinking with epichlorohydrin

3.4.1.3.Synthesis of CNF-CD and CNF-PCD

The first indication of successful grafting of CD and PCD to the CNF was given by the appearance and texture of each system. In Figure 3.5, the observable differences in the physical state between the different products can be seen, from a fine powder for CD (far left pan), to a more flake-like of the crosslinked PCD, up to gels from the CNF-CD and CNF (far right pans). Both the CNF-CD and CNF-PCD (center) sample had a solid content of 22 wt.%. However, CNF-PCD appeared more solid-like than CNF-CD, which looked more like a gel.

The charge density was reduced to 128.8 ± 10.1 μeq/g for the CNF-CD and to 166.6 ± 24.0 μeq/g for the CNF-PCD. The reduction in charge densities of modified CNFs was likely caused by the reactions of carboxyl and hydroxyl groups with EPI and with the CD or PCD. Moreover, the charge density difference between the CNF-CD and CNF-PCD might be related to the higher amount of hydroxyl groups that were added with the PCD and with the EPI linkages than obtained by the reaction with the pristine CD, or to a less efficient reaction of PCD with CNF leaving more unreacted sites in the fibrils.

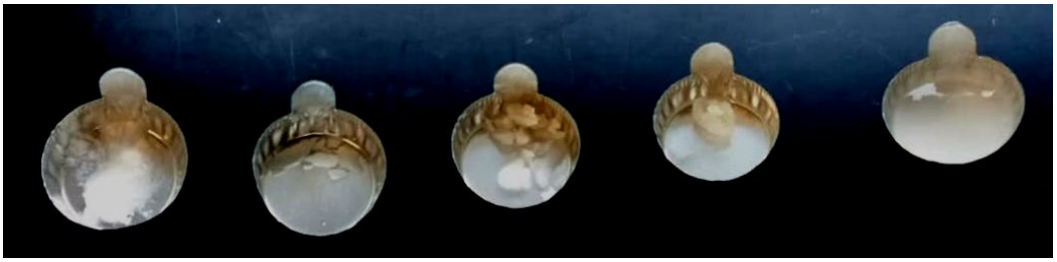

Figure 3.5.. Aluminum pans with the materials used for this work, from left to right: CD, PCD, CNF-PCD, CNF-CD, and CNF suspensions

The modification of the CNF was then confirmed through FTIR analysis. In Figure 3.6 the spectra of the modified CNFs are shown. The main changes between them are in the intensity of the bands of C-H stretching (2900 cm^{-1}) and the increase in intensity related to the glucose ring out-of-phase stretching (890 cm^{-1}), which can also be seen to be more pronounced in the system with PCD as more anhydroglucose units are present. Similarly, we also see an increase in H_2-O bending (1650 cm^{-1}) related to adsorbed water in the structures. Finally, the definition of the bands related to C-C and C-OH stretching (1020 cm^{-1}) confirm the etherification of the materials, as well as the increase of secondary alcohols from either epoxy derivates or CD.

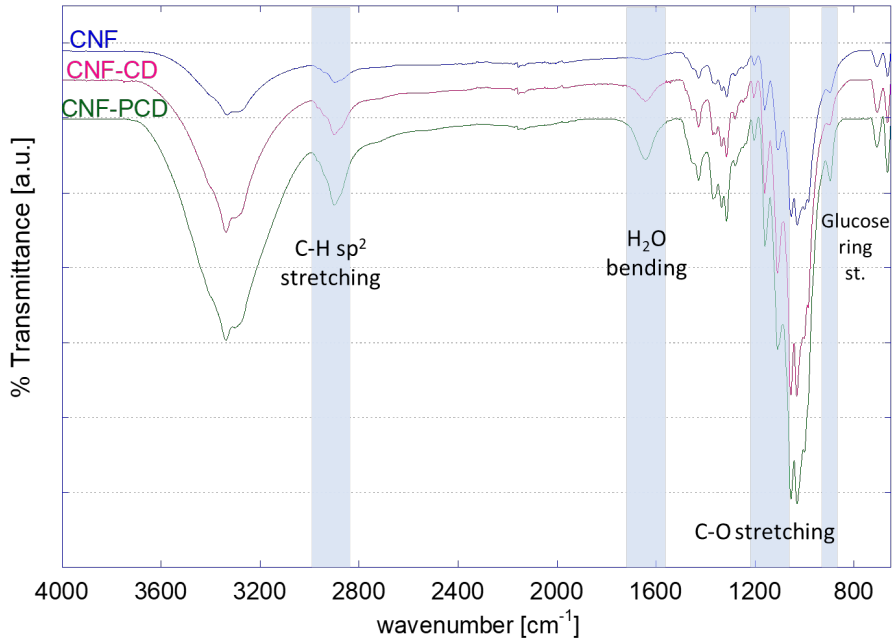

Figure 3.6. FTIR-ATR spectra comparing cellulose nanofibrils (CNF) and modified cellulose nanofibrils (CNF-CD and CNF-PCD)

Similarly, the modification can be observed in Figure 3.7 where the XPS wide energy region spectra of the three materials (CNF, CNF-CD, and CNF-PCD) are shown as well as a reference of 100% pure cellulose. The main differences were observed in the C 1s high resolution spectra, where the ratio of CO/OCO increased from 3.9 to 4.4 as a result of modification. This indicates the presence of other surface elements besides anydroglucose monomers. The increase in the CC component, i.e., carbons without oxygen neighbors, is typical to CNF, and most possibly related to the ultra-high vacuum conditions of XPS (Johansson et al., 2011). It is further increased in the modified materials, which could be linked with the presence of the EPI linkages.

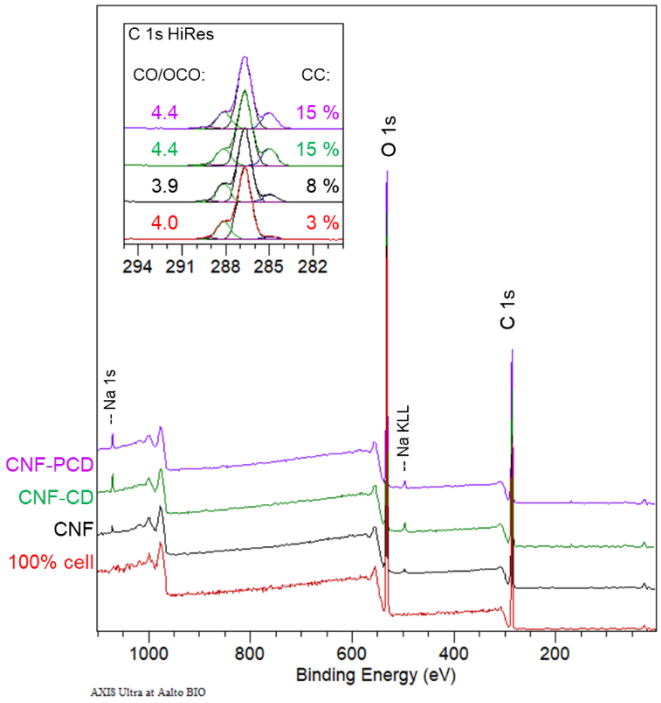

Figure 3.7. XPS wide energy region spectra comparing a pure cellulose reference, cellulose nanofibrils (CNF) and modified cellulose nanofibrils (CNF-CD and CNF-PCD). The insert shows the high-resolution C 1s spectra

TGA data also suggested the successful modifications of the CNF as the onset degradation temperatures were increased when compared to that of the unmodified CNF (Figure 3.8). As expected, CNF-PCD was the most stable as it possesses a higher crosslinking density, i.e., the onset degradation temperature of CNF-PCD was 13°C higher than that of CNF-CD. When the first derivative was observed, there was no significant difference in the maximums of both products. However, they are set in between the CNF and CD with a single peak which can be considered indicative for a successful modification. Furthermore, a second change in slope from 450 to 554 °C for CNF-CD and from 450 to 585 °C for CNF-PCD was observed, both of which can be related to a bridge formation by EPI.

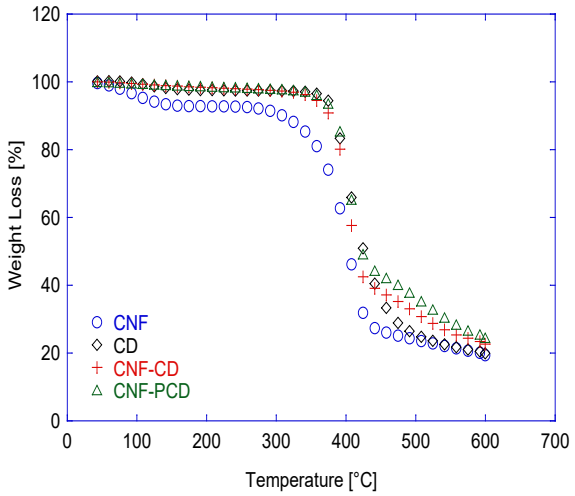

Sample	Onset Temperature [°C]	Maximum degradation [°C]
CNF	244	407
CD	314	388
CNF-CD	317	394
CNF-PCD	330	394

Figure 3.8 Thermogravimetric analysis of the CNF, CD, and the modified cellulose nanofibrils (CNF-CD and CNF-PCD). The thermogram (left) shows the behavior of the material, and the table (right) presents the main extracted data for each sample.

3.4.2. Formation of surfaces in situ on QCM-D and adsorption of microcystin-LR

To test the adsorption capacity of modified CNF in capturing microcystin-LR, surfaces were generated *in situ* on the QCM-D by flowing solutions of the unmodified and modified cellulose, followed by the toxin once stable. Two media, water and TRIS-buffer were used in order to compare the changes in adsorption of MC under different ionic concentrations. A simplified scheme of the layers used is presented in Figure 3.9. PEI was used as an anchoring polymer (first layer) in which the (co)polymers CNF, CNF-CD or CNF-PCD were then adsorbed. A layer by layer (CNF + CD) approach was also studied to assure that the capture of the microcystin was due to its chemical bonding with β-cyclodextrin instead of merely physical adsorption on the unmodified CNF surface or to the surface of the CD, independently of the availability of the hydrophobic cavity that can be blocked by H-bonding with the CNF fibrils.

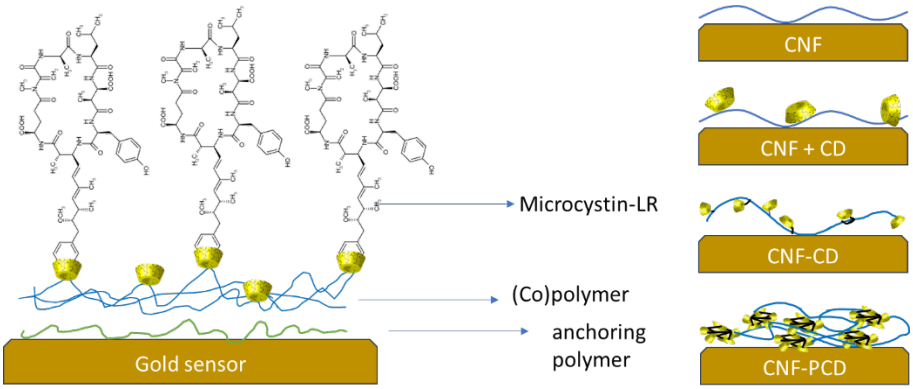

Figure 3.9. Scheme of the sequece used in the QCM-D to monitor the adsorption of the microcystinon the generated (co)polymerlayers

QCM-D sensograms of the studied systems were split to facilitated discussion, with the first part being the surface generation and the second, the microcystin adsorption. The first part of the sensograms (*in situ* surface generation) is shown in Figure 3.10 and is discussed with the AFM images. For comparison, the surfaces were also generated by using spin coating and drop casting techniques.

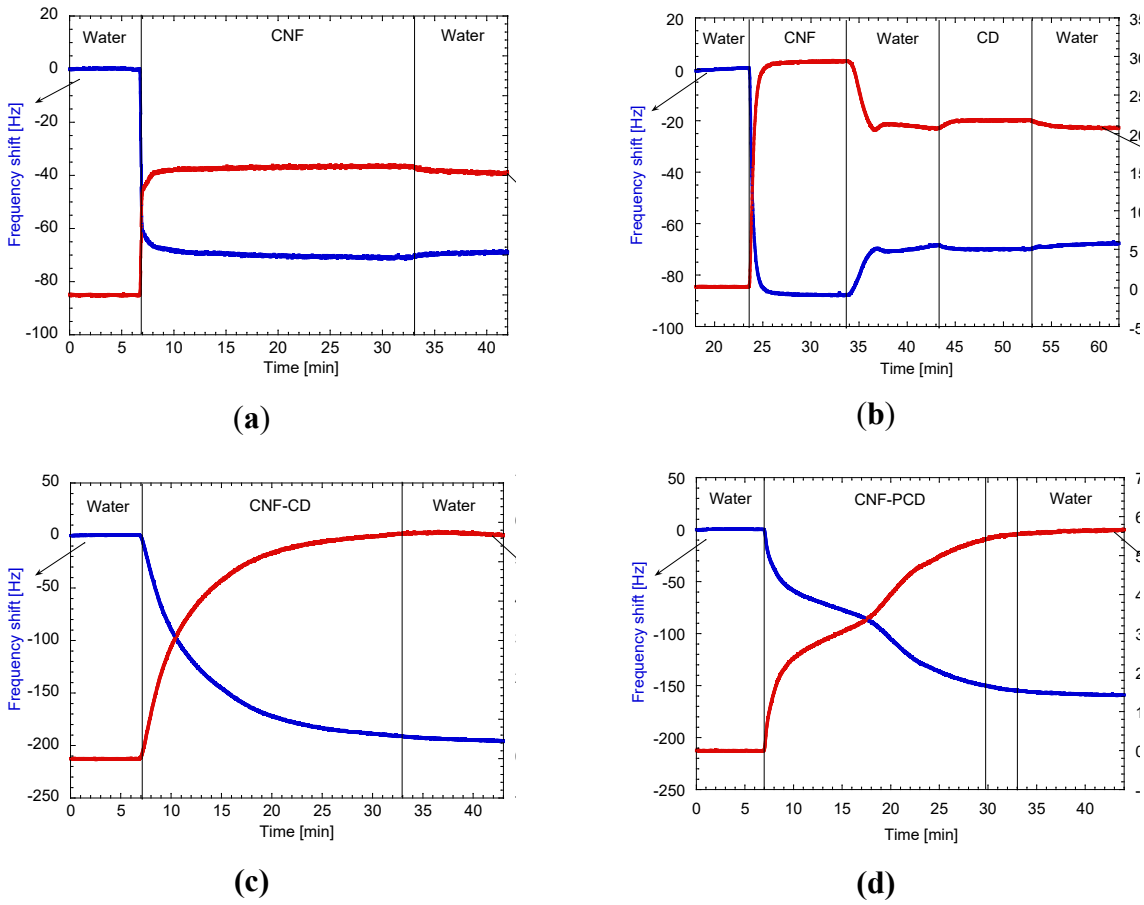

Figure 3.10. QCM-D sensograms of the in situ surface generation from (a) CNF, (b) CNF and flushed CD (CNF+CD), (c) CNF-CD, and (d) CNF-PCD. CNF, cellulose nanofibrils; CD, cyclodextrin; CNF-CD, cellulose nanofibrils grafted with cyclodextrin; CNF-PCD, cellulose nanofibrils grafted with poly-cyclodextrin

3.4.2.1.Surface generation and characterization

As mentioned, the first part of the sensograms is related to the generation of the surface *in situ* on the QCM-D. The formation of CNF surfaces was done twice with the first being as a control without any modification on the surface (Figure 3.10a), and the second is including the addition of pure CD (Figure 3.10b). When the changes in frequency were observed, both CNF surfaces had a negative shift of -69 Hz and changes in dissipation between 15 and 20 ppm in all repetitions, showing good consistency in the approach. When the adsorption of the CD on the CNF surface was completed (Figure 3.10b), the change in frequency only amounted to -2 Hz, which is not

considered representative in rigid surfaces. However, the change in dissipation was more than 0.5 ppm, suggesting a change in the viscoelasticity of the surface showing there was some molecular adsorption of the CD.

For the adsorption of CNF-CD and CNF-PCD, larger changes in frequency and dissipation were observed (Figure 3.10c and 3.10d). Herein, the frequency shifts were -195 HZ, and -158 Hz and dissipation were increased by 55 ppm and 56 ppm for CNF-CD and CNF-PCD, respectively. Both materials thus showed viscoelastic behavior. Likewise, the frequency and dissipation shifts were more significant than in the case of unmodified CNF. These differences in the frequency and dissipation shifts were almost three times higher for both modified materials than for the pristine CNF; these differences can be related to the difference in viscosity of the modified materials as well as improved interactions with the amino groups of the anchoring polymer. The changes in dissipation can be associated with the water uptake, which is known to occur in highly hydrated fibrillar systems (Fält et al., 2003; Kasemo et al., 2001). This water uptake could lead to osmotic effects that in turn would absorb pollutants into the fibrillar-based structures.

AFM images of the different surfaces are shown in Figure 3.11. After spin coating, the CNF films showed well dispersed fibril network which is not observed for CD or PCD modified fibrils. In the case of modified fibrils, agglomeration was visible, as well as higher points or mounds along the surface. This can be an indication of the CD binding. Furthermore, when the average rugosity (Ra) of the images is compared, the CNF-PCD image is approximately two times of Ra for the CNF-CD image. This confirms a higher grafting density for CNF-PCD which agrees with the higher charge density and the higher dissipation shift from QCM-D experiments.

The CNF surface had a smoother appearance when compared to the other materials. However, it is visible that microfibers and finer nanofibrils are present in all. While comparing the

CNF-CD and CNF-PCD, wider fibrils are found in the surface of CNF-PCD Moreover, the AFM images of CNF-CD and CNF-PCD show some larger particles which is likely due to presence of the CD on the surface.

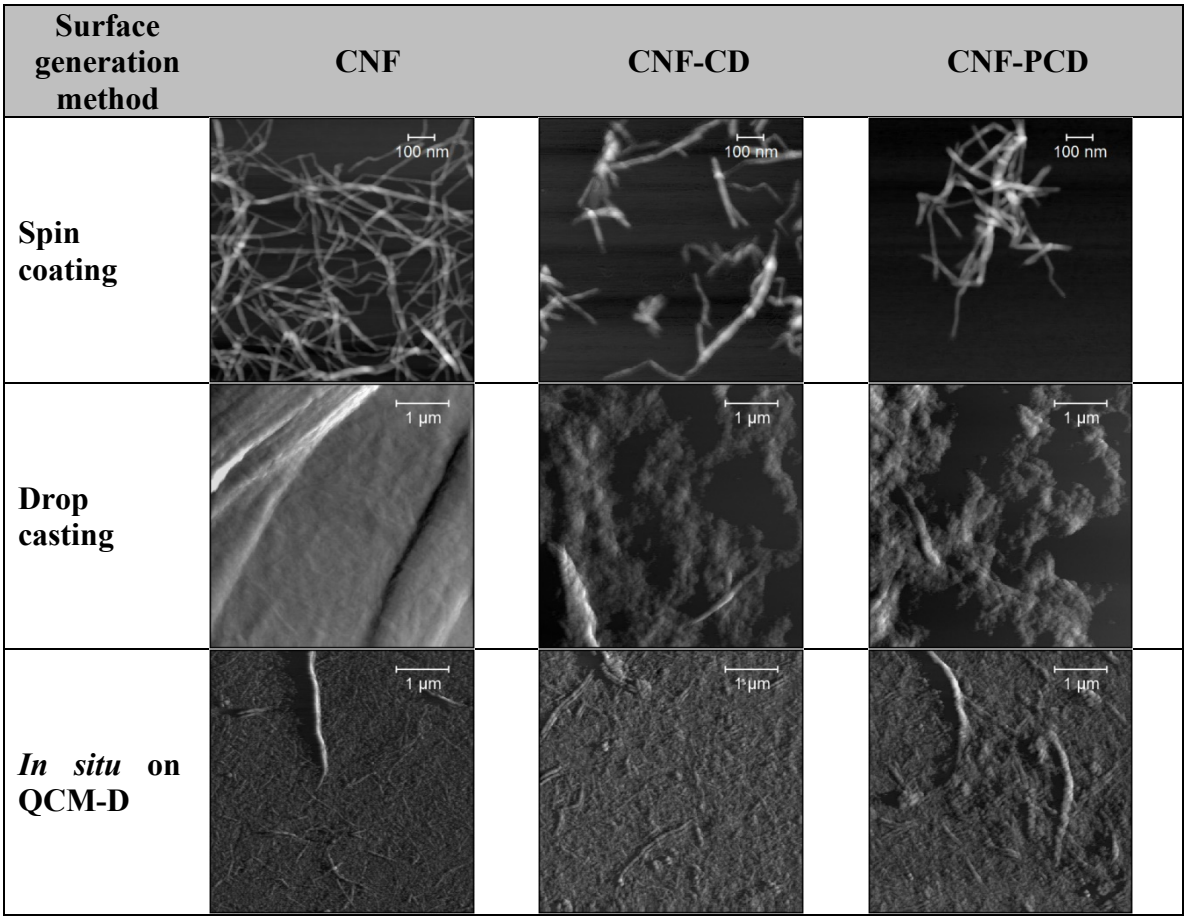

Figure 3.11. AFM images of the cellulose nanofibrils (CNF) and the modified cellulose nanofibrils (CNF-CD and CNF-PCD) and the average rugosity (Ra), each row was generated by a different technique, while the last one was measured after adsorption of microcystin in the QCM-D

Table 3.1 compares the roughness between the surfaces of CNF, CNF-CD, and CNF-PCD generated by the three methods (spin-coating, drop-casting, and *in-situ* adsorption in the QCM-D). One can observe that the roughness increases with the increased grafting on the surface. It is worth to mention here that the spin-coated surfaces are not fully covered, which made the surface roughness data less comparable as it is virtually impossible to accurately correct for uncoated

areas. However, including this skew in the data, Ra and Rq for CNF-PCD is significantly higher than CNF-CD and CNF.

Drop-casting produced thicker surfaces as more material was deposited. The rugosity difference between CNF and CNF-CD was less than 1 nm. However, the roughness of CNF-PCD surface was higher indicating the apparent relationship between the grafting density and surface rugosity. Finally, a similar behavior was conserved even after the adsorption of MC.

Table 3.1. Roughness comparison between the systems surfaces

System	Average roughness (Ra) [nm]	Root mean square roughness (Rq) [nm]	Average maximum height of the roughness (Rz ISO) [nm]
Spin coated			
CNF	1.43	1.80	14.7
CNF-CD	0.84	1.25	10.9
CNF-PCD	1.95	2.46	15.0
Drop Casted			
CNF	2.00	3.00	13.0
CNF – CD	2.80	3.90	14.7
CNF – PCD	4.20	4.90	16.8
In situ on QCM-D			
CNF / MC	0.30	0.53	1.99
CNF – CD /MC	1.18	1.45	6.00
CNF – PCD/MC	2.06	2.44	9.23

3.4.2.2.Capture of MC followed by QCM-D.

In the second part of the sensograms shown in Figure 3.12 the adsorption of MC was monitored first with water as a medium, followed by an adsorption in hypersaline conditions. In Figure 10a, the adsorption of MC on the unmodified surface of CNF seemed to be reversible, as the frequency level decreased to -72 Hz and went up again to -69 Hz upon rinsing with ultrapure water. When the adsorption was done in hypersaline conditions, however, a frequency shift of -

2 Hz was sustained after rinsing, suggesting that this condition helped the adsorption. The adsorption in hypersaline conditions is likely due to entropic effects where having the MC on the surface is energetically more convenient than having ions form the salts, thus hurdling desorption.

In Figure 3.12b, the adsorption of CD was first tested with no apparent adsorption but when the MC was flown through the QCM-D, a frequency decrease of 2 Hz as well as an increase in the dissipation shift were observed, indicating adsorption of MC on the surface. Under hypersaline conditions, there was also a decrease in frequency but smaller than the first one, probably indicating less available free space and less entropic effects as the surface energy was lowered with the adsorption of the CD.

For CNF-CD as shown in Figure 3.12c, the adsorption can be seen from the decrease in the frequency shift was -5 Hz in water and -2 Hz under hypersaline conditions, again showing extra adsorption when which can also relate to the exchange of salts for MC and then facilitating the contact with less available active spaces. The increased adsorption under hypersaline conditions can be due to the easier contact of the hydrophobic tail to the CD as well as some other types of interactions like hydrogen bonding from the aromatic at the end of the tail and the electrons on the surface of the anhydro glucose units of cellulose or CD. To investigate the driving force for the interaction, Isothermal Titration Calorimetry experiments were also carried out. Herein, the interaction of CNF-CD and MC were measured. In these experiments, the enthalpic interactions between the CNF-CD and MC were always too low for detection indicating that the CD-MC interaction is not driven by preferential enthalpic interactions but are instead driven by entropy where the release of the water from the corona around MC and from inside the CD are released upon interaction and decrease the Gibbs-free energy of the system.

As shown in Figure 3.12d, adsorption on the CNF-PCD surface had a frequency shift of -4 Hz in water and -2 Hz in in hypersaline water, both of which were lower than in the observed from using CNF-CD. These differences are likely related to the denser crosslinked CD that are present in PCD which can block the access to the hydrophobic cavities on the surface.

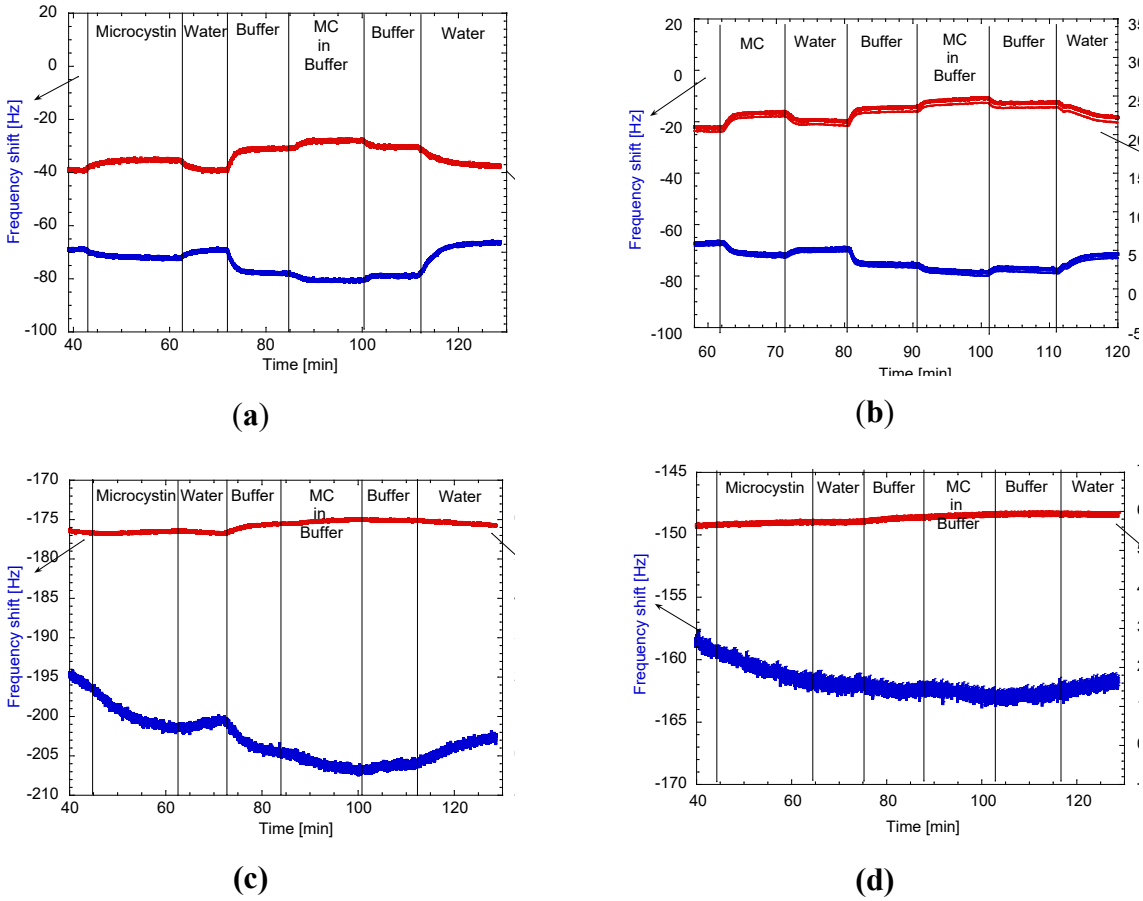

Figure 3.12. QCM-D sensograms of the adsorption of microcystin in water and Tris-HCl buffer from (a) CNF, (b) CNF and flushed CD (CNF+CD), (c) CNF-CD, and (d) CNF-PCD. CNF, cellulose nanofibrils; CD, cyclodextrin; CNF-CD, cellulose nanofibrils grafted with cyclodextrin; CNF-PCD, cellulose nanofibrils grafted with poly-cyclodextrin

3.4.2.3.Mass modelling from QCM-D data

After modeling the data obtained from the sensograms with QSense DFind software, the mass contribution of each layer was calculated considering densities, frequency, and dissipation

shifts. The average masses obtained in each event is presented in Figure 3.13a and the ratios of MC to CNF, CNF+CD, CNF-CD, and CNF-PCD are presented in Figure 3.13b. The total MC mass was calculated from the frequency shift values obtained after a final rinse with ultrapure water.

When the masses of the materials on the surface were calculated and compared (Figure 3.13a), the CNF presented a higher mass with *ca.* 7 mg on both surfaces (CNF and CNF+CD). After CNF, CNF-PCD presented more adsorbed mass than CNF-CD, this latter one had a higher frequency shift drop in Figure 3.10c but also had lower density than CNF-PCD, then the interdependency between these two parameters and the dissipation gave a mass of 3.5 mg for CNF-CD and 5.3 mg for CNF-PCD.

For CNF-CD, even when the frequency shift was minimal in the adsorption step of the CD, a mass of 143.3 ng was calculated which can explain the decrease in frequency that was observed in the MC step. This adsorption amounted to 112 ng of MC in water and an extra 83 ng in the hypersaline Tris buffer. This total mass adsorbed in water equaled 281 ng of MC adsorbed on pure CNF which indicates that the CD competed with the MC for free space.

Overall, the adsorption increased with the presence of crosslinking, as both CNF-CD and CNF-PCD had better adsorptions than the CNF and CNF-CD. CNF-PCD had a maximum adsorption of 64.4 mg/g, with 51.4 mg/g of it corresponding to adsorption in water. The adsorption under hypersaline conditions was negative in the step calculation, however, after the final rinse with water the final adsorption value was higher meaning that some adsorption occurred also during the hypersaline step.

CNF-CD was the only material that presented a different trend in the adsorption values, as herein the highest adsorption was under hypersaline conditions. This difference is likely due to a

different mechanism for adsorption compared with other three, and this can only correspond to the active capturing by the hydrophobic cavity of the available CD. After the final rinse with ultrapure water, the maximum adsorption stable on the surface was 196 mg/g.

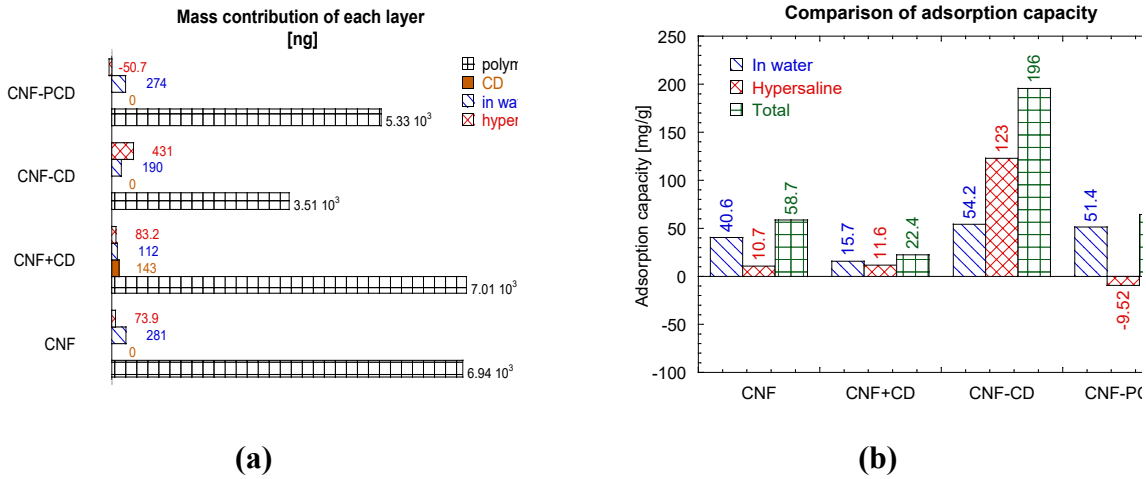

(a) **(b)**

Figure 3.13. Charts of the mass obtained after the modeling the frequency and dissipation shift of the QCM-D sensograms in QSense DFind software. (a) Mass contribution of each layer added to the surfaces, and (b) microcystin-LR adsorption capability of each CNF polymer. CNF, cellulose nanofibrils; CD, cyclodextrin; CNF-CD, cellulose nanofibrils grafted with cyclodextrin; CNF-PCD, cellulose nanofibrils grafted with poly-cyclodextrin

It is important to mention that even though the adsorption capacities were obtained using a non-standardized technique; the adsorption capacity of the CNF-CD is more than double that some other bio-based materials reported in the literature. [CS+CEL] composite generated by Tran *et al.* (Tran et al., 2013), was reported to adsorb 96 mg/g, while a magnetic nanocomposite (G-Fe_2O_3-CD) had a β-cyclodextrin removal capacity of 140 mg/g (Arjyabaran Sinha & Jana, 2015).

3.5. Conclusion

The present work demonstrates that cellulose nanofibrils (CNF) can be modified with

β-cyclodextrin, which in turn was able to remove microcystin-LR from aqueous solutions. Two different modification approaches were investigated and one step crosslinking onto the surface was found to be the most effective by removing up to 196 mg/g according to the modelled QCM-D measurements. This material presents an opportunity to develop novel sustainable materials that can help improve the water quality by using non-specific interaction. While the cyclodextrin hydrophobic cavity allows to adsorb hydrophobic substrates and aromatic pollutants from water sources, the nanofibrillar matrix of CNF provides an increased surface area for the adsorption. The combination of both phenomena can then be maximized when complex structures, such as membranes or aerogels, are generated from this material.

3.6. Future work

Even though the CNF-CD was a good material to adsorb microcystin, the non-specific nature of the interactions with this material possesses a great capacity to capture other hydrophobic compounds that might be in the same water sources. Furthermore, competition between these different pollutants at diverse pH and ionic strength are phenomena that could have an impact on the performance. One of the big challenges that was presented in this work was assessing the amount of cyclodextrin attached. This due to the similarities in chemical structure between the base materials for the composites—solid state nuclear magnetic resonance was tried but good results were not obtained. Consequently, the increase in expertise of collaborations with ionic liquid assisted NMR could lead to a better understanding of the material. Finally, another challenge for the utilization of this material is the formation of 3-D structures that are stable enough that cycles of washing, adsorption, and desorption are possible. There is some literature on how to break complexes between microcystin and cyclodextrin, however the 3-D formation should be studied in parallel.

An edited version of this chapter was published as:

Gomez-Maldonado D, Vega Erramuspe IB, Filpponen I, et al (2019) Cellulose-Cyclodextrin Co-Polymer for the Removal of Cyanotoxins on Water Sources. Polymers (Basel) 11:2075. https://doi.org/10.3390/polym11122075

3.7. Literature Cited

Abdolali, A., Guo, W. S., Ngo, H. H., Chen, S. S., Nguyen, N. C., & Tung, K. L. (2014). Bioresource Technology Typical lignocellulosic wastes and by-products for biosorption process in water and wastewater treatment: A critical review. *Bioresource Technology*, *160*, 57–66. https://doi.org/10.1016/j.biortech.2013.12.037

Ali, I., & Gupta, V. K. (2007). Advances in water treatment by adsorption technology. *Nature Protocols*, *1*(6), nprot.2006.370. https://doi.org/10.1038/nprot.2006.370

Archimandritis, A. S., Papadimitriou, T., Kormas, K. A., Laspidou, C. S., Yannakopoulou, K., & Lazarou, Y. G. (2016). Theoretical investigation of microcystin-LR, microcystin-RR and nodularin-R complexation with α-, β-, and γ-cyclodextrin as a starting point for the targeted design of efficient cyanotoxin traps. *Sustainable Chemistry and Pharmacy*, *3*, 25–32. https://doi.org/10.1016/j.scp.2016.02.001

Bouhadiba, A., Belhocine, Y., Rahim, M., Djilani, I., Nouar, L., & Khatmi, D. E. (2017). Host-guest interaction between tyrosine and β-cyclodextrin: Molecular modeling and nuclear studies. *Journal of Molecular Liquids*, *233*, 358–363. https://doi.org/10.1016/j.molliq.2017.03.029

Briggs, D., & Beamson, G. (1993). XPS Studies of the Oxygen 1s and 2s Levels in a Wide Range of Functional Polymers. *Analytical Chemistry*, *65*(11), 1517–1523. https://doi.org/10.1021/ac00059a006

Carpenter, A. W., de Lannoy, C.-F., & Wiesner, M. R. (2015). Cellulose Nanomaterials in Water Treatment Technologies. *Environmental Science & Technology*, *49*(9), 5277–5287. https://doi.org/10.1021/es506351r

Chen, L., Zhu, J. Y., Baez, C., Kitin, P., & Elder, T. (2016). Highly thermal-stable and functional cellulose nanocrystals and nanofibrils produced using fully recyclable organic acids. *Green Chem.*, *18*(13), 3835–3843. https://doi.org/10.1039/C6GC00687F

Espinosa, E., Tarrés, Q., Delgado-Aguilar, M., González, I., Mutjé, P., & Rodríguez, A. (2016). Suitability of wheat straw semichemical pulp for the fabrication of lignocellulosic nanofibres and their application to papermaking slurries. *Cellulose*, *23*(1), 837–852. https://doi.org/10.1007/s10570-015-0807-8

Example, A. (1991). Dissipative QCM. *Langmuir*, 1–3.

Fält, S., Wågberg, L., & Vesterlind, E. L. (2003). Swelling of model films of cellulose having different charge densities and comparison to the swelling behavior of corresponding fibers. *Langmuir*, *19*(19), 7895–7903. https://doi.org/10.1021/la026984i

Filpponen, I., Kontturi, E., Nummelin, S., Rosilo, H., Kolehmainen, E., Ikkala, O., & Laine, J. (2012). Generic method for modular surface modification of cellulosic materials in aqueous medium by sequential “click” reaction and adsorption. *Biomacromolecules*, *13*(3), 736–742. https://doi.org/10.1021/bm201661k

Gidwani, B., & Vyas, A. (2014). Synthesis, characterization, and application of Epichlorohydrin-β-cyclodextrin polymer. *Colloids and Surfaces B: Biointerfaces*, *114*, 130–137. https://doi.org/10.1016/j.colsurfb.2013.09.035

Gomez-Maldonado, D., Vega Erramuspe, I. B., & Peresin, M. S. (2019). Natural Polymers as Alternative Adsorbents and Treatment Agents for Water Remediation. *BioResources*, *14*(4). https://doi.org/10.15376/biores.14.4.Gomez-Maldonado

Hitzfeld, B. C., Hoger, S. J., & Dietrich, D. R. (2000). Cyanobacterial Toxins: Removal during Drinking Water Treatment, and Human Risk Assessment Cyanobacteria. *Environmental Health Perspectives*, *108*(1), 113–122.

Jagur-Grodzinski, J. (2006). Nanostructured polyolefins / clay composites: role of the molecular interaction at the interface. *Polym. Adv. Technol.*, *17*(April), 395–418. https://doi.org/10.1002/pat

Ji, B., Tang, P., Yan, K., & Sun, G. (2015). Catalytic actions of alkaline salts in reactions between 1,2,3,4-butanetetracarboxylic acid and cellulose: II. Esterification. *Carbohydrate Polymers*, *132*, 228–236. https://doi.org/10.1016/j.carbpol.2015.06.070

Johansson, L. S., & Campbell, J. M. (2004). Reproducible XPS on biopolymers: Cellulose studies. *Surface and Interface Analysis*, *36*(8), 1018–1022. https://doi.org/10.1002/sia.1827

Johansson, L. S., Tammelin, T., Campbell, J. M., Setälä, H., & Österberg, M. (2011). Experimental evidence on medium driven cellulose surface adaptation demonstrated using nanofibrillated cellulose. *Soft Matter*, *7*(22), 10917–10924. https://doi.org/10.1039/c1sm06073b

Kasemo, B., Fant, C., Sott, K., Elwing, H., & Qcm-d, T. (2001). *Variations in Coupled Water , Viscoelastic Properties , and Film Thickness of a Mefp-1 Protein Film during Adsorption and Cross-Linking : A Quartz Crystal Microbalance with Dissipation Monitoring , Ellipsometry , and Surface Plasmon*. *73*(24), 5796–5804.

Kim, S., Yun, Y. S., & Choi, Y. E. (2018). Development of waste biomass-based sorbent for removal of cyanotoxin microcystin-LR from aqueous phases. *Bioresource Technology*, *247*(June 2017), 690–696. https://doi.org/10.1016/j.biortech.2017.09.164

KSV Instruments Ltd. (2002). *What Is a Quartz Crystal Microbalance – Qcm* (pp. 1–10).

Kuo, P. Y., Barros, L. de A., Yan, N., Sain, M., Qing, Y., & Wu, Y. (2017). Nanocellulose composites with enhanced interfacial compatibility and mechanical properties using a hybrid-toughened epoxy matrix. *Carbohydrate Polymers*, *177*(August), 249–257. https://doi.org/10.1016/j.carbpol.2017.08.091

Lahti, K., Rapala, J., Färdig, M., Niemelä, M., & Sivonen, K. (1997). Persistence of cyanobacterial hepatotoxin, microcystin-LR in particulate material and dissolved in lake water. *Water Research*, *31*(5), 1005–1012. https://doi.org/10.1016/S0043-1354(96)00353-3

Lee, J., & Walker, H. W. (2011). Adsorption of microcystin-Lr onto iron oxide nanoparticles. *Colloids and Surfaces A: Physicochemical and Engineering Aspects*, *373*(1–3), 94–100. https://doi.org/10.1016/j.colsurfa.2010.10.032

Li, C., Wen, T., Yan, L., Li, B., Wang, W., Yang, J., Xu, M., T-f, W., L-n, Y., W-t, W., J-y, Y., & M-q, X. (2017). Develpment of waste biomass-based sorbent for removal of cyanotoxin microcystin-LR from aqueous phases. *Bioresource Technology*. https://doi.org/10.1016/j.ijsu.2017.05.034

Li, R., Yu, J. C., Jiang, Z. T., Zhou, R. H., & Liu, H. Y. (2003). A solid-phase fluorescent, quenching method for the determination of trace amounts of nitrite in foods with neutral red. *Journal of Food and Drug Analysis*, *11*(3), 251–257.

Lombardo, S., & Thielemans, W. (2019). Thermodynamics of adsorption on nanocellulose surfaces. *Cellulose*, *26*(1), 249–279. https://doi.org/10.1007/s10570-018-02239-2

Mahfoudhi, N., & Boufi, S. (2017). Nanocellulose as a novel nanostructured adsorbent for environmental remediation: a review. *Cellulose*, *24*(3), 1171–1197. https://doi.org/10.1007/s10570-017-1194-0

Medronho, B., Andrade, R., Vivod, V., Ostlund, A., Miguel, M. G., Lindman, B., Voncina, B., & Valente, A. J. M. (2013). Cyclodextrin-grafted cellulose: Physico-chemical characterization. *Carbohydrate Polymers*, *93*(1), 324–330. https://doi.org/10.1016/j.carbpol.2012.08.109

Meriluoto, J., & Codd, G. A. (2005). *Cyanobacterial Monitoring and Cyanotoxin Analysis*. https://doi.org/10.1002/9781119068761

Parvinzadeh, M., Alimohammadi, F., & Shamei, A. (2012). Surface & Coatings Technology Preparation of water-repellent cellulose fi bers using a polycarboxylic acid / hydrophobic silica nanocomposite coating. *Surface & Coatings Technology*, *206*(14), 3208–3215. https://doi.org/10.1016/j.surfcoat.2012.01.006

Pinto, L. M. A., Fraceto, L. F., Santana, M. H. A., Pertinhez, T. A., Oyama, S., & De Paula, E. (2005). Physico-chemical characterization of benzocaine-β-cyclodextrin inclusion complexes. *Journal of Pharmaceutical and Biomedical Analysis*, *39*(5), 956–963. https://doi.org/10.1016/j.jpba.2005.06.010

Saenger, W., & Steiner, T. (1998). *Cyclodextrin Inclusion Complexes: Host ± Guest Interactions and Hydrogen-Bonding Networks*. 798–805. https://doi.org/10.1107/S0108767398010733

Sinha, A., & Jana, N. R. (2015). Separation of microcystin-LR by cyclodextrin-functionalized magnetic composite of colloidal graphene and porous silica. *ACS Applied Materials and Interfaces*, *7*(18), 9911–9919. https://doi.org/10.1021/acsami.5b02038

Sun, T., & Lindsay, J. D. (2004). *Cyclodextrins covalently bound to polysaccharides* (Patent No. US 6,689,378 B1).

Szejtli, J., Zsadon, B., Fenyvesi, É., & Tüdös, F. (1982). *Sorbents of cellulose basis capable of forming inclusion complexes and a process for the preparation thereof* (Patent No. 4,357,468).

TAPPI. (1993). T550 Determination of equilibrium moisture in pulp, paper and paperboard for chemical analysis. *TAPPI T550 Om-08*, 1–3. https://doi.org/10.1002/rcm.5278

Tran, C. D., Duri, S., Delneri, A., & Franko, M. (2013). Chitosan-cellulose composite materials: Preparation, Characterization, and application for removal of microcystin. *Journal of Hazardous Materials*, *253*, 355–366.

Turon, X., Rojas, O. J., & Deinhammer, R. S. (2008). Enzymatic kinetics of cellulose hydrolysis: A QCM-D study. *Langmuir*, *24*(8), 3880–3887. https://doi.org/10.1021/la7032753

USEPA - Office of Water. (2016). *Human Health Recreational Ambient Water Quality Criteria or Swimming Advisories for Microcystins and Cylindrospermopsin Draft Human Health Recreational Ambient Water Quality Criteria or Swimming Advisories for Microcystins and Cylindrospermopsin* (Issue December).

Voinova, M. V., Jonson, M., & Kasemo, B. (2002). "Missing mass" effect in biosensor's QCM applications. *Biosensors and Bioelectronics*, *17*(10), 835–841. https://doi.org/10.1016/S0956-5663(02)00050-7

Voinova, M. V., Rodahl, M., Jonson, M., & Kasemo, B. (1998). *Viscoelastic acoustic response of layered polymer films at fluid-solid interfaces: Continuum mechanics approach*. 1–22. https://doi.org/10.1238/Physica.Regular.059a00391

Walls, J. T., Wyatt, K. H., Doll, J. C., Rubenstein, E. M., & Rober, A. R. (2018). Hot and toxic: Temperature regulates microcystin release from cyanobacteria. *Science of the Total Environment*, *610–611*, 786–795. https://doi.org/10.1016/j.scitotenv.2017.08.149

Wang, R., Chen, L., Zhu, J. Y., & Yang, R. (2017). Tailored and integrated production of carboxylated cellulose nanocrystals (CNC) with nanofibrils (CNF) through maleic acid hydrolysis. *ChemNanoMat*, *3*(5), 328–335. https://doi.org/10.1002/cnma.201700015

World Health Organization. (2014). Guidelines for drinking-water quality, 2011. *Switzerland: WHO Library Cataloguing-in-Publication Data, Fourth Google Scholar*, *1*, 595. https://doi.org/10.1016/S1462-0758(00)00006-6

Zhang, F., Wu, W., Sharma, S., Tong, G., & Deng, Y. (2015). Synthesis of Cyclodextrin-functionalized Cellulose Nanofibril Aerogel as a Highly Effective Adsorbent for Phenol Pollutant Removal. *BioResources*, *10*(4), 7555–7568.

Zhou, Z.-Y., Tian, N., Li, J.-T., Broadwell, I., & Sun, S.-G. (2011). Nanomaterials of high surface energy with exceptional properties in catalysis and energy storage. *Chem. Soc. Rev.*, *40*(7), 4167–4185. https://doi.org/10.1039/C0CS00176G

4. Fabrication of aerogels from cellulose nanofibril grafted with β-cyclodextrin for capture of water pollutants.

4.1.Abstract

Interactions at the molecular and surface chemistry are some of the key factors that determine the adsorption capacity of pollutants and emerging contaminants in porous materials. As filtration-based purification of water sources expands, the generation of green materials, such as biopolymers is priority. However, to increase the removal capacity, modification of natural polymers appears necessary. Nanomaterials, especially bio-based materials like cellulose nanofibrils, inherently have large surface areas as a consequence of their high aspect ratios. Their capacity to modulate the interactions with contaminants present in water can be modulated by incorporating selective active points, such as hydrophobic cavities, that can further improve their overall adsorption capability. A bio-based material that can fulfill this requirement is β-cyclodextrin, a cyclic oligosaccharide with glucose as monomer, which provides an easy grafting strategy onto cellulose due to structural affinity. Another advantage of using cellulose nanofibril is their film formability, aerogels, and hydrogels without the need of harsh chemicals or processes.

In this work, an oligosaccharide with a hydrophobic centre – β-cyclodextrin – was immobilized onto bleached softwood cellulose nanofibrils, and then used to generate high surface area aerogels with a density of 175 kg/m^3 and porosities above 88%. Charge density titration, Fourier Transform Infrared (FTIR), X-Ray Photoelectron Spectroscopy (XPS), Thermogravimetric Analysis (TGA), and Atomic Force Microscopy (AFM) characterization techniques were used to assess the successful modification of the fibrils. Inductive Coupled Plasma Mass Spectroscopy (ICP-MS) was used to determine the lack of trace chlorine in the material from

the grafting process, while Scanning Electron Microscopy (SEM) and Dynamic Vapor Sorption (DVS) were used to determine porosity and surface area of the aerogels. Adsorption capacity was tested with two molecules of different natures: a cyanotoxin (microcystin-LR) and a dye (methylene blue), using High-Performance Liquid Chromatography with a UV detector (HPLC-UV) and UV-Vis spectroscopy, respectively. The adsorption in equilibrium for CNF-CD aerogels was calculated to be 0.078 mg/g of microcystin-LR and 3.46 mg/g of methylene blue, enlightening its possible use to improve water quality.

4.1.1. Index Words

Cellulose nanofibril, β-cyclodextrin, aerogels, water remediation, physical adsorption, microcystin-LR, methylene blue.

4.1.2. Project Partners

The Forest Products Development Center worked in collaboration with the School of Pharmacy and the Department of Crops, Soils and Environmental Science from Auburn University and with Surface Measurement Systems Ltd. This research was supported by the Alabama Agricultural Experiment Station, and the Hatch program of the National Institute of Food and Agriculture, United States Department of Agriculture. The School of Forestry and Wildlife Sciences at Auburn University financial support to complete this work is greatly appreciated.

4.2. Introduction

As clean water sources are negatively impacted by increasing industrial and agricultural activities, and global urbanization, there is a rising need to develop low cost, renewable and widely available sorbents that can be used to increase water quality (United Nations, n.d.; United Nations Department of Economic and Social Affairs, 2014; World Health Organization, 2017). The efficiency of these sorbents is linked to the material surface chemistry and surface area as well as the possible molecular interactions between the material and the given pollutants (J. Lee & Walker, 2011; N. Lin & Dufresne, 2013; Piñeiro et al., 2007).

When selecting materials for the development of filtration sorbents, worldwide efforts to lower carbon emissions need to be taken into consideration. These efforts have prompted the development of green materials and processing technologies that aim at replacing widely used fossil fuel-derived analogues. Along these lines, the utilization of bio-based materials to develop of sorbent for water treatment is of particular interest (Ali, 2012; Carpenter, de Lannoy, et al., 2015; Carpenter, Lannoy, et al., 2015; Devrimci et al., 2012; Gomez-Maldonado, Vega Erramuspe, & Peresin, 2019; Papageorgiou et al., 2012; Vakili et al., 2019; Zeng et al., 2008). Out of a variety of bio-based materials, cellulose nanofibrils (CNF) are considered a versatile substrate due to their wide availability, well-established structures, and chemical reactivity, allowing for their modification to target specific interactions towards particular pollutants of interest (Kumar Dutta et al., 2004; K. Y. Lee et al., 2011; Missoum et al., 2013). Cellulose, as a molecule, is a polysaccharide made of β-(1□4) glucopyranoside units with chain conformations that vary in length and crystalline structure from organism to organism. Cellulose chains are organized in highly packed bundles by intra- and intermolecular hydrogen bonds, that interact with the additional plant cell wall components conforming the so-called lignocellulosic materials (Oksman

et al., 2014; Sixta, 2006). Lignocellulosic materials can be treated by chemical, mechanical, or enzymatic ways to produce cellulose fibers in dimensions that can vary from the micro to the nanoscale (Iglesias et al., 2020). In particular, CNF present characteristic high surface area along with inherent biocompatibility, high mechanical strength, and light weight which make them highly suitable for a range of applications, including water treatment applications (Jin et al., 2015; Orelma et al., 2011; Ristić et al., 2014). CNFs can be assembled into 3-D structures that not only maintain a high surface area, but also provide dimensional stability so they can be further manipulated, such as highly porous and low-density aerogels (Sehaqui et al., 2011; Toivonen et al., 2015).

Cellulose nanomaterials have been proven to adsorb positively charged pollutants like metallic ions (Gurgel et al., 2008; Kardam et al., 2014) or polypeptides (Koshani & Madadlou, 2018; Raghuwanshi et al., 2017). These interactions are mainly driven by electrostatic or van der Waals interactions, which increase the total entropy of the systems by liberating adsorbed water (Lombardo & Thielemans, 2019). This is highly appealing as the capturing a wide variety of pollutants is driven by these same mechanisms. In addition to this, multiple emerging contaminants such as dyes, aromatics, or hydrocarbons are complex molecules for which their adsorption on the sorbent could be benefited by the addition of hydrophobic active points on the cellulose nanofibril surface, with straightforward routs such as grafting of β-cyclodextrin. β-cyclodextrin has been shown to improve the adsorption of pollutants when was grafted onto magnetic graphene sheets and porous silica (Sinha & Jana, 2015), chitosan/graphene sheets (Fan et al., 2013), carbonaceous nanofibrils (Chen et al., 2011), biomass/polysulfone/polyethylenimine (Kim et al., 2018), and cellulose-based materials (Celebioglu et al., 2014; Cova et al., 2018; Dong, Qian, et al., 2014; Gomez-Maldonado, Vega Erramuspe, Filpponen, et al., 2019; Zhang et al., 2013).

However, the formation of aerogels with pre-grafted cellulose nanofibril has not been widely explored. The potential impact of this approach on the adsorption of organic pollutants is intriguing and holds great potential for removal of such pollutants and for increasing water quality.

In this work, bleached softwood cellulose nanofibrils (CNF) were crosslinked with β-cyclodextrin (CD) via epichlorohydrin, and aerogels were formed from this material by solvent exchange (ethanol and tert-butanol), followed by freeze drying. Charge density, Fourier transform infrared (FTIR), X-ray photoelectron spectroscopy (XPS) thermogravimetric analysis (TGA), and atomic force microscopy (AFM) characterization techniques were used to confirm modification of the fibrils; inductive coupled plasma optical emission spectroscopy (ICP-OES) was used to monitor traces of chlorine after grafting reaction. Scanning electron microscopy (SEM) and dynamic vapor sorption (DVS) were used to determine surface area and surface energy of the aerogel. For testing adsorption capability, two different target molecules were chosen: a cyclic oligopeptide with a prominent hydrophobic residue: microcystin-LR- (a cyanotoxin) and methylene blue (a commonly used cationic dye) to elucidate preferred adsorption mechanisms between pristine CNF and the CNF grafted with β-cyclodextrin (CNF-CD). The adsorption of microcystin-LR was followed by high-performance liquid chromatography with an UV detector (HPLC-UV), UV-Vis spectroscopy (UV-Vis) was the chosen analytical tool to monitor adsorption of methylene blue. A schematic flowline of this study can be found in Figure 4.1.

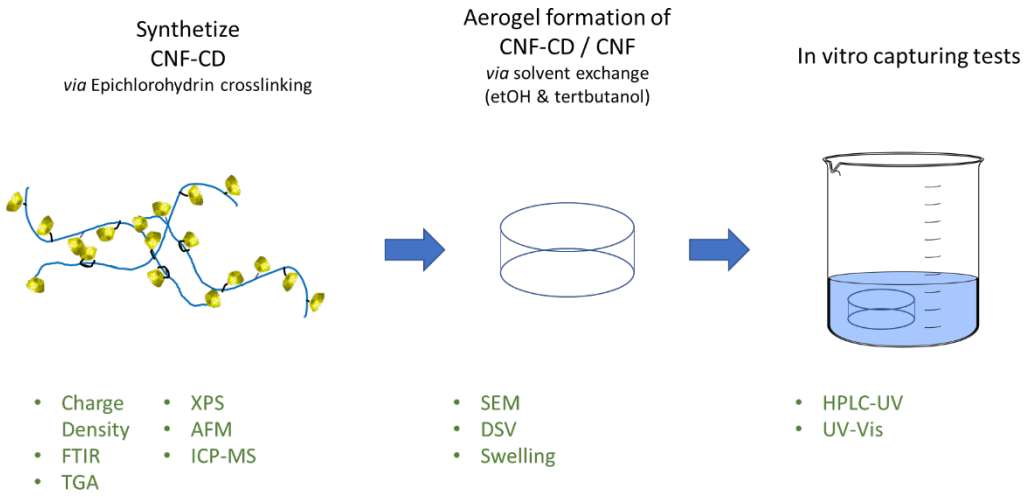

Figure 4.1.Schematic outline of this work

4.3. Materials and Methods

4.3.1. Materials

Bleached cellulose nanofibrils (2.76%, pH 6.3) were produced at the Forest Products Development Center at Auburn University from bleached pulp from mixed softwood kindly provided by International Paper; ß-cyclodextrin (> 98%, CD) was purchased from Tokyo Chemical Industry America (Portland, OR, U.S.); epichlorohydrin (99% EPI) was obtained from Acros Organics (Geel, Belgium); microcystin-LR (> 95%, MC) from Cayman Chemicals (Ann Arbor, MI, U.S.); methylene blue and 2,4-dichlorophenol were purchased from Merck KGaA (Darmstadt, Germany); hydrochloric acid (37.6% solution) purchased from Fisher Scientific (Waltham, MA, U.S.); sodium hydroxide (50% w/w solution) purchased from J.T. Baker (Phillipsburg, NJ, U.S.); ammonium hydroxide (18-30 % solution) purchased from VWR International, LLC., (Radnor, PA, U.S.); ethanol (200 proof pure) purchased from Decon Labs, Inc. (King of Prussia, PA, U.S.); and

tert-butanol (> 99%) was acquired from Sigma-Aldrich Co., (San Luis, MO, U.S.). The water used was deionized and purified with a Thermo Scientific Barnstead nanopure (18.2 mΩ cm).

4.3.2. Cellulose nanofibrils (CNF) production

For the preparation of the CNF solution, the bleached pulp was diluted to a 2% wt. suspension. A washing was done as pre-treatment of the pulp to eliminate residual metals and another component. The washing consisted in first lowering the pH to 3 with a 1 M HCl solution; after 30 min washings of the pulp were done with DI water until pH increased to 4.5-5, then NaHCO3 was added to obtain a 0.001 M concentration and pH was adjusted to 9 with 1 M NaOH. After 30 min, washings were performed until no changes in conductivity were measurable. Finally, the washed pulp was then processed by Masuko super mass colloider (MKZA-10-15J). The pulp was first refined 10 times with stone no. 46 and then 10 more times with stone no. 80. A final consistency of 2.76% wt. was obtained with a pH of 6.3.

4.3.3. Synthesis of crosslinked cellulose nanofibrils/β-cyclodextrin (CNF-CD)

A low concentration solution of CNF was prepared (625 mL, 0.004% w/v) and left overnight stirring at 4 °C. Then, 75 mL of 40% v/v NaOH was mixed with 12.5 g β-cyclodextrin. Once dissolved, the solution was added to the CNF solution and stirred for one hour. The temperature was then raised to 65 °C in a water bath. Meanwhile, 38 mL of epichlorohydrin were added dropwise to obtain a final ratio of (1:5:25 moles of CNF:CD:EPI). The solution was left to react for 2 hours while stirring at 160 rpm. After cooling to room temperature, the solution was vacuum filtered with a PYREX Buchner funnel (using Whatman TM glass microfiber filters diameter 70 mm Cat No. 1820-070) until cake released no more water. After removal, the material was put in an extraction glass fiber thimble inside a Soxhlet extractor system with 375 mL of

acetone at 80 °C and left for 16 cycles. The material produced was then re-suspended in 375 mL of ultrapure water and neutralized to a pH of 7.03 with 1 M HCl. Once neutralized, the CNF-CD solution was vacuum filtrated and stored at 4 °C.

4.3.4. Aerogels formation

CNF and CNF-CD were resuspended in ultrapure water to a 0.35% wt. consistency. From these solutions 21 mL were vacuum filtrated in a filtration system assembled with diameter of 25 mm with glass fiber filter paper. The filtration was done until a cake of approximately 1 cm was obtained, which was then transferred to a Teflon film (1.6 mm of thickness, 4 cm diameter) inside 6 cm petri dishes. A total of seven solvent changes were done, four in ethanol and three changes with tert-butanol with 15 mL steps and waits of 1 h. After the last removal of tert-butanol, the filtrated cakes were frozen and freeze-dried in a Freezone 12 (Labconco).

4.3.5. Characterization techniques

4.3.5.1. Charge density.

Charge densities of the CNF, CNF-CD and CD were measured using a method adapted from Espinosa *et al* (2016). Measurements were repeated 6 times and averaged. In brief, suspensions with 0.04% wt. consistency were prepared and pH was adjusted to 6.5 for both solutions using 1 M HCl or NaOH. 15 mL of this suspension were mixed with 25 mL of pDADMAC and centrifuged at 3000 rpm for 15 min. After centrifugation, 10 mL of the supernatant were separated and analyzed using a Laboratory Charge Analyzer Chemtrac LCA-1, (Norcross, GA). For this analysis, the solution was titrated with PSVK until the equipment reached 0 streaming current value (SCV). The volume of titrant consumed was used for the final calculations using the following equation (Eq. (4.1))

$$Charge\ density = \frac{([pDADMAC]*V_{p-DADMAC})-([PVSK])*V_{PVSK}}{W_{dry\ sample}} \quad (4.1)$$

where [pDADMAC] is the concentration of the cationic polymer, Vp-DADMAC is the used volume of p-DADMAC, [PVSK] is the concentration of the anionic titrant, V_PVSK is the consumed volume of titrant, and W (dry sample) is the weight of the dry CNF, CNF-CD or CD sample.

4.3.5.2.Fourier-transform infrared spectroscopy with attenuated total reflectance (FTIR-ATR).

Air-dried samples were analyzed for characterization of the surface modification on a PerkinElmer Spotlight 400 FT-IR Imaging System (Massachusetts, US) with an ATR accessory with diamond/ZnSe crystal and a resolution of 4 cm-1. First, a background spectrum with the clean sensor was measured; this was carried-out before each set of measurements with the same number of scans. To archive a high resolution at the spectrum bands, 512 scans per spectrum were performed. Data was processed with Spectrum 6 Spectroscopy Software (PerkinElmer, Massachusetts, US).

4.3.5.3.X-ray photoelectron spectroscopy (XPS).

*4.3.5.4.*Surfaces of the CNF and CNF-CD were mounted on an XPS sample holder using UHV compatible carbon tape. The chamber with the samples and a piece of pure cellulose -as the in-situ reference monitoring analysis conditions during the measurement (Johansson et al., 2020)- were pre-evacuated overnight together. The gathered data were recorded using monochromatic Al Kα irradiation at only 100 W and under neutralization. For the data analysis, high-resolution C 1s regions were fitted with Gaussian components of equal half widths, and the binding energies of all spectra were charge-corrected using the main component of cellulose, namely C–O at 286.7 eV, as the BE reference (Briggs & Beamson, 1993).

4.3.5.5.Thermogravimetric analysis (TGA).

Air-dried samples were tested on aluminum pans in a TGA-50 from Shimadzu (Kyoto, Japan). Samples were heated from room temperature to 600 °C at a rate of 10 °C/min under a nitrogen atmosphere and data was processed with ta60 software version 2.11 from Shimadzu.

4.3.5.6.Atomic force microscopy (AFM).

Surface characterization of the CNF and CNF-CD were done in spin-coated silicon wafers (2x2 cm) with a Tosca 400 equipment from Anton-Paar (Gratz, At). Height images were obtained by tapping mode with a Nano World (Innovative Technologies) ARROW-NCR-20 silicon SPM-sensor cantilever with a resonance frequency of 285 kHz and constant force of 42 N/m; scan sizes were 5x5 µm and 10x10 µm. Processing of the images was done with Gwyddion software 2.49 (SourceForge) and roughness calculations were done with ProfilmOnline (KLA Corporation).

4.3.5.7.Inductive coupled plasma optical emission spectroscopy (ICP-MS).

Samples of CNF and CNF-CD were analyzed for chloride concentrations using a Thermo Electron iCAP-RQ inductively coupled plasma mass spectrometer (ICP-MS) per Standard Method 3125-B.(American Public Health Association & American Water Works Association and Water Environment Federation, n.d.) Samples and calibration standards were prepared in a matrix of 2% nitric acid by volume.

4.3.5.8.Scanning electron microscopy (SEM).

Freeze-dried CNF and CNF-CD aerogels were placed on aluminum studs and sputtered with gold for 60 s in a Q150R ES sputter coating device acquired form Electron Microscopy Sciences (Hatfield, PA, U.S.). Images were recorded using 20 kW, working distance between 6 and 8 mm and with magnification of 1000X in a Zeiss Evo 50VP scanning electron microscope (SEM).

4.3.5.9.Dynamic vapor sorption (DVS).

For all experiments, approximately 125 mg of each aerogel were packed into individual silanized glass columns (300 mm long by 4 mm inner diameter) using the SMS Column Packing Accessory. Each column was conditioned for a period of 2 h at 30°C and 0% RH with helium gas prior to any measurements. All experiments were conducted at 30°C with 25 sccm total flow rate of helium gas, using methane for dead volume corrections. Samples were run at a series of surface coverages with n-alkanes (nonane, octane, heptane and hexane; Aldrich, HPLC grade) and polar probe molecules (acetone, ethanol, acetonitrile, ethyl acetate, and dichloromethane; Aldrich, HPLC grade) to determine the dispersive surface energy as well as the specific free energies of adsorption, respectively. The complete IGC experiment over all surface coverages measured took

approximately 24 h for one sample. Repeat experiments were completed in succession on the same column to investigate if the elapsed time or exposure to vapors caused any measurable surface changes. Dispersive surface energy values were repeatable within ± 1.0 mJ/m2 and acid-base surface energy values were repeatable within ± 0.5 mJ/m2. All surface energy analyses were carried out using iGC Surface Energy Analyzer (SMS, Alperton, UK) and the data were analyzed using both standard and advanced SEA Analysis Software.

4.3.5.10. Water uptake and swelling.

To calculate water uptake, the dried aerogels were immersed in 20 mL of ultrapure water, from which they were removed at regular time intervals up to 240 min and weighted. The averaged results for water uptake were calculated by the following equation (Eq 4.2).

$$Water\ uptake\ (\%) = \frac{Wt-Wd}{Wd} * 100 \quad (4.2)$$

where Wt is the weighted mass, and Wd is the dry weight of the aerogels. Meanwhile, for the swelling, the aerogels were left for 24 h in 20 mL of ultrapure water before weighting. The average results were then calculated with the next equation (Eq 4.3).

$$Swelling\ (\%) = \frac{Ws}{Wd} * 100 \quad (4.3)$$

where Ws is the weight obtain after swelling.

Density and porosity. Dimensional measurement of the aerogels was done using a digital caliper and used to calculate volume and density (ρa). The porosity was obtained by equation (Eq. 4.4), where the density of the cellulose (ρc) was assumed to be 1460 kg/m3, as reported in literature (Sehaqui et al., 2011).

$$Porosity\ (\%) = 1 - \frac{\rho_a}{\rho_c} * 100 \quad (4.4)$$

4.3.6. Adsorption Experiments

4.3.6.1.High Pressure Liquid Chromatography (HPLC).

For the analysis of microcystin, the aerogels were placed in 20 mL of solutions containing 1.5 and 0.8 µg/mL at room temperature and constant stirring. 150 µL aliquots were taken at the corresponding time and analyzed in a Waters Alliance HPLC (Model No. e2695, Waters Corp., Milford, MA, USA) system equipped with a solvent management system 2695 and detected by a photodiode array detector (PDA, 2998). The system also counts with a thermostatically controlled column compartment and an autosampler. The method used was adapted from the one described by Meriluoto & Codd (2005). Briefly, a C-18 column (55x4 mm) was used as stationary phase, and 0.5% trifluoroacetic acid (TFA) aqueous solution/0.5% TFA acetonitrile with linear gradient at a flow rate of 1 mL/min, and 10 µL injections using the autosampler in cycles of 9 min. The retention time was 4.2 min and correlation of the samples to the standard curve was of 0.9997. All experiments were done by triplicates and averaged. The analysis of the data was performed using Empower® 3 software (Waters Corp., Milford, MA, USA).

4.3.6.2.UV-Vis spectroscopy.

All absorbance data was collected in a SpectraMax M2 from Molecular Devices (Silicon Valley, CA, USA) and data was visualized on the software SoftMax Pro 6.5.1. For methylene blue adsorption and desorption experiments, filters were immersed in 50 mL of a 15 mg/L solution and kept at 25 °C with constant stirring; absorbance measurements were done at λ=664 nm. All experiments were done by triplicated and averaged.

4.3.6.3.Kinetics.

The fitting of the data to calculate rate constants (k1 and k2) and adsorbed amounts in equilibrium (qe) was done for a pseudo-first order and pseudo-second order models when possible, following the equations given in (Tran et al., 2013). Briefly, for pseudo-first order:

$$\ln(qe - qt) = \ln qe - k_1 t \quad (4.5)$$

For pseudo-second order:

$$\frac{t}{qt} = \frac{1}{h} + \frac{t}{qe} \quad (4.6)$$

where h=k2qe2, with k1 and k2 being the pseudo-first and pseudo-second order rate constant of sorption, respectively. qe is the amount of analyte adsorbed at equilibrium (mg/g), and qt is the amount of analyte adsorbed at any time (mg/g).

The linear plots for the pseudo-second order were first done to obtain qe and h, and the obtained qe was used for the pseudo-first order when possible, for the fitting.

4.4. Results and Discussions

4.4.1. Synthesis of CNF-CD.

The success of the grafting reaction was followed by a combination of analytical techniques. Comparing the charge densities (see Table 4.1) of pristine CNF and CNF-CD, the CD-grafted CNF shows an increase of 37.4% compared to the charge density of the pristine CNF. This increase can be related to an increase of functional groups as a side reaction of the grafting in alkaline conditions (Mozdyniewicz et al., 2013), or by the formation of aldehyde and other ionizable groups with the additions of side chains occurring upon the inclusion of the epichlorohydrin into the fibre (Morin-Crini et al., 2018).

Table 4.1. Charge density values of the different elements used.

Sample	Charge Density [μeq/g]	St. Dev	pH
CNF	126.67	64.89	6.5
CNF-CD	202.22	48.57	6.5

When analyzing FTIR spectra (shown in Figure 4.2A), changes in the C-H stretching band (2900 cm-1) are perceptible in the CNF-CD; due to the introduction of aliphatic CH2 with the molecular bridges, product of the crosslinking via EPI (Morin-Crini et al., 2018; Udoetok et al., 2016). These bonds can also be seen in the changes in the bands related to OCH/CH2 bending at 1423 cm-1, where it can be observed that the main band decreases and the shoulder is more defined. Finally, the band at 1640 cm-1 is traditionally related to the adsorbed water. In this band, the shoulder that is present in the CNF spectrum increases in intensity for the crosslinked polymer which reveals a greater similarity of the CNF-CD to the CD spectrum, showing the presence of these components in the conjugated system.

These changes can also be observed in the XPS wide energy region and the high-resolution C 1s spectra (Figure 4.2B), where there is a 2.8% increase in the C-O bonds in the surface from the pristine CNF to the modified CNF-CD. There we can also see a reduction in the proportion of O-C-O bonds where there was a 2.2% decrease that indicates the introduction of EPI bonds. In other words, the decrease can be explained due to the presence of more aliphatic carbons on the surfaces, which translates to a lower proportion of the O-C-O signal coming from the cyclic ring than the monomers. Moreover, a decrease in the C/O ratio was observed from 0.64 to 0.62, further confirming the modification of the fibers.

(a)

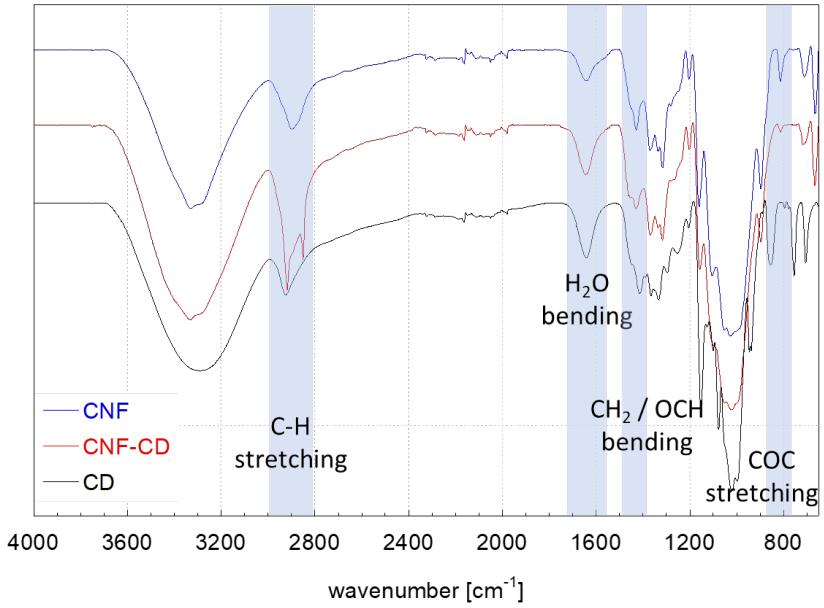

(b)

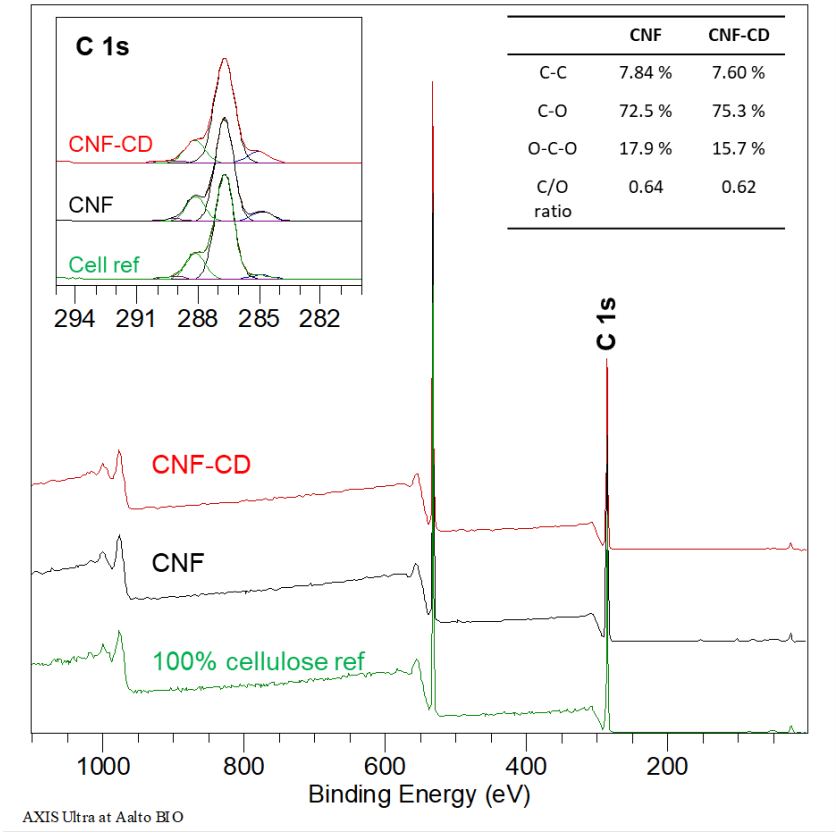

Figure 4.2. Chemical and thermal comparison of the used cellulose nanofibrils (CNF), β-cyclodextrin (CD), and the crosslinked CNF-CD. (A) FTIR spectra; (B) XPS wide energy region spectra and inserts showing the high-resolution C 1S spectra and the elemental data

Alternatively, thermal analysis of the samples was conducted to collect additional evidence of the chemical modification using TGA. Thermograms can be found in Figure 4.3. From these tests, it can be observed that the grafting of the CD increased the onset temperature of the modified CNF, however keeping it lower than free CD. These results are in accordance with other cellulose and cyclodextrin systems found in literature (Medronho et al., 2013). However, in this work, the addition of the cyclodextrin to the CNF increased the max degradation temperature, as more packing of the fibers is present (Dong, Ye, et al., 2014); which also can be confirmed with the AFM images presented in Figure 4.4.

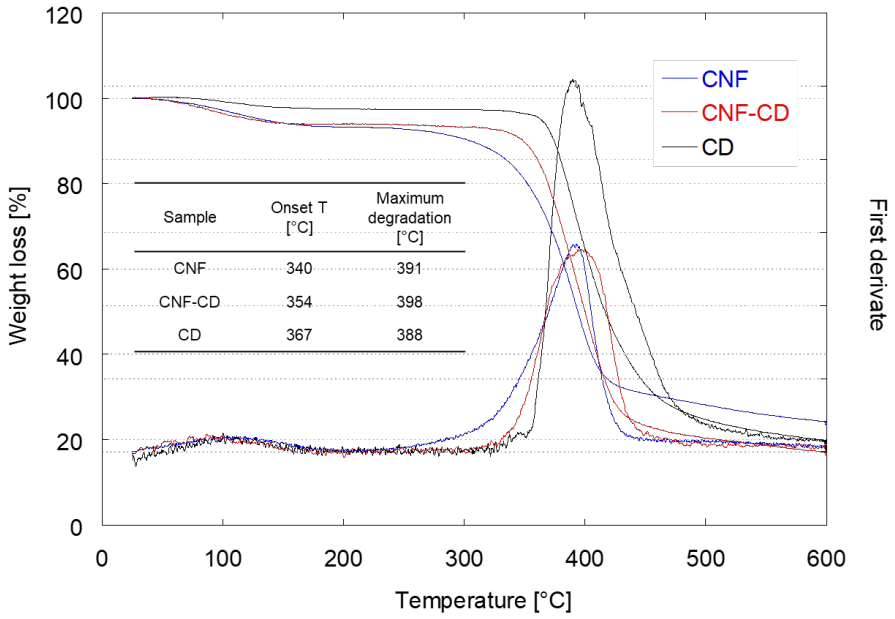

Figure 4.3. Thermograms comparing the used cellulose nanofibrils (CNF), β-cyclodextrin (CD) and inserts of the first derivate and the main thermal degradation data.

When analyzing the morphology of the surfaces using AFM (Figure 4.4), the mean rugosity root square height (Rsq) of the grafted fibers showed an increment of 49% on respect of the pristine CNF. Such rugosity increase could be related to the additional bonding created between CNF fibrils and cyclodextrin molecules. This also correlates with a perceptible increased thickness on the fibers and the more granular appearance of the surface. No traces

of chloride were found in either the CNF or the CNF-CD as revealed by ICP-MS assuring that its use for applications such as water remediation would not be jeopardized by the crosslinking methodology, as not extra pollutants -such as chloride- could leach from this system.

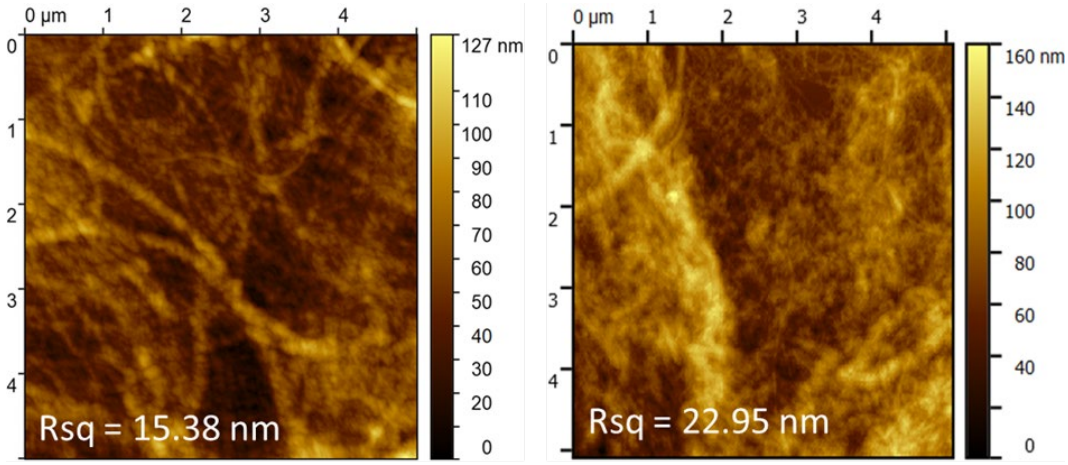

Figure 4.4 AFM images of spin coated surfaces from CNF (left) and CNF-CD (right).

4.4.2. Aerogel formation.

The first observable difference between the aerogels was visible after freeze-drying, there the pristine CNF lost more height than the modified fibers, indicating that the dragging forces where stronger as more hydrogen bonding and hydration was present in the unmodified systems (Ajdary et al., 2020).

Physical properties of the aerogels are listed in Table 2. Further differences between the two aerogels are presented there; for example, it can be observed that the modified aerogels presented 20% more weight than the aerogels formed from only CNF. This is important as the total dry mass used for the formation of both types of aerogels was 73.5 mg, showing that the CNF lost more fibril fines during the vacuum-filtration than the

crosslinked material, further confirming the difference in thickness observed in the AFM images (Figure 3). The density values obtained also correlate to these observations, as the CNF-CD aerogels were 84% denser, which consequently presented a porosity decrease of 5.8% compared with the pure CNF. Additionally, the BET of the freshly prepared aerogels revealed a surface area 30% lower for CNF-CD, which can likewise be linked to the lower porosity and increase of thickness of the fibrils after the reaction. Additionally, the images obtained by SEM also present these visible differences between the two materials, where a more packed surface is also observed, even when the height of the aerogels formed from the CNF-CD were higher.

All the differences found between the two materials could then be tracked down to the modification of the fibrils. Which in turns indicates that, if lighter or less dense materials are desire, a finer control during the reaction would be needed to avoid undesired crosslinking between the fibrils.

Table 4.2. Physical properties of the CNF and CNF-CD aerogels

Property	CNF aerogel	CNF-CD aerogel
Mass [mg]	54 .0± 2.0	65.0 ± 9.6
Density [kg/m3]	95.0 ± 21	175 ± 49
Porosity [%]	93.4 ± 1.4	88.0 ± 3.3
BET surface area [m2/g]	10.4	7.24
Total surface energy [mJ/m2] (min, max)	(59.4, 74.9)	(50.6, 60.6)

Dry aerogel		
SEM images 1000x	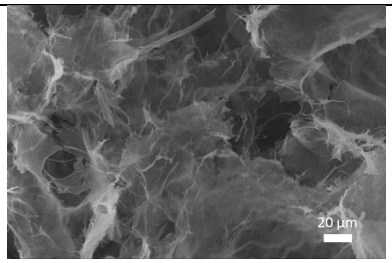	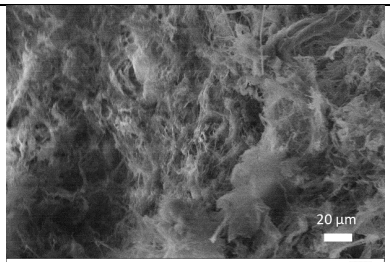

Figure 4.5A shows the total surface energy profile of the aerogels obtained from DVS tests. The modified CNF-CD shows a significant lower surface energy, as expected by the presence of the β-cyclodextrin hydrophobic cavities and the aliphatic extensions contributed by the epichlorohydrin. When comparing wettability of the pristine CNF and CNF-CD (Figure 4.5B), a higher wettability profile is observed for the later. Wettability is defined as the ratio between the acid-base surface component and the total surface energy of the material. A higher wettability for CNF-CD was expected, which correlates with the higher charge density of the modified fibrils when compared to pristine CNF. Moreover, the swelling capacity and water uptake was also higher for the CNF-CD with a 60% water uptake and 1200% swelling capacity compared to 50% and 800% for the aerogels obtained with CNF alone (Figure 4.5C and 4.5D).

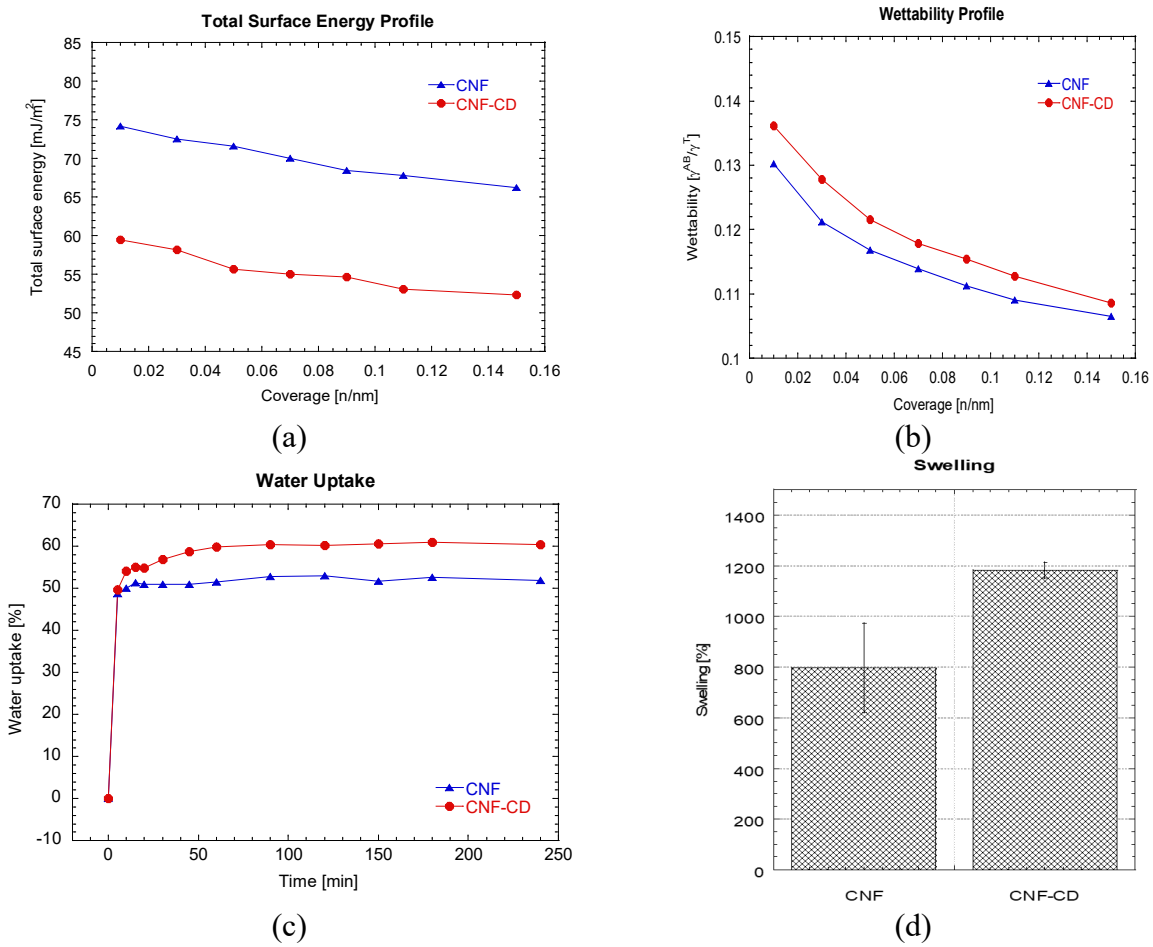

Figure 4.5. Comparison between on surface energy (a), wettability (b), water uptake (c), and swelling (d) of the aerogels obtained from the CNF and the modified CNF-CD.

4.4.3. Molecular interactions

As previously discussed, interactions between pristine CNF and CNF-CD fibrils and water were significantly different. Thus, similar effects are expected upon interaction with pollutants. When comparing the microcystin-LR (MC) kinetics of adsorption on CNF at different concentrations (Figure 4.6), in both cases CNF showed negative results. This is most likely due to the adsorption of water from the solution, rather than MC adsorption. As a result, a higher concentration of microcystin in the remaining solution is expected. On the other hand, the microcystin adsorption on CNF-CD showed a maximum at 180 min with 0.043 mg MC/g of filter for the solution with 0.8 µg/mL and 0.097 mg MC/g of filter in the 1.5 µg/mL solution. This

translates to a removal capacity of 20.5% and 18.4% of the total toxin in the solution, respectively. However, adsorption decreased at longer monitored times, suggesting a reversible process driven by the interactions of water with the other residues from the amino acids present in the structure, as well as water interactions with the hydroxyl groups on the edge of the cyclodextrin structure (Archimandritis et al., 2016). When the adsorption was analyzed using a pseudo-second order fitting (Table 3), the equilibrium adsorption capacity (qe) was calculated to 0.078 mg/g and 0.034 mg/g for each concentration, respectively. These results from the fitting are like the values observed during the first minutes after the beginning of the interaction. This could imply that the interaction between the hydrophobic cavities and the targeted molecule occur rapidly, suggesting then that the rest of the adsorption observed could be mostly driven by some weak interactions (probably van der Waals) that are later lost as the water interacts with the surface of the sorbent and the more polar residues of the toxin. These weak interactions mentioned to occur during the first minutes can also be seen for the CNF aerogel, where some adsorption is presented but is quickly lost to instead adsorb water in these used active points on the surface.

Regarding the fitting into a pseudo-first order, as the adsorption capacity was never in total equilibrium, which in turn made some of the values obtained after the difference to have negative values. These negative values do not have a real logarithm value, making the fitting unviable. However, using the chemical theoretical universal rate law for kinetic reactions logic, from which this pseudo models are based (Liu, 2008), the second order should consider the first level as a factor in the progressive addition (J. Lin & Wang, 2009; Wu et al., 2009).

The maximum adsorption capacity observed is lower than the equilibrium adsorption found in the previous work on model films with a similar CNF-CD material followed by QCM-D with a constant MC concentration in a flow cell (Chapter 3). This different behavior could be explained

with the difference in technique, residency times and the concentration pressure that the flow presents versus static adsorption used for this work.

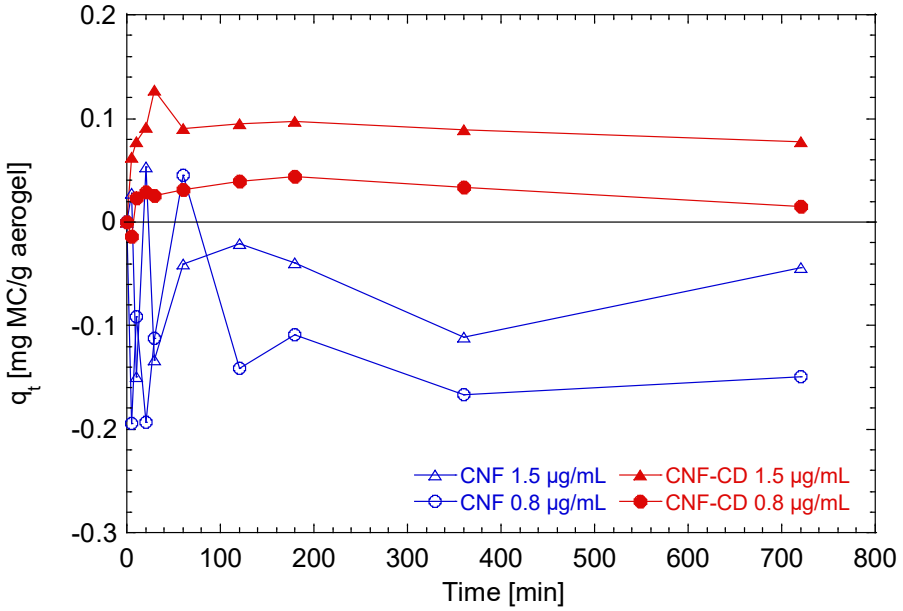

Figure 4.6. (a) Adsorption of microcystin-LR from solutions with concentrations 0.8 and 1.5 µg/mL by aerogels prepared with CNF and CNF-CD.

In the case of adsorption of methylene blue (MB) (Figure 4.7A), the fitted maximum adsorption capability in equilibrium for CNF filters was 203% higher in the case of pristine CNF when compared to CNF-CD. As suggested by the different nature of the pollutants, the main difference in this behavior may relate to the different adsorption mechanisms involved. In the case of microcystin-LR, the target for the adsorption is the hydrophobic ADDA group, while in the case of MB, the interaction with the CNF aerogels is mainly with the partially charged nitrogen present at both ends of the dye molecule. Finally, when the desorption of MB was followed (Figure 4.7B), the CNF-CD released up to 42% of the adsorbed load after 24 h (1440 min), while the CNF released only 14% over that time. This further confirms that the interactions between the CNF and the MB were stronger than the CNF-CD and MB.

Overall, this difference in adsorption capacity -with a higher capturing of the MB into CNF- can be related to the higher surface energy of the material as discussed in section 3.2, caused by the higher number of charged points on the surface of the CNF aerogels. As electrostatic interactions are the main driving force in the adsorption of charged molecules like MB onto cellulose, this is favorable for CNF-only filters (Lombardo & Thielemans, 2019). Meanwhile, adsorption into CNF-CD surface needs a different driving force, which is mainly hydrophobic due to the cavities available with the immobilized cyclodextrin, just as observed with the preferent adsorption of the microcystin-LR and seen on the model surfaces (Gomez-Maldonado, Vega Erramuspe, Filpponen, et al., 2019).

Overall, these adsorption experiments prove the capacity of the CNF-CD to capture and remove pollutants with short residency times. However successful, the process by which the aerogels were formed came with a high loss of surface area compared with other aerogels that had BET surface area 10-fold higher (Long et al., 2018). A change in the fabrication approach could increase the surface area of the nanofibrils that is kept while structuring, which would consequently increase their capacity to capture pollutants, therefore enhancing the benefits of these bio-based adsorbents.

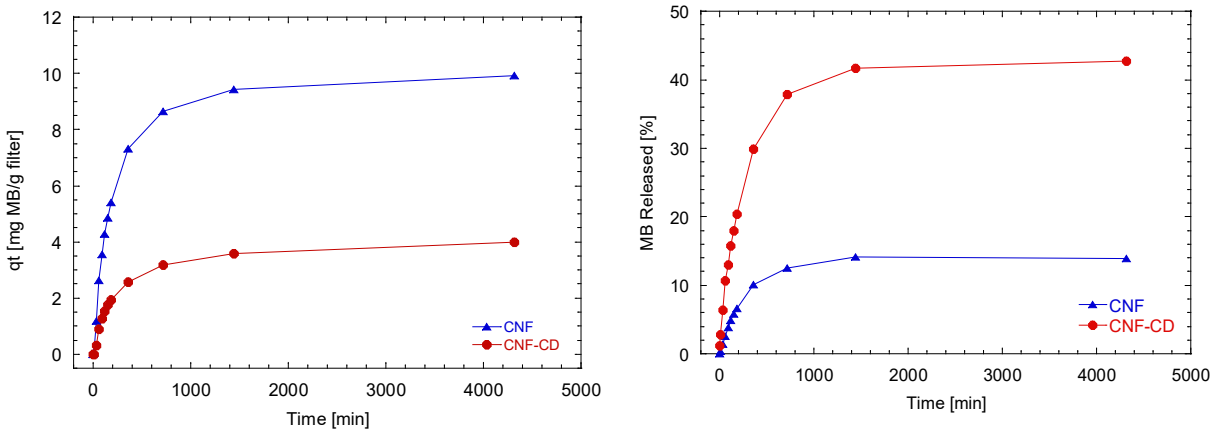

(A) (B)

Figure 4.7. (A) Adsorption and (B) desorption of methylene blue (MB) from a 15 mg/L solution by aerogels prepared with CNF and CNF-CD.

Table 4.3. Parameters for adsorption of microcystin-LR (MC) and methylene blue (MB) by aerogel filters

Adsorption system		Pseudo-first order			Pseudo-second order		
Sorbent	**Adsorbate**	**q_e (mg/g)**	**k_1 (min^{-1})**	**R^2**	**q_e (mg/g)**	**k_2 (g/mg min)**	**R^2**
CNF	MC 1.5	N.A.	N.A.	N.A.	-0.047	10.678	0.8603
	MC 0.8	N.A.	N.A.	N.A.	-0.143	0.2370	0.8781
	MB	9.086	0.0024	0.9439	10.51	0.0004	0.9760
CNF-CD	MC 1.5	N.A.	N.A.	N.A.	0.078	1.048	0.9947
	MC 0.8	N.A.	N.A.	N.A.	0.034	8.211	0.9789
	MB	3.463	0.0023	0.9474	3.935	0.1050	0.8920

4.5. Conclusion

In this work, wood derived cellulose nanofibrils were successfully decorated with β-cyclodextrin, which were then used to successfully form aerogels by solvent exchange and freeze-drying. These CNF-CD aerogels had lower surface area, porosity, and surface energy than those generated from pure cellulose nanofibrils; however, they presented higher water uptake, swelling and wettability.

When the aerogels were tested for adsorption of pollutants, the CNF-CD aerogels presented a higher adsorption of aromatic components such as microcystin-LR, which are driven by hydrophobic interactions, while pristine CNF aerogels had a higher adsorption of electrostatic driven molecules such as methylene blue. Even when limitations were presented in the surface area that was achieved by this solvent exchange/freeze-drying process, this work sets a precedent on the potential use of these bio-based and green materials to remove multiple types of pollutants from water sources.

4.6. Future Work

The main limitation found on this study was the loss of surface area, which was consequent of the drying process used. For upscaling this material, besides the improvement in surface area, another challenge is the quantification od the cyclodextrin added into the structure and whether the cyclodextrin is on the surface. Furthermore, even if the cyclodextrin is still present on a surface level, the percentage them that are oriented to allow the formation of complexes needs to be improved.

4.7. Literature Cited:

Ajdary, R., Tardy, B. L., Mattos, B. D., Bai, L., & Rojas, O. J. (2020). Plant Nanomaterials and Inspiration from Nature: Water Interactions and Hierarchically Structured Hydrogels. Advanced Materials, 2001085. https://doi.org/10.1002/adma.202001085

Ali, I. (2012). New generation adsorbents for water treatment. Chemical Reviews, 112(10), 5073–5091. https://doi.org/10.1021/cr300133d

American Public Health Association, & American Water Works Association and Water Environment Federation. (n.d.). 3125 METALS BY INDUCTIVELY COUPLED PLASMA—MASS SPECTROMETRY (2017). https://doi.org/10.2105/SMWW.2882.048

Archimandritis, A. S., Papadimitriou, T., Kormas, K. A., Laspidou, C. S., Yannakopoulou, K., & Lazarou, Y. G. (2016). Theoretical investigation of microcystin-LR, microcystin-RR and nodularin-R complexation with α-, β-, and γ-cyclodextrin as a starting point for the targeted design of efficient cyanotoxin traps. Sustainable Chemistry and Pharmacy, 3, 25–32. https://doi.org/10.1016/j.scp.2016.02.001

Briggs, D., & Beamson, G. (1993). XPS Studies of the Oxygen 1s and 2s Levels in a Wide Range of Functional Polymers. Analytical Chemistry, 65(11), 1517–1523. https://doi.org/10.1021/ac00059a006

Carpenter, A. W., de Lannoy, C.-F., & Wiesner, M. R. (2015). Cellulose Nanomaterials in Water Treatment Technologies. Environmental Science & Technology, 49(9), 5277–5287. https://doi.org/10.1021/es506351r

Carpenter, A. W., Lannoy, C. F. de, & Wiesner, M. R. (2015). Cellulose Nanomaterials in Water Treatment Technologies. Environ Sci Technol., 49(9), 209–220. https://doi.org/10.1021/es506351r.Cellulose

Celebioglu, A., Demirci, S., & Uyar, T. (2014). Cyclodextrin-grafted electrospun cellulose acetate nanofibers via "click" reaction for removal of phenanthrene. Applied Surface Science, 305, 581–588. https://doi.org/10.1016/j.apsusc.2014.03.138

Chen, P., Liang, H. W., Lv, X. H., Zhu, H. Z., Yao, H. Bin, & Yu, S. H. (2011). Carbonaceous nanofiber membrane functionalized by beta-cyclodextrins for molecular filtration. ACS Nano, 5(7), 5928–5935. https://doi.org/10.1021/nn201719g

Cova, T. F. G. G., Murtinho, D., Pais, A. A. C. C., & Valente, A. J. M. (2018). Combining cellulose and cyclodextrins: fascinating designs for materials and pharmaceutics. Frontiers in Chemistry, 6(July), 271. https://doi.org/10.3389/fchem.2018.00271

Devrimci, H. A., Yuksel, A. M., & Sanin, F. D. (2012). Algal alginate: A potential coagulant for drinking water treatment. Desalination, 299, 16–21. https://doi.org/10.1016/j.desal.2012.05.004

Dong, C., Qian, L. Y., Zhao, G. L., He, B. H., & Xiao, H. N. (2014). Preparation of antimicrobial cellulose fibers by grafting β-cyclodextrin and inclusion with antibiotics. Materials Letters, 124, 181–183. https://doi.org/10.1016/j.matlet.2014.03.091

Dong, C., Ye, Y., Qian, L., Zhao, G., He, B., & Xiao, H. (2014). Antibacterial modification of cellulose fibers by grafting β-cyclodextrin and inclusion with ciprofloxacin. Cellulose, 21(3), 1921–1932. https://doi.org/10.1007/s10570-014-0249-8

Espinosa, E., Tarrés, Q., Delgado-Aguilar, M., González, I., Mutjé, P., & Rodríguez, A. (2016). Suitability of wheat straw semichemical pulp for the fabrication of lignocellulosic nanofibres and their application to papermaking slurries. Cellulose, 23(1), 837–852. https://doi.org/10.1007/s10570-015-0807-8

Fan, L., Luo, C., Sun, M., Qiu, H., & Li, X. (2013). Synthesis of magnetic β-cyclodextrin-chitosan/graphene oxide as nanoadsorbent and its application in dye adsorption and removal. Colloids and Surfaces B: Biointerfaces, 103, 601–607. https://doi.org/10.1016/j.colsurfb.2012.11.023

Gomez-Maldonado, D., Vega Erramuspe, I. B., Filpponen, I., Johansson, L.-S., Lombardo, S., Zhu, J., Thielemans, W., & Peresin, M. S. (2019). Cellulose-Cyclodextrin Co-Polymer for the Removal of Cyanotoxins on Water Sources. Polymers, 11(12), 2075. https://doi.org/10.3390/polym11122075

Gomez-Maldonado, D., Vega Erramuspe, I. B., & Peresin, M. S. (2019). Natural Polymers as Alternative Adsorbents and Treatment Agents for Water Remediation. BioResources, 14(4), 10093–10160. https://doi.org/10.15376/biores.14.4.10093-10160

Gurgel, L. V. A., Júnior, O. K., Gil, R. P. de F., & Gil, L. F. (2008). Adsorption of Cu(II), Cd(II), and Pb(II) from aqueous single metal solutions by cellulose and mercerized cellulose chemically modified with succinic anhydride. Bioresource Technology, 99(8), 3077–3083. https://doi.org/10.1016/j.biortech.2007.05.072

Iglesias, M. C., Gomez-Maldonado, D., Via, B. K., Jiang, Z., & Peresin, M. S. (2020). Pulping processes and their effects on cellulose fibers and nanofibrillated cellulose properties: A review. Forest Products Journal, 70(1), 10–21. https://doi.org/10.13073/FPJ-D-19-00038

Jin, L., Sun, Q., Xu, Q., & Xu, Y. (2015). Adsorptive removal of anionic dyes from aqueous solutions using microgel based on nanocellulose and polyvinylamine. Bioresource Technology, 197, 348–355. https://doi.org/10.1016/j.biortech.2015.08.093

Johansson, L., Campbell, J. M., & Rojas, O. J. (2020). Cellulose as the in situ reference for organic XPS . Why ? Because it works. Surface and Interface Analysis, February, 1–5. https://doi.org/10.1002/sia.6759

Kardam, A., Raj, K. R., Srivastava, S., & Srivastava, M. M. (2014). Nanocellulose fibers for biosorption of cadmium, nickel, and lead ions from aqueous solution. Clean Technologies and Environmental Policy, 16(2), 385–393. https://doi.org/10.1007/s10098-013-0634-2

Kim, S., Yun, Y. S., & Choi, Y. E. (2018). Development of waste biomass based sorbent for removal of cyanotoxin microcystin-LR from aqueous phases. Bioresource Technology, 247(June 2017), 690–696. https://doi.org/10.1016/j.biortech.2017.09.164

Koshani, R., & Madadlou, A. (2018). A viewpoint on the gastrointestinal fate of cellulose nanocrystals. Trends in Food Science and Technology, 71(October 2017), 268–273. https://doi.org/10.1016/j.tifs.2017.10.023

Kumar Dutta, P., Dutta, J., & Tripathi, V. S. (2004). Chitin and chitosan: Chemistry, properties and applications. Journal of Scientific & Industrial Research, 63(January), 20–31. https://doi.org/10.1002/chin.200727270

Lee, J., & Walker, H. W. (2011). Adsorption of microcystin-Lr onto iron oxide nanoparticles. Colloids and Surfaces A: Physicochemical and Engineering Aspects, 373(1–3), 94–100. https://doi.org/10.1016/j.colsurfa.2010.10.032

Lee, K. Y., Quero, F., Blaker, J. J., Hill, C. A. S., Eichhorn, S. J., & Bismarck, A. (2011). Surface only modification of bacterial cellulose nanofibres with organic acids. Cellulose, 18(3), 595–605. https://doi.org/10.1007/s10570-011-9525-z

Lin, J., & Wang, L. (2009). Comparison between linear and non-linear forms of pseudo-first order and pseudo-second-order adsorption kinetic models for the removal of methylene blue by activated carbon. Frontiers of Environmental Science and Engineering in China, 3(3), 320–324. https://doi.org/10.1007/s11783-009-0030-7

Lin, N., & Dufresne, A. (2013). Supramolecular hydrogels from in situ host-guest inclusion between chemically modified cellulose nanocrystals and cyclodextrin. Biomacromolecules, 14(3), 871–880. https://doi.org/10.1021/bm301955k

Liu, Y. (2008). New insights into pseudo-second-order kinetic equation for adsorption. Colloids and Surfaces A: Physicochemical and Engineering Aspects, 320(1–3), 275–278. https://doi.org/10.1016/j.colsurfa.2008.01.032

Lombardo, S., & Thielemans, W. (2019). Thermodynamics of adsorption on nanocellulose surfaces. Cellulose, 26(1), 249–279. https://doi.org/10.1007/s10570-018-02239-2

Long, L. Y., Weng, Y. X., & Wang, Y. Z. (2018). Cellulose aerogels: Synthesis, applications, and prospects. Polymers, 8(6), 1–28. https://doi.org/10.3390/polym10060623

Medronho, B., Andrade, R., Vivod, V., Ostlund, A., Miguel, M. G., Lindman, B., Voncina, B., & Valente, A. J. M. (2013). Cyclodextrin-grafted cellulose: Physico-chemical characterization. Carbohydrate Polymers, 93(1), 324–330. https://doi.org/10.1016/j.carbpol.2012.08.109

Meriluoto, J., & Codd, G. A. (2005). Cyanobacterial Monitoring and Cyanotoxin Analysis. https://doi.org/10.1002/9781119068761

Missoum, K., Belgacem, M. N., & Bras, J. (2013). Nanofibrillated cellulose surface modification: A review. Materials, 6(5), 1745–1766. https://doi.org/10.3390/ma6051745

Morin-Crini, N., Winterton, P., Fourmentin, S., Wilson, L. D., Fenyvesi, É., & Crini, G. (2018). Water-insoluble β-cyclodextrin–epichlorohydrin polymers for removal of pollutants from aqueous solutions by sorption processes using batch studies: A review of inclusion mechanisms. Progress in Polymer Science, 78, 1–23. https://doi.org/10.1016/j.progpolymsci.2017.07.004

Mozdyniewicz, D. J., Nieminen, K., & Sixta, H. (2013). Alkaline steeping of dissolving pulp. Part I: Cellulose degradation kinetics. Cellulose, 20(3), 1437–1451. https://doi.org/10.1007/s10570-013-9926-2

Oksman, K., Mathew, A. P., Pia Qvintus, A. B., Rojas, O., & Sain, M. (2014). Handbook of Green Materials, Bionanomaterials: separation processes, characterization and properties Vol.5. https://doi.org/10.1142/8975

Orelma, H., Filpponen, I., Johansson, L.-S., Laine, J., & Rojas, O. J. (2011). Modification of Cellulose Films by Adsorption of CMC and Chitosan for Controlled Attachment of Biomolecules. Biomacromolecules, 12(12), 4311–4318. https://doi.org/10.1021/bm201236a

Papageorgiou, S. K., Katsaros, F. K., Favvas, E. P., Romanos, G. E., Athanasekou, C. P., Beltsios, K. G., Tzialla, O. I., & Falaras, P. (2012). Alginate fibers as photocatalyst immobilizing agents applied in hybrid photocatalytic/ultrafiltration water treatment processes. Water Research, 46(6), 1858–1872. https://doi.org/10.1016/j.watres.2012.01.005

Piñeiro, Á., Banquy, X., Pérez-Casas, S., Tovar, E., García, A., Villa, A., Amigo, A., Mark, A. E., & Costas, M. (2007). On the characterization of host-guest complexes: Surface tension,

calorimetry, and molecular dynamics, of cyclodextrins with a non-ionic surfactant. Journal of Physical Chemistry B, 111(17), 4383–4392. https://doi.org/10.1021/jp0688815

Raghuwanshi, V. S., Su, J., Garvey, C. J., Holt, S. A., Holden, P. J., Batchelor, W. J., & Garnier, G. (2017). Visualization and Quantification of IgG Antibody Adsorbed at the Cellulose-Liquid Interface. Biomacromolecules, 18(8), 2439–2445. https://doi.org/10.1021/acs.biomac.7b00593

Ristić, T., Mohan, T., Kargl, R., Hribernik, S., Doli??ka, A., Stana-Kleinschek, K., & Fras, L. (2014). A study on the interaction of cationized chitosan with cellulose surfaces. Cellulose, 21(4), 2315–2325. https://doi.org/10.1007/s10570-014-0267-6

Sehaqui, H., Zhou, Q., & Berglund, L. A. (2011). High-porosity aerogels of high specific surface area prepared from nanofibrillated cellulose (NFC). Composites Science and Technology, 71(13), 1593–1599. https://doi.org/10.1016/j.compscitech.2011.07.003

Sinha, A., & Jana, N. R. (2015). Separation of microcystin-LR by cyclodextrin-functionalized magnetic composite of colloidal graphene and porous silica. ACS Applied Materials and Interfaces, 7(18), 9911–9919. https://doi.org/10.1021/acsami.5b02038

Sixta, H. (2006). Handbook of pulp (Vol. 1). Wiley Online Library.

Toivonen, M. S., Kaskela, A., Rojas, O. J., Kauppinen, E. I., & Ikkala, O. (2015). Ambient-Dried Cellulose Nanofibril Aerogel Membranes with High Tensile Strength and Their Use for Aerosol Collection and Templates for Transparent, Flexible Devices. Advanced Functional Materials, 25(42), 6618–6626. https://doi.org/10.1002/adfm.201502566

Tran, C. D., Duri, S., Delneri, A., & Franko, M. (2013). Chitosan-cellulose composite materials: Preparation, Characterization, and application for removal of microcystin. Journal of Hazardous Materials, 253, 355–366.

Udoetok, I. A., Dimmick, R. M., Wilson, L. D., & Headley, J. V. (2016). Adsorption properties of cross-linked cellulose-epichlorohydrin polymers in aqueous solution. Carbohydrate Polymers, 136(September), 329–340. https://doi.org/10.1016/j.carbpol.2015.09.032

United Nations. (n.d.). Human Rights to Water and Sanitation | UN-Water. UN Water. Retrieved August 1, 2018, from http://www.unwater.org/water-facts/human-rights/

United Nations Department of Economic and Social Affairs. (2014). International Decade for Action "Water for Life" 2005-2015. Focus Areas: The human right to water and sanitation. https://www.un.org/waterforlifedecade/human_right_to_water.shtml

Vakili, M., Deng, S., Cagnetta, G., Wang, W., Meng, P., Liu, D., & Yu, G. (2019). Regeneration of chitosan-based adsorbents used in heavy metal adsorption: A review. Separation and Purification Technology, 224(February), 373–387. https://doi.org/10.1016/j.seppur.2019.05.040

World Health Organization. (2017). WHO | Water safety and quality. WHO; World Health Organization. http://www.who.int/water_sanitation_health/water-quality/en/

Wu, F. C., Tseng, R. L., Huang, S. C., & Juang, R. S. (2009). Characteristics of pseudo-second-order kinetic model for liquid-phase adsorption: A mini-review. Chemical Engineering Journal, 151(1–3), 1–9. https://doi.org/10.1016/j.cej.2009.02.024

Zeng, D., Wu, J., & Kennedy, J. F. (2008). Application of a chitosan flocculant to water treatment. Carbohydrate Polymers, 71(1), 135–139. https://doi.org/10.1016/j.carbpol.2007.07.039

Zhang, L., Zhou, J., & Zhang, L. (2013). Structure and properties of β-cyclodextrin/cellulose hydrogels prepared in NaOH/urea aqueous solution. Carbohydrate Polymers, 94(1), 386–393. https://doi.org/10.1016/j.carbpol.2012.12.077

5. Oriented β-cyclodextrin/chitosan polymer as an active coating on 2D and 3D nanocellulose surfaces and its efficiency in microcystin-LR capture

5.1. Abstract

In the search for more environmentally friendly adsorbent materials, the use of polysaccharides as coatings to add functionality to common materials is a new avenue to explore. Their inherent tendency to adsorb into each other is valuable as it adds a variety of functional groups on the outmost surface layer. Our project focusses on the pre-modification of the bio-polymer chitosan (Ch) with a 2,2,6,6-Tetramethylpiperidine-1-oxyl (TEMPO) oxidized β-cyclodextrin, which was then adsorbed on the CNF surface. Furthermore, the mechanism driving the adsorption of the modified chitosan onto the cellulose backbone was studied, thus different Ch:TOCD molar ratios (1:2, 1:1, and 3:1) were tested. This to evaluate if the adsorption was impacted by the change on the available electrostatic interaction between amino groups in chitosan and the carboxyl groups of cellulose or if those were driven by the dispersive forces of the hydroxyl groups. Finally, to assess the viability of the added hydrophobic cavities of the cyclodextrins, adsorption of an amphipathic toxin categorized as a monitored pollutant (microcystin-LR) was tested and followed by QCM on a surface level and by HPLC when the coating was used in nanocellulose beads. Results showed that the adsorption was accomplished in similar levels independent of the degree of substitutions. Adsorption was best observed in the chitosan modified with cyclodextrins at 20.5 mg/g on the surface and 2.36 mg/g in the case of nanocellulose beads. The successful coating of two nanocellulose systems and the positive adsorption of the microcystin suggests broad-scale application of this bio-based, low energy input coating in high-end fields such as drug delivery, textile, and water restoration.

5.1.1. Index Words

Active coatings, chitosan, β-cyclodextrin, cellulose beads, model surfaces, water remediation, physical adsorption, microcystin-LR.

5.1.2. Project Partners

The Forest Products Development Center worked in collaboration with the Samuel Ginn College of Engineering, the School of Pharmacy, and the Department of Crops, Soils and Environmental Science from Auburn University and with the Department of Chemical Engineering of Aalto University, Finland. This research was supported by the Alabama Agricultural Experiment Station, and the Hatch program of the National Institute of Food and Agriculture, United States Department of Agriculture. The School of Forestry and Wildlife Sciences at Auburn University financial support to complete this work is greatly appreciated. This work also made use of Aalto University Bioeconomy Facilities (XPS).

5.2. Introduction

Active coatings are a novel approach to modify surfaces by adding a specific functionality to existing materials, without disrupting their bulk composition and modifying the interactions of the surface-medium interphase.(Shim, 2013) This added functionality can provide catalytic power to the material,(Guo et al., 2016; Solgi et al., 2020) stabilize it from oxidation,(P. K. Huang et al., 2004) moisture,(P. K. Huang et al., 2004; Isimjan et al., 2012; Parvinzadeh et al., 2012) heat,(Larsson et al., 2013) or UV exposure;(Isimjan et al., 2012; M. Zhang et al., 2020) or increase adhesion and bonding of other molecules(Karim et al., 2016; Kayaci et al., 2013; M. Zhang et al., 2020) or cells (Fang et al., 2018; Groll et al., 2005). It is an enhanced adsorption of the molecules

that is needed when looking into water treatment, as the capacity of the material to remove pollutants is linked to its surface interaction with the water and the different pollutants. (Ali, 2012; Gomez-Maldonado et al., 2019; W. J. Huang et al., 2007; Peresin et al., 2014; Spence et al., 2010) Therefore, a variety of surface interactions is preferred when developing new water adsorbents, ranging from electrostatic charges (Trygg et al., 2014; Zeng et al., 2008) to hydrophobic interactions (Adebajo et al., 2003; Arkles, 2006), which drive most pollutants capturing onto the sorbent surfaces.

The development of an active coating that could be used for water treatment should enhance the activity of natural and low-cost materials – like cellulose-based filters – without the need of complex processing to develop, or when acting as a scaffold to other polymers. For this, the intrinsic affinity of β-linked polysaccharides could be easily exploited as they possess the capacity to irreversibly adsorb similar glucans – such as cellulose – onto their surface via dispersive forces (Junka et al., 2014; Mishima et al., 1998), thus allowing larger structures, like cellulose fibers that have the ability to be built into yarns, aerogels, textiles, and more. (Dong et al., 2013; Dufresne, 2017; Dunlop & Fratzl, 2010; Pillai et al., 2014) Among the available polysaccharides, chitosan is favorable as it is obtained by the partial deacetylation of chitin. Chitin is found in exoskeletons of crustaceous and fungi, and it is known to be the second most abundant polymer in nature, only after cellulose.(Blackburn, 2004; Kumar Dutta et al., 2004; Tran et al., 2013) The structure of chitosan is a linear backbone of β-(1 → 4) 2-acetamido-2-deoxy-β-D-glucose and β-(1→4) 2-amino-2-deoxy-β-D-glucose with more than 65% of the deacetylated monomeric units. Because of the amino functional groups in chitosan (with pKa 6.5) (Sashiwa et al., 2004), the polymer has a positive charge in acidic pH and brings the possibility for making

polyelectrolyte complexes by self-assembly with negatively charged polyelectrolytes via electrostatic interactions (Mocchiutti et al., 2016).

Conversely, cyclodextrins are cyclic oligosaccharides formed by α-(1→4) D-glucopyranose, and, depending on the number of monomers they have, are called α-cyclodextrin (6 monomers), β-cyclodextrin (7 monomers), or γ-cyclodextrin (8 monomers). One distinguishing property of cyclodextrins is the formation of a ring that provides a cone shape structure. This structure orients the hydroxyl groups at C2 and C3 in the wider extreme to allow hydrogen bonding, and hydroxyl groups at C6 are placed at the lower part of the cone in the exterior, forming a highly hydrophobic cavity that can be used to form complexes with the different molecules and pollutants (Saenger & Steiner, 1998), making cyclodextrins a highly intriguing natural approach for the capture of pollutants from water sources. However, the low molecular weight of these oligosaccharides requires the attachment of them onto the surface of larger carriers to facilitate the recovery of the microcystin-cyclodextrin complex (e.g., using filtration or other mechanisms such as magnetic attraction). Examples of previously studied carriers are magnetic graphene,(Sinha & Jana, 2015) porous silica,(Sinha & Jana, 2015) and a decarboxylated PEI-coated polysulfone-biomass composite fiber.(Kim et al., 2018) Furthermore, additional capturing systems have been developed and tested with other target molecules such as: regenerated cellulose nanofibers for toluene,(Yuan et al., 2017) chitosan via glutaraldehyde for methyl orange,(Jiang et al., 2018) iron oxide for heavy metals,(Badruddoza et al., 2013) multi-walled carbon nanotubes for besphenyls,(Shao et al., 2010) carbonaceous nanofibers for phenolphthalein,(Chen et al., 2011)or simply crosslinked β-cyclodextrin-based systems with larger particle size.(Khaoulani et al., 2015; Kono et al., 2013; Liu et al., 2011) Unfortunately, many of these methodologies involve a chemical reaction with undistinguished hydroxyl groups of cyclodextrin, thus making the reaction not

selective and with a high risk of blocking the active cavities. To try to overcome this problem, selective modification can be done in C6 by green processes such as TEMPO oxidation (Khan et al., 1998), which recently has been improved to use neutral pH conditions instead of the traditional alkaline media which might imply chemical degradation (Orelma et al., 2018; Tsuguyuki Saito & Isogai, 2004).

The main advantage of the neutral TEMPO-NaClO/NaClO2 oxidation in aqueous media is that it allows the selective oxidation of the primary alcohol functional groups of β-cyclodextrin to carboxylic functional groups under mild conditions, which allows the preparation of TEMPO-mediated β-cyclodextrin (TOCD) with low degradation rates. This further permits us to use simple chemistry as N-ethyl-N'-(3-(dimethylamino)propyl) carbodiimide (EDC) and N-hydroxy succinimide (NHS). The EDC/NHS activation approach can be used to bind the TOCD to other compounds that contain amino groups such as chitosan (D'Este et al., 2014; Orelma et al., 2012; Prabaharan & Gong, 2008).

As before mentioned, chitosan possesses amino functional groups that can be used as active sites for crosslinking with other molecules that have carboxyl groups via EDC/NHS reaction or similar chemistry. For example, Jiang et al. (Jiang et al., 2018) used maleic anhydride and EDC to link cyclodextrin to chitosan and to form a network with the chitosan molecules. Similarly, glutaraldehyde can be used to immobilize CD to chitosan as Li et al. (L. Li et al., 2013) did before anchoring it to graphene. Nevertheless, in both approaches the orientation of the CD or the use of only the amino groups is not favored, which the previous TEMPO-oxidation of CD could help to prevent.

This modification of chitosan with TEMPO-oxidized β-cyclodextrin was previously performed on a chitosan pre-coated cellulose yarn. However, the present work aims to modify in

homogenous solution chitosan with TEMPO-oxidized β-cyclodextrin in different molar ratios (Ch:TOCD 1:2, 1:1, and 3:1) and measure the adsorption onto the surface of cellulose when amino groups of the chitosan where previously used in the immobilization. This would allow us to compare the influence of the electrostatic interactions and van der Waals forces in the self-assembly. Furthermore, the system will be used to capture microcystin-LR for synthetic water as a model of active coating material that can be used for water treatment.

Microcystin-LR is a toxin in water that can negatively impact human health due to its ability to promote the growth of tumors, mainly in the liver (T. Li et al., 2011; Loftin et al., 2016). The concentration of this toxin is increasing and surpassing the upper limit established by the World Health Organization (WHO) of 1 μg/L (Word Health Organization (WHO), 1998) in water reservoirs as a consequence of the increase in the occurrence and duration of cyanobacteria blooms (Merel et al., 2013). As shown in Figure 5.1, the microcystins are a family of toxins composed by cyclic oligomers with 7 amino acids, including the unique amino acid (2S,3S,8S,9S)-3-Amino-9-methoxy-2,6,8-trimethyl-10-phenyldeca-4,6-dienoic acid (Adda) at position 5. The difference between the microcystin variants is given by the substitutions in positions 2 and 4, which are leucine and arginine for microcystin-LR (Al-Ammar et al., 2015; Meriluoto & Codd, 2005). The Adda amino acid shared by all microcystins is highly hydrophobic due to the phenyl terminal group and the long unsaturated tail, making it an ideal anchoring point on hydrophobic active sites. As shown by Archimandritis *et al* (2016), β-cyclodextrin (CD) is able to effectively capture microcystin-LR (MC), making it an interesting molecule to assess the viability of the cavities on the active coating, while targeting an emerging contaminant that is accumulating in water sources every day.

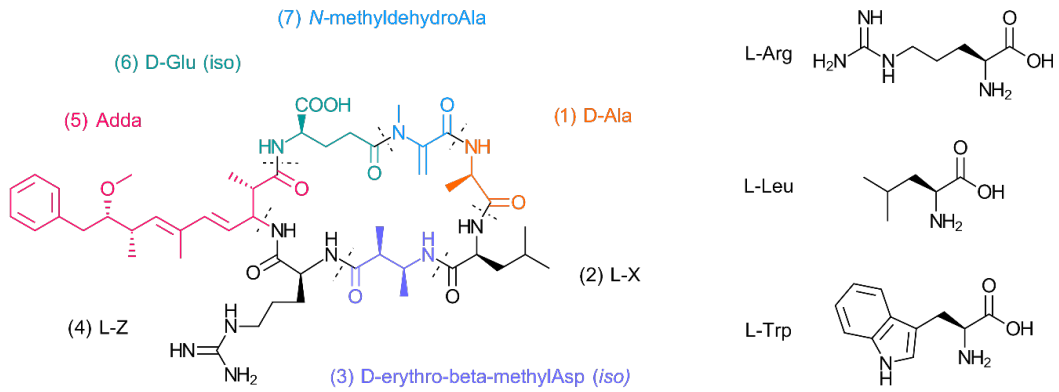

X-Z	
MC-RR	Arg-Arg
MC-YR	Tyr-Arg
MC-LR	Leu-Arg
MC-LY	Leu-Tyr
MC-LW	Leu-Trp
MC-LF	Leu-Phe

Figure 5.1. Basic structure of microcystins, where residues 2 and 4 show variability in residues, those variations are used to name the different molecules derivates, being microcystin-LR the most prominent related to liver cancer and other hepatoxic reactions.

Therefore, the aim of this work was to generate a cyclodextrin-chitosan polymer which were able to form complexes with microcystin-LR and were used as active coating on cellulose nanofibrillar-based films and hydrogels. To evaluate the impact on the adsorption capacity of the chitosan after the modification of the amino groups, different ratios were evaluated (1:2, 1:1, and 3:1). After chemical characterization, the adsorption of the modified chitosan was first evaluated on surface level by Quartz, Crystal Microbalance with Dissipation monitoring (QCM-D), as well as the capacity to remove the toxin. Finally, the best performing coating was used to coat cellulose nanofibril-based hydrogel beads and used to remove the toxin while the kinetic was followed by High Pressure Liquid Chromatography (HPLC).

5.3.Materials and Methods

5.3.1. Materials

Bleached cellulose nanofibrils (CNF, 2.76%, pH 6.3) were produced at the Forest Products Development Center at Auburn University from mixed-softwood bleached pulp kindly provided by a North American Mill ; β-cyclodextrin (CD, > 95 % purity) and N-hydroxysuccinimide (NHS, 98.0% purity) were obtained from Tokyo Chemical Industry (Portland, OR, U.S.); chitosan (DSacetylation of 0.15, MRU 167.3 g/mol) was purchased from Alfa Aesar (Haverhill, MA, U.S.), sodium chlorite (80% purity) was obtained from BeanTown Chemical (Hudson, NH, U.S.); sodium hypochlorite (12.5 % w/w, 2 M in water) was obtained from VWR chemicals (Radnor, PA, U.S.); 2,2,6,6-tetramethylpiperidinooxy (TEMPO, 98 % purity) was bought from Acros Organics (Geel, Belgium); 3-(3-Dimethylaminopropil)-1-ethyl-carbodiimide hydrochloride (EDC, 99.9% purity) was obtained from Chem-Impex International (Wood Dale, IL, U.S.); polyethylene glycol (PEG, Mw 10 000) and polyethylenimine, branched (PEI, Mw 25 000, Mn 10 000) were obtained from Aldrich (San Luis, MO, U.S.); microcystin-LR (MC, > 95 %) was purchased from Cayman Chemicals (Ann Arbor, MI, U.S.); sodium hydroxide (50 % w/w) was purchased from J.T. Baker (Phillipsburg, NJ, U.S.). The water used was deionized and purified with a Thermo Scientific Barnstead Nanopure (18.2 MΩ cm). Unless specified, all the weights in this paper are expressed in oven dry basis.

5.3.2. Synthesis of TEMPO oxidized β-cyclodextrin (TOCD).

β-cyclodextrin was carboxylated by neutral TEMPO-NaClO-NaClO2 oxidation in aqueous media (Orelma et al., 2018; Tsuguyuki Saito et al., 2009). For this, 5 g of β-cyclodextrin was dissolved in 450 mL of sodium phosphate buffer (0.05 M, pH 6.8). Then 0.08 g of TEMPO (0.1

mmol/g) and 5.65 g of sodium chlorite (80 %, 10 mmol) was added to the cyclodextrin solution. Simultaneously, the 2 M sodium hypochlorite was diluted to a 0.1 M in the buffer and 23 mL of this dilution was added in one step to the reactive solution to obtain a final concentration of 5 mmol (1.0 mmol NaClO/g of CD). The reaction was conducted in a closed flask for 19.5 h under ambient condition and a constant stirring of 500 rpm.

After modification, TEMPO-oxidize β-cyclodextrin (TOCD) was purified by dialysis against ultrapure water (18.2 Ω) in a 100-500 Da dialysis membrane tube, then concentrated with reverse dialysis in PEG, before freeze-drying.

5.3.3. Synthesis of chitosan-cyclodextrin polymers (Ch-TOCD).

The synthesis of Ch-TOCD was performed for all tested molar ratios of the functional groups NH:COOH (Ch:TOCD 1:2, 1:1 and 3:1) in a total of 50 mL volume using the same sequence of steps. First, the TOCD was dissolved in 1% acetic acid (125, 50, and 50 mg, respectively) to obtain a final concentration of 0.05%, then EDC was added to a final concentration of 0.05 M EDC and let stir before adding NHS to obtain a final concentration of 0.2 M NHS. From a stock solution of chitosan (1% in 1% acetic acid, w/w), the corresponding milliliters were added to obtain 25, 25, and 50 mg, respectively. The reaction was stopped after 24 h by adding ethanol-amide (61 µL) to obtain a final concentration of 0.1 M. Purification and concentration was done by five washings in 30 KDa Pall-membrane centrifugation tubes (Macrosep Advance Centrifugal Device, Pall Corporation) at 3000 rpm for 1 h.

5.3.4. Nanocellulose bead generation.

A 1.4% consistency cellulose nanofibril alkaline solution was generated targeting a final concentration of 7% w/w NaOH and 12% w/w urea mixed at -10°C with a recirculating bath. Once

dissolved, the cold solution was added dropwise to 50 mL of 2 M nitric acid solution in a graduated cylinder. After 10 min in the coagulation bath, the obtained beads were transferred into a reservoir with ultrapure water and thoroughly washed under a continuous flow of ultrapure water overnight.

Coating was done by immersing the neutralized beads into a 50 mM NaOAc buffer pH 5 containing 0.05 wt.% or the chitosan or the Ch-TOCD coatings for 24 h, followed by washing with ultrapure water until neutral pH was obtained.

5.3.5. Characterization techniques

5.3.5.1.TEMPO oxidized β-cyclodextrin (TOCD) titration.

Degree of oxidation (DO) was determined by pH and conductivity titration methods, based on the calculations reported by da Silva Perez.(da Silva Perez et al., 2003) For this, TOCD suspension was first brought to pH 3 with 10 mM HCl to assure the protonation of all present acid moieties. After freeze drying, 30-40 mg of TOCD in acidic form were dissolved in 15 mL of 10 mM HCl and titrated with 10 mM NaOH by adding 1 mL every 5 min and measuring pH and conductivity with a VWR symphony B30PCI multiprobe conductometer. The degree of oxidation was then calculated by the following equation:

$$DO = 162(V2 - V1)c/[w - 36(V2 - V1)c] \quad (5.1)$$

Where V1 and V2 are the amount in L of NaOH used to reach the end points 1 and 2, respectively; c is the concentration of the base in mol/L, and w is the dry weight of the sample. V1 and V2 were determined by the second derivative of pH curve (or conductivity curve), using the volumes where the graph crossed the origin.

5.3.5.2.Fourier-transform infrared spectroscopy with attenuated total reflectance (FTIR).

The degree of oxidation (DO) was also estimated by FTIR spectroscopy measurements. Before the measurements, TOCD was treated with a 0.01 M HCl until a final pH of 3 was achieved to get the compound in the acid form. This eliminated the interference between the band involving the out-of-phase COO- stretching vibration in the carboxylic salt, and the band observed due to the presence of adsorbed water (~1640 cm^{-1}) (Larkin, 2011). DO was then measured by calculating the ratio of the intensity of the carbonyl band (1730 cm^{-1}) to the stronger cellulose backbone band (1050 cm-1). Both TOCD and Ch-TOCD samples were analyzed for characterization of KBr pellets on a PerkinElmer Spotlight 400 FT-IR Imaging System (Massachusetts, US) with a transmission accessory and a resolution of 4 cm^{-1}. First, a background spectrum was measured, which was carried out before each set of measurements with the same number of scans. To lower the noise in the spectrum bands, 128 scans per spectrum were measured by duplicates in different areas of the sensor. Data was processed with Spectrum 6 Spectroscopy Software (PerkinElmer, Massachusetts, US).

5.3.5.3.X-Ray Spectroscopy (XPS).

Surface characterization of neat and modified chitosan powders was carried out using the AXIS Ultra DLD Photoelectron spectrometer (Kratos Analytical, Manchester, UK), under neutralization. Samples were mounted on the sample holder with UHV compatible carbon tape, together with an in-situ reference of pure cellulose (L. Johansson et al., 2020) and pre-evacuated overnight. Surface elemental content was calculated from low-resolution wide scans, while C 1s, O 1s, and N 1s high-resolution regional spectra were utilized for more detailed chemical information. Data was collected from 2-4 locations for each sample. The data was analyzed using

CasaXPS software, with the C-O component of high-resolution C 1s signal at 286.7 eV as the binding energy reference. (Beamson & Briggs, 1992; L. S. Johansson & Campbell, 2004).

5.3.5.4.Elemental Analysis (EA).

Freeze-dried samples were processed in an ECS 4010 Elemental Combustion System CHNS-O from Costech Analytical technologies, Inc (Firenze, Italy) and data analyzed with the ECS60 software. Carbon and Nitrogen content were collected and fitted into standard curves with correlations of 0.99996 and 0.9999799 for N and C, respectively.

5.3.5.5.Quartz Crystal Microbalance with Dissipation Monitoring (QCM-D) measurements.

The generation of the CNF surfaces, adsorption of Ch-CD, and capture of microcystin-LR (MC) were studied on gold-coated quartz sensors in a QSense Analyzer from Biolin Scientific (Västra Frölunda, Sweden). The basic principle of the QCM-D is the following: changes in frequency (Hz) of a piezoelectric sensor that has a base resonance of 5 MHz and its overtones 15, 25, 35, 45, 55 and 75 MHz are measured; the changes in the frequency resonance are proportional to the change in mass on the sensor. Because the surface is interacting with a flow of matter only, those changes are correlated to the mass adsorption on the sensors surface (Example, 1991; KSV Instruments Ltd, 2002; Voinova et al., 2002). Sauerbrey (1959) determined the relationship between changes in frequency and mass for rigid layers, uniformly distributed on the surface of the sensor and with lower values of mass than the mass of the crystal with the following equation:

$$\Delta m = C * \Delta F * n^{-1} \quad (5.2)$$

Where the constant for 5 MHz crystals (C) is equal to -17.7 ng/cm^2, ΔF is the change in frequency and n is the overtone number. Because most of the polymeric systems do not generate

a rigid layer, Sauerbrey's equation underestimates the adsorbed mass, some other models have been generated to address the changes of mass, like Voigt's and Maxwell's. These models take into the account the density, dynamic and static viscosity of the adsorbed materials as well as the crystal's (Voinova et al., 1998).

The dissipation factor ΔD is related to the viscoelastic properties of the layers formed on the crystal, as it translates the relationship of energy dissipation from the sensor to the fluid and the energy stored (5.3); it can be measured as it is inversely proportional to the decay time constant (τ) and the resonant frequency (f) as it is shown in equation 4 (Voinova et al., 1998).

$$D = \frac{E_{dissipated}}{2\pi E_{stored}} \tag{5.3}$$

$$D = \frac{1}{\pi f \tau} \tag{5.4}$$

If the generated film is viscous, energy would be dissipated due to the oscillation of the layer, then more energy is loss and longer decay times are present which translates to a decrement in the D factor; while when more energy is stored, as the surface is being rigidize, increments in the D-factor will be observable (Turon et al., 2008).

All measurements were made at 25 °C with a constant flow of 100 µL/min on gold coated crystals using PEI as anchoring solution with concentrations of 0.1 % (m/v), 0.1 % (m/v) CNF solution flown; for the chitosan-cyclodextrin polymers, a concentration of 0.5 mg/mL was used in a 50 mM NaOAc buffer at pH 5, and 50-mM ionic strength adjusted with NaCl; and 10 µg/mL for microcystin-LR in the same buffer. Only the changes of the third overtone are presented to make

the figures clearer. Mass was calculated using the Broadfit model (based on the Voight model) with dissipation dependency from frequency changes, this at the DFind Software from Biolin Scientific (Västra Frölunda, Sweden); densities were 1030, 1200, 1770, and 1299 g L-1, for PEI, CNF, chitosan and derivates, and Microcystin-LR, respectively.

Gold crystals were previously cleaned with NH4O, H2O, H2O2 hot solution (at ratio of 5:1:1, w:w) at 60 °C for 15 min, following by 15 min in ultrapure water, 1 min in piranha solution (at ratio of 3:1, w:w of H2SO4 and H2O2, respectively) with abundant rinsing and 30 min in Novascan PSD Series Digital UV Ozone System (Iowa, US).

5.3.5.6.High Pressure Liquid Chromatography (HPLC).

For the analysis of microcystin, ca. 200 mg of swollen uncoated and coated bead were placed in 10 mL of solutions containing 6.5 µg/mL at room temperature and constant stirring. 150 µL aliquots were taken at the corresponding time and analyzed in a Waters Alliance HPLC (Model No. e2695, Waters Corp., Milford, MA, USA) system equipped with a solvent management system 2695 and detected by a photodiode array detector (PDA, 2998). The system also counts with a thermostatically controlled column compartment and an autosampler. The method used was adapted from the one described by Meriluoto & Codd (2005). Briefly, a C-18 column (55x4 mm) was used as stationary phase, and 0.05% trifluoroacetic acid (TFA) aqueous solution/0.05% TFA acetonitrile with linear gradient at a flow rate of 1 mL/min, and 10 µL injections using the autosampler in cycles of 9 min. The retention time was 4.2 min and correlation of the samples to the standard curve was of 0.9997. All experiments were done by duplicates and averaged. The analysis of the data was performed using Empower® 3 software (Waters Corp., Milford, MA, USA).

5.3.5.7.Kinetics.

The fitting of the data to calculate rate constants (k_2) and adsorbed amounts in equilibrium (q_e) was done for a pseudo-first order and pseudo-second order models when possible, following the equations given in (Tran et al., 2013). Briefly, for pseudo-second order:

$$\frac{t}{qt} = \frac{1}{h} + \frac{t}{qe} \quad (5.5)$$

where $h = k_2 q_e^2$, and k_2 being the pseudo-second order rate constant of sorption, respectively. q_e is the amount of analyte adsorbed at equilibrium (mg/g), and qt is the amount of analyte adsorbed at any time (mg/g).

5.4. Results and Discussion

5.4.1. TEMPO oxidation of β-cyclodextrin.

To investigate the degree of oxidation of the β-cyclodextrin, the inflexions points found in the pH titration graph presented in Figure 5.2 were used to identify the point in which the functional groups reached a pKa point. Such inflexion points were observed between the volumes 14 and 16 mL for the first point, and 20 and 24 mL in the different repetitions: giving an averaged DO of 0.29. Considering that only C6 in the glucose monomer should be reactive in the TEMPO-mediated oxidation reaction, the maximum DO possible is equal to 1. (T. Saito et al., 2005) Therefore, 0.29 is approximate two sevenths of it, indicating the modification of at least one C6 in each β-CD. This more selective modification would ideally help in the further grafting onto the chitosan, as it would assure that C6 is the carbon interacting with the polymers, leave the cavity exposed to capture the pollutant and avoiding the closure of the cavity by random immobilization.

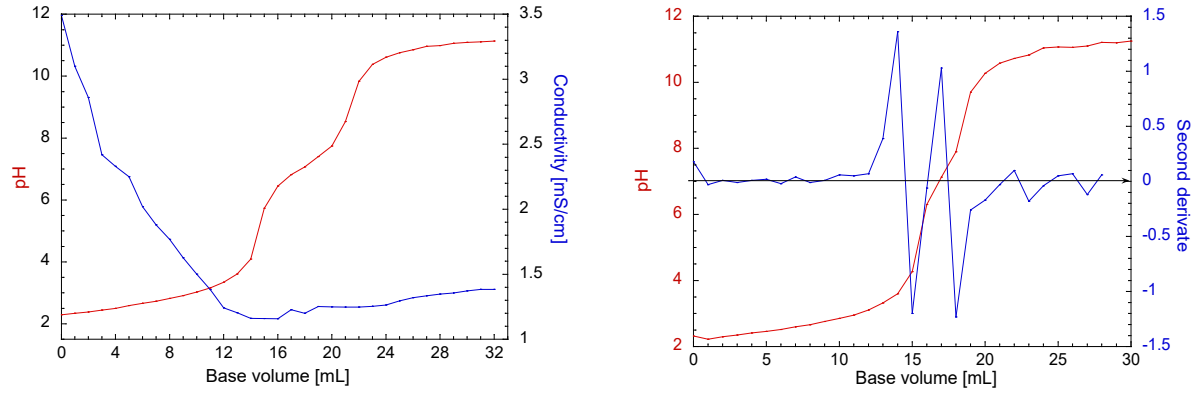

Figure 5.2. Conductivity and pH titration of TEMPO oxidized beta-cyclodextrin (left) and determination of inflexion points for volumes determination (right).

With the FTIR spectrum in Figure 5.3 there is a small shift in the C-O stretching band (1050 cm^{-1}) which might be caused by the cyclic structure. Nevertheless, the ratio of this band with the acid carboxyl band after normalization and baseline correction was of 0.18, meaning that between 1 and 2 out of the 7 monomers are modified. This result is aligned with the reported theory described by Khan *et al.* (1998) where it is explained that the maximum number of monomers that can be modified in β-cyclodextrin is 3, as possible steric problems begin to occur.

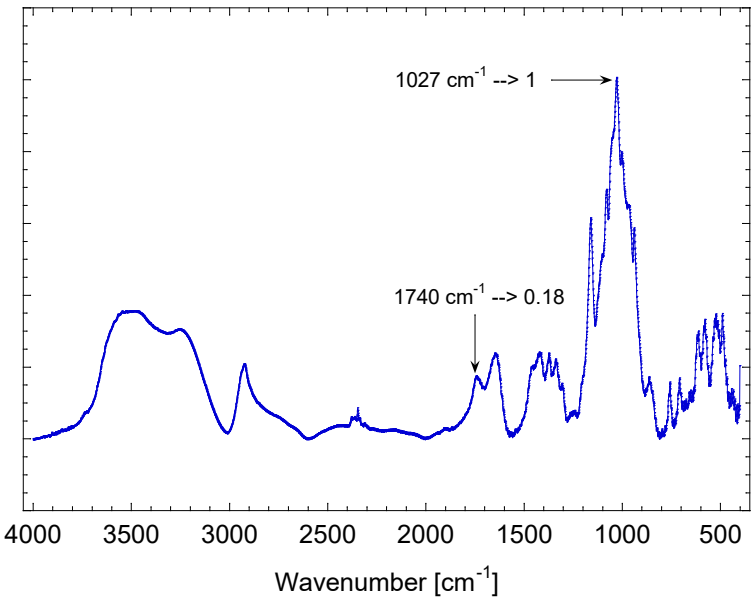

Figure 5.3. FT-IR spectrum (KBr method) of the acid TEMPO-mediated oxidization of beta-cyclodextrin.

As titration is more accurate than FTIR for the degree of oxidation, several repetitions were performed with similar results, confirming this modification also between different batches.

5.4.2. TOCD grafting to chitosan.

To assure the successful modification of chitosan, elemental analysis, FTIR and DSC measurements were performed. In Table 5.1 the percentages of C and N are presented as well as the C:N ratio, which was used to calculate the degree of substitution for both chitosan, and three-oxidized β-cyclodextrin. From these data, we can see that there is some discrepancies between the estimations for the chitosan monomers, as the calculated DS is 0.03 in the case of pure chitosan.

For the derivatives, 0.85 is the maximum expected DS, considering the maximum degree of deacetylation for raw chitosan. The 1:2 molar ratio (NH: COOH) is the one that has the higher DS with 0.57, while the 1:1 and 3:1 have similar results with 0.28 and 0.30, respectively. It is worth noticing that the standard deviation of the 1:1 is higher than the 3:1 which can be related to the apparent higher DS of the Ch-TOCD 3:1, being this difference equivalent to the error.

Table 5.1. Elemental Analysis of Chitosan derivates and Degree of substitution estimation.

	%C	%N	C/N	DS
Chitosan	40.38	7.35	6.41 ± 0.01	0.03
Ch-TOCD 1:2 (NH: COOH)	40.05	5.22	8.95 ± 0.4	0.57
Ch-TOCD 1:1 (NH: COOH)	40.03	6.27	7.44 ± 0.3	0.28
Ch-TOCD 3:1 (NH: COOH)	39.91	5.95	7.81 ± 0.1	0.30

To verify the presence of the modification of amine groups of the chitosan, surfaces were analyzed in XPS, and the results of the wide energy region spectra are shown in Figure 5.4. Herein, the main changes can be observed at the high-resolution C1s graph, where an increase in the C-N signal can be observed. This can be attributed to the linkage between TOCD and the chitosan. There again the Ch-TOCD 1:2 has the larger intensity, but more similar in the case of Ch-TOCD 1:1. The N1 peaks, also shows less free nitrogen in Ch-TOCD 1:2, confirming a higher degree of substitution.

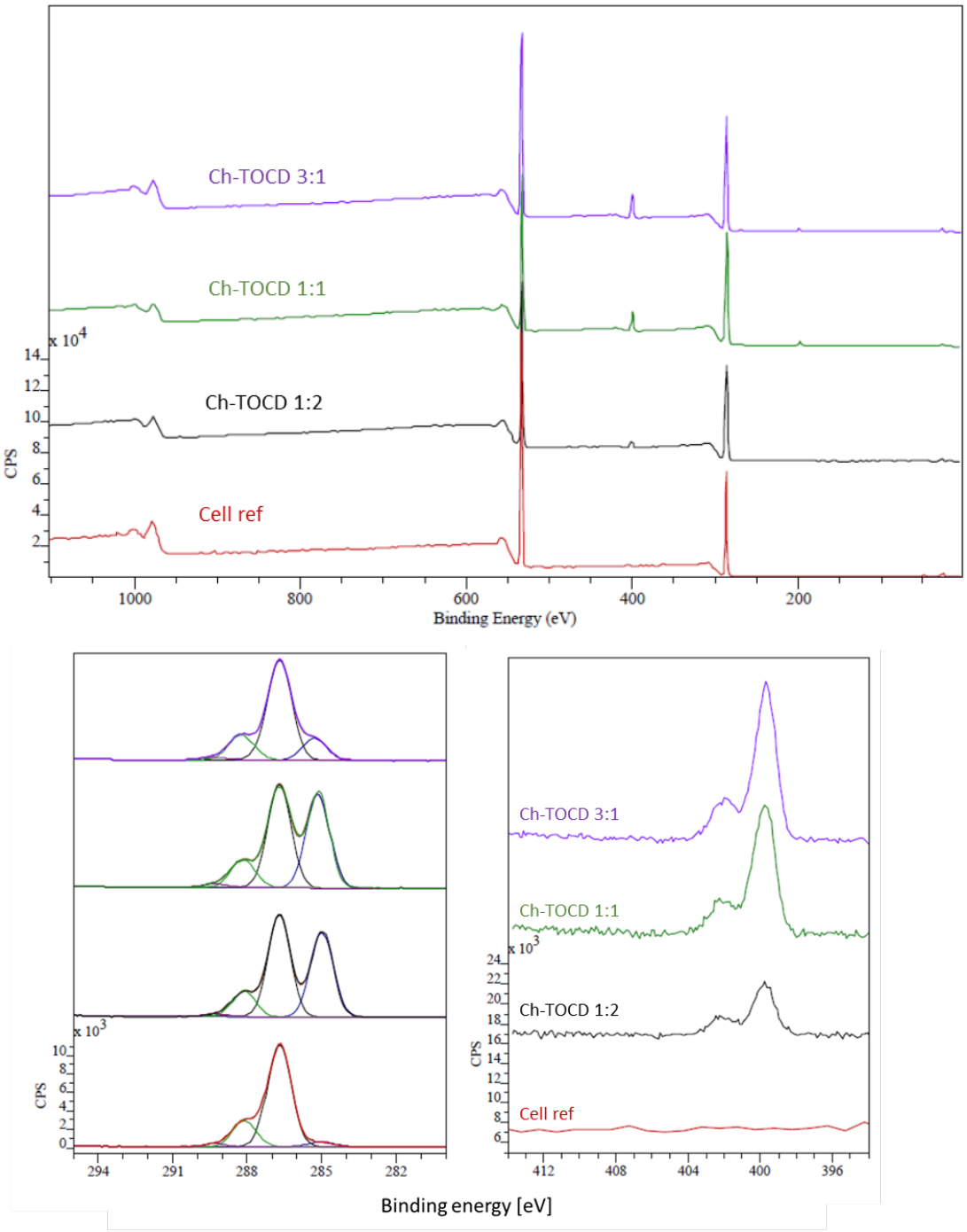

Figure 5.4 XPS wide energy region spectra of chitosan and its derivates. High resolution C 1s graphs (left) and N (left).

Furthermore, FTIR spectra was obtained for all the different derivates (Figure 5.5). In the TOCD spectrum in 1710 cm^{-1} the added carboxyl group is present. The primary difference between

the pristine chitosan and derivatives is observed in the NH bending band which decreases due to the new linkage between COO and NH. Other bands that present a change are those related to the CH bonding, this mainly due to the presence of a higher number of this link but with different opportunities for mobility between the polymer chains. Finally, the signals used to normalize the spectra were the bands at 1079 cm^{-1} for chitosan and all the derivatives, while for TOCD C-O-C at 1027 cm^{-1} was used. The spectrum for Ch-TOCD 2:1 displayed nearly the same intensity in both bands, confirming a higher content of TOCD.

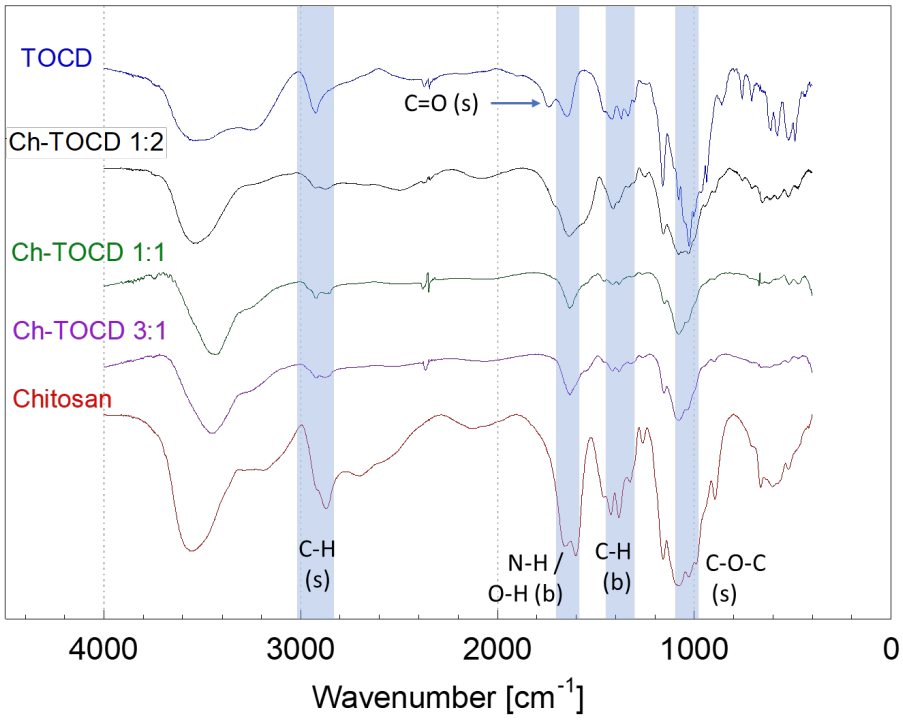

Figure 5.5 FTIR spectra comparison of the chitosan derivatives and the pristine materials.

5.4.3. Adsorption of Ch-TOCD onto CNF and microcystin-LR capture on surface.

The sensograms of the formation of the CNF surface, the adsorption of the materials and the capturing of microcystin-LR is shown in Figure 5.6. All sensograms have a reproducible

frequency shift of – 5.08 and -124.50 Hz and dissipation shift of 1.15 and 43.17 ppm for the adsorption of both PEI and CNF, respectively.

For the adsorption of the Ch and Ch-TOCD in the 50 mM buffer medium, the frequency shift was -24.71 ± 0.04, -22.76 ± 0.07, -27.13 ± 0.05, and -35.56 ± 0.16 Hz for chitosan, Ch-TOCD 1:2, Ch-TOCD 1:1, and Ch-TOCD 3:1, respectively. Even when the total adsorbed mass is different, the variation does not seem to correlate with the DS, as the unmodified chitosan had adsorption values comparable to the chitosan-cyclodextrin with 57% DS.

Meanwhile, for the adsorption of the MC, a decrease of ca. 5 Hz was observed for the modified materials and -4 Hz for the Ch. However, after rinsing, a loss of mass from the surface was observed, with a simultaneous reduction of dissipation in the case of chitosan, Ch-TOCD 1:1, and 3:1 below the initial level of MC adsorption. Additionally, the surface containing Ch-TOCD 2:1 also showed desorption, but with final dissipation values higher than the original values. These shift in frequency and its consequent difference in mass can be attributed to desorption of salts and water previously bounded onto the surfaces, rather than interactions of the polymers with MC.

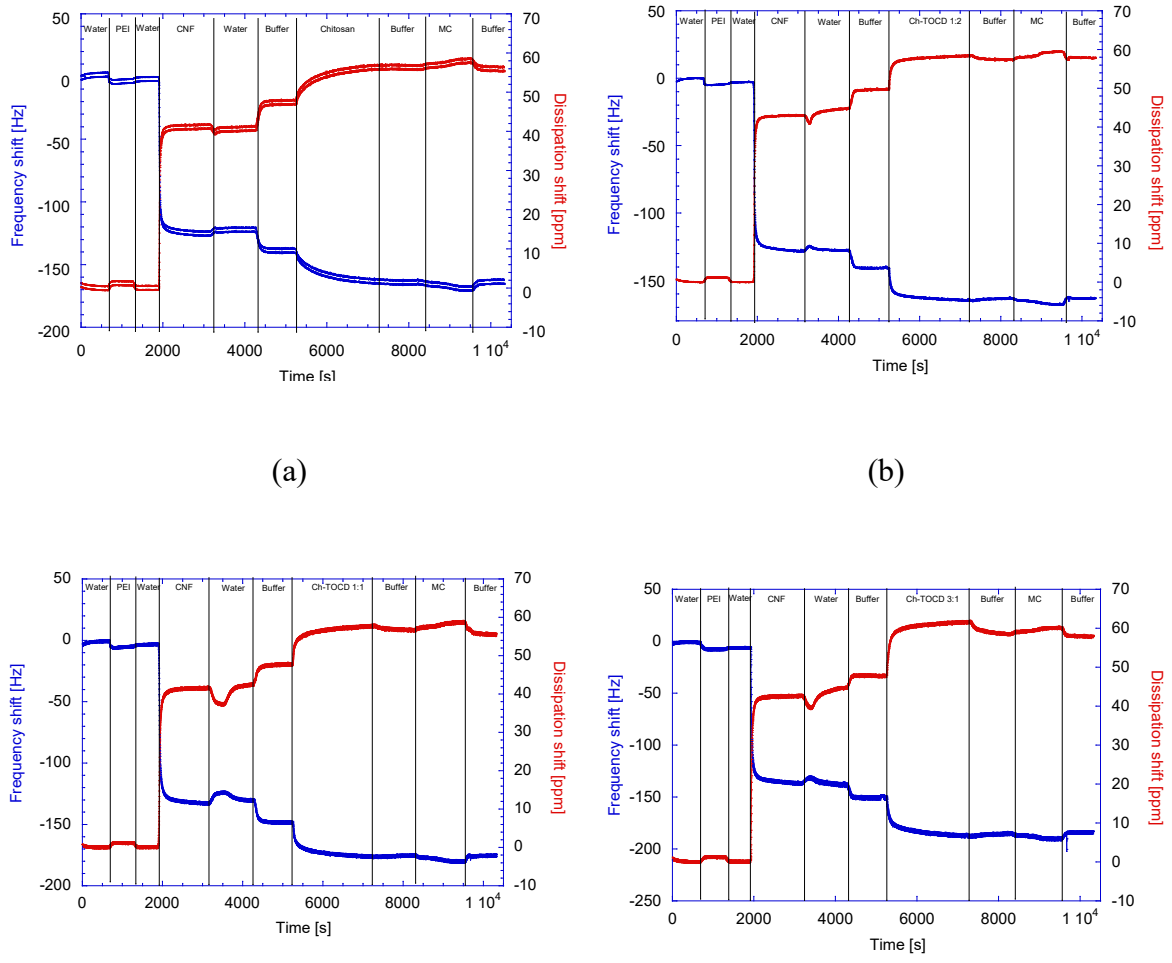

Figure 5.6. QCM-D isotherms of surface generation with chitosan and derivates, followed by adsorption of microcystin on 50 mM NaOAc buffer. Chitosan surface (a), Chitosan-TOCD molar ratio 1:2 (b), 1:1 (c), and 3:1 (d).

Adsorbed mass values were calculated fitting the data from the sensograms into the BroadFit model and the obtained results are shown in Figure 5.7. Similar to the frequency shift previously mentioned, the Chitosan and the Ch-TOCD 1:3 showed the highest interaction with the CNF surface, which can be partially due to more amino groups left available for hydrogen bonding interactions. However, the adsorption behavior of the rest of the polymers did not follow a

correlation with the amount of amino groups, evidencing the effect of H-bonding between β-(1 → 4) polysaccharides.

Positive MC adsorption was only observed in the case of the surface coated with Ch-TOCD 1:2. However, as previously suggested, frequency values returned to the original ones before the MC adsorption while changes in dissipation were irreversible, indicating swelling. This suggests that the changes observed in adsorbed mass are most like a tradeoff between toxin adsorption and loss of salts and release of water molecules. Adsorption capacity was estimated by the software to be 20.5 mg/g for the case of Ch-TOCD 1:2.

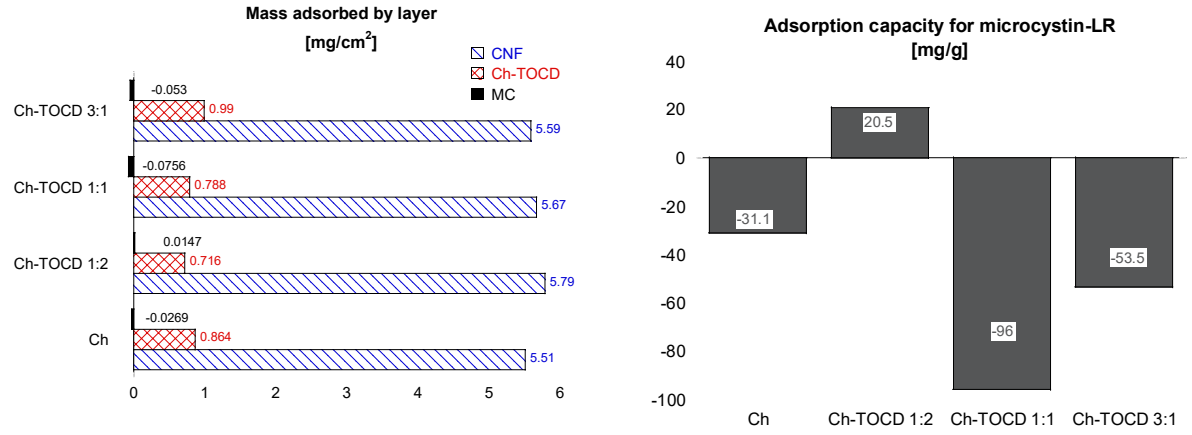

Figure 5.7. Mass adsorbed onto the CNF layers of each component (left), and microcystin adsorbed on each chitosan derivate (right).

5.4.4. Adsorption of Ch-TOCD onto CNF and microcystin-LR capture on beads.

MC adsorption was tested on a 3-D model, where cellulose beads were produced by regeneration of a solution of lignocellulosic material in sodium/urea solution, and subsequent coagulation in nitric acid. (O'Neill & Reichardt, 1951; Trivedi et al., 2018; Trygg et al., 2013) In this work, we used mechanically produced bleached softwood nanocellulose as a starting material, instead of dissolving pulp. We obtained beads of similar size, shape, and structure as those

produced using dissolving pulp (Gomez-Maldonado et al., 2021). Successful adsorption of the modified chitosan was indicated by the increase on solid content on the spheres, from a 2.1 ± 0.3% for the uncoated CNF to a maximum of 3.3 ± 0.2% for the ones coated with the Ch-TOCD 1:2 (Figure 5.8a). The modification was monitored by elemental analysis (Figure 5.8b) were the C% decreased from 54.98% for the CNF to around 39% for the coated beads; however, the N% was between 0.12 and 0.15% showing no clear trend. Finally, FTIR spectra of the coated and uncoated systems were not conclusive regarding nitrogen containing groups for coated and non-coated CNF. Contrary to what it was observed with the coated CNF, in the case of TOCD with higher content of TOCD, a clear band of unmodified carboxyl groups was observed around 1750 cm^{-1} and the stretching of the freer C-H of the cyclodextrin around 2900 cm-1 (Figure 5.8c).

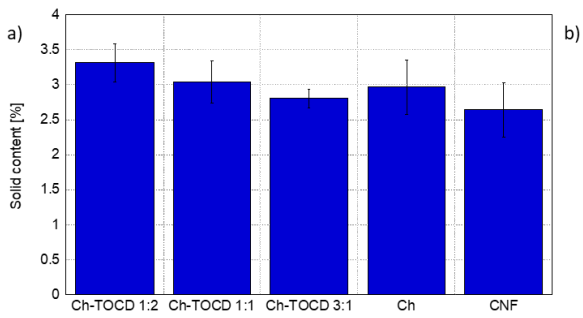

b)

	%C	%N	C/N
CNF	54.98	N/A	N/A
Chitosan	40.28	0.15	268.5
Ch-TOCD 1:2 (NH: COOH)	39.55	0.13	304.2
Ch-TOCD 1:1 (NH: COOH)	39.33	0.14	280.9
Ch-TOCD 3:1 (NH: COOH)	39.80	0.12	331.7

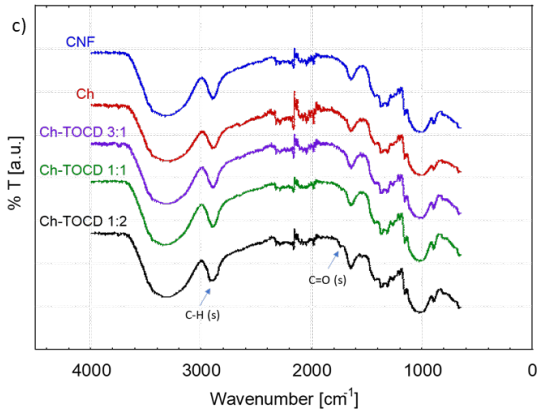

Figure 5.8. Physicochemical comparison of the uncoated CNF beads coated with chitosan (Ch) and chitosan modified with oriented cyclodextrin (Ch-TOCD) in the proportions 3:1, 1:1, and 1:2 by a) solid content: b) elemental analysis; and c) FTIR spectra.

Based on the previous results, the system coated with Ch-TOCD 1:2 was the selected system to evaluate MC adsorption, which was followed by HPLC analysis. When observing the adsorption kinetics (Figure 5.9), pure CNF beads appeared to adsorb MC more quickly at the beginning than in the case of coated beads. After 24 h, adsorption reached 2.4 mg/g for the coated beads compared with 1.9 mg/g in the case of pristine CNF. These values were higher than those reported for cellulose surface generated by dissolving the cellulose in ionic liquids without chitosan, but lower than the composite generated with 20% of chitosan (Tran et al., 2013) which had an adsorption around 20 mg/g. Even though the quantification techniques ware different, these values were closer to the observed on surface experiments on QCM-D, suggesting that part of the difference on the adsorption capacity could be related to the structure.

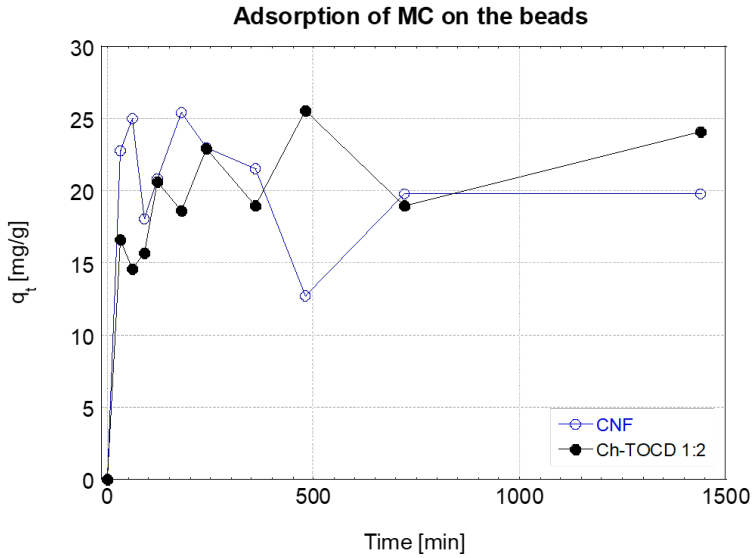

Figure 5.9. Adsorption kinetics of the CNF beads and CNF beads coated with Ch-TOCD 1:2 on a 6.5µg/mL solution over 24 h.

After fitting the adsorption data into pseudo-second order kinetic (Figure 5.10), the adsorption in equilibrium was of 1.92 mg/g for the CNF beads and of 2.36 mg/g for the coated beads with a R^2 of 0.96 and 0.98, respectively. When the k value was analyzed, the saturation half-time of them was 7.97 min for the CNF while the 81.3 min for the coated, once again demonstrating

that the adsorption mechanism for coated is a more passive adsorption than the electrostatic adsorption observed traditionally on cellulose (Lombardo & Thielemans, 2019). Furthermore, as only 0.7% of the mass of the coated bead correspond to the coating, the slow kinetics can be also related to the slower availability of active points on the surface rather than osmotic equilibrium of the concentration of MC on the media and the bead.

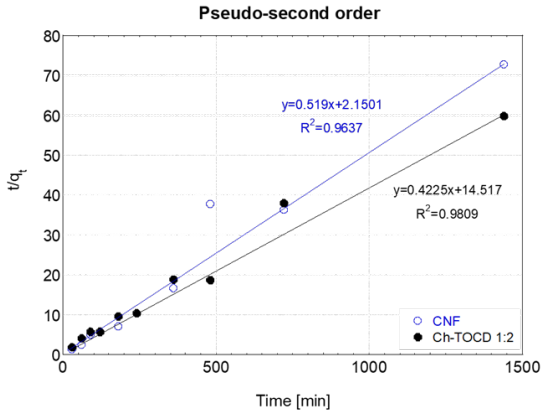

	CNF	Ch-TOCD 1:2
q_e	1.925	2.367
h	0.465	0.069
k_2	0.125	0.012
R^2	0.963	0.981
$t_{0.5}$	7.97	81.3

Figure 5.10. Pseudo-second order kinetic model for the CNF beads and CNF beads coated with Ch-TOCD 1:2

These results show a successful coating of the CNF beads with the chitosan-cyclodextrin polymer, which had an active site that interact with MC through a different mechanism than the uncoated beads, as expected. However, the data obtained from the HPLC is lower than the adsorption calculated in the 2D model with QCM-D in ten-fold. This difference can be attributed to the difference in coverage of the cellulose and diffusion profiles caused by the beads higher surface area, when compared to thin films.

This methodology for CNF coating opens new opportunities for the use of this bio-based polymer as a material that can be used to add hydrophobic active sites in multiple lignocellulosic-based products. These modified materials can be used for either capturing aromatic molecules or for slow-delivery of active molecules in sutures or other fibers as suggested; for example with

molecules such as estradiol (Orelma et al., 2018), phenols (F. Zhang et al., 2015), pentachlorophenol or other chlorophenolic compounds (Wilson et al., 2011).

5.5. Conclusions

Chitosan was successfully modified with TEMPO oxidized β-cyclodextrin in order to obtain an oriented hydrophobic cavity, and the modification was tested with different NH:COOH molar proportions 3:1, 1:1, and 1:2. These materials were used as a coating for nanocellulose surface – thin films (2D) as well as nanocellulose beads (3D) with the successful addition of cyclodextrin.

The coated cellulose-based materials were tested for their capacity to adsorb microcystin, showing an adsorption of 20.5 mg/g for the surface coated with the Ch-TOCD 1:2 monitored by QCMD and an adsorption of 2.36 mg/g on the coated bead as monitored by HPLC. The difference on these values obtained by these different technique is most likely a consequence of incomplete coating of the beads; however, the difference in the kinetic modeling between the non-coated and coated beads reflects a clear variation in adsorption mechanisms between the two materials. The successful adsorption of the coating on the lignocellulosic structure, as well as their capacity to adsorb an amphipathic molecule driven by its hydrophobic residue, airs that this bio-based coating has potential for a wide range of applications from drug delivery to water treatment.

5.6. Future work

As the cyclodextrin on the obtained cyclodextrin-chitosan co-polymer were oriented on the surface of both film and three-dimensional structure. The next goal is to develop a high surface cellulose materials with high surface area and porosity. A low energy input process is proposed in the next chapter of this dissertation.

5.7. Literature Cited

Adebajo, M. O., Frost, R. L., Kloprogge, J. T., Carmody, O., & Kokot, S. (2003). Porous Materials for Oil Spill Cleanup: A Review of Synthesis and Absorbing Properties. Journal of Porous Materials, 10(3), 159–170. https://doi.org/10.1023/A:1027484117065

Al-Ammar, R., Nabok, A., Hashim, A., & Smith, T. (2015). Microcystin-LR produced by bacterial algae: Optical detection and purification of contaminated substances. Sensors and Actuators, B: Chemical, 209, 1070–1076. https://doi.org/10.1016/j.snb.2014.11.063

Ali, I. (2012). New generation adsorbents for water treatment. Chemical Reviews, 112(10), 5073–5091. https://doi.org/10.1021/cr300133d

Archimandritis, A. S., Papadimitriou, T., Kormas, K. A., Laspidou, C. S., Yannakopoulou, K., & Lazarou, Y. G. (2016). Theoretical investigation of microcystin-LR, microcystin-RR and nodularin-R complexation with α-, β-, and γ-cyclodextrin as a starting point for the targeted design of efficient cyanotoxin traps. Sustainable Chemistry and Pharmacy, 3, 25–32. https://doi.org/10.1016/j.scp.2016.02.001

Arkles, B. (2006). Hydrophobicity, Hydrophilicity and Silanes. Paint & Coatings Industry, October, 114. https://doi.org/10.1016/j.micromeso.2005.05.031

Badruddoza, A. Z. M., Shawon, Z. B. Z., Tay, W. J. D., Hidajat, K., & Uddin, M. S. (2013). Fe 3O 4/cyclodextrin polymer nanocomposites for selective heavy metals removal from industrial wastewater. Carbohydrate Polymers, 91(1), 322–332. https://doi.org/10.1016/j.carbpol.2012.08.030

Beamson, G., & Briggs, D. (1992). High resolution XPS of organic polymers: The Scienta ESCA 300 database. John Wiley & Sons.

Blackburn, R. S. (2004). Natural polysaccharides and their interactions with dye molecules: Applications in effluent treatment. Environmental Science and Technology, 38(18), 4905–4909. https://doi.org/10.1021/es049972n

Chen, P., Liang, H. W., Lv, X. H., Zhu, H. Z., Yao, H. Bin, & Yu, S. H. (2011). Carbonaceous nanofiber membrane functionalized by beta-cyclodextrins for molecular filtration. ACS Nano, 5(7), 5928–5935. https://doi.org/10.1021/nn201719g

D'Este, M., Eglin, D., & Alini, M. (2014). A systematic analysis of DMTMM vs EDC/NHS for ligation of amines to Hyaluronan in water. Carbohydrate Polymers, 108(1), 239–246. https://doi.org/10.1016/j.carbpol.2014.02.070

da Silva Perez, D., Montanari, S., & Vignon, M. R. (2003). TEMPO-mediated oxidation of cellulose III. Biomacromolecules, 4(5), 1417–1425. https://doi.org/10.1021/bm034144s

Dong, H., Snyder, J. F., Tran, D. T., & Leadore, J. L. (2013). Hydrogel, aerogel and film of cellulose nanofibrils functionalized with silver nanoparticles. Carbohydrate Polymers, 95(2), 760–767. https://doi.org/10.1016/j.carbpol.2013.03.041

Dufresne, A. (2017). Nanocellulose: From nature to high performance tailored materials. In Nanocellulose: From Nature to High Performance Tailored Materials, 2. Edition (2nd ed.). De Gruyter.

Dunlop, J. W. C., & Fratzl, P. (2010). Biological Composites. Annual Review of Materials Research, 40(1), 1–24. https://doi.org/10.1146/annurev-matsci-070909-104421

Example, A. (1991). Dissipative QCM. Langmuir, 1–3.

Fang, R. H., Kroll, A. V., Gao, W., & Zhang, L. (2018). Cell Membrane Coating Nanotechnology. Advanced Materials, 30(23), 1–34. https://doi.org/10.1002/adma.201706759

Gomez-Maldonado, D., Vega Erramuspe, I. B., Filpponen, I., Johansson, L.-S., Lombardo, S., Zhu, J., Thielemans, W., & Peresin, M. S. (2019). Cellulose-Cyclodextrin Co-Polymer for the Removal of Cyanotoxins on Water Sources. Polymers, 11(12), 2075. https://doi.org/10.3390/polym11122075

Groll, J., Fiedler, J., Engelhard, E., Ameringer, T., Tugulu, S., Klok, H. A., Brenner, R. E., & Moeller, M. (2005). A novel star PEG-derived surface coating for specific cell adhesion. Journal of Biomedical Materials Research - Part A, 74(4), 607–617. https://doi.org/10.1002/jbm.a.30335

Guo, J., Filpponen, I., Su, P., Laine, J., & Rojas, O. J. (2016). Attachment of gold nanoparticles on cellulose nanofibrils via click reactions and electrostatic interactions. Cellulose, 23(5), 3065–3075. https://doi.org/10.1007/s10570-016-1042-7

Huang, P. K., Yeh, J. W., Shun, T. T., & Chen, S. K. (2004). Multi-principal-element alloys with improved oxidation and wear resistance for thermal spray coating. Advanced Engineering Materials, 6(1–2), 74–78. https://doi.org/10.1002/adem.200300507

Huang, W. J., Cheng, B. L., & Cheng, Y. L. (2007). Adsorption of microcystin-LR by three types of activated carbon. Journal of Hazardous Materials, 141(1), 115–122. https://doi.org/10.1016/j.jhazmat.2006.06.122

Isimjan, T. T., Wang, T., & Rohani, S. (2012). A novel method to prepare superhydrophobic, UV resistance and anti-corrosion steel surface. Chemical Engineering Journal, 210, 182–187. https://doi.org/10.1016/j.cej.2012.08.090

Jiang, Y., Liu, B., Xu, J., Pan, K., Hou, H., Hu, J., & Yang, J. (2018). Cross-linked chitosan/β-cyclodextrin composite for selective removal of methyl orange: Adsorption performance and

mechanism. Carbohydrate Polymers, 182(July 2017), 106–114. https://doi.org/10.1016/j.carbpol.2017.10.097

Johansson, L., Campbell, J. M., & Rojas, O. J. (2020). Cellulose as the in situ reference for organic XPS . Why ? Because it works. Surface and Interface Analysis, February, 1–5. https://doi.org/10.1002/sia.6759

Johansson, L. S., & Campbell, J. M. (2004). Reproducible XPS on biopolymers: Cellulose studies. Surface and Interface Analysis, 36(8), 1018–1022. https://doi.org/10.1002/sia.1827

Junka, K., Filpponen, I., Johansson, L. S., Kontturi, E., Rojas, O. J., & Laine, J. (2014). A method for the heterogeneous modification of nanofibrillar cellulose in aqueous media. Carbohydrate Polymers, 100, 107–115. https://doi.org/10.1016/j.carbpol.2012.11.063

Karim, Z., Claudpierre, S., Grahn, M., Oksman, K., & Mathew, A. P. (2016). Nanocellulose based functional membranes for water cleaning: Tailoring of mechanical properties, porosity and metal ion capture. Journal of Membrane Science, 514, 418–428. https://doi.org/10.1016/j.memsci.2016.05.018

Kayaci, F., Aytac, Z., & Uyar, T. (2013). Surface modification of electrospun polyester nanofibers with cyclodextrin polymer for the removal of phenanthrene from aqueous solution. Journal of Hazardous Materials, 261, 286–294. https://doi.org/10.1016/j.jhazmat.2013.07.041

Khan, A. R., Forgo, P., Stine, K. J., & D'Souza, V. T. (1998). Methods for selective modifications of cyclodextrins. Chemical Reviews, 98(5), 1977–1996. https://doi.org/10.1021/cr970012b

Khaoulani, S., Chaker, H., Cadet, C., Bychkov, E., Cherif, L., Bengueddach, A., & Fourmentin, S. (2015). Wastewater treatment by cyclodextrin polymers and noble metal/mesoporous

TiO2photocatalysts. Comptes Rendus Chimie, 18(1), 23–31. https://doi.org/10.1016/j.crci.2014.07.004

Kim, S., Yun, Y. S., & Choi, Y. E. (2018). Development of waste biomass-based sorbent for removal of cyanotoxin microcystin-LR from aqueous phases. Bioresource Technology, 247(June 2017), 690–696. https://doi.org/10.1016/j.biortech.2017.09.164

Kono, H., Onishi, K., & Nakamura, T. (2013). Characterization and bisphenol A adsorption capacity of β-cyclodextrin-carboxymethylcellulose-based hydrogels. Carbohydrate Polymers, 98(1), 784–792. https://doi.org/10.1016/j.carbpol.2013.06.065

KSV Instruments Ltd. (2002). What Is a Quartz Crystal Microbalance – Qcm (pp. 1–10).

Kumar Dutta, P., Dutta, J., & Tripathi, V. S. (2004). Chitin and chitosan: Chemistry, properties and applications. Journal of Scientific & Industrial Research, 63(January), 20–31. https://doi.org/10.1002/chin.200727270

Larkin, P. J. (2011). "IR and Raman Spectroscopy - Principles and Spectral Interpretation." In Vasa. https://doi.org/10.1016/b978-0-12-386984-5.10001-1

Larsson, E., Sanchez, C. C., Porsch, C., Karabulut, E., Wågberg, L., & Carlmark, A. (2013). Thermo-responsive nanofibrillated cellulose by polyelectrolyte adsorption. European Polymer Journal, 49(9), 2689–2696. https://doi.org/10.1016/j.eurpolymj.2013.05.023

Li, L., Fan, L., Sun, M., Qiu, H., Li, X., Duan, H., & Luo, C. (2013). Adsorbent for hydroquinone removal based on graphene oxide functionalized with magnetic cyclodextrin-chitosan. International Journal of Biological Macromolecules, 58, 169–175. https://doi.org/10.1016/j.ijbiomac.2013.03.058

Li, T., Huang, P., Liang, J., Fu, W., Guo, Z., & Xu, L. (2011). Microcystin-LR (MCLR) Induces a Compensation of PP2A Activity Mediated by α 4 Protein in HEK293 Cells.

Liu, H., Cai, X., Wang, Y., & Chen, J. (2011). Adsorption mechanism-based screening of cyclodextrin polymers for adsorption and separation of pesticides from water. Water Research, 45(11), 3499–3511. https://doi.org/10.1016/j.watres.2011.04.004

Loftin, K. A., Clark, J. M., Journey, C. A., Kolpin, D. W., Van Metre, P. C., Carlisle, D., & Bradley, P. M. (2016). Spatial and temporal variation in microcystin occurrence in wadeable streams in the southeastern United States. Environmental Toxicology and Chemistry, 35(9), 2281–2287. https://doi.org/10.1002/etc.3391

Lombardo, S., & Thielemans, W. (2019). Thermodynamics of adsorption on nanocellulose surfaces. Cellulose, 26(1), 249–279. https://doi.org/10.1007/s10570-018-02239-2

Merel, S., Villarín, M. C., Chung, K., & Snyder, S. (2013). Spatial and thematic distribution of research on cyanotoxins. Toxicon, 76(SEPTEMBER), 118–131. https://doi.org/10.1016/j.toxicon.2013.09.008

Meriluoto, J., & Codd, G. A. (2005). Cyanobacterial Monitoring and Cyanotoxin Analysis. https://doi.org/10.1002/9781119068761

Mishima, T., Hisamatsu, M., York, W. S., Teranishi, K., & Yamada, T. (1998). Adhesion of β-D-glucans to cellulose. Carbohydrate Research, 308(3–4), 389–395. https://doi.org/10.1016/S0008-6215(98)00099-8

Mocchiutti, P., Schnell, C. N., Rossi, G. D., Peresin, M. S., Zanuttini, M. A., & Galván, M. V. (2016). Cationic and anionic polyelectrolyte complexes of xylan and chitosan. Interaction with

lignocellulosic surfaces. Carbohydrate Polymers, 150, 89–98. https://doi.org/10.1016/j.carbpol.2016.04.111

O'Neill, J. J. J., & Reichardt, E. P. (1951). Method of producing cellulose pellets (Patent No. 2543928).

Orelma, H., Filpponen, I., Johansson, L. S., Österberg, M., Rojas, O. J., & Laine, J. (2012). Surface functionalized nanofibrillar cellulose (NFC) film as a platform for immunoassays and diagnostics. Biointerphases, 7(1–4), 1–12. https://doi.org/10.1007/s13758-012-0061-7

Orelma, H., Virtanen, T., Spoljaric, S., Lehmonen, J., Seppälä, J., Rojas, O. J., & Harlin, A. (2018). Cyclodextrin-Functionalized Fiber Yarns Spun from Deep Eutectic Cellulose Solutions for Nonspecific Hormone Capture in Aqueous Matrices. Biomacromolecules, 19(2), 652–661. https://doi.org/10.1021/acs.biomac.7b01765

Parvinzadeh, M., Alimohammadi, F., & Shamei, A. (2012). Surface & Coatings Technology Preparation of water-repellent cellulose fi bers using a polycarboxylic acid / hydrophobic silica nanocomposite coating. Surface & Coatings Technology, 206(14), 3208–3215. https://doi.org/10.1016/j.surfcoat.2012.01.006

Peresin, M. S., Vesterinen, A. H., Habibi, Y., Johansson, L. S., Pawlak, J. J., Nevzorov, A. A., & Rojas, O. J. (2014). Crosslinked PVA nanofibers reinforced with cellulose nanocrystals: Water interactions and thermomechanical properties. Journal of Applied Polymer Science, 131(11), 1–12. https://doi.org/10.1002/app.40334

Pillai, K., Navarro Arzate, F., Zhang, W., & Renneckar, S. (2014). Towards Biomimicking Wood: Fabricated Free-standing Films of Nanocellulose, Lignin, and a Synthetic Polycation. Journal of Visualized Experiments, 88, 1–14. https://doi.org/10.3791/51257

Prabaharan, M., & Gong, S. (2008). Novel thiolated carboxymethyl chitosan-g-β-cyclodextrin as mucoadhesive hydrophobic drug delivery carriers. Carbohydrate Polymers, 73(1), 117–125. https://doi.org/10.1016/j.carbpol.2007.11.005

Sauerbrey G (1959) Verwendung von Schwingquarzen zur Wägung dünner Schichten und zur Mikrowägung. Zeitschrift für Phys 155:206–222. https://doi.org/10.1007/BF01337937

Saenger, W., & Steiner, T. (1998). Cyclodextrin Inclusion Complexes: Host ± Guest Interactions and Hydrogen-Bonding Networks. 798–805. https://doi.org/10.1107/S0108767398010733

Saito, T., Shibata, I., Isogai, A., Suguri, N., & Sumikawa, N. (2005). Distribution of carboxylate groups introduced into cotton linters by the TEMPO-mediated oxidation. Carbohydrate Polymers, 61(4), 414–419. https://doi.org/10.1016/j.carbpol.2005.05.014

Saito, Tsuguyuki, Hirota, M., Tamura, N., Kimura, S., Fukuzumi, H., Heux, L., & Isogai, A. (2009). Individualization of Nano-Sized Plant Cellulose Fibrils by Direct Surface Carboxylation Using TEMPO Catalyst under Neutral Conditions. Biomacromolecules, 10(7), 1992–1996. https://doi.org/10.1021/bm900414t

Saito, Tsuguyuki, & Isogai, A. (2004). TEMPO-mediated oxidation of native cellulose. The effect of oxidation conditions on chemical and crystal structures of the water-insoluble fractions. Biomacromolecules, 5(5), 1983–1989. https://doi.org/10.1021/bm0497769

Sashiwa, H., Shigemasa, Y., & Roy, R. (2004). Dissolution of Chitosan in Dimethyl Sulfoxide by Salt Formation. Chemistry Letters, 29(6), 596–597. https://doi.org/10.1246/cl.2000.596

Shao, D., Sheng, G., Chen, C., Wang, X., & Nagatsu, M. (2010). Removal of polychlorinated biphenyls from aqueous solutions using β-cyclodextrin grafted multiwalled carbon nanotubes. Chemosphere, 79(7), 679–685. https://doi.org/10.1016/j.chemosphere.2010.03.008

Shim, E. (2013). Smart surface treatments for textiles for protection. In Smart Textiles for Protection (pp. 87–126). Elsevier. https://doi.org/10.1533/9780857097620.1.87

Sinha, A., & Jana, N. R. (2015). Separation of microcystin-LR by cyclodextrin-functionalized magnetic composite of colloidal graphene and porous silica. ACS Applied Materials and Interfaces, 7(18), 9911–9919. https://doi.org/10.1021/acsami.5b02038

Solgi, S., Ghorbani-Vaghei, R., & Alavinia, S. (2020). Application of copper iodide nanoparticles immobolized porous polysulfonamide gel as an effective nanocatalyst for synthesis of aminoindolizines. Journal of Porous Materials, 0123456789. https://doi.org/10.1007/s10934-020-00989-8

Spence, K. L., Venditti, R. A., Rojas, O. J., Habibi, Y., & Pawlak, J. J. (2010). The effect of chemical composition on microfibrillar cellulose films from wood pulps: Water interactions and physical properties for packaging applications. Cellulose, 17(4), 835–848. https://doi.org/10.1007/s10570-010-9424-8

Tran, C. D., Duri, S., Delneri, A., & Franko, M. (2013). Chitosan-cellulose composite materials: Preparation, Characterization, and application for removal of microcystin. Journal of Hazardous Materials, 253, 355–366.

Trivedi, P., Saloranta-Simell, T., Maver, U., Gradišnik, L., Prabhakar, N., Smått, J.-H., Mohan, T., Gericke, M., Heinze, T., & Fardim, P. (2018). Chitosan–Cellulose Multifunctional Hydrogel Beads: Design, Characterization and Evaluation of Cytocompatibility with Breast Adenocarcinoma and Osteoblast Cells. Bioengineering, 5(1), 3. https://doi.org/10.3390/bioengineering5010003

Trygg, J., Fardim, P., Gericke, M., Mäkilä, E., & Salonen, J. (2013). Physicochemical design of the morphology and ultrastructure of cellulose beads. Carbohydrate Polymers, 93(1), 291–299. https://doi.org/10.1016/j.carbpol.2012.03.085

Trygg, J., Yildir, E., Kolakovic, R., Sandler, N., & Fardim, P. (2014). Anionic cellulose beads for drug encapsulation and release. Cellulose, 21(3), 1945–1955. https://doi.org/10.1007/s10570-014-0253-z

Turon, X., Rojas, O. J., & Deinhammer, R. S. (2008). Enzymatic kinetics of cellulose hydrolysis: A QCM-D study. Langmuir, 24(8), 3880–3887. https://doi.org/10.1021/la7032753

Voinova, M. V., Jonson, M., & Kasemo, B. (2002). "Missing mass" effect in biosensor's QCM applications. Biosensors and Bioelectronics, 17(10), 835–841. https://doi.org/10.1016/S0956-5663(02)00050-7

Voinova, M. V., Rodahl, M., Jonson, M., & Kasemo, B. (1998). Viscoelastic acoustic response of layered polymer films at fluid-solid interfaces: Continuum mechanics' approach. 1–22. https://doi.org/10.1238/Physica.Regular.059a00391

Wilson, L. D., Mohamed, M. H., & Berhaut, C. L. (2011). Sorption of aromatic compounds with copolymer sorbent materials containing β-cyclodextrin. Materials, 4(9), 1528–1542. https://doi.org/10.3390/ma4091528

Word Health Organization (WHO). (1998). Cyanobacterial toxins: Microcystin-LR in Drinking-water. Guidelines for Drinking-Water Quality, 2.

Yuan, G., Prabakaran, M., Qilong, S., Lee, J. S., Chung, I. M., Gopiraman, M., Song, K. H., & Kim, I. S. (2017). Cyclodextrin functionalized cellulose nanofiber composites for the faster

adsorption of toluene from aqueous solution. Journal of the Taiwan Institute of Chemical Engineers, 70, 352–358. https://doi.org/10.1016/j.jtice.2016.10.028

Zeng, D., Wu, J., & Kennedy, J. F. (2008). Application of a chitosan flocculant to water treatment. Carbohydrate Polymers, 71(1), 135–139. https://doi.org/10.1016/j.carbpol.2007.07.039

Zhang, F., Wu, W., Sharma, S., Tong, G., & Deng, Y. (2015). Synthesis of Cyclodextrin-functionalized Cellulose Nanofibril Aerogel as a Highly Effective Adsorbent for Phenol Pollutant Removal. BioResources, 10(4), 7555–7568.

Zhang, M., Ma, W., Cui, J., Wu, S., Han, J., Zou, Y., & Huang, C. (2020). Hydrothermal synthesized UV-resistance and transparent coating composited superoloephilic electrospun membrane for high efficiency oily wastewater treatment. Journal of Hazardous Materials, 383(September 2019), 121152. https://doi.org/10.1016/j.jhazmat.2019.121152

6. Delignified wood aerogel as scaffolds coated with chitosan-cyclodextrin co-polymer for removal of microcystin-LR.

6.1. Abstract

Nano-porous aerogels are an advantageous approach to produce low-density materials with a high surface area, particularly when they are produced from biobased materials. Frequently, most biobased aerogels are synthesized through a bottom-up approach, which requires high energy inputs to break and rebuild the raw materials, with the elimination of water occurring through traditional freeze-drying method. To curb this, we focused this work on the generation of aerogels by a top-down approach through the delignification of a solid wood substrate while incorporating a solvent exchange step to eliminate water without extra energetic inputs. To diversify the surface chemistry for use of aerogels in water treatment, the delignified wood -nanowood- was coated with a chitosan-cyclodextrin co-polymer and tested in the capture of the toxin microcystin-LR -an amphipathic molecule known to form inclusion complexes with cyclodextrins. We were able to generate a nanowood structure with 75% porosity after coating, with up to 339% water swelling and an adsorption capacity of 0.12 mg/g of the microcystin from initial 5.4 µg/mL stock solution. This simple approach of generating aerogels also allowed the use of a coating with hydrophobic active sites by self-assembling driven interactions. This top-down technique enables the generation of low-cost aerogels by reducing steps and costly input.

6.1.1. Index Words

Wood aerogels, active coatings, chitosan, β-cyclodextrin, microcystin-LR, water quality.

6.1.2. Project Partners

The Forest Products Development Center worked in collaboration with the School of Pharmacy, and the Department of Crops, Soils and Environmental Science from Auburn University and with Surface Measurement Systems Ltd. This research was supported by the Alabama Agricultural Experiment Station, and the Hatch program of the National Institute of Food and Agriculture, United States Department of Agriculture. The School of Forestry and Wildlife Sciences at Auburn University financial support to complete this work is greatly appreciated.

6.2. Introduction

Wood is one of the most used materials since pre-historian dates for fuel, constructions (first wood house made 10,000 years ago), and as a material for tools and weapons (Woods, 2016). Even in more modern times, its application has made incursions into furniture and paper, which makes it an important day-to-day resource. Furthermore, it is estimated that up to 1.6 billion people depend on this industry for their sustenance, products and services as it translates in a market of about $ 450 billion USD (Munang et al., 2011). It is estimated that there were 530.5 billion cubic meters of wood stock in 2015, but regions like Europe, East Asia, and North America have consistently reported an increase in their forest coverage (Howard, 2016; Howard & Liang, 2019; Köhl et al., 2015).

As wood is a biosynthesize product, its chemical composition varies depending on the selected tree, specie, geographical location, available soil nutrients, age, and other environmental factors (Iglesias, Gomez-Maldonado, et al., 2020; Pettersen & Rowell, 1984). For wood products,

the three main components are cellulose, hemicellulose and lignin. With the polysaccharide components -cellulose and hemicellulose- accounting for 65 to 70% of the dry weight (Rowell et al., 2012). Traditional processing for goods such as commodities and high-end products is based in the break of the inherent structure, homogenization, and separation of the components (Sixta, 2006). Thereafter, the products development takes a bottom-up route, rebuilding the components into new structure such as paper and films (Avila-Suarez et al., 2013; Dahl, 1884), or more complex structures such as aerogels and hydrogels (Ajdary et al., 2020; De France et al., 2020; Pillai et al., 2014). While this is an important process, a great side effect is the hornification of the cellulose nanofibrils that were present in the cellular wall (Fernandes Diniz et al., 2004). To return the pulp into nano-scale diameters, high energetic demanding processes such as high-pressure homogenizer and grinding by super mass colloider are required (de Assis et al., 2018; Oksman et al., 2014; Rojas, 2014; Solala et al., 2020).

As some of the more novel applications, such as water treatment, want to maintain the high surface area of the cellulose nanofibrils and a low densities such as the aerogels and hydrogels that can be developed; a recently alternative has been the separation of the lignin and hemicellulose from the wood natural structure by softer processes derived from the more traditional pulping methods (Ajdary et al., 2020; Chu et al., 2020; Li et al., 2017; Tsuguyuki Saito et al., 2006; Wu et al., 2020; Zhu et al., 2016). However, most of these processes still use a high energy step, freeze-drying.

Even with the high surface area that is obtained from this wood aerogels (also called nanowood); some applications such as water treatment still need extra processing as the surface chemistry is limited to the inherent cellulose side groups, and consequent partial negative charge that comes with some side reactions on the delignification process (Iglesias, Gomez-Maldonado,

et al., 2020). Therefore, some extra modification is needed, which ideally will be done with little to no energy input and green materials. This could be achieved like in traditional bottom-up aerogels and other porous materials, with active nanoscale coatings, such as adsorption of nanoparticles (Dong et al., 2013; Sullivan et al., 2017; Toivonen, Kaskela, et al., 2015), or other active polymers (Awaja et al., 2009; Guo et al., 2016; Lombardo & Villares, 2020).

A good strategy to add functionality to polysaccharides is to adsorb other β-linked polysaccharides that have the desired functional group, such as chitosan or alginates (Mishima et al., 1998; Orelma et al., 2011). Furthermore, when chitosan is used, the amino groups that are added serve both as functionality by their positive charge that can interact with negative charged pollutants (Mao et al., 2019; Zeng et al., 2008), as well as a new surface group that can be easily modified with other active molecules with different molecular interactions like β-cyclodextrin or with enzymes by green chemistry such as EDC/NHS chemistry (Orelma et al., 2018; Prabaharan & Mano, 2005; Smith et al., 2020).

Based on the downfalls described above the generation of a wood aerogel without freeze-drying and coated with a polysaccharide derivate was made. To avoid freeze-drying, solvent exchange adapted from Toivonen *et al.* was done (2015), where the final solvent is octane which can then be air dried avoiding the energy input. On the other hand, coating was done with a pre-modified chitosan with TEMPO oxidized β-cyclodextrin; the coating was done by sole immersion of the aerogels in a buffer solution with a ionic strength of 50 mM, which promotes the adsorption of chitosan and cellulose by hydrogen bonding. Finally, to assess the activity of the coating material, adsorption on the increasingly concerning cyanotoxin -microcystin-LR- was done, as it has a known to form inclusion complexes with β-cyclodextrin (Archimandritis et al., 2016; Gomez-Maldonado et al., 2019).

6.3. Materials and Methods

6.3.1. Materials

Pine wood was obtain from the School of Forestry and Wildlife Science at Auburn University; β-cyclodextrin (CD, > 95 % purity) and N-hydroxysuccinimide (NHS, 98.0% purity) were purchased from Tokyo Chemical Industry (Portland, OR, U.S.); chitosan (DSacetylation of 0.15, MRU 167.3 g/mol) and octane (98 + %) were purchased from Alfa Aesar (Haverhill, MA, U.S.); microcystin-LR (MC, > 95 %) was purchase from Cayman Chemicals (Ann Arbor, MI, U.S.); sodium hydroxide (50 % w/w) was obtained from J.T. Baker (Phillipsburg, NJ, U.S.); sodium chlorite (80% purity) was purchased from BeanTown Chemical (Hudson, NH, U.S.); sodium hypochlorite (12.5 % w/w, 2 M in water), peroxide (35% w/w) and Isopropanol were obtained from VWR chemicals (Radnor, PA, U.S.); sodium sulfate (Na_2SO_3) was bought from Fisher Scientific company (Walthman, MA, U.S.); sulfuric acid (72% w/w) was obtained from Ricca Chemical company (Arlington, TX, U.S.); 2,2,6,6-tetramethylpiperidinooxy (TEMPO, 98 % purity) was bought from Acros Organics (Geel, Belgium); 3-(3-Dimethylaminopropil)-1-ethyl-carbodiimide hydrochloride (EDC, 99.9% purity) was obtained from Chem-Impex International (Wood Dale, IL, U.S.);. ethanol (200 proof pure) purchased from Decon Labs, Inc. (King of Prussia, PA, U.S.); The water used was deionized and purified with a Thermo Scientific Barnstead Nanopure (18.2 MΩ cm). Unless specified, all the weights in this paper are expressed in oven dry basis.

6.3.2. Synthesis of TEMPO oxidized β-cyclodextrin (TOCD).

β-cyclodextrin was carboxylated by neutral TEMPO-NaClO-NaClO2 oxidation in aqueous media. (Orelma et al., 2018; Tsuguyuki Saito et al., 2009) For this, 5 g of β-cyclodextrin were dissolved in 450 mL of sodium phosphate buffer (0.05 M, pH 6.8). Then 0.08 g of TEMPO (0.1 mmol/g) and 5.65 g sodium chlorite (80 %, 10 mmol) were added to the cyclodextrin solution. Simultaneously, the 2 M sodium hypochlorite stock solution was diluted to a 0.1 M in the same buffer and 23 mL of this dilution were added in one step to the reactive solution to obtain a final concentration of 5 mmol (1.0 mmol NaClO/g of CD). The reaction was conducted in a closed flask for 19.5 h under ambient condition and a constant stirring of 500 rpm. After modification, TEMPO-oxidize β-cyclodextrin (TOCD) was purified by dialysis against ultrapure water (18.2 Ω) in a 100-500 Da dialysis membrane tube, then freeze-dried.

6.3.3. Synthesis of chitosan-cyclodextrin polymers (Ch-CD).

The synthesis of Ch-CD was performed considering a 2:1 molar ratio of the functional groups COOH:NH (TOCD:Ch) in a total of 50 mL volume with the same steps sequence. First, the TOCD was dissolved in 1% acetic acid (125 mg) to obtain a final concentration of 0.05%, then pre-dissolved EDC was added to obtain a final concentration of 0.05 M EDC and let stir before adding a pre-dissolved NHS to obtain a final concentration of 0.2 M NHS. From a stock solution of chitosan (1% in 1% acetic acid, w/w), the corresponding milliliters were added to obtain a 0.05% solution. The reaction was left for 24 h before stopping it by adding ethanol-amide (61 µL) to obtain a final concentration of 0.1 M. Purification and concentration was done by five washings in 50 KDa Pall-membrane centrifugation tubes (Macrosep Advance Centrifugal Device, Pall Corporation) at 3000 rpm for 45 min each time.

6.3.4. Delignified wood aerogels (nanowood) production.

The delignification process was adapted from Zhu et al. (2016). Briefly, wood pieces cut perpendicularly to the growth axis (10x10x3 mm) were immersed in 100 mL of 2.5 M NaOH, 0.4 M Na_2SO_3 and allowed ti boil for 8 h. Thereafter, the samples were rinsed with hot water and placed in another 100 mL of 2.5 M H_2O_2 and boiled for 1 h. The samples were then rinsed with cold DI water and placed in ethanol overnight to eliminate water excess. Solvent was then exchanged 3-4 times with fresh isopropanol and left overnight; the same was done with octane which was left to air dry after overnight exchange (ca. 72 h).

6.3.5. Coating of wood aerogels.

Treated dry wood pieces were immersed in 10 mL of acetate buffer 50 mM (ionic strength was adjusted to the same molarity with NaCl) containing 0.5 mg/mL of the Ch-CD polymer. The nanowood was left in the solution for 24 h, then they were rinsed with ultrapure water until no changes in conductivity were measured.

6.3.6. Adsorption of microcystin-LR (MC) by High Pressure Liquid Chromatography (HPLC).

For the analysis of the adsorption of the untreated wood, nanowood and coated nanowood of the microcystin, the materials were placed in 28 mL of solutions containing 5.4 μg/mL at room temperature and constant stirring. 150 μL aliquots were taken at the corresponding time and analysed in a Waters Alliance HPLC (Model No. e2695, Waters Corp., Milford, MA, USA) system equipped with a solvent management system 2695 and detected by a photodiode array detector (PDA, 2998). The system also counts with a thermostatically controlled column compartment and an autosampler. The method used was adapted from the one described by Meriluoto & Spoof (Meriluoto & Codd, 2005). Briefly, a C-18 column (55x4 mm) was used as stationary phase, and

0.05% trifluoroacetic acid (TFA) aqueous solution/0.05% TFA acetonitrile with linear gradient at a flow rate of 1 mL/min, and 10 µL injections using the autosampler in cycles of 9 min. The retention time was 4.2 min and correlation of the samples to the standard curve was of 0.9997. All experiments were done in triplicate and averaged. The analysis of the data was performed using Empower® 3 software (Waters Corp., Milford, MA, USA).

The data was then fitted to calculate rate constants (k_2) and adsorbed amounts in equilibrium (q_e) was done for a pseudo-second order models when possible following the equations (Tran et al., 2013).

$$\frac{t}{qt} = \frac{1}{h} + \frac{t}{qe} \quad (6.1)$$

where $h=k_2qe^2$, with k_2 being the pseudo-second order rate constant of sorption, respectively. qe is the amount of analyte adsorbed at equilibrium (mg/g), and qt is the amount of analyte adsorbed at any time (mg/g).

6.3.7. Characterization

6.3.7.1. TEMPO oxidized β-cyclodextrin (TOCD) titration.

Degree of oxidation (DO) was determined by pH titration methods, based on the calculations reported by da Silva Perez (da Silva Perez et al., 2003). For this, TOCD suspension was previously brought to pH 3 with 10 mM HCl, this to assure the protonation of all present acid moieties. After freeze drying, 30-40 mg of TOCD in acidic form were dissolved in 15 mL of 10 mM HCl and titrated with 10 mM NaOH by adding 1 mL every 5 min and measuring pH with a VWR symphony B30PCI multiprobe conductometer. The degree of oxidation was then calculated by the following equation:

$$DO = 162(V2 - V1)c/[w - 36(V2 - V1)c] \quad (6.2)$$

were V1 and V2 are the amount in L of NaOH used to reach the end points 1 and 2, respectively; c is the concentration of the base in mol L-1, and w is the dry weight of the sample. V1 and V2 were determined by the second derivative of pH curve (or conductivity curve), using the volumes where the graph crossed the origin.

6.3.7.2.Elemental Analysis (EA).

Freeze-dried samples were processed in an ECS 4010 Elemental Combustion System CHNS-O from Costech Analytical technologies, Inc (Firenze, Italy) and data analyzed with the ECS60 software. Carbon and Nitrogen content were collected and fitted into standard curves with correlations of 0.99996 and 0.9999799 for N and C respectively.

6.3.7.3.Fourier-transform infrared spectroscopy with attenuated total reflectance (FTIR-ATR).

Dried samples were analyzed for characterization of the surface modification on a PerkinElmer Spotlight 400 FT-IR Imaging System (Massachusetts, US) with an ATR accessory with diamond/ZnSe crystal and a resolution of 4 cm-1. First, a background spectrum with the clean sensor was measured; this was carried-out before each set of measurements with the same number of scans. To archive a high resolution at the spectrum bands, 128 scans per spectrum were performed. Data was processed with Spectrum 6 Spectroscopy Software (PerkinElmer, Massachusetts, US).

6.3.7.4.Thermogravimetric analysis (TGA).

After solvent exchange, dried samples were tested on aluminum pans in a TGA-50 from Shimadzu (Kyoto, Japan). Samples were heated from room temperature to 600 °C at a rate of 10 °C/min under a nitrogen atmosphere and data was processed with ta60 software version 2.11 from Shimadzu.

6.3.7.5.Scanning electron microscopy (SEM).

Dried aerogels were placed on aluminum studs and sputtered with gold for 45 s in a Q150R ES sputter coating device acquired form Electron Microscopy Sciences (Hatfield, PA, U.S.). Images were recorded using 20 kW, working distance between 6 and 8 mm in a Zeiss Evo 50VP scanning electron microscope (SEM).

6.3.7.6.Water uptake and swelling.

To calculate water uptake, the dried aerogels were immersed in 25 mL of ultrapure water, from which they were removed at regular time intervals up to 240 min and weighted. The averaged results for water uptake were calculated by the following equation.

$$Water\ uptake\ (\%) = \frac{Wt-Wd}{Wd} * 100 \quad (6.3)$$

where Wt is the weighted mass, and Wd is the dry weight of the aerogels. Meanwhile, for the swelling, the aerogels were left for 24 h in 20 mL of ultrapure water before weighting. The average results were then calculated with the next equation.

$$Swelling\ (\%) = \frac{Ws}{Wd} * 100 \quad (6.4)$$

where Ws is the weight obtain after swelling.

6.3.7.7.Density and porosity.

Dimensional measurement of the wood, nanowood and coated nanowood were done using a digital caliper and used to calculate volume and density (ρa), at least two distinct samples were measured. The porosity was then obtained by equation, where the density of the cellulose (ρc) was assumed to be 1460 kg/m3, as reported in literature (Sehaqui et al., 2011).

$$Porosity\ (\%) = 1 - \frac{\rho_a}{\rho_c} * 100 \quad (5)$$

6.4. Results and Discussion

6.4.1. TEMPO oxidation of β-cyclodextrin and grafting to chitosan.

One of the first indications of the success of the reaction was the red tint that the product acquired when frozen after the dialysis. When the titration was done to investigate the degree of oxidation (DO), the inflexion points were visualized by doing a second derivate to the pH curve. In Figure 6.1 it can be observed that the 13 and 18 mL, which after applying the equation 1 gave a DO of 0.27, which considering that only the hydroxyl groups from C6 can be modified (T. Saito et al., 2005) equals that 2 of every 7 glucose units are modified, or 2 on each β-cyclodextrin.

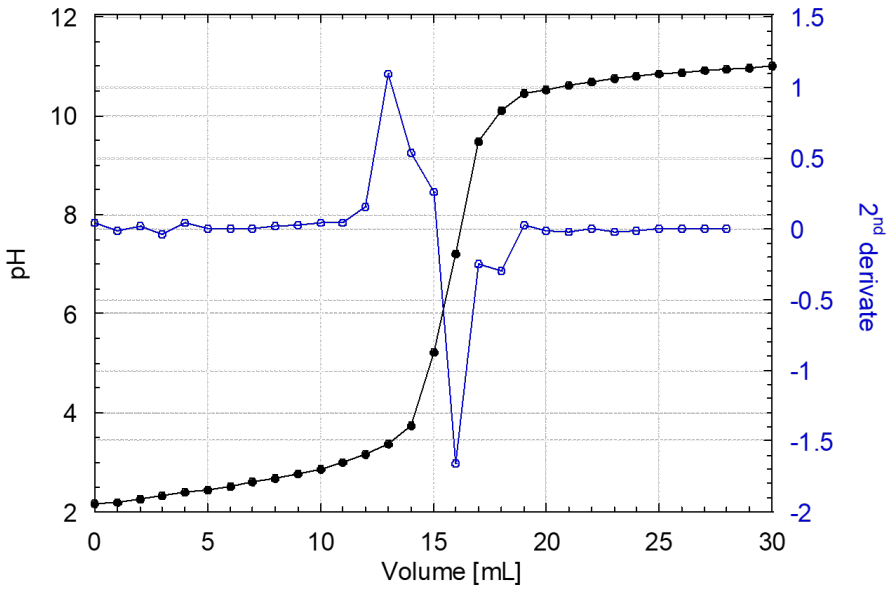

Figure 6.1. pH titration of TEMPO oxidized β-cyclodextrin (TOCD) and 2 derivate to identify inflexion groups for DO determination.

After determination of the DO on the TO-CD, the reaction with chitosan was calculated to be done into a 2:1 ratio between the amino and carboxyl groups. One of the main differences was the solubility in water of the modified Ch-CD, that did not need an acid pH to solubilized like the

pure chitosan. As a first test, C and N elemental analysis was done, showing a C/N ratio of 6.41 ± 0.01 for chitosan and 8.95 ± 0.4 for the grafted molecule. If the molecular weight is used to calculate the degree of substitution for the chitosan, then after grafting there is a DS of 0.57 from a possible maximum of 0.85 of the deacetylated groups. When the FTIR-ATR spectra of the samples were compared (Figure 6.2), it can be observed that the stretching C-H (2950 – 2800 cm^{-1}) of the grafted material fits in between the signals from the unmodified materials. Similar behavior is observed with the bending of the O-H (1600-1590 cm^{-1}). The signal of the carboxyl added (1750 cm^{-1}) to CD disappears in the grafted material, but the stretching of the C-N appears (1490 cm^{-1}), confirming the EDC/NHS reaction. Finally, the bending of the ring of chitosan is kept but slight shift to the blue is perceptible as a more pronounce shoulder, closer to the signal that is seen in the TOCD.

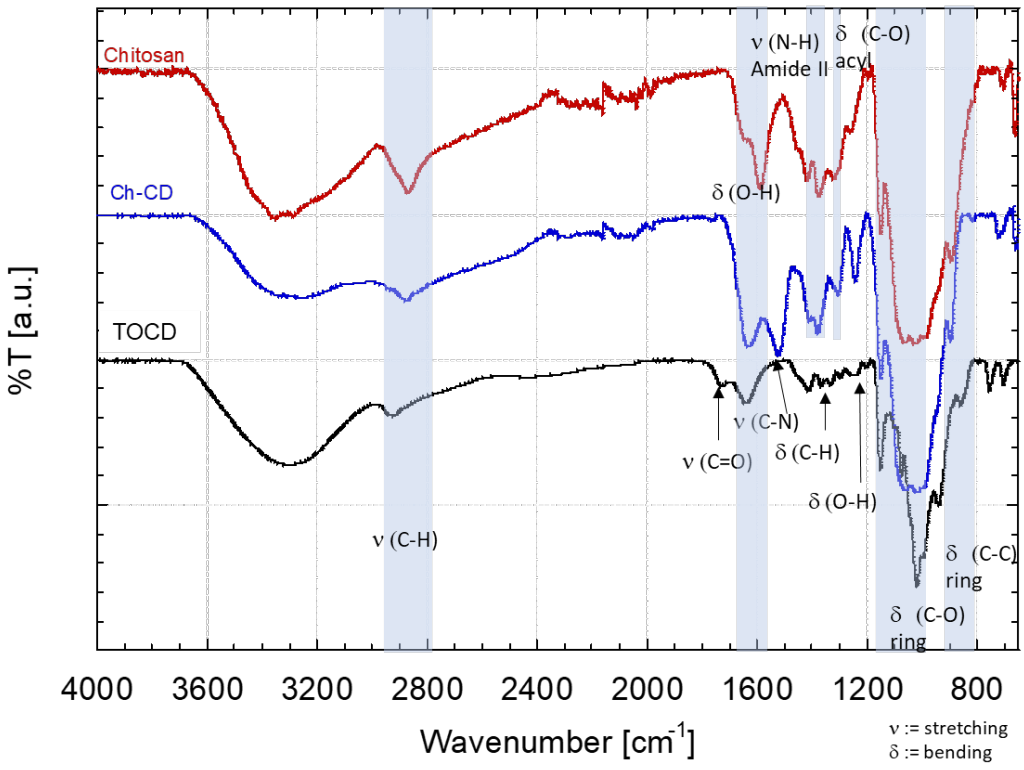

Figure 6.2. FTIR-ATR spectra of the TEMPO oxidized β-cyclodextrin (TOCD), chitosan and the grafter material of both (Ch-CD). There the formation of the C-N bond is visible ca. 1490 cm^{-1} as well as the reduction of the carboxyl bond at 1750 cm^{-1}added to TOCD, confirming the reaction.

6.4.2. Characterization of nanowood and coated nanowood.

For the chemical characterization, FTIR-ATR and TGA were done for wood, nanowood and after coating to compare each step on the preparation. In the FTIR-ATR spectra showed in Figure 6.3a, the higher difference is between the wood and the other two, as the wood has more bands related to the aromatic rings of lignin, its side chains as well as the side C-O and C-H groups of the hemicelluloses (Emmanuel et al., 2015). After extraction of most of the lignin, the spectrum is closer to the one of pure cellulose, with the bands related to bending of the polysaccharide rings having the highest intensity. As the coating material is meant to be only at the surface, the intensity of its signal is lower than the ones from the cellulose nanofibrils of the nanowood. However, some changes are clear; first there is a reduction on the C-H stretching close to 2900 cm^{-1}, this as the side groups have a more restricted movement and only the glucose side C-H on sp_3 configuration can better emit. Similarly, there is the apparition of a shoulder close to 1590 cm^{-1}, close to where the N-H amide stretching should appear, suggesting the presence of chitosan.

This modification can also be confirmed by the elemental analysis results shown in Table 6.1. The untreated wood had an average carbon content of 56.02 ± 4.1% and a nitrogen content of 0.055 ± 0.007%, close to values found in other wood-species (Martius, 1992; Strickland et al., 2009; Waliszewska et al., 2015). However, for the nanowood, the nitrogen content was removed, confirming the delignification and removal of other components besides of the cellulose and hemicelluloses, as the carbon content was of 52.09 ± 2.3%. Furthermore, after coating, nitrogen was again found in the material with a 0.015 ± 0.007% confirming the addition of the amino groups of the chitosan joined by a decrease on the C% to 47.54 ± 0.2% which can be a result of the oxygens added with the coating.

The difference between them is clearer in the thermogravimetrical analysis (Figure 6.3b). Between the wood and the nanowood there is little differences, with only 10 °C higher degradation of the nanowood and higher ash content afterward. The higher max temperature can be related to a faster degradation on the untreated wood due to the lignin, that when removed allows for a slower degradation as the lignin is not promoting it (Iglesias, Shivyari, et al., 2020). A contrary effect is observed after the coating, as the Ch-CD on the surface prone to a faster degradation and a stiffer slope than the other two materials, lowering the maximum degradation to 375 °C. The addition of these polysaccharides also lowered the residual content to a similar value than wood, as more oxygen was introduced in the structure with the coating.

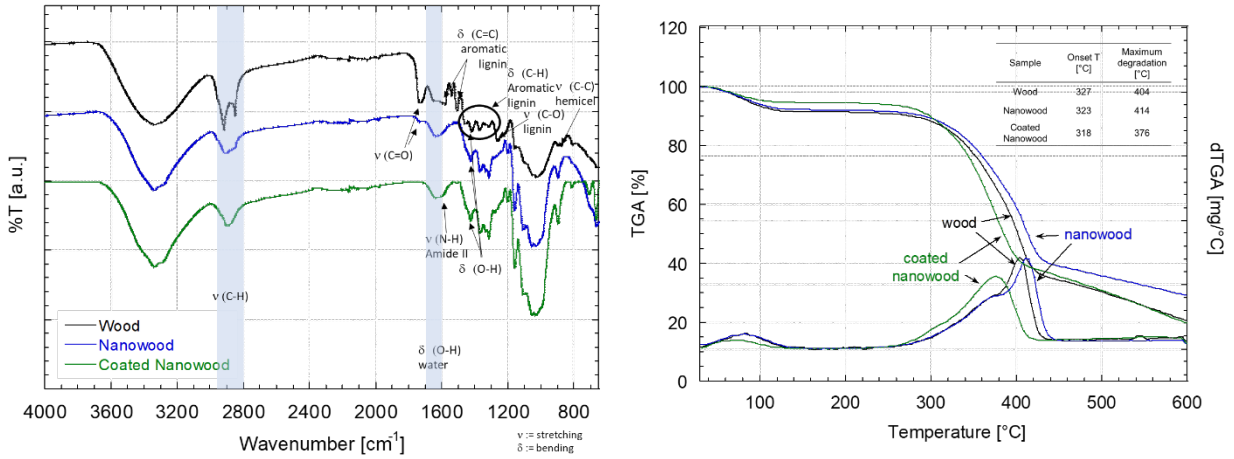

(a) (b)

Figure 6.3. (a) FTIR-ATR spectra of the wood, nanowood and coated nanowood and (b) shows the thermogravimetrical analysis of the three components with an insert table presenting the onset and max degradation temperatures of each one.

Table 6.1. Results from the elemental analysis of the wood, nanowood and coated nanowood.

Sample	% N	% C	C/N ratio
Wood	0.055 ± 0.007	56.02 ± 4.1	1018.6
Nanowood	0	52.09 ± 2.3	N/A
Coated Nanowood	0.015 ± 0.007	47.54 ± 0.2	3169.3

The first perceptible change between the samples is the loss of the color after delignification. The nanowood and the coated nanowood have higher dispersion of light, appearing white instead of the natural wood color of the pine wood pieces. Similarly, the density of the samples decreased to almost half after treatment. Furthermore, when the porosity and SEM images (Table 6.2) are compared between the different stages, the porosity increased about 10% after each step from 55.6 ± 3.28% to 75.1 ± 4.53% after delignification and coating with the Ch-CD. However, the more visible change is perceptible with the SEM images, where the structure changes from plate-like to a more cell-like structures, where the fibers are now noticeable after the delignification process. The difference is not visible in the SEM images with the molecular coating, but as mention above this change can be measured with the changes in porosity, which increased again, probably due to the new cavities introduced by the cyclodextrins.

Table 6.2. Porosity and SEM image comparison between pinewood before and after treatment.

System	Porosity [%]	SEM image
Wood 	55.6 ± 3.28	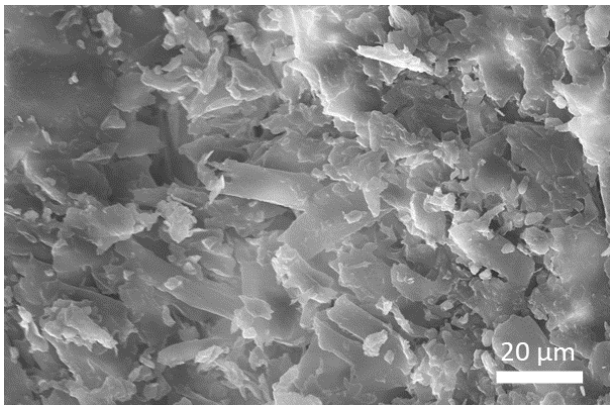
Nanowood 	65.8 ± 2.74	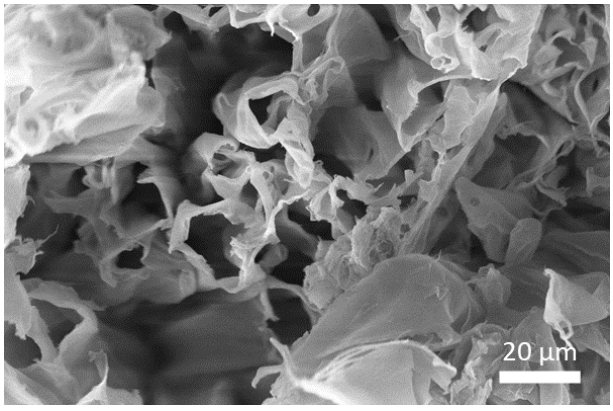
Coated nanowood 	75.1 ± 4.53	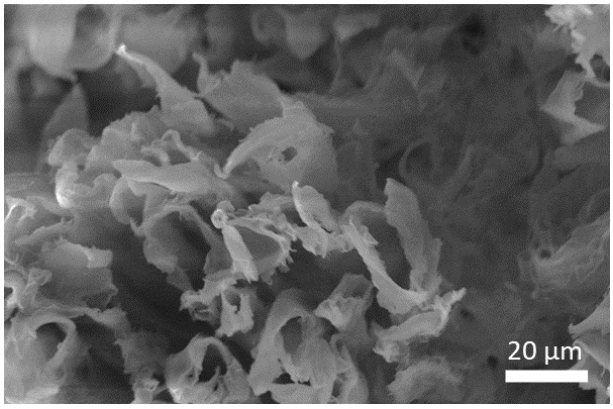

The difference between the coated nanowood and the pristine nanowood is also perceptible in their interactions with water. As a first observation, the untreated wood floated during most of

the swelling time, even if the mass did not change after sinking. Meanwhile, the nanowood coated and pristine, sank in the first couple minutes.

When the water uptake and swelling values were compared in Figure 6.4, the nanowood before coating was the one that took the most water, with almost 300% in equilibrium, while the untreated wood had only an increment of 100%. After coating, the nanowood decreased to 260%, which also indirectly suggest the surface modification after the adsorption of the Ch-CD material. Another interesting trend was that the wood reached stability before the other two materials, in less than 1 h, while the nanowood needed 2 h to reach similar stability. When the swelling was plotted, the behavior is maintained with the most swelling present in the nanowood, followed by the coated nanowood and the untreated wood in last.

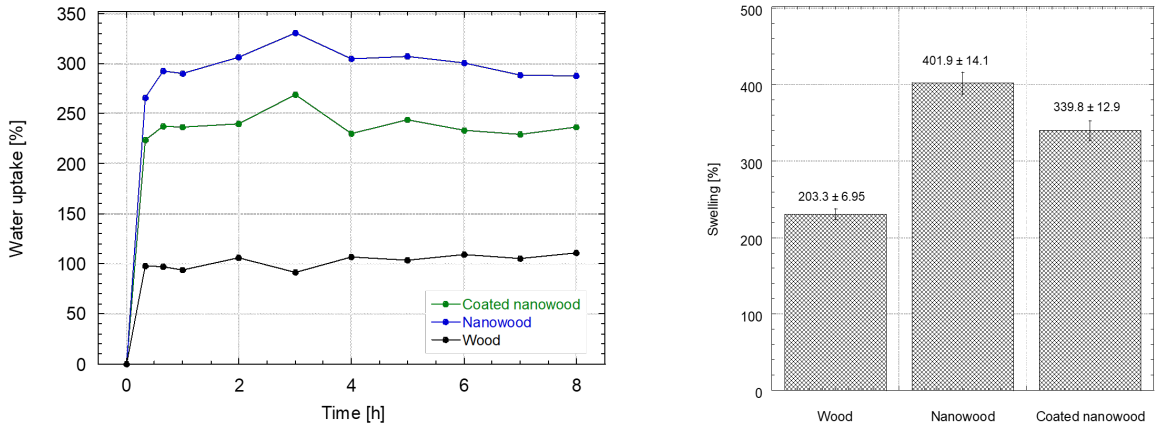

(a) (b)

Figure 6.4. (a) Plot comparing the water uptake on wood, nanowood and coated nanowood and (b) swelling percentage of each material after stability.

Reswelling test were also done of the materials. For this, a new solvent exchange was done to the swollen aerogels to dry them once more before letting them reswell on ultrapure water. The redrying was successful with no significant change on the initial mass in either of the three systems,

assessing that the coated material remained disregarding the different solvents. Similarly, the masses after swelling were not different to the ones obtained the first time, confirming the possibility of reusing the structures after redrying.

6.4.3. Microcystin adsorption

Whenever the aerogels were immersed in the solution containing the microcystin, in Figure 5 it can be observed that the wood and nanowood increased the concentration as water was absorbed on the dry material, but non-microcystin seem to be removed of the solution. This behavior is congruent with other literature using cellulose structures with microcystin (Tran et al., 2013) were there is no adsorption on the unmodified material. Furthermore, the decrease observed is like the swelling times that are presented in Figure 6.4.

In contrast, the nanowood coated with the chitosan-cyclodextrin polymer presented a clear adsorption since the beginning, with an adsorption peak at 40 min that is then decrease to a more stable value close to the q_e that was calculated with the kinetic of 0.12 mg/g. When the total removal of the microcystin was measured, a removal of 16% was measured at the end of the 360 min.

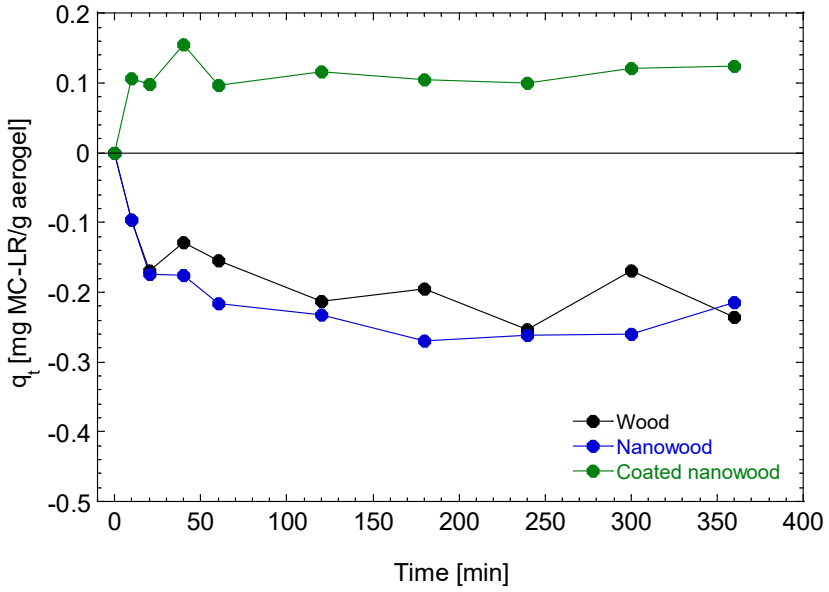

Figure 6.5. Adsorption kinetic of wood, nanowood and the coated nanowood on a 5.4 µg/mL on a solution for 6 h.

As mentioned before, the data was fitted into a pseudo-second kinetic model (Figure 6), the adsorption for wood and nanowood with -0.22 and -0.24 mg/g and R2 of 0.92 and 0.97. However, for the coated nanowood had a value of adsorption in equilibrium of 0.12 mg/g with a fitting of 0.98; even as the value is low, probably due to the surface not being saturated, it can be observed that the coating was successful in capturing the microcystin molecule driven by the hydrophobic cavities added with the coating. Furthermore, the half-time saturation was of only 0.84 min, indicating that the surface area and porosity was enough to allow the toxin to be captured easily without any energy input.

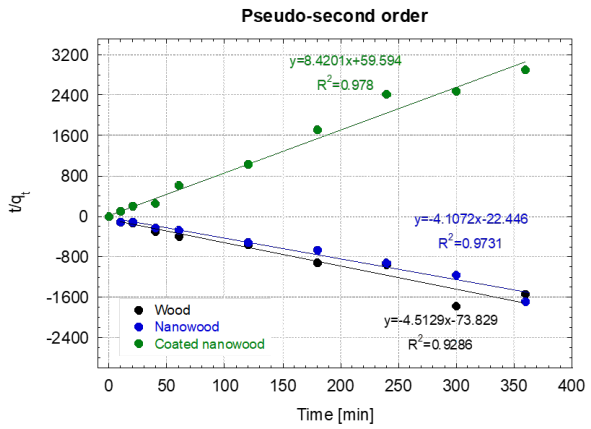

	Wood	Nanowood	Coated nanowood
q_e [mg/g]	-0.22	-0.24	0.12
h [mg/g min]	-0.01	-0.04	0.02
k_2 [g/mg min]	-0.27	-0.75	1.19
R^2	0.92	0.97	0.98
$t_{0.5}$ [min]	-3.62	-1.33	0.84

Figure 6.6. Pseudo-second order kinetic model and data of the adsorption of microcystin-LR with wood, nanowood and the coated nanowood.

6.5. Conclusions

This work proves that nano-porous bio-based aerogels can be generated by low-energy input procedures using a top-down approach instead of the more common bottom-up. The delignification of the wood to obtain the nanowood was achieved by a simple process that do not require extensive pressures or hard chemicals. The removal of the lignin allows the wood to increase its swelling 2 folds compared with the untreated wood to up to 400%. Furthermore, the solvent exchange process can be done more than once, allowing the easy regeneration of the material.

Beside the properties obtained after the delignification, the aerogels can be passively coated with the chitosan-cyclodextrin material that increased the surface reactivity by adding the hydrophobic cavity, which can be used to capture molecules with hydrophobic moieties as exemplified with the capturing of the microcystin toxin without sacrificing much of the swelling capacity of the material.

6.6. Future Work

As the capturing of the microcystin-LR was successful on the coated nanowood in lab-controlled conditions, the next step should be to evaluate it on spiked sample water from natural sources as the base conditions would be different than the ones controlled.

Furthermore, the levels of saturation of the coating on the surface should be tested to increase the removal capacity of the overall system, an the percentage of coverage is not known at the moment.

6.7. Literature Cited

Avila-Suarez, S., Palma-Rodriguez, H. M., Rodriguez-Hernandez, A. I., Hernandez-Uribe, J. P., Bello-Perez, L. A., & Vargas-Torres, A. (2013). Characterization of films made with chayote tuber and potato starches blending with cellulose nanoparticles. Carbohydrate Polymers, 98(1), 102–107. https://doi.org/10.1016/j.carbpol.2013.05.022

Ajdary, R., Tardy, B. L., Mattos, B. D., Bai, L., & Rojas, O. J. (2020). Plant Nanomaterials and Inspiration from Nature: Water Interactions and Hierarchically Structured Hydrogels. Advanced Materials, 2001085. https://doi.org/10.1002/adma.202001085

Archimandritis, A. S., Papadimitriou, T., Kormas, K. A., Laspidou, C. S., Yannakopoulou, K., & Lazarou, Y. G. (2016). Theoretical investigation of microcystin-LR, microcystin-RR and nodularin-R complexation with α-, β-, and γ-cyclodextrin as a starting point for the targeted design of efficient cyanotoxin traps. Sustainable Chemistry and Pharmacy, 3, 25–32. https://doi.org/10.1016/j.scp.2016.02.001

Awaja, F., Gilbert, M., Kelly, G., Fox, B., & Pigram, P. J. (2009). Adhesion of polymers. Progress in Polymer Science (Oxford), 34(9), 948–968. https://doi.org/10.1016/j.progpolymsci.2009.04.007

Chu, Z., Zheng, P., Yang, Y., Wang, C., & Yang, Z. (2020). Compressible nanowood/polymer composite adsorbents for wastewater purification applications. Composites Science and Technology, 198(April), 108320. https://doi.org/10.1016/j.compscitech.2020.108320

da Silva Perez, D., Montanari, S., & Vignon, M. R. (2003). TEMPO-mediated oxidation of cellulose III. Biomacromolecules, 4(5), 1417–1425. https://doi.org/10.1021/bm034144s

Dahl, G. F. (1884). Process of manufacturing cellulose from wood. In US Patent 0,002,969 35.

de Assis, C. A., Iglesias, M. C., Bilodeau, M., Johnson, D., Phillips, R., Peresin, M. S., Bilek, E. M. T., Rojas, O. J., Venditti, R., & Gonzalez, R. (2018). Cellulose micro- and nanofibrils (CMNF) manufacturing - financial and risk assessment. Biofuels, Bioproducts and Biorefining, 12(2), 251–264. https://doi.org/10.1002/bbb.1835

De France, K., Zeng, Z., Wu, T., & Nyström, G. (2020). Functional Materials from Nanocellulose: Utilizing Structure–Property Relationships in Bottom-Up Fabrication. Advanced Materials, 2000657. https://doi.org/10.1002/adma.202000657

Dong, H., Snyder, J. F., Tran, D. T., & Leadore, J. L. (2013). Hydrogel, aerogel and film of cellulose nanofibrils functionalized with silver nanoparticles. Carbohydrate Polymers, 95(2), 760–767. https://doi.org/10.1016/j.carbpol.2013.03.041

Emmanuel, V., Odile, B., & Céline, R. (2015). FTIR spectroscopy of woods: A new approach to study the weathering of the carving face of a sculpture. Spectrochimica Acta - Part A: Molecular and Biomolecular Spectroscopy, 136(PC), 1255–1259. https://doi.org/10.1016/j.saa.2014.10.011

Fernandes Diniz, J. M. B., Gil, M. H., & Castro, J. A. A. M. (2004). Hornification - Its origin and interpretation in wood pulps. Wood Science and Technology, 37(6), 489–494. https://doi.org/10.1007/s00226-003-0216-2

Gomez-Maldonado, D., Vega Erramuspe, I. B., Filpponen, I., Johansson, L.-S., Lombardo, S., Zhu, J., Thielemans, W., & Peresin, M. S. (2019). Cellulose-Cyclodextrin Co-Polymer for the Removal of Cyanotoxins on Water Sources. Polymers, 11(12), 2075. https://doi.org/10.3390/polym11122075

Guo, H., Fuchs, P., Cabane, E., Michen, B., Hagendorfer, H., Romanyuk, Y. E., & Burgert, I. (2016). UV-protection of wood surfaces by controlled morphology fine-tuning of ZnO nanostructures. Holzforschung, 70(8), 699–708. https://doi.org/10.1515/hf-2015-0185

Howard, J. L. (2016). U. S. Timber Production, Trade, Consumption, and Price Statistics, 1965 – 2013. February 1965–2013.

Howard, J. L., & Liang, S. (2019). U.S. Timber Production, Trade, Consumption, and Price Statistics, 1965-2017. July, 96.

Iglesias, M. C., Gomez-Maldonado, D., Via, B. K., Jiang, Z., & Peresin, M. S. (2020). Pulping processes and their effects on cellulose fibers and nanofibrillated cellulose properties: A review. Forest Products Journal, 70(1), 10–21. https://doi.org/10.13073/FPJ-D-19-00038

Iglesias, M. C., Shivyari, N., Norris, A., Martin- Sampedro, R., Eugenio, M. E., Lahtinen, P., Auad, M. L., Elder, T., Jiang, Z., Frazier, C. E., & Peresin, M. S. (2020). The effect of residual lignin on the rheological properties of cellulose nanofibril suspensions. Journal of Wood Chemistry and Technology.

Köhl, M., Lasco, R., Cifuentes, M., Jonsson, Ö., Korhonen, K. T., Mundhenk, P., de Jesus Navar, J., & Stinson, G. (2015). Changes in forest production, biomass and carbon: Results from the 2015 UN FAO Global Forest Resource Assessment. Forest Ecology and Management, 352, 21–34. https://doi.org/10.1016/j.foreco.2015.05.036

Li, Y., Fu, Q., Rojas, R., Yan, M., & Lawoko, M. (2017). Lignin-Retaining Transparent Wood. 3445–3451. https://doi.org/10.1002/cssc.201701089

Lombardo, S., & Villares, A. (2020). Engineered Multilayer Microcapsules Based on Polysaccharides Nanomaterials. Molecules, 25(19), 4420. https://doi.org/10.3390/molecules25194420

Mao, J., Li, S., He, C., Tang, Y., Chen, Z., Huang, J., & Lai, Y. (2019). Robust amphiprotic konjac glucomannan cross-linked chitosan aerogels for efficient water remediation. Cellulose, 26(11), 6785–6796. https://doi.org/10.1007/s10570-019-02549-z

Martius, C. (1992). Density, humidity, and nitrogen content of dominant wood species of floodplain forests (várzea) in Amazonia. Holz Als Roh- Und Werkstoff, 50(7–8), 300–303. https://doi.org/10.1007/BF02615357

Meriluoto, J., & Codd, G. A. (2005). Cyanobacterial Monitoring and Cyanotoxin Analysis. https://doi.org/10.1002/9781119068761

Mishima, T., Hisamatsu, M., York, W. S., Teranishi, K., & Yamada, T. (1998). Adhesion of β-D-glucans to cellulose. Carbohydrate Research, 308(3–4), 389–395. https://doi.org/10.1016/S0008-6215(98)00099-8

Munang, R., Thiaw, I., Thompson, J., Ganz, D., Girvetz, E., & Rivington, M. (2011). Sustaining Forests: Sustaining forests: Investing in our common future (Issue 5).

Oksman, K., Mathew, A. P., Pia Qvintus, A. B., Rojas, O., & Sain, M. (2014). Handbook of Green Materials, Bionanomaterials: separation processes, characterization, and properties Vol.5. https://doi.org/10.1142/8975

Orelma, H., Filpponen, I., Johansson, L. S., Laine, J., & Rojas, O. J. (2011). Modification of cellulose films by adsorption of cmc and chitosan for controlled attachment of biomolecules. Biomacromolecules, 12(12), 4311–4318. https://doi.org/10.1021/bm201236a

Orelma, H., Virtanen, T., Spoljaric, S., Lehmonen, J., Seppälä, J., Rojas, O. J., & Harlin, A. (2018). Cyclodextrin-Functionalized Fiber Yarns Spun from Deep Eutectic Cellulose Solutions for Nonspecific Hormone Capture in Aqueous Matrices. Biomacromolecules, 19(2), 652–661. https://doi.org/10.1021/acs.biomac.7b01765

Pettersen, R. C., & Rowell, R. M. (1984). The Chemical Compostition of Wood. In R. Rowell (Ed.), The chemistry of solid wood (Issue 2, pp. 57–126). American Chemical Society. https://doi.org/10.1021/ba-1984-0207.ch002

Pillai, K., Navarro Arzate, F., Zhang, W., & Renneckar, S. (2014). Towards Biomimicking Wood: Fabricated Free-standing Films of Nanocellulose, Lignin, and a Synthetic Polycation. Journal of Visualized Experiments, 88, 1–14. https://doi.org/10.3791/51257

Prabaharan, M., & Mano, J. F. (2005). Hydroxypropyl chitosan bearing β-cyclodextrin cavities: Synthesis and slow release of its inclusion complex with a model hydrophobic drug. Macromolecular Bioscience, 5(10), 965–973. https://doi.org/10.1002/mabi.200500087

Rojas, O. J. (2014). Outlook for nanocellulose production and materials Function of the Nanomaterial Anticaking agent Antimicrobial Filtration Hardness and Sorbent. 2017, 1–22.

Rowell, R., Pettersen, R., & Tshabalala, M. (2012). Cell Wall Chemistry. In Handbook of Wood Chemistry and Wood Composites, Second Edition (pp. 33–72). https://doi.org/10.1201/b12487-5

Saito, T., Shibata, I., Isogai, A., Suguri, N., & Sumikawa, N. (2005). Distribution of carboxylate groups introduced into cotton linters by the TEMPO-mediated oxidation. Carbohydrate Polymers, 61(4), 414–419. https://doi.org/10.1016/j.carbpol.2005.05.014

Saito, Tsuguyuki, Hirota, M., Tamura, N., Kimura, S., Fukuzumi, H., Heux, L., & Isogai, A. (2009). Individualization of Nano-Sized Plant Cellulose Fibrils by Direct Surface Carboxylation

Using TEMPO Catalyst under Neutral Conditions. Biomacromolecules, 10(7), 1992–1996. https://doi.org/10.1021/bm900414t

Saito, Tsuguyuki, Nishiyama, Y., Putaux, J. L., Vignon, M., & Isogai, A. (2006). Homogeneous suspensions of individualized microfibrils from TEMPO-catalyzed oxidation of native cellulose. Biomacromolecules, 7(6), 1687–1691. https://doi.org/10.1021/bm060154s

Sehaqui, H., Zhou, Q., & Berglund, L. A. (2011). High-porosity aerogels of high specific surface area prepared from nanofibrillated cellulose (NFC). Composites Science and Technology, 71(13), 1593–1599. https://doi.org/10.1016/j.compscitech.2011.07.003

Sixta, H. (2006). Handbook of pulp (Vol. 1). Wiley Online Library.

Smith, S., Goodge, K., Delaney, M., Struzyk, A., Tansey, N., & Frey, M. (2020). A comprehensive review of the covalent immobilization of biomolecules onto electrospun nanofibers. Nanomaterials, 10(11), 1–39. https://doi.org/10.3390/nano10112142

Solala, I., Iglesias, M. C., & Peresin, M. S. (2020). On the potential of lignin-containing cellulose nanofibrils (LCNFs): a review on properties and applications. Cellulose, 27(4), 1853–1877. https://doi.org/10.1007/s10570-019-02899-8

Strickland, M. S., Osburn, E., Lauber, C., Fierer, N., & Bradford, M. A. (2009). Litter quality is in the eye of the beholder: Initial decomposition rates as a function of inoculum characteristics. Functional Ecology, 23(3), 627–636. https://doi.org/10.1111/j.1365-2435.2008.01515.x

Sullivan, R. K., Erickson, M., & Oyanedel-Craver, V. A. (2017). Understanding the microbiological, organic and inorganic contaminant removal capacity of ceramic water filters doped with different silver nanoparticles. Environmental Science: Nano, 4(12), 2548–2555. https://doi.org/10.1039/c7en00443e

Toivonen, M. S., Kaskela, A., Rojas, O. J., Kauppinen, E. I., & Ikkala, O. (2015). Ambient-Dried Cellulose Nanofibril Aerogel Membranes with High Tensile Strength and Their Use for Aerosol Collection and Templates for Transparent, Flexible Devices. Advanced Functional Materials, 25(42), 6618–6626. https://doi.org/10.1002/adfm.201502566

Toivonen, M. S., Kurki-Suonio, S., Schacher, F. H., Hietala, S., Rojas, O. J., & Ikkala, O. (2015). Water-Resistant, Transparent Hybrid Nanopaper by Physical Cross-Linking with Chitosan. Biomacromolecules, 16(3), 1062–1071. https://doi.org/10.1021/acs.biomac.5b00145

Tran, C. D., Duri, S., Delneri, A., & Franko, M. (2013). Chitosan-cellulose composite materials: Preparation, Characterization, and application for removal of microcystin. Journal of Hazardous Materials, 253, 355–366.

Waliszewska, B., Pradzynski, W., Zborowska, M., Stachowiak-Wencek, A., Waliszewska, H., & Spak-Dzwigala, A. (2015). The diversification of chemical composition of pine wood depending on the tree age. Annals of Warsaw University of Life Sciences - SGGW. Forestry and Wood Technology, 91, 182–187.

Woods, S. (2016). A History of Wood from the Stone Age to the 21st Century | Architect Magazine. Ecobuilding Pulse. https://www.architectmagazine.com/technology/products/a-history-of-wood-from-the-stone-age-to-the-21st-century_o

Wu, M. B., Huang, S., Liu, C., Wu, J., Agarwal, S., Greiner, A., & Xu, Z. K. (2020). Carboxylated wood-based sponges with underoil superhydrophilicity for deep dehydration of crude oil. Journal of Materials Chemistry A, 8(22), 11354–11361. https://doi.org/10.1039/d0ta03844j

Zeng, D., Wu, J., & Kennedy, J. F. (2008). Application of a chitosan flocculant to water treatment. Carbohydrate Polymers, 71(1), 135–139. https://doi.org/10.1016/j.carbpol.2007.07.039

Zhu, M., Song, J., Li, T., Gong, A., Wang, Y., Dai, J., Yao, Y., Luo, W., Henderson, D., & Hu, L. (2016). Highly Anisotropic, Highly Transparent Wood Composites. Advanced Materials, 28(26), 5181–5187. https://doi.org/10.1002/adma.201600427

7. Adsorption of microcystin-LR by coated nanowood aerogels from spiked samples of Lake Ogletree of Auburn, AL

7.1. Abstract

To assess the viability of the generated delignified wood aerogels -nanowood- coated with chitosan-cyclodextrin co-polymer on close to real conditions, surface water from Lake Ogletree was obtained and spiked with microcystin-LR to follow the sorbent adsorption capacity. The generated nanowood was coating by immersion on a 2 mg/mL chitosan-cyclodextrin copolymer in a acetate buffer solution and characterized by gravimetry, elemental analysis and Fourier Transformed Infrared. pH, conductivity, ion concentration, and total dissolved solids of the sampled water were also measured prior to spiking. The results showed that the coated nanowood (CNW) was not able to adsorb any toxin under these conditions, probably due by low salt concentrations which favor water adsorption and other more hydrophobic molecules rather than MC.

7.1.1. Index Words

Wood aerogels, active coatings, chitosan, β-cyclodextrin, cyanotoxins, water treatment, natural water sample.

7.1.2. Project Partners

The Forest Products Development Center worked in collaboration with the School of Pharmacy, and the Department of Crops, Soils and Environmental Science from Auburn University and with the Soil, Forage & Water Testing Laboratory of Auburn University and the Alabama Agricultural Experiment Station. This research was supported by the Alabama

Agricultural Experiment Station, and the Hatch program of the National Institute of Food and Agriculture, United States Department of Agriculture. The School of Forestry and Wildlife Sciences at Auburn University financial support to complete this work is greatly appreciated.

7.2. Introduction

Access to clean water is one of the main human rights, however 29% of the population do not have access to it, even after a 30-minute round trip to the closest source (World Health Organization, 2019). Furthermore, it is estimated that by 2025, half of the global population will be living in water-stressed areas (World Health Organization, 2019). Even in places where surface water is available and could be easily processed to make drinkable, recurrent algae blooms threat these sources by increasing the concentration of harmful byproducts such as microcystin-LR (Carmichael & Boyer, 2016; Grattan et al., 2016; Pam Wright, 2018; Wells et al., 2015).

In the city of Auburn, located in the state of Alabama, U.S., the main water source is Lake Ogletree which contains an estimated 1.7 billion gallons of clean water and is supplied by the Chewacla Creek and its tributaries Nash Creek and Robinson Creek, all located in the Chewacla watershed (SunCrest Laboratories, 2010). The city of Auburn has permitted an extraction capacity of 8 million gallons/day (MGD), with the remaining water needs met by Well No. 3 (1.3 MGD) and the Saugahatchee Lake from Opelika, AL (3.6 MGD) (Water Resource Management - City of Auburn, 2020). The normal consumption is 7.2 MGD which means that most water comes from the main lake. Once the water is extracted from the lake, it is subjected to flocculation through addition of alum, followed by a sedimentation basin and filtration to eliminate particles and the abundant metamorphic rock, sand and silt. Thereafter, sodium hypochlorite, lime, fluoride, and anticorrosion compounds (zinc) are mixed before being distributed to customers (Figure 7.1).

Organic byproducts are often formed due to the described disinfection process. These byproducts are also considered pollutants such as haloacetic acids, chloroacetic acids. Additionally, this process are not able to eliminate natural erosion components such as copper, lead and other metals, or leaching of agricultural runoffs (i.e., nitrate). Even more, some upstream discharged elements also remain, such as barium (The Water Works Board of The City of Auburn, 2019). Finally, toxins and other organic molecules have been detected from the water purchased from the Opelika service, resulting in the halt of import of water from there until the concentration has decreased (Dorton, 2019) but without any active removal of the toxins.

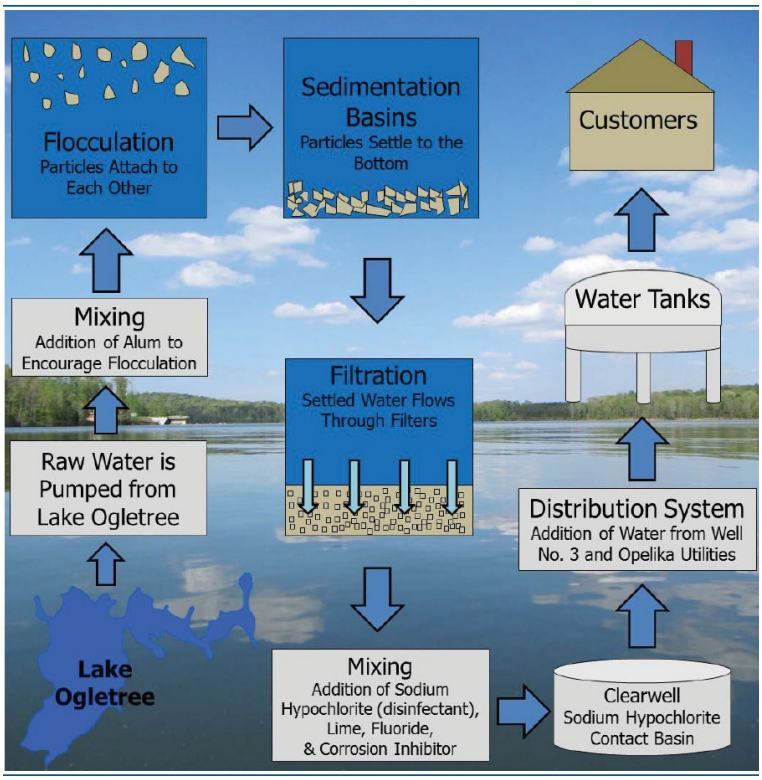

Figure 7.1. Water Treatment Process of the City of Auburn (The Water Works Board of The City of Auburn, 2019).

Like these toxins, other emerging contaminants that are not currently stated in the regulations to be removed and monitored for drinking water exist (Rosenfeld & Feng, 2011; USEPA - Office of Ground Water and Drinking Water, 2017). Nevertheless, new technologies are

being developed to efficiently remove them from water sources, most of which also are considering the use of natural-derived materials to decrease the carbon footprint of the processes and avoid cross contamination (Ali, 2012; Gomez-Maldonado, Vega Erramuspe, & Peresin, 2019).

Interestingly, most of these adsorbents are based on passive filtration driven by molecular interactions (Abbas et al., 2020; Ahmad et al., 2015; Blackburn, 2004; Tran et al., 2013) or by reduction of the entropy via hydrophobic complexation (Archimandritis et al., 2016; Gomez-Maldonado, Vega Erramuspe, Filpponen, et al., 2019; Ozmen et al., 2008; Sinha & Jana, 2015). Overall, the adsorption capacity in 3D structures is mostly limited by the surface area in contact with the contaminated water (Adebajo et al., 2003; Chu et al., 2020). As microcystin-LR is an amphipathic molecule, meaning that it has a hydrophobic section and charged residues, the use of cyclodextrins has been proved to remove them efficiently by capturing the hydrophobic (2S,3S,8S,9S)-3-Amino-9-methoxy-2,6,8-trimethyl-10-phenyldeca-4,6-dienoic acid (ADDA) residue in position 5 in complexes with the hydrophobic center of the cyclodextrin structure (Archimandritis et al., 2016; Gomez-Maldonado, Vega Erramuspe, Filpponen, et al., 2019; Ozmen et al., 2008; Sinha & Jana, 2015).

As the recurrence of algae blooms is estimated to rise due to global warming (Wells et al, 2015), in this work we focus on the generation of a bio-based nanoporous aerogel with functional cyclodextrin hydrophobic cavities available in the surface. The aerogel was generated in a top-down approach to decrease energy inputs generally consequent of the breaking down of the lignocellulosic source and rebuild of the cellulose materials to nanoporous structures by bottom-up approaches. Furthermore, the cyclodextrins was pre-grafted to chitosan by the green method of NHS/EDC reaction, and attached to the aerogel by passive adsorption in 50 mM ionic strength buffer. This approach facilitates the natural tendency of β(1→4)polysaccharides to irreversibly

adsorb to each other (Mishima et al., 1998; Orelma et al., 2011). Once the material was obtained, water samples of the Lake Ogletree were collected, characterized, and spiked with a known concentration of the microcystin-LR toxin, to then follow the adsorption of the toxin on the material using High-Pressure Liquid Chromatography (HPLC).

7.3.**Materials and Methods**

7.3.1. Materials

Pine wood was obtain from the School of Forestry and Wildlife Science at Auburn University; β-cyclodextrin (CD, > 95 % purity) and N-hydroxysuccinimide (NHS, 98.0% purity) were purchased from Tokyo Chemical Industry (Portland, OR, U.S.); chitosan (DSacetylation of 0.15, MRU 167.3 g/mol) and octane (98 + %) were purchased from Alfa Aesar (Haverhill, MA, U.S.); microcystin-LR (MC, > 95 %) was purchase from Cayman Chemicals (Ann Arbor, MI, U.S.); sodium hydroxide (50 % w/w) was obtained from J.T. Baker (Phillipsburg, NJ, U.S.); sodium chlorite (80% purity) was purchased from BeanTown Chemical (Hudson, NH, U.S.); sodium hypochlorite (12.5 % w/w, 2 M in water), peroxide (35% w/w) and Isopropanol were obtained from VWR chemicals (Radnor, PA, U.S.); sodium sulfate (Na2SO3) was bought from Fisher Scientific company (Walthman, MA, U.S.); sulfuric acid (72% w/w) was obtained from Ricca Chemical company (Arlington, TX, U.S.); 2,2,6,6-tetramethylpiperidinooxy (TEMPO, 98 % purity) was bought from Acros Organics (Geel, Belgium); 3-(3-Dimethylaminopropil)-1-ethyl-carbodiimide hydrochloride (EDC, 99.9% purity) was obtained from Chem-Impex International (Wood Dale, IL, U.S.);. ethanol (200 proof pure) purchased from Decon Labs, Inc. (King of Prussia, PA, U.S.); The water used was deionized and purified with a Thermo Scientific Barnstead

Nanopure (18.2 MΩ cm). Unless specified, all the weights in this paper are expressed in oven dry basis.

7.3.2. Water sample of Lake Ogletree

Water samples were obtained by immersing one-gallon bottles at least 15 m from the shore of Lake Ogletree (Figure 2, coordinates 32.55, -85.43) the 30th of January 2021 at 13:30; outside temperature was 14°C. Samples were stored at 4°C until further use. Conductivity and pH were measured using a VWR B30PCI potentiometer (Radnor, PA, U.S.), while total dissolved solids (TDS) were obtained with a ZeroWater (Zero Technologies LLC, Trevose, PA, U.S.) tested at least 10 times in the different samples obtained and averaged. The results of TDS were validated repeating test while following the SM 2540C (Baird et al., 2017). Ion concentrations were calculated by Ion Chromatography coupled with Argon Plasma by the Soil Testing Laboratory of the Department of Agronomy and Soils from Auburn University and Alabama Agricultural Experiment Station, Alabama Cooperative Extension System.

Figure 7.2. Location where the water samples were obtained.

7.3.3. Synthesis of TEMPO oxidized β-cyclodextrin (TOCD).

β-cyclodextrin was carboxylated by neutral TEMPO-NaClO-$NaClO_2$ oxidation in aqueous media. (Orelma et al., 2018; Saito et al., 2009). For this, 5 g of β-cyclodextrin were dissolved in 450 mL of sodium phosphate buffer (0.05 M, pH 6.8). Then 0.08 g of TEMPO (0.1 mmol/g) and 5.65 g sodium chlorite (80 %, 10 mmol) were added to the cyclodextrin solution. Simultaneously, the 2 M sodium hypochlorite stock solution was diluted to a 0.1 M in the same buffer and 23 mL of this dilution were added in one step to the reactive solution to obtain a final concentration of 5 mmol (1.0 mmol NaClO/g of CD). The reaction was conducted in a closed flask for 19.5 h under ambient condition and a constant stirring of 500 rpm. After modification, TEMPO-oxidize β-cyclodextrin (TOCD) was purified by dialysis against ultrapure water (18.2 Ω) in a 100-500 Da dialysis membrane tube, then freeze-dried.

7.3.4. Synthesis of chitosan-cyclodextrin polymers (Ch-CD).

The synthesis of Ch-CD was performed considering a 2:1 molar ratio of the functional groups COOH:NH (TOCD:Ch) in a total of 100 mL volume with the same steps sequence. First, the TOCD was dissolved in 1% acetic acid (250 mg) to obtain a final concentration of 0.05%, then pre-dissolved EDC was added to obtain a final concentration of 0.05 M EDC and let stir before adding a pre-dissolved NHS to obtain a final concentration of 0.2 M NHS. From a stock solution of chitosan (1% in 1% acetic acid, w/w), the corresponding milliliters were added to obtain a 0.05% solution. The reaction was left for 24 h before stopping it by adding ethanol-amide (122 µL) to obtain a final concentration of 0.1 M. Purification and concentration was done by washings in 50 KDa Pall-membrane centrifugation tubes (Macrosep Advance Centrifugal Device, Pall Corporation) at 3000 rpm for 45 min each time.

7.3.5. Delignified wood aerogels (nanowood) obtention.

The delignification process was adapted from Zhu et al. (2016). Briefly, wood pieces cut perpendicularly to the growth axis (10x10x3 mm) were immersed in 100 mL of 2.5 M NaOH, 0.4 M Na2SO3 and left boil for 8 h. Thereafter, the samples were rinsed with hot water and placed in another 100 mL of 2.5 M H2O2 and boiled for 1 h. The samples were then rinsed with cold DI water and placed in ethanol overnight to eliminate water excess. Solvent was then exchanged 3-4 times with fresh isopropanol and left overnight; the same was done with octane which was left to air dry after overnight exchange (ca. 72 h).

7.3.6. Coating of wood aerogels and characterization

Treated dry wood pieces were immersed in 10 mL of acetate buffer 50 mM (ionic strength was adjusted to the same molarity with NaCl) containing 2 mg/mL of the Ch-CD polymer. The

nanowood was left in the solution for 24 h, then they were rinsed with ultrapure water until no changes in conductivity were measured. To assess correct coating, the mass changes were followed and described by the following equation:

$$\text{Mass change (\%)} = (mf-mi)/mi \times 100\ \% \quad (7.1)$$

where mf is final mass and mi is the initial mass before treatment or coating.

Coated and untreated wood were also studied by Fourier-transform infrared spectroscopy with attenuated total reflectance (FTIR-ATR) to assess the introduction of the coating; for this aerogel samples were placed on a PerkinElmer Spotlight 400 FT-IR Imaging System (Massachusetts, US) with an ATR accessory with diamond/ZnSe crystal and a resolution of 4 cm-1. First, a background spectrum with the clean sensor was measured; this was carried-out before each set of measurements with 128 scans. To archive a high resolution at the spectrum bands, 128 scans per spectrum were performed. Data was processed with Spectrum 6 Spectroscopy Software (PerkinElmer, Massachusetts, US). Elemental analysis was performed for both samples as well in an ECS 4010 Elemental Combustion System CHNS-O from Costech Analytical technologies, Inc (Firenze, Italy) and data analyzed with the ECS60 software. Carbon and Nitrogen content were collected and fitted into standard curves with correlations of 0.99996 and 0.9999799 for N and C, respectively.

7.3.7. Adsorption of microcystin-LR (MC) by High Pressure Liquid Chromatography (HPLC).

For the analysis of the adsorption of the untreated wood, and coated nanowood of the microcystin, pre-swelled materials -on ultrapure water- were placed in 28 mL of water obtained from Lake Ogletree spiked with microcystin-LR in a concentration of 5.4 µg/mL at room temperature and constant stirring. 150 µL aliquots were taken at the corresponding time and

analyzed in a Waters Alliance HPLC (Model No. e2695, Waters Corp., Milford, MA, USA) system equipped with a solvent management system 2695 and detected by a photodiode array detector (PDA, 2998). The system also counts with a thermostatically controlled column compartment and an autosampler. The method used was adapted from the one described by Meriluoto & Spoof (Meriluoto & Codd, 2005). Briefly, a C-18 column (55x4 mm) was used as stationary phase, and 0.05% trifluoroacetic acid (TFA) aqueous solution/0.05% TFA acetonitrile with linear gradient at a flow rate of 1 mL/min, and 10 µL injections using the autosampler in cycles of 9 min. The retention time was 4.2 min and correlation of the samples to the standard curve was of 0.9997. All experiments were done in triplicate and averaged. The analysis of the data was performed using Empower® 3 software (Waters Corp., Milford, MA, USA).

The data was then fitted to calculate rate constants (k2) and adsorbed amounts in equilibrium (qe) was done for a pseudo-second order models when possible following the equations (Tran et al., 2013).

$$t/qt=1/h+t/qe \quad (7.2)$$

where h=k2qe2, with k2 being the pseudo-second order rate constant of sorption, respectively. qe is the amount of analyte adsorbed at equilibrium (mg/g), and qt is the amount of analyte adsorbed at any time (mg/g).

7.4. Results and discussion

7.4.1. Lake water characterization

Lake water properties are presented in Table 7.1. The measured value of pH was 0.4 points above the 2019 annual report, while the TDS were a fifth lower (The Water Works Board of The City of Auburn, 2019). Overall, the properties of the water presented little change after the

potabilization process, which further indicates the acceptable properties of the lake water for human consumption.

When the ion concentration was measured, the only quantifiable ones were calcium, sodium, magnesium, potassium, sulfate, nitrate, and aluminum. From these, the cations are known to interact with cellulose fibers to improve swelling (Stana-Kleinschek et al., 1999); while nitrate and sulfates are most likely related to agricultural runoffs and are the elements directly necessary for the occurrence of algae blooms (Boopathi & Ki, 2014).

Table 7.1. Characterization of the water obtained from Lake Ogletree.

Property	Value
pH	7.67 ± 0.11
Conductivity [µS/cm]	61.7 ± 0.14
Total dissolved solids [ppm]	20.2 ± 0.21
Calcium [ppm]	5.00 ± 0.00
Potassium [ppm]	2.00 ± 0.00
Magnesium [ppm]	3.00 ± 0.00
Phosphorus [ppm]	<0.1
Aluminum [ppm]	0.25 ± 0.07
Arsenic [ppm]	< 0.1
Boron [ppm]	< 0.1
Cadmium [ppm]	< 0.1
Chromium [ppm]	< 0.1
Copper [ppm]	< 0.1
Iron [ppm]	< 0.1

Manganese [ppm]	< 0.1
Sodium [ppm]	5.00 ± 0.00
Nickel [ppm]	< 0.1
Lead [ppm]	< 0.1
Zinc [ppm]	< 0.1
Sulfate – Sulfur [ppm]	1.5 ± 0.71
Nitrate-Nitrogen [ppm]	0.4 ± 0.00

7.4.2. Coated Nanowood characterization

Weight of coated nanowood material was 1.38 ± 0.23% higher than the nanowood after the delignification process, indicating the successful coating of the nanowood. Furthermore, elemental analysis data (Table 7.2), showed 0.05 ± 0.0% nitrogen content, which is 0.035% higher than the results obtained when a quarter of the concentration of the coating was used in chapter 6. However, in this instance it was noticed that the coating was present on the more external layers, as evidenced by the absence of nitrogen in nanowood core samples.

FTIR-ATR spectra (Figure 7.3) shows the differences between the wood and the coated-nanowood. The higher difference between the two are the bands related to the aromatic rings of lignin, the side chains of this polymer as well as the side C-O and C-H groups of the hemicelluloses (Emmanuel et al., 2015). Like explained previously, the coating material is expected to be only at the surface; therefore, the intensity of its signals is lower than the others presented from both the untreated wood and the nanowood. However, the presence of the signal around 1590 cm^{-1}, the band related to N-H amide stretching confirms the presence of chitosan. While the bands at 700

cm^{-1} indicates the presence of α-C-O-C, which can only come from the β-cyclodextrin attached in the coating (Jiang et al., 2018).

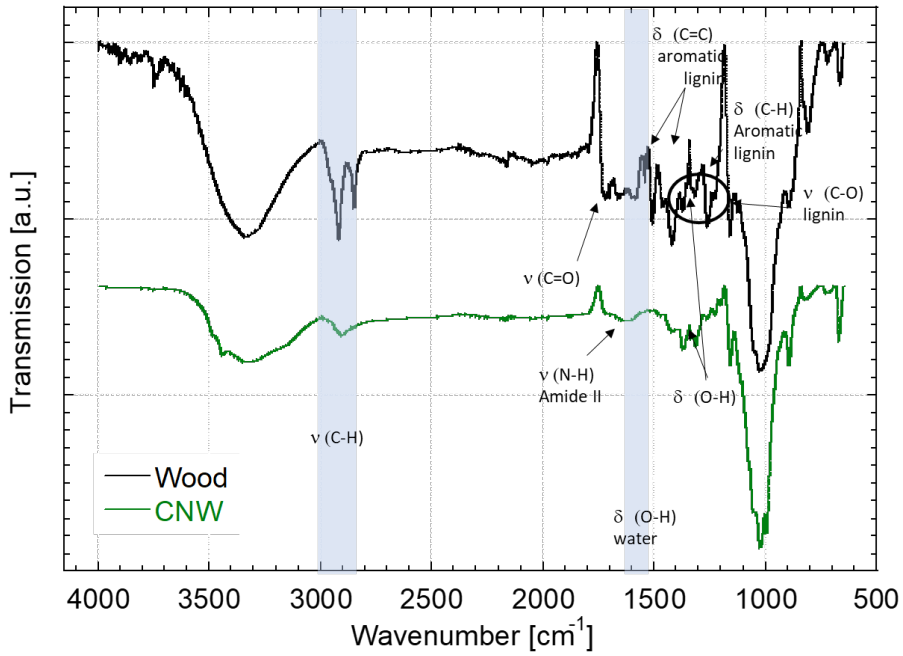

Figure 7.3. FTIR-ATR spectra of the wood and coated nanowood.

7.4.3. Adsorption of microcystin from the spiked Ogletree water

The adsorption of the toxin in the spiked water was followed for 6 h (Figure 7.4). Uncoated wood presented some adsorption, while the coated nanowood did not, contrary to the results observed on Chapter 6. The main difference that could affect the adsorption capacity of the material is attributed to ion concentration, which for the buffer used in the previous chapter had a conductivity of 1841.1 ± 0.11 µS/cm, which is almost 30 folds higher that the conductivity on the water obtained from the lake. This has a high impact on the formation of the inclusion complexes between the cyclodextrins and amphipathic molecules, like in this case, MC (Kotake & Janzen, 1989; Zhu et al., 2017). The presence of higher saline content, increases the ability of the active

coating to capture more microcystin, which was low in this case, making the adsorption of water onto the surface of the coating and nanofibrils the preferred route.

Similarly, porosity of the nanowood was higher than the original wood as expected, also presenting higher water swelling in ultrapure water. Furthermore, before adsorption experiments, both materials -wood and coated nanowood- were pre-swelled in ultrapure water; then the swelled adsorbents were placed into the lake water. However,osmotic pressure seemed to have driven dewatering in the coated nanowood (2.67 ± 0.29% loss), this did not happen in case of the wood, that in turn further swelled 5.52 ± 0.23%.

This input of extra water to the spiked lake water could help explain the decrease of concentration observed on the aliquots extracted from the coated nanowood. The change is clearly attributed to loss of water, as no mass loss was measured when the adsorbents were dried after use, with resulting weights similar to the values present before swelling.

Likewise, a possible phenomenon occurring in this system is that other hydrophobic molecules present in the natural lake's water present a higher affinity to the hydrophobic cavities, competing selectively for this active points. However, this was not clearly observed in the chromatograms obtained using the acidic acetonitrile/water method.

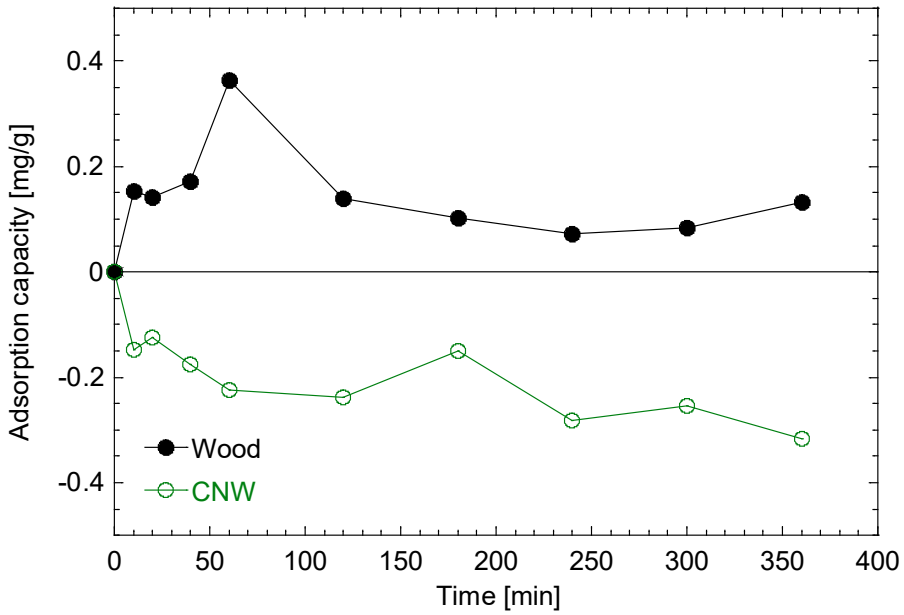

Figure 7.4. Adsorption kinetic of wood and coated nanowood on water from Lake Ogleetree spiked with 5.4 µg/mL.

Another indication that the observed results are due to changes on water interactions could be seen in the pseudo-second order modeling of the results (Figure 7.5), where both materials presented negative constant rates. These values indicate desorption rates rather than adsorption, contrary to the positive 1.19 g/ mg min from the coated nanowood reported in Chapter 6. These negative values indicate that molecules are desorbing from both wood and CNW at higher rates than the microcystin adsorption observed on the wood. These trends are similar to the QCM-D data observed in Chapter 5, where the loss of water was higher than any positive adsorption of the toxin on the surfaces.

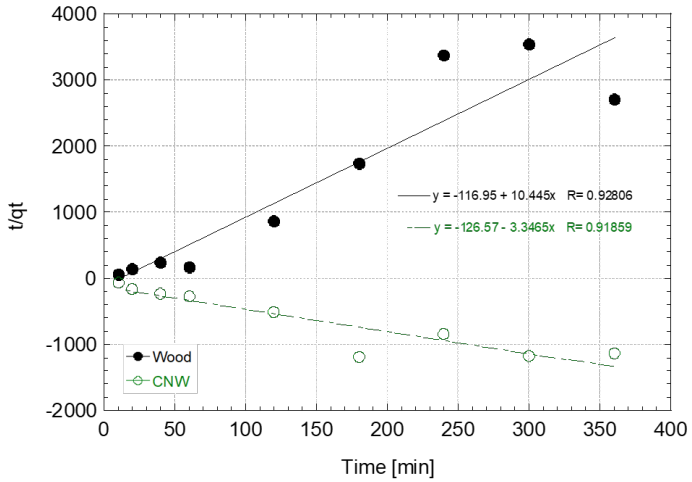

	Wood	Coated nanowood
q_e [mg/g]	0.09	-0.29
h [mg/g min]	-0.01	-0.01
k_2 [g/mg min]	-0.93	-0.09
R^2	0.93	0.92
$t_{0.5}$ [min]	-1.07	-11.3

Figure 7.5. Pseudo-second order kinetic model and data of the adsorption of microcystin-LR with wood and the coated nanowood from spiked water of Ogletree Lake.

Another possibility for the lack of MC adsorption onto the coating could be due to the formation of crystals by the oriented cyclodextrins on the surface caused by higher concentration of the coating and the uneven distribution on the material as observed with the elemental analysis. Cyclodextrins are known to form liquid crystals by intermolecular hydrogen bonding to avoid the exposure of the hydrophobic cavities (Luviano et al., 2020; Saenger & Steiner, 1998). It is possible that the liquid crystal formation could be occurring during coating and drying of the material, occluding the cyclodextrin cavities, and therefore impeding the formation of inclusion complexes between the sorbent and MC. To better understand if this is happening, rheology measurement should be done with the coating at different concentrations as next steps.

7.5. Conclusions

On this chapter, the successful generation of coated nanowood was performed, using a higher quantity of coating on the surface (1.5%) compared to the previous chapter. Furthermore, surface water from Lake Ogleetree was obtained and analyzed. The water showed good quality for

drinking purposes, even before potabilization of it. This water had low dissolved solids, as well as low conductivity because of little ions present on it.

When the lake water was spiked with the microcystin-LR at comparable concentrations that those tested on the previous chapter, it was observed that the lower salt concentration had a significant impact on the behavior of the sorbent. The pristine wood presented certain level of adsorption, resulting on the removal of 0.09 mg/g of the toxin from the tested water; meanwhile, the coated nanowood did not presented active adsorption of the microcystin. This lack of adsorption could be a consequence of the higher concentration of CD used for the coating, or by the lower salt concentration in the natural water sample.

7.6. Future Work

To determine if liquid crystals are being formed on the interface with the modified chitosan-cyclodextrin prior to coating, the rheological behavior of the Ch-TOCD coating at different concentrations should be evaluated. Similarly, different concentrations and atmospheric pressures on the coating process could be evaluated to ensure that the surface is completely coated and active.

Conversely, additional lab-controlled adsorption testing should be performed at different ionic strength in order to evaluate the behavior of the coating at different conditions.

7.7. Literature Cited

Abbas, T., Kajjumba, G. W., Ejjada, M., Masrura, S. U., Marti, E. J., Khan, E., & Jones-Lepp, T. L. (2020). Recent Advancements in the Removal of Cyanotoxins from Water Using Conventional and Modified Adsorbents—a Contemporary Review. Water, 12(10), 2756. https://doi.org/10.3390/w12102756

Adebajo, M. O., Frost, R. L., Kloprogge, J. T., Carmody, O., & Kokot, S. (2003). Porous Materials for Oil Spill Cleanup: A Review of Synthesis and Absorbing Properties. Journal of Porous Materials, 10(3), 159–170. https://doi.org/10.1023/A:1027484117065

Ahmad, M., Ahmed, S., Swami, B. L., & Ikram, S. (2015). Adsorption of Heavy Metal Ions: Role of Chitosan and Cellulose for Water Treatment. International Journal of Pharmacognosy, 2(6), 280–289. https://doi.org/10.13040/IJPSR.0975-8232.IJP.2(6).280-89

Ali, I. (2012). New generation adsorbents for water treatment. Chemical Reviews, 112(10), 5073–5091. https://doi.org/10.1021/cr300133d

Archimandritis, A. S., Papadimitriou, T., Kormas, K. A., Laspidou, C. S., Yannakopoulou, K., & Lazarou, Y. G. (2016). Theoretical investigation of microcystin-LR, microcystin-RR and nodularin-R complexation with α-, β-, and γ-cyclodextrin as a starting point for the targeted design of efficient cyanotoxin traps. Sustainable Chemistry and Pharmacy, 3, 25–32. https://doi.org/10.1016/j.scp.2016.02.001

Baird, R. B., Eaton, A. D., & Rice, E. W. (Eds.). (2017). Standard Methods for the Examination of Water and Wastewater (23rd Editi). American Public Health Association, American Water Works Association, Water Environment Federation. https://www.awwa.org/Store/Product-Details/productId/65266295

Blackburn, R. S. (2004). Natural polysaccharides and their interactions with dye molecules: Applications in effluent treatment. Environmental Science and Technology, 38(18), 4905–4909. https://doi.org/10.1021/es049972n

Boopathi, T., & Ki, J.-S. (2014). Impact of Environmental Factors on the Regulation of Cyanotoxin Production. Toxins, 6(7), 1951–1978. https://doi.org/10.3390/toxins6071951

Carmichael, W. W., & Boyer, G. L. (2016). Health impacts from cyanobacteria harmful algae blooms: Implications for the North American Great Lakes. Harmful Algae, 54, 194–212. https://doi.org/10.1016/j.hal.2016.02.002

Chu, Z., Zheng, P., Yang, Y., Wang, C., & Yang, Z. (2020). Compressible nanowood/polymer composite adsorbents for wastewater purification applications. Composites Science and Technology, 198(April), 108320. https://doi.org/10.1016/j.compscitech.2020.108320

Dorton, D. D. (2019). Auburn limits use of water source to lessen taste, odor issues - Auburn News. Auburn News. https://news.auburnalabama.org/article/City News/3005

Emmanuel, V., Odile, B., & Céline, R. (2015). FTIR spectroscopy of woods: A new approach to study the weathering of the carving face of a sculpture. Spectrochimica Acta - Part A: Molecular and Biomolecular Spectroscopy, 136(PC), 1255–1259. https://doi.org/10.1016/j.saa.2014.10.011

Gomez-Maldonado, D., Vega Erramuspe, I. B., Filpponen, I., Johansson, L.-S., Lombardo, S., Zhu, J., Thielemans, W., & Peresin, M. S. (2019). Cellulose-Cyclodextrin Co-Polymer for the Removal of Cyanotoxins on Water Sources. Polymers, 11(12), 2075. https://doi.org/10.3390/polym11122075

Gomez-Maldonado, D., Vega Erramuspe, I. B., & Peresin, M. S. (2019). Natural Polymers as Alternative Adsorbents and Treatment Agents for Water Remediation. BioResources, 14(4), 10093–10160. https://doi.org/10.15376/biores.14.4.10093-10160

Grattan, L. M., Holobaugh, S., & Morris, J. G. (2016). Harmful algal blooms and public health. Harmful Algae, 57, 2–8. https://doi.org/10.1016/j.hal.2016.05.003

Jiang, Y., Liu, B., Xu, J., Pan, K., Hou, H., Hu, J., & Yang, J. (2018). Cross-linked chitosan/β-cyclodextrin composite for selective removal of methyl orange: Adsorption performance and mechanism. Carbohydrate Polymers, 182(July 2017), 106–114. https://doi.org/10.1016/j.carbpol.2017.10.097

Kotake, Y., & Janzen, E. G. (1989). Effect of pH and Salt Concentration on Bimodal Inclusion of a Nitroxide by Cyclodextrins. Journal of the American Chemical Society, 111(19), 7319–7323. https://doi.org/10.1021/ja00201a006

Luviano, A. S., Hernández-Pascacio, J., Ondo, D., Campbell, R. A., Piñeiro, Á., Campos-Terán, J., & Costas, M. (2020). Highly viscoelastic films at the water/air interface: α-Cyclodextrin with anionic surfactants. Journal of Colloid and Interface Science, 565, 601–613. https://doi.org/10.1016/j.jcis.2019.12.012

Mishima, T., Hisamatsu, M., York, W. S., Teranishi, K., & Yamada, T. (1998). Adhesion of β-D-glucans to cellulose. Carbohydrate Research, 308(3–4), 389–395. https://doi.org/10.1016/S0008-6215(98)00099-8

Orelma, H., Filpponen, I., Johansson, L.-S., Laine, J., & Rojas, O. J. (2011). Modification of Cellulose Films by Adsorption of CMC and Chitosan for Controlled Attachment of Biomolecules. Biomacromolecules, 12(12), 4311–4318. https://doi.org/10.1021/bm201236a

Orelma, H., Virtanen, T., Spoljaric, S., Lehmonen, J., Seppälä, J., Rojas, O. J., & Harlin, A. (2018). Cyclodextrin-Functionalized Fiber Yarns Spun from Deep Eutectic Cellulose Solutions for Nonspecific Hormone Capture in Aqueous Matrices. Biomacromolecules, 19(2), 652–661. https://doi.org/10.1021/acs.biomac.7b01765

Ozmen, E. Y., Sezgin, M., Yilmaz, A., & Yilmaz, M. (2008). Synthesis of β-cyclodextrin and starch-based polymers for sorption of azo dyes from aqueous solutions. Bioresource Technology, 99(3), 526–531. https://doi.org/10.1016/j.biortech.2007.01.023

Pam Wright. (2018). Florida's Blue-Green Algae Bloom 10 Times Too Toxic to Touch, Testing Shows | The Weather Channel. Weather.Com. https://weather.com/science/environment/news/2018-08-10-florida-algae-bloom-st-lucie-microcystin

Rosenfeld, P. E., & Feng, L. G. H. (2011). Emerging Contaminants. In Risks of Hazardous Wastes (pp. 215–222). Elsevier. https://doi.org/10.1016/b978-1-4377-7842-7.00016-7

Saenger, W., & Steiner, T. (1998). Cyclodextrin Inclusion Complexes: Host ± Guest Interactions and Hydrogen-Bonding Networks. 798–805. https://doi.org/10.1107/S0108767398010733

Saito, T., Hirota, M., Tamura, N., Kimura, S., Fukuzumi, H., Heux, L., & Isogai, A. (2009). Individualization of Nano-Sized Plant Cellulose Fibrils by Direct Surface Carboxylation Using TEMPO Catalyst under Neutral Conditions. Biomacromolecules, 10(7), 1992–1996. https://doi.org/10.1021/bm900414t

Sinha, A., & Jana, N. R. (2015). Separation of microcystin-LR by cyclodextrin-functionalized magnetic composite of colloidal graphene and porous silica. ACS Applied Materials and Interfaces, 7(18), 9911–9919. https://doi.org/10.1021/acsami.5b02038

Stana-Kleinschek, K., Strnad, S., & Ribitsch, V. (1999). Surface characterization and adsorption abilities of cellulose fibers. Polymer Engineering & Science, 39(8), 1412–1424. https://doi.org/10.1002/pen.11532

SunCrest Laboratories, L. L. C. (2010). Lake Ogletree Source Water Assessment Report.

The Water Works Board Of The City Of Auburn. (2019). 2019 Consumer Confidence Report.

Tran, C. D., Duri, S., Delneri, A., & Franko, M. (2013). Chitosan-cellulose composite materials: Preparation, Characterization, and application for removal of microcystin. Journal of Hazardous Materials, 253, 355–366.

USEPA - Office of Ground Water and Drinking Water. (2017). The Fourth Unregulated Contaminant Monitoring Rule (UCMR 4) Public Meeting and Webinar

Water Resource Management - City of Auburn. (n.d.). Lake Ogletree - City of Auburn. Retrieved January 20, 2021, from https://www.auburnalabama.org/water-resource-management/water-operations/Lake-ogletree/

Wells, M. L., Trainer, V. L., Smayda, T. J., Karlson, B. S. O., Trick, C. G., Kudela, R. M., Ishikawa, A., Bernard, S., Wulff, A., Anderson, D. M., & Cochlan, W. P. (2015). Harmful algal blooms and climate change: Learning from the past and present to forecast the future. Harmful Algae, 49, 68–93. https://doi.org/10.1016/j.hal.2015.07.009

World Health Organization. (2019, June 14). Drinking-water. https://www.who.int/news-room/fact-sheets/detail/drinking-water

Zhu, Z., Kang, W., Yang, H., Wang, P., Zhang, X., Yin, X., & Lashari, Z. A. (2017). Study on salt thickening mechanism of the amphiphilic polymer with betaine zwitterionic group by β-

cyclodextrin inclusion method. Colloid and Polymer Science, 295(10), 1887–1895. https://doi.org/10.1007/s00396-017-4169-7

Zhu, M., Song, J., Li, T., Gong, A., Wang, Y., Dai, J., Yao, Y., Luo, W., Henderson, D., & Hu, L. (2016). Highly Anisotropic, Highly Transparent Wood Composites. Advanced Materials, 28(26), 5181–5187. https://doi.org/10.1002/adma.201600427